Isolation and characterisation of thirteen pterosins and pterosides from bracken (*Pteridium aquilinum* (L.) Kuhn) rhizome

Rizgar Hassan Mohammad, Mohammad Nur e-Alam, Martina Lahmann, Ifat Parveen Shah, Graham J. Tizzard, Simon J. Coles, Mark Fowler, Alex F. Drake, Derren Heyes, Vera Thoss*

Thirteen previously undescribed pterosins and pterosides were isolated from bracken rhizomes in north of Wales. Their structures were elucidated using NMR spectroscopic and high resolution FT-ICR-MS data.

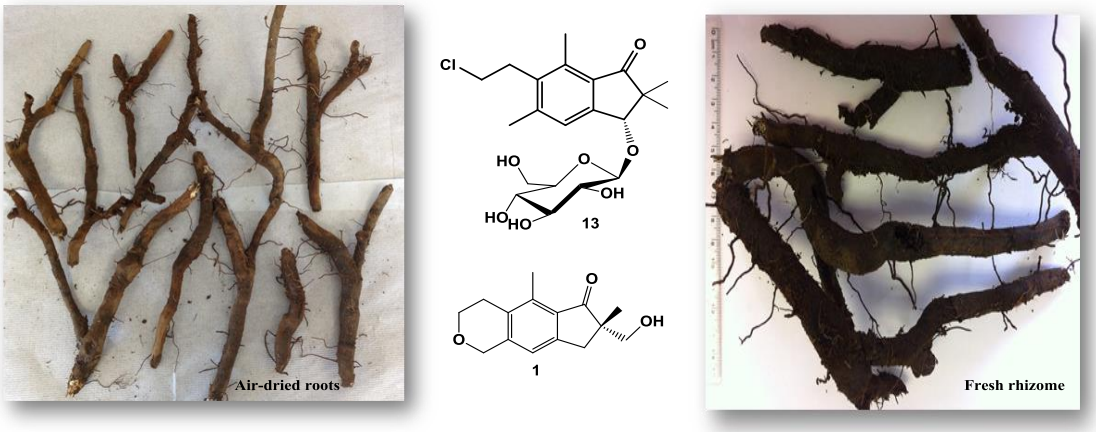

Isolation and characterisation of 13 pterosins and pterosides from bracken (*Pteridium aquilinum* (L.) Kuhn) rhizome

Rizgar Hassan Mohammad[a], Mohammad Nur-e-Alam[a,b] , Martina Lahmann[a], Ifat Parveen[c], Graham J. Tizzard[d], Simon J. Coles[d], Mark Fowler[e], Alex F. Drake[f], Derren Heyes[g], Vera Thoss[a,*]

[a] School of Chemistry, Bangor University, Bangor LL57 2UW, United Kingdom

[b] Department of Pharmacognosy, College of Pharmacy, King Saud University, P.O. Box 2457, Riyadh 11451, Saudi Arabia

[c] IBERS, Aberystwyth University, Penglais, Aberystwyth SY23 3DA, UK

[d] UK National Crystallography Service, School of Chemistry, University of Southampton, University Road, Southampton SO17 1BJ, United Kingdom

[e] Strategic Science Group, Unilever R&D, Colworth Science Park, Bedford, MK44 1LQ, UK

[f] Biomolecular Spectroscopy Centre, Pharmaceutical Optical & Chiroptical Spectroscopy Facility, King's College London, The Wolfson Wing, WWB10 Hodgkin Building, Guy's Campus, London SE1 1UL, UK

[g] Manchester Institute of Biotechnology, University of Manchester, 131 Princess St, Manchester M1 7DN

*Corresponding Author vera.thoss@bangor.ac.uk

ABSTRACT

Systematic phytochemical investigations of the underground rhizome of *Pteridium aquilinum* (L.) Kuhn (Dennstaedtiaceae) afforded thirty-five pterosins and pterosides. By detailed analysis of one- and two-dimensional nuclear magnetic resonance spectroscopy, circular dichroism (CD) and high-resolution mass spectrometric data, thirteen previously undescribed pterosins and pterosides have been identified. Interestingly, for the first time 12-*O*-*β*-D-glucopyranoside substituted pterosins, rhedynosides C and D, and the sulfate-containing pterosin, rhedynosin H, alongside the two known compounds, histiopterosin A and (2*S*)-pteroside A2, were isolated from the rhizomes of subsp. *aquilinum* of bracken. In addition, six-membered cyclic ether pterosins and pterosides, rhedynosin A and rhedynoside A, are the first examples of this type of pterosin-sesquiterpenoid. Additionally, the three previously reported compounds (rhedynosin I, (2*S*)-2-hydroxymethylpterosin E and (2*S*)-12-hydroxypterosin A) were obtained for the first time from plants as opposed to mammalian metabolic products. Single crystal X-ray diffraction analysis was applied to the previously undescribed compounds (2*R*)-rhedynoside B, (2*R*)-pteroside B and (2*S*)-pteroside K, yielding the first crystal structures for pterosides, and three known pterosins, (2*S*)-pterosin A, *trans*-pterosin C and *cis*-pterosin C. Rhedynosin C is the only example of the cyclic lactone pterosins with a keto group at position C-14. Six selected pterosins ((2*S*)-pterosin A, (2*R*)-pterosin B and *trans*-pterosin C) and associated glycosides ((2*S*)-pteroside A, (2*R*)-pteroside B and pteroside Z) were assessed for their anti-diabetic activity using an intestinal glucose uptake assay; all were found to be inactive at 300 µM.

Keywords: *Pteridium aquilinum*; Dennstaedtiaceae; Bracken Pterosins; Pterosides; Norsesquiterpenes; Sesquiterpenoids; Pterosins A and B; Circular Dichroism, SGLT1 and GLUT2 Transporters

1. Introduction

One of the most widely distributed vascular plant species in the world is bracken (*Pteridium aquilinum* (L.) Kuhn). In the UK, *P. aquilinum* subsp. *aquilinum* comprises the majority of bracken, with a dense coverage estimated at 4782 km^2 (dense) or 17000 km^2 (presence), representing 7% of the land area in the UK, including sparse bracken (Pakeman et al., 1996). This corresponds to 1.1 - 5 Gigatonne (Gt) of plant material above ground and 5 - 20 Gt of rhizome biomass (dry weight, calculated from data in (Marrs and Watt, 2006)). Bracken has long been recognised for its potential pharmaceutical uses and its toxicity. Furthermore, bracken has been used medicinally as an anthelminthic agent (Marrs and Watt, 2006). Bracken crosiers have been eaten as a delicacy in Japan and Brazil. The rhizome has been used as a source of starch (Alonso-Amelot and Avendano, 2002; Madeja et al., 2009).

Phytochemical studies of bracken are most often concerned with the norsesquiterpene glycoside ptaquiloside, because of its established carcinogenicity (Fenwick, 1988; Hirono, 1986). Research has been concentrated on the quantification of this compound in the plant (Alonso-Amelot et al., 1992; Rasmussen et al., 2003) and in biological samples, such as urine, milk and plasma (Aranha et al., 2014). Ptaquiloside is unstable due to the presence of a spirocyclopropane moiety. The main degradation product of ptaquiloside is pterosin B (Hirono, 1986). Other pterosins have been isolated from different subsp. of *Pteridium aquilinum* (Fukuoka et al., 1978; Kuraishi et al., 1985; Murakami et al., 1980; Sengupta et al., 1976; Tanaka et al., 1982; Yoshihira et al., 1971). Pterosins are sesquiterpenoids and their structures are derivatives of 1-indanone. They are biosynthesised in all parts of the bracken, including fronds and rhizomes (Hikino et al., 1976; Kigoshi et al., 1989). Bracken has historically been associated with incidents of livestock poisoning (Hopkins, 1990; Vetter, 2009) resulting in many mechanistic studies on distinct pterosins and their biological targets. For example, pterosin B was found to inhibit the Gram-positive bacterium *Bacillus subtilis* at minimum inhibitory concentration (MIC) of 30 µg ml^{-1} (Kobayashi et al., 1975). Pterosins B, F, H, I, O, Z and V showed cytotoxic effects on *Paramecium caudatum* and caused abnormal development of sea urchin embryos but did not inhibit DNA synthesis (Kobayashi and Koshimizu, 1980). Pterosin Z is a potent relaxant to smooth muscle (EC_{50} = 1.3 ± 0.1 µM) (Sheridan et al., 1999). In addition, the interaction of bracken extract with vitamin C in human submandibular and oral epithelial cell lines has been assessed (Campos-da-Paz et al., 2008) and the dependency of the biological effect of bracken extract in different cell assays has been evaluated (Almeida Santos et al., 2006). Anti-diabetic activity has also been associated with pterosins (Hsu et al., 2014), and studies using distinct pterosins, methanolic extracts of bracken have been used to investigate glycophenotypic alterations in mice gastric mucosa (Gomes et al., 2012).

The toxicity of North Wales bracken, 'Rhedyn' in the Welsh language, to cattle has been studied previously (Potter, D.M., Baird, 2000; Yamada et al., 2007). Recently, a traditional phytochemical investigation of bracken rhizomes using various analytical techniques led to the isolation of thirteen novel compounds (**1**-**13**) (Figs. 1 & 2), together with twenty two known compounds: rhedynosin I (**14**), (2*S*)-pterosin A (**15**), (2*R*)-pterosin B (**16**), (2*R*, 3*R*)-pterosin C (*trans*-pterosin C) (**17**), (2*S*, 3*R*)-pterosin C (*cis*-pterosin C) (**18**), (3*S*)-pterosin D (**19**), (2*R*)-pterosin E (**20**), (2*R*)-pterosin F (**21**), (2*S*, 3*S*)-pterosin J (**22**), (2*S*)-pterosin K (**23**), (2*S*)-pterosin N (**24**), (2*S*)-pterosin P (**25**), pterosin Z (**26**), (2*S*)-2-hydroxymethylpterosin E (**27**), histiopterosin A (**28**), (2*S*)-12-hydroxypterosin A (**29**), (2*S*)-pteroside A (**30**), (2*R*)-pteroside B (**31**), (3*S*)-pteroside D (**32**), pteroside Z (**33**), (2*S*)-pteroside A2 (**34**) and (2*S*)-pteroside K (**35**), of which compounds **14** and **27-29** are identified for the first time from the genus *Pteridium* which belongs to Dennstaedtiaceae

family (Figs. 1-3). Herein described are the isolation and structural elucidation of these compounds.

2. Results and Discussion:

The underground parts (rhizomes) of bracken (*Pteridium aquilinum* (L.) Kuhn) were air-dried, chopped and then extracted with chloroform. More than twenty sesquiterpenoid constituents have been identified with UV absorption spectra profiles in the 340 to 205 nm region characteristic of 1-indanone derivatives (Fukuoka et al., 1978; Kuraishi et al., 1985; Murakami et al., 1980; Yoshihira et al., 1971). The chloroform extract was repeatedly subjected to thin-layer, normal-phase column, and automated reversed phase flash chromatography to afford thirty five compounds (**1-35)**. One- and two-dimensional NMR experiments combined with mass spectrometry were used to identify thirteen novel natural products (**1-13**) (Supplementary Information 1) belonging to the sesquiterpenoid family. The structures of twenty two previously reported pterosins and pterosides **14**, **27**, **29** (Lee et al., 2012), **15-18**, **30-33**, **35** (Kuroyanagi et al., 1979), **19-25** (Fukuoka et al., 1978), **26** (Kuraishi et al., 1985; Tanaka et al., 1982), **28** (Murakami et al., 1980), **34** (Castillo et al., 2003) were determined by the comparison of their spectroscopic data with those reported in the literature (Figs. 1-3). The structures of compound **1-13** are shown in Figs. 1 & 2 and their ^{1}H and ^{13}C data is listed in Tables 1-4.

X-ray crystallography remains the definitive tool to determine the absolute configuration but requires the existence of good crystals. Circular Dichroism (CD) is a technique that can be used to assign the absolute configuration in solution with less than 1 mg of compound (Warnke and Furche, 2012). However, CD is only reliable for the determination of absolute configuration if chromophores are in close spatial proximity allowing for exciton coupling. Unfortunately, this is not the case with the compounds discussed here. In the past, sector rules (eg octant rules) were invoked in order to assign the absolute configuration of compounds composed of a chromophore in a dissymmetric environment. However, such rules are now considered with scepticism. Nevertheless, careful pair-wise comparison of the CD of compounds with identical chromophore cores (Fig. 4) and similar dissymmetric environments enables correlation. Unfortunately, the large perturbing influence of a glycosyl-residue in the structure can hamper comparison with glucose-free compounds.

The UV and CD spectra in the 380 nm to 260 nm region associated with the keto group $n \rightarrow \pi^*$ transition can be deceptively complex. The electron transitions primarily observed in an UV spectrum produce fairly straightforward spectral data. However, the presence of vibronic effects (coincidental change of vibrational and electronic energy levels) may add complexity to the signal, e.g., in form of additional shoulders. The corresponding CD spectra obey different selection rules. The CD associated with the $n \rightarrow \pi^*$ transition may mimic the absorption spectrum and be relatively plain or may be fine structured indicating the importance of particular vibronic progressions. In the series outlined here, compound **1**, **14**, **15**, **23**, **27**, **29** and **30** present CDs with vibronic fine structure, while compounds **2**, **7**, **34**, **35** render relatively featureless spectra. Comparison of the CD spectra with X-ray data or published CD data (Kuroyanagi et al, 1979) revealed that the stereogenic centre in the core aglycone (Fig. 4) of all compounds **1**, **2**, **7**, **14**, **15**, **23**, **27**, **29**, **30**, **34**, **35** can be assigned as 2*S*.

2.1. Structural Elucidation

Compound **1** was obtained as a yellow powder and its molecular formula was established as $C_{15}H_{18}O_3$ based on the positive mode quasi-molecular ion peak at *m/z* 247.1330 $[M+H]^+$ (calcd for $C_{15}H_{19}O_3$, 247.1334) showing 7 degrees of unsaturation. The UV absorbance maxima at 211, 258 and 306 nm were consistent with 1-indanone derivatives. The IR absorption bands at 3014, 1605, 3418 and 1704 cm^{-1} indicated the presence of aromatic C-H, C=C, hydroxyl and carbonyl groups, respectively, which concur with the presence of a 1-indanone skeleton (Fukuoka et al., 1978; Kuroyanagi et al., 1979).

The full assignment of ^1H and ^{13}C NMR resonances was deduced from ^1H-^1H COSY, DEPTQ, HSQC and HMBC analysis (Tables 1 & 4, Fig. 5 and Supplementary Information 1). The signals for all protonated carbons were assigned by analysis of the DEPTQ and HSQC spectra to establish the connectivity. The ^1H NMR spectrum of **1** shows signals of one secondary methyl [δ_H 2.56 (3H, s, H-15)], one tertiary methyl [δ_H 1.23 (3H, s, H-10)], two methylenes [δ_H 2.77, 3.06 (2H, d, J = 17.5 Hz, H-3) and 2.76 (2H, t, J = 5.9 Hz, H-13)], three oxygenated methylenes [δ_H 3.62, 3.78 (2H, d, J = 10.8 Hz, H-11), 4.80 (2H, s, H-12) and 4.01 (2H, td, J = 1.3, 5.9, 11.8 Hz, H-14)] and one methine [δ_H 6.93 (1H, s, H-4)] signal in the aromatic region. The DEPTQ spectrum, in combination with HSQC and HMBC data, displays 15 carbon resonances, including two quaternary methyls at δ_C 21.1 (C-10) and δ_C 13.1 (C-15), five methylenes (including three oxygenated carbons), one methine at δ_C 120.0 (C-4) and seven quaternary carbons. As three of the 7 degrees of unsaturation are accounted for by a tricyclic system of **1**, the remaining 4 degrees of unsaturation require 4 double bonds. The key HMBC correlations are shown in Fig. 5. In the HMBC spectrum, the signals at δ_H 2.77 and 3.06 (2H, d, J = 17.5 Hz, H-3) shows correlations with δ_C 50.9 (C-2), δ_C 138.2 (C-7), δ_C 131.3 (C-8), δ_C 151.0 (C-9), δ_C 21.1 (C-10) and δ_C 68.3 (C-11). δ_H 4.80 (2H, s, H-12) displays correlations with δ_C 120.0 (C-4), δ_C 142.1 (C-5), δ_C 131.8 (C-6) and δ_C 65.6 (C-14). δ_H 2.76 (2H, t, J = 5.9 Hz, H-13) exhibits correlations with δ_C 142.1 (C-5), δ_C 131.8 (C-6) and δ_C 138.2 (C-7). δ_H 4.01 (2H, td, J = 1.3, 5.9, 11.8 Hz, H-14) reveals correlations with δ_C 131.8 (C-6), 68.8 (C-12) and δ_C 25.8 (C-13). δ_H 3.62, 3.78 (2H, d, J = 10.8 Hz, H-11) is correlated with δ_C 210.5 (C-1), δ_C 50.9 (C-2), δ_C 37.1 (C-3) and δ_C 21.1 (C-10). The latter correlations confirmed the position of the hydroxymethylene (CH_2OH) group at C-2. Other connectivities shown in this spectrum are: δ_H 6.93 (1H, s, H-4) with C-3, C-6 & C-12, δ_H 1.23 (3H, s, H-10) with C-1, C-2, C-3 & C-11 and δ_H 2.56 (3H, s, H-15) with C-6, C-7 & C-8. The presence of an ether link was assigned to be between positions C-12 and C-14 as their proton and carbon chemical shifts appeared at the low field region due to the deshielding influence of the oxygen atom. This was further confirmed with the HMBC spectrum that showed the correlations from H-12 (δ_H 4.80) to C-14 (δ_C 65.6) and from H-14 (δ_H 4.01) to C-12 (δ_C 68.8). The *J*-coupling systems were confirmed by COSY data that displays couplings between signals: δ_H 2.76 & δ_H 4.01, δ_H 2.77 & δ_H 3.06, and δ_H 3.62 & δ_H 3.78, respectively.

The CD spectrum of **1** shows a vibronic n → π* transition (Fig. 6) which concurs with C-2 having 2*S* configuration. The observed transitions for the assignment of the absolute stereochemistry were based on the comparison of CD spectra of **1** with X-ray crystallography data of **15** (Fig. 7) and the CD interpretation provided for **15** by Kuroyanagi et al., 1979. Based on the above analysis, the structure of this compound was determined as a new natural product and named rhedynosin A (**1**). Its physical and spectroscopic features were consistent with the proposed structure in Fig. 1.

Compound **2** was isolated as a white powder exhibiting negative optical rotation ($[\alpha]_D^{24.2}$ -26.07 (*c* 0.33, MeOH)). The IR spectrum showed absorption bands in the region 1602, 1692 and 3369 cm^{-1} attributable to the aromatic ring, carbonyl and hydroxyl groups, respectively. UV spectrum absorption maxima were observed at 304 (log ε 2.99), 259 (log ε 3.92) and 216 (log ε 4.27) nm. The molecular formula, $C_{21}H_{28}O_8$, of **2** was determined by the quasi-molecular ion peak at *m/z*: 409.1865 ($[M+H]^+$, calcd. 409.1862) in the FT-ICR-MS spectrum (Fig. S14, SI1). Compound **2** exhibited ^1H and ^{13}C NMR data closely resembling to those of **1**. Comparison of the UV, IR and NMR spectroscopic data of **2** (Tables 1 and 4) with those of rhedynosin A (**1**) showed the following differences, the main one being the presence of an additional hexose sugar moiety having a signal for an anomeric-H at δ_H 4.21 (d, J = 7.8 Hz) and remaining sugar proton signals at δ_H 3.03-3.78. The ^{13}C NMR spectrum of **2** contained an anomeric carbon signal of a hexose moiety at δ_C 104.7 and signals for the remaining five sugar carbons at δ_C 62.7 - 78.1, which were in good agreement with those reported for glucoside compounds (Fukuoka et al., 1983). This indicated that compound **2** was a glycoside of compound **1**. The coupling constant (J = 7.8 Hz) is consistent with *trans* $^3J_{H\text{-}H}$, showing that it is a *β*-hexoside and that the adjacent proton on the sugar is axial in the chair conformation of the pyranose ring. The 8.9 Hz *trans*-diaxial coupling between H-2′ and H-3′ indicates an equatorial OH at C-3′. Thus, the sugar must be glucose or galactose. Since the ^1H NMR signals for H-3′ and H-4′ overlap in the spectrum of **2**, a sample was peracetylated forming the tetraacetate. The introduction of the electron withdrawing groups shifts the signals for the ring protons H-2′, H-3′, H-4′ and H-6′ downfield and resolves them clearly (method and spectra in SI1). The $J_{H3',H4'}$ coupling was determined to be *ca*. 8 Hz. This value is consistent with a *trans*-diaxial relationship between these protons in the chair conformation of the hexopyranose. Three *trans*-diaxial relationships derived from the ring protons of a pyranose are indicating a glucosyl residue. To our knowledge, no L-glucose has been reported being isolated from a plant source yet. Thus, it is most likely that this glycosyl residue belongs to the D-series. Carbon resonances at δ_C 104.7, 78.1, 77.9, 74.9, 71.5 and 62.7 in the ^{13}C NMR spectrum (Table 4) provided further evidence for the presence of a glucopyranyl residue. The linkage position of the sugar moiety to C-11 of the aglycone was confirmed by an HMBC experiment, which shows correlations between the anomeric resonance H-1′ (δ4.21) and C-11 (δ75.0), and between H-11 (δ4.13 and 3.48) and the anomeric carbon C-1′ (δ104.7). The CD spectrum shows a plain positive n $\rightarrow\pi^*$ component at ~330 nm that can be correlated with the configuration at C-2 being 2*S* (Kuroyanagi et al., 1979). Based upon the above evidence, the structure of **2** was identified as rhedynosin A 11-*O*-β-D-glucoside and named rhedynoside A (Fig. 1).

A new natural product, compound **3**, was isolated as a yellow powder with an accurate mass similar to **1** at *m/z* 247.0967 $[M+H]^+$, consistent with a molecular formula of $C_{14}H_{15}O_4$ and 8 degrees of unsaturation. The IR bands were due to a hydroxyl, carbonyl and aromatic carbon-carbon double bond observed at 3419, 1715 and 1603 cm^{-1}, respectively. The ^1H NMR spectrum (Table 1) of **3** closely resembles that of **1** but the ^{13}C NMR (HMBC) data, displays only 14 carbon resonances instead of the 15 signals that appear in the spectrum of **1**. These signals were ascribed to three methylenes, two methyls, one methine, six quaternary carbons and two carbonyl groups (Tables 1 & 4). The major difference in the NMR data for compound **3** is the absence of a methylene signal at δ_H 4.80 (CH_2-12, ^1H NMR) and the appearance of a quaternary carbon at δ_C 165.0 (^{13}C NMR) corresponding to an ester, thus indicating that the methylene group (CH_2-12) of **1** is oxidised to a carbonyl in **3**. This interpretation explains the downfield shift (δ_H 8.05) of the methine signal (H-4) due to the influence of the carbonyl at position C-12. The HMBC spectrum

confirmed the location of the carbonyl group. Furthermore, in the HMBC experiment strong correlations were observed from both proton signals at δ_H 8.05 (H-4) & 4.55 (H-14) to the carbon signal at δ_C 165.0 (C-12). The other significant difference was the absence of CH_2 signals at δ_H 3.78 and δ_H 3.62 (CH_2-11) in the ^1H NMR spectrum. The ^{13}C NMR spectrum showed that the methylene signal from C-11 was absent and that the signal for C-2 had moved downfield to δ_C 78.0, showing the presence of an oxygen. While CD spectra were obtained for **3**, the absolute stereochemistry was not assignable as there was neither an X-ray reference with hydroxyl substitution on C-2 nor a previous literature report of a CD spectrum of a compound with a suitable chromophore core. Compound **3** was identified as a previously unreported natural product and named rhedynosin B (Fig. 1).

Compound **4** was obtained as a white powder with an optical rotation $[\alpha]_D^{24.2}$ +3.76. The negative mode mass spectrum showed a molecular ion peak at *m/z* 245.0821 $[M-H]^-$, compatible with the molecular formula of $C_{14}H_{13}O_4$. In the IR spectrum, strong bands at ν_{max} 1703 and 3428 cm^{-1} were indicative of carbonyl and hydroxyl groups, respectively. The maximum UV absorbances of **4** appeared at 214, 258 and 306 nm, in agreement with 1-indanone compounds (Tanaka et al., 1982; Yoshihira et al., 1971). Analysis of the NMR and MS spectral data showed that **4** is structural similar to **3**. The major differences were detected by NMR experiments, for example the presence of two isolated methylene signals at δ_H 5.40 (2H, s, H-12) and δ_H 3.83 (2H, s, H-13) which appear as singlets and thus indicated that the carbonyl group was at position 14 in **4**. The chemical shift for CH_2-12 (δ_H 5.40) also indicated a very electron-deficient environment, consistent with $ArCH_2OC{=}O$. The HMBC spectrum confirmed the assignments and connectivities, and also shows a cross peak between H-12 (δ_H 5.40) and C-14 (δ_C 173.5). The data provided further evidence for the carbonyl being present at the C-14 position. Thus, the structure of **4** was identified as a new compound, named rhedynosin C (Fig. 1). However, the absolute configuration in C-2 remains undetermined.

Compound **5** was obtained as a yellow solid. In the positive mode spectrum, *pseudo*-molecular ion peaks at *m/z* 269.0941 and *m/z* 271.0912 $[M + H]^+$ in the ratio 3:1, indicate the presence of one chlorine atom and suggested a molecular formula of $C_{14}H_{18}ClO_3$. The IR spectrum showed major absorption bands at 3418 cm^{-1} (OH), 1714 cm^{-1} (C=O) and 1602 and 1447 cm^{-1} (aromatic C=C). The UV spectrum exhibits UV signals at 212, 215 and 303 nm. The ^1H NMR data (Table 1) of **5** indicates a penta-substituted benzene ring with a single aromatic proton signal at δ_H 7.39 (1 H, s). Two coupled methylene groups at δ_H 3.21 (2H, t, J = 8.0 Hz) and δ_H 3.62 (2 H, t, J = 8.0 Hz) indicate an $ArCH_2CH_2X$ system, with the chemical shift of the latter triplet suggesting that X = Cl. The remaining ^1H NMR signals were in agreement with a pterosin-type structure (Fukuoka et al., 1978; Kovganko et al., 2004; Kuraishi et al., 1985; Tanaka et al., 1982). The ^{13}C NMR data of **5** (Table 4) shows fourteen distinct carbon environments, confirming the presence of a penta-substituted aromatic ring, including a low-field signal at δ_C 208.9 ppm (C=O) assigned as the C-1 of a pterosin-type sesquiterpene skeleton. The HMBC proton-carbon correlations confirmed a pterosin K side chain, a 2-chloroethyl group (CH_2CH_2Cl) attached to C-6 of benzene ring. A singlet methylene signal at δ_H 4.84 was assigned as the hydroxymethylene (CH_2OH) group attached to C-5 of the benzene ring. All assignments were confirmed by HMBC correlations and **5** was thus identified as rhedynosin D (Fig. 1). However, the absolute configuration in C-2 remains undetermined.

Compound **6** was obtained as an off-white powder and its molecular formula was determined from the positive mode FT-ICR-MS to be $C_{15}H_{19}O_4$ (*m/z* 263.1280 $[M+H]^+$, calcd 263.1283). The UV, IR, and NMR data of **6** were very similar to histiopterosin A (**28**) (Murakami et al., 1980). Two carbonyl resonances were evident in the ^{13}C NMR spectrum, with the ketone signal at δ_C 211.6 and a carboxylic acid signal at δ_C 175.3. In the ^1H NMR spectrum of **6**, an additional methyl signal is present, which was shown to be connected to C-2 by HMBC. Thus, two magnetically inequivalent methyl groups are attached to C-2, which resonate as singlets at δ_H 1.05 and δ_H 1.19.The application of CD spectroscopy to compound **6** showed a non-vibronic n→π* transition which was compared to the CD spectrum for **19** reported by Kuroyanagi et al., 1979 and assigned the configuration as *S* on C-3. Therefore, the structure of **6** was confirmed as rhedynosin E (Fig. 1).

Compound **8** was obtained as a yellow gum. In the FT-ICR-MS, **8** gave the same molecular formula as **5** ($C_{14}H_{17}ClO_3$). The UV spectrum showed absorption bands at 218, 260 and 299 nm. The IR, NMR and MS data of **8** were similar to those of **5**, with detailed exceptions which allowed identification of **8**. Differences were found in the NMR signals for the C-12 and C-13 positions for these two compounds. The ^1H NMR spectrum of **8** showed a methyl group resonating at δ_H 2.55 that gave a proton-carbon correlation to the carbon resonating at δ_C 22.0 in the HSQC spectrum and by HMBC this was assigned as C-12. A methine group, resonating at δ_H 5.45 (1 H, dd, J = 5.2, 8.7 Hz), that gave proton-carbon correlation to the carbon resonating at δ_C 71.4 in the HSQC spectrum, was assigned as the C-13. This suggested that the hydroxy group, which had been at C-12 in **5**, was in position C-13 in **8**. Compound **8** was thus identified as rhedynosin G (Fig. 1). However, the absolute configuration in C-2 remains undetermined.

Compound **7** was obtained as a pale yellow crystalline powder. In the accurate mass spectrum, **7** gave the molecular formula $C_{15}H_{19}ClO_3$, suggesting an additional methylene group when compared to **8**. The UV, IR and NMR data were similar to those of **8**. However, the additional methylene group was evident from the NMR data of **7**, with two geminally coupled doublets δ_H 3.79 (1 H, d, J = 10.7 Hz) and δ_H 3.59 (1 H, d, J = 10.7 Hz), correlating through one-bond with a new carbon signal at δ_C 68.1. The chemical shifts indicated that this new methylene was attached to the oxygen and thus the hydroxymethylene group was in position C-2. On the basis of the above mentioned evidence, the structure of **7** was confirmed as rhedynosin F (Fig. 1). CD spectroscopy allowed a 2*S* assignment of configuration.

Compound **9** was isolated as an off-white powder and its mass spectrum in the negative ion mode showed a molecular ion peak at *m/z* 297.0802 $[M-H]^-$ corresponding to a molecular formula of $C_{14}H_{17}O_5S$ (calcd as 297.0797). The UV, IR, and NMR data of **9** were very similar to those of pterosin B (**16**) (Fig. 3). This molecular formula suggested that the primary alcohol of **16** had been sulfated. This was confirmed by a downfield shift of the ^1H NMR resonance for the adjacent CH_2 (CH_2-14) to δ_H 4.05. Sulfated monoesters are common in marine natural products (McKee et al., 1994; Uddin et al., 2011). Compound **9** and **12** were subjected to CD spectroscopy, however, no significant spectra were observed and it is hypothesised that **9** and **12** racemised due to the presence of an acidic proton in the α-position to the carbonyl group. The structure of **9** was confirmed by full analysis of the data as rhedynosin H (Fig. 1).

Compound **10**, obtained as a white crystalline product, exhibited a molecular ion peak at *m/z* 415.1527 $[M+H]^+$ in the mass spectrum and correlated to the molecular formula $C_{20}H_{28}ClO_7$ (calcd as 415.1523). The UV, IR, and NMR data for **10** was very similar to that reported for pterosin F (**21**) (Fukuoka et al., 1978; Kuroyanagi et al., 1979), except for the presence of a sugar moiety in **10** which was connected to the aglycone through C-2, as determined by the HMBC experiment. Careful study of the coupling constants around the hexopyranose in the ^{1}H NMR spectrum suggested that the sugar was a glucose; $J_{1',2'}$ = 7.8 Hz, $J_{2',3'}$ = 8.0 Hz and $J_{3',4'}$ = 8.9 Hz, consistent with *trans*-diaxial arrangements of these protons. X-ray crystallography confirmed **10** as rhedynoside B and assigned the configuration at C-2 as *R* (Figs. 2 & 8).

Compound **11** was obtained as an off-white crystalline powder. In the FT-ICR-MS, **11** was shown to have the molecular formula $C_{21}H_{29}ClO_7$, with a molecular mass 14 Da higher than **10**. The UV, IR and NMR data of **11** were similar to those of pterosin H (Hayashi et al., 1972; Padwa et al., 1996; Tanaka et al., 1982) with the exception that **11** contained a sugar moiety. Of particular interest was a pair of geminally coupled doublets in the ^{1}H NMR spectrum at δ_H 5.11 (1 H, d, *J* = 12.4 Hz) and δ_H 4.78 (1 H, d, *J* = 12.4 Hz). These signals gave a one-bond H-C correlation with the ^{13}C NMR signal at δ_C 70.2. The chemical shifts corresponded to an $ArCH_2O$ system. An HMBC experiment assigned this carbon signal being connected to C-12. Moreover, the HMBC also linked the sugar to this methylene. The ^{1}H NMR spectrum of **11** confirmed the sugar as a hexopyranoside and identified the configuration of the glycosidic bond as β, with $J_{1',2'}$ = 7.7 Hz (also suggesting that the sugar was glucose or galactose). Peracetylation of the sugar separated the ^{1}H NMR signals of the sugar sufficiently to provide a full diastereomeric assignment of the sugar as glucose (see the discussion for **2** above). On the basis of this evidence, compound **11** was identified as rhedynoside C (Fig. 1).

Compound **12**, a novel natural product, was obtained as a yellow powder with the negative optical rotation $[\alpha]_D^{24.6}$ -0.643 (*c* 0.33, MeOH). In the FT-ICR-MS, **12** gave a quasi-molecular ion peak at *m/z* 413.1374 $[M-H]^-$, appropriate for a molecular formula $C_{20}H_{26}ClO_7$ (calcd as 413.1367), and indicating that it was an isomer of **10**. The UV, IR and NMR data of **12** were broadly similar to those of **10** except that the point of attachment of the sugar was clearly different. As for **11**, a diastereotopic methylene group was observed in the NMR spectra at δ_H 5.10 (1 H, d, *J* = 12.3 Hz) & 4.78 (1 H, d, *J* = 12.3 Hz) and δ_C 70.2. Using the same rationale as for determination of the location of the sugar as for **11**, HMBC data confirmed that the sugar was attached through a glycosidic linkage to C-12. Examination of the ^{1}H NMR coupling constants for protons around the hexopyranose in native and peracetylated forms demonstrated that it was β-linked glucose. Also notable was the presence of only one methyl group at C-2, δ_H 1.25 (3 H, d, *J* = 7.2 Hz), with the ^{13}C NMR signal for C-2 now reported as a methine. The structure of **12** was thus established as rhedynoside D (Fig. 1). However, the absolute configuration in C-2 remains undetermined.

Compound **13** was isolated as an off-white crystalline powder. Its molecular formula, $C_{21}H_{29}ClO_7$, was deduced from the FT-ICR-MS, indicating that it was another isomer of **11**. The UV, IR and NMR data for the aglycone of **13** were very similar to those of (3*R*)-hydroxypterosin H (Tanaka et al., 1982) indicating that it has the same structure in the aglycone part. A NOESY study of compound **13** showed through-space correlations between H-1′ and H-3′ and between H-1′ and H-5′, confirming that these three protons are all axial and that the sugar is glucose. Singlet signals for three methyl groups were evident in the ^{1}H NMR spectrum, with HMBC confirming that two methyl signals (δ_H 1.28 and δ_H 1.09) formed a geminal pair. The third (δ_H 2.49) was in an ArMe

environment and was confirmed by HMBC data to correspond to C-12. The signal for H-3 was identified as being at δ_H 4.85, appropriate to ArCHO. HMBC correlations from H-3 (δ_H 4.85, s) to C-1′ (δ_C 105.9), and from H-1′ (δ_H 4.58, d, J = 7.7 Hz) to C-3 (δ_C 86.10) evidence that the glycosyl residue is connected through C-3 (Fig. S113, Supplementary Information 1). The application of CD spectroscopy to compound **13** shows a non-vibronic n→π* transition which is opposite to the transition observed for **6**. Based on the comparison of CD data of **13** to that for **19** reported by Kuroyanagi et al., 1979, **13** was assigned the *R* configuration in C-3. The reported compounds, 13-chloro-spelosin 3-*O*-*β*-D-glucopyranoside (Chen et al., 2015) and (2*R*,3*R*)-pterosin L 3-*O*-*β*-D-glucopyranoside (Chen et al., 2008), whose ^{1}H and ^{13}C NMR data are very similar to compound **13**, also show *R* configuration in C-3. As a result of these observations, **13** was identified as rhedynoside E (Fig. 1).

2.2. Structural Relationships between New and Known Pterosins and Pterosides

Rhedynoside B (**10**) is the first example of a pteroside bearing the glucose moiety at the position C-2 and hence being directly attached to the five membered ring in α-position to the keto group. In addition, this is also the first report of glycosylation at C-12 with the 12-*O*-*β*-D-glucopyranoside substituted pterosins: rhedynosides C (**11**) and D (**12**). Most previously reported pterosides have had the sugar moiety at the following positions: C-11, for example, pterosides A2 and K (Castillo et al., 2003; Kuroyanagi et al., 1979); C-14, such as pterosides A, B, C, D, P and Z (Hikino et al., 1972, 1971; Kuroyanagi et al., 1979) or C-3, e.g. (2*R*, 3*R*)-pterosin L 3-*O*-*β*-D-glucopyranoside (Chen et al., 2008) and (2*S*, 3*S*)-pterosin C 3-*O*-*β*-D-glucoside (wallichoside) (Sengupta et al., 1976). Furthermore, rhedynosin A (**1**) and rhedynoside A (**2**) are novel compounds, being the first examples of a six-membered cyclic ether containing pterosin and pteroside.

For the first time rhedynosin C (**4**) was isolated from the rhizomes of *P. aquilinun* (L.) Kuhn, as a new cyclic lactone pterosin with a keto group at position C-14. However, another cyclic lactone pterosin, (*S*)-12-hydroxy-2-hydroxymethylpterosin E 14, 12-lactone, with one extra methylene has been reported as a metabolic product of (2*S*)-pterosin A in rat urine via oral administration (100 mg/kg) (Lee et al., 2012). Other metabolites of (2*S*)-pterosin A were compounds **14**, **27** and **29**, which we isolated for the first time from plant material. We hence suggest rhedynosin I as common name for compound **14**. Moreover, (2*S*)-pteroside A2 and histiopterosin A are being reported for the first time from the rhizomes of subsp. *aquilinum* of bracken fern, as they have previously been isolated from the young fronds of *P. aquilinum* (L.) Kuhn var. *caudatum* (syn *Pteridium caudatum L.* Maxon) (Castillo et al., 2003) and *Histiopteris incisa* (Murakami et al., 1980), respectively. More interestingly, a novel sulfated-pterosin, rhedynosin H (**9**), was isolated from belowground rhizomes of *P. aquilinum* (L.) Kuhn. Previously, (2*R*, 3*S*)-sulfated pterosin C and (2*S*, 3*S*)-sulfated pterosin C have been reported from the aerial parts of *Acrostichum aureum* (Uddin et al., 2011).

The absolute stereochemistry of the novel compound rhedynoside B (**10**) was determined by single crystal X-ray diffraction analysis (Figs. 2 & 8, and SI2). The CD spectrum of **15** exhibited negative and positive vibronic components associated with the n→π* transition in the range of 320-360 nm (Fig. 6). Thus, compound **15** was assigned 2*S* configuration (Kuroyanagi et al., 1979) and confirmed by X-ray diffraction (Fig. 7). The n→π* CD components of compounds **17** and **18** exhibit a strong negative Cotton effect around 330 nm (Fig. 9) which is in agreement with the reported CD data and thus, the configurations of **17** and **18** were determined to be 2*R*, 3*R* and 2*S*, 3*R* (Kuroyanagi et al., 1979). Again, X-ray diffraction confirmed this (Fig. 7). X-ray data for the two known pterosides (**31** and **35**) confirmed the absolute configuration determined previously by

CD, i.e. (2*R*)-pteroside B (**31**) and (2*S*)-pteroside K (**35**) (Fukuoka et al., 1978; Kuroyanagi et al., 1979; Ng and McMorris, 1984) (Figs. 2 & 7, SI2, and deposited with the Cambridge Crystallographic Data Centre).

The pterosins and pterosides isolated from bracken rhizomes showed surprising structural diversity, which even encompassed chloride and sulphate substituents. The biosynthesis of pterosin B is thought to be derived from the sesquiterpenoid biosynthetic pathway established by using the incorporation of radiolabelled mevalonate. Specifically Hikino et al. (1976) suggested pterosin B (**16**) to be derived from mevalonic acid via farnesyl pyrophosphate and humulene. It is hypothesised that at least compounds **9** and **12** derive from ptaquiloside degradation *in planta* as the major ptaquiloside degradation product, pterosin B (**16**), originates from a nucleophilic addition of present nucleophiles. The less abundant nucleophiles *in planta* Cl^- and SO_4^{2-} can also act by a similar mechanism to yield the chlorinated rhedynosins (**5**, **7** and **8**) and rhedynosides (**10**-**13**). Their presence in crude rhizome extracts, using MeOH and Et_2O instead of chloroform, was confirmed by HPLC/ESI-MS^n analysis. Both negative molecular ions (427 and 429 Da) of compounds **11**, **13** and **35** showed a constant neutral loss of 162 Da to give ions at *m/z* 265 and 267, respectively, which corresponded to the loss of an *O*-linked hexose moiety (glucose) (Felipe et al., 2014; Levandi et al., 2014; Qu et al., 2004; Scholz et al., 2005) (Figs. SD1-4, Supplementary Data 2). The presence of only one sulfated metabolite amongst the group of reported pterosins is rather a degradation product than a compound of biosynthetic origin. The other reported sulfated pterosins (Uddin et al., 2011) occurred as both *trans* and *cis* isomers at C2-C3, which also suggests their origin from degradation of ptaquiloside rather than through direct biosynthesis (Yamada et al., 2007). Similarly, *cis* and *trans* motifs at C2-C3 were identified in compounds **17** and **18** (Figs. 2 & 7). The C-2 position adjacent to the keto group readily epimerises if there is simply a methyl substituent. Unfortunately, at this stage it was not possible to assign the absolute configurations for compounds **9**, **12**, **16**, **20**, **21**, **25**, and **31**. A hydroxymethyl group at C-2 is apparently optically stable as in compounds **1**, **2**, **7**, **14**, **15**, **23**, **27**, **29**, **30**, **34** and **35**. Epimerisation may well be inhibited through intermolecular hydrogen bonding in these compounds (Kuroyanagi et al., 1979).

2.3. Biological Activity Assessment

Hsu *et al*. (2014) patented the use of pterosins and pterosides, including 86 distinct compounds of natural and synthetic origin. Their biological activity for treating diabetes and obesity was investigated predominantly with pterosin A but claimed for all described compounds. On this basis we were particularly interested whether pterosins or pterosides were more active. Hence a selection of pterosins (**15** - **17**) and their associated pterosides (**30**, **31** and **33**) were assessed for their anti-diabetic activity using an intestinal glucose uptake assay *in vitro*, specifically seeking inhibitors of the SGLT1 and GLUT2 transporters. However, no compound was active at 300 μM (more details can be found in the Supplementary Data 2) in contrast to activity reported by Hsu *et al*. (2014). However, Hsu *et al*. (2014) studied the antidiabetic activity for extracts of bracken against STZ-induced disease in mice at 100 mg/Kg/d for 14 days by activating GLUT4. Thus, the discrepancy could have multiple origins, including the dosing schedule and activity in the latter assay through a mechanism other than through SGLT1 and GLUT2 transporters.

3. Conclusion

This study describes the successful isolation and identification of 35 pterosin-type sesquiterpenoids from the rhizome of *Pteridium aquilinum* (L.) Kuhn, including eight new pterosins (**1** & **3**-**9**) and five new pterosides (**2** & **10**-**13**). Their chemical structures were elucidated by 1D and 2D NMR spectroscopic analysis. The absolute configuration were also determined for five compounds by using either single crystal X-ray diffraction (**10**) or CD spectroscopy (**15**, **31**, **35**) or both techniques (**17**, **18**). In addition, CD spectroscopy yielded the absolute configuration for **1**, **2**, **6**, **7**, and **13**. To the best of our knowledge, rhedynosides C (**11)** and D (**12)** are the first reported glucosides with the glucose moiety on the C-12 of the aglycone. In addition, one previously unreported sulfate-containing pterosin, rhedynosin H (**9**), together with two other reported compounds, histiopterosin A (**28**) and (2*S*)-pteroside A2 (**34**), were isolated for the first time from the rhizomes of bracken, subsp. *aquilinum*. Furthermore, compounds **1** and **2** have a relatively rare aglycone, containing a six-membered cyclic ether.

4. Experimental

4.1. General experimental procedures:

1D and 2D NMR spectra were recorded on a Bruker Avance (DRX) instrument (Bruker BioSpin Group, Germany) (400 or 500 MHz) NMR spectrometer in CD_3OD, $CDCl_3$, or $(CD_3)_2CO$ with TMS as internal standard. Ultra-high mass accuracy analysis was performed on a Nano-Flow (Triversa Nanomate; Advion biosciences limited, Norfolk, UK) linear trap quadrupole Fourier Transformation Ion Cyclotron Resonance Mass Spectrometry Ultra (FT-ICR-MS), where ultra refers to the high sensitivity ICR cell. Samples were reconstituted in 100 µL of HPLC grade MeOH / ultra-pure water (7:3). Samples were vortexed, and were centrifuged for 4 min, at 13,000 rpm at a temperature of 0 ºC. 20 µL of supernatant was then transferred to a clean well on a 128-well plate. 13 µL of sample was injected by the nano-flow injection system, with a 5 µL aliquot being delivered to the ICR cell. Gas pressure was maintained at 0.5 psi with an applied voltage of 1.5 kV to maintain a consistent current of 60-120 nA. When operating in narrow SIM mode, the resolution was 100,000 and the scan window 30 *m/z*. Each scan window was acquired in 60 s.

Specific rotations were acquired using ADP 440+ Polarimeter (Bellingham + Stanley Ltd). IR spectra were recorded on a PerkinElmer Spectrum 100 FT-IR Spectrometer using NaCl disc, and the samples were prepared as a solution. Column chromatography (CC) used silica gel (LC60A 40-63 MICRON, Germany). UV spectra were recorded on PerkinElmer (Singapore) Lambda 35 UV/VIS Spectrometer.

CD spectra for the compounds were recorded at 25 °C using a Chirascan CD spectrometer (Applied Photophysics Ltd). Samples (~1 mg/ml) were measured in methanol using a 1 mm pathlength quartz cuvette. Data were recorded every 0.5 nm between 280 nm and 400 nm with a 1 nm spectral bandwidth and an integration time of 2 seconds per data point.

Chromatographic profiling, method development and assessment of purity of isolated pterosins and pterosides from each fraction of bracken rhizome chloroform extract were performed using a Dionex UltiMate 3000 HPLC system from Thermo Scientific equipped with Binary gradient pump, Autosampler and diode array detector (DAD) monitoring 190-400 nm (UV-VIS detector).

Chromatographic analysis of each fraction was achieved using reverse phase analytical column, 250 × 4.6 mm, packed with Spherisil ODS-2 (C18), 5µm as a stationary phase. Different ratios of two mobile phases of MeOH-H_2O and ACN-H_2O (acidified with 0.1% formic acid) at a flow rate of 1.0 mL/min at 40 °C were used to obtain high resolution chromatograms. Ultraviolet detection was set at 254 nm. The Chromeleon 7 Software was used to control gradient setting, data acquisition and auto-sampler.

The Reveleris® Flash Chromatography system was used for purification of pterosins and pterosides. The samples were pre-adsorbed onto silica gel and subsequently run on the Reveleris® C18 (40 µm, 12 g) column for 64 min using two different solvent systems, MeOH-H_2O and ACN-H_2O (acidified with 0.1% formic acid), at a flow rate of 18 mL/min. The peaks were visualised and recorded with UV-Vis (254 nm and 280 nm) and ELSD detectors.

Preparative TLC was conducted using glass plates pre-coated with silica gel (TLC Silica gel 60 F_{254}, Germany, 1.0 mm thickness, 20 × 20 cm). Mixture of chloroform extract fractions were applied to TLC plates using suitable solvent systems. These compounds were visualized using UV-light and / or phosphomolybdic acid (PMA).

Single crystal X-ray diffraction data were collected either on a Rigaku AFC11 quarter chi goniometer equipped with an enhanced sensitivity (HG) Saturn944+ detector mounted at the window of 007 HF copper rotating anode generator with Varimax optics (*cis*-pterosin C, *trans*-pterosin C and (2*S*)-pterosin A), or on a Rigaku AFC12 goniometer equipped with an enhanced sensitivity (HG) Saturn724+ detector mounted at the window of an FR-E+ SuperBright molybdenum rotating anode generator with VHF Varimax optics (70 µm focus) ((2*R*)-pteroside B, (2*S*)-pteroside K and rhedynoside B). Rigaku CrystalClear (Rigaku Corporations, The Woodlands, Texas, USA) was used to record images. Data integration was carried out using Agilent CrysAlisPro (Agilent- Technologies UK Ltd). (*cis*-pterosin C, *trans*-pterosin C, (2*S*)-pterosin A and rhedynoside B) or Rigaku CrystalClear ((2*R*)-pteroside B, (2*S*)-pteroside K). The structures were solved by charge-flipping methods using SUPERFLIP (Palatinus and Chapuis, 2007) and refined on F_o^2 by full-matrix least squares refinement using SHELXL-2014 (Sheldrick, 2008). All non-hydrogen atoms were refined with anisotropic displacement parameters. Hydrogen atoms were added at calculated positions and refined using a riding model with isotropic displacement parameters based on the equivalent isotropic displacement parameter (Ueq) of the parent atom. The structures were deposited on the Cambridge Structural Database with the deposition numbers CCDC 1050917, 1050918, 1050920, 1406891, 1418452 and 1418453.

In order to confirm the presence of isolated chlorinated compounds, bracken rhizomes (10 g, dry weight) were extracted with 100 ml of methanol and ethyl acetate, and the extracts were analysed by reverse-phase HPLC using photodiode array detection with and without electrospray ionisation-ion trap mass spectrometry (HPLC/ESI-MS^n) (more details are in the SI2).

4.2. Plant material

The bracken rhizomes (11.8 kg) were collected from Llanberis in Wales N 53º 07′ and W 04º 08′, on 21 February 2013. They were confirmed as *Pteridium aquilinum* (L.) Kuhn by Nigel Brown. A voucher specimen was deposited at Treborth Botanical Garden, Bangor.

4.3. Extraction and isolation

The air-dried chopped bracken rhizomes (3.45 kg) were macerated with chloroform (14 L) at room temperature for 3 × 24 h. After filtration, the organic solvent was reduced under pressure to give the crude extract (7.1 g) which was pre-adsorbed onto silica gel and subjected to CC using $CHCl_3$-MeOH mixture with increasing polarity (100:0 → 0:100) to give thirteen fractions (BR1-BR13). From these fractions, 13 new compounds (**1**, 6.0 mg; **2**, 11.0 mg; **3**, 5.8 mg; **4**, 2.6 mg; **5**, 4.5 mg; **6**, 6.0 mg; **7**, 4.1 mg; **8**, 13.0 mg, **9**, 3.0 mg; **10**, 11.6 mg; **11**, 3.2 mg; **12**, 9.1 mg, and **13**, 3.8 mg) and 22 known compounds (**14**, 6.0 mg; **15**, 160.0 mg; **16**, 110.0 mg; **17**, 18.0 mg; **18**, 20.0 mg; **19**, 60.0 mg; **20**, 17.0 mg; **21**, 10.0 mg; **22**, 5.0 mg; **23**, 3.0 mg; **24**, 15.4 mg; **25**, 4.0 mg; **26**, 14.0 mg; **27**, 14.7 mg; **28**, 3.0 mg; **29**, 4.0 mg; **30**, 10.2 mg; **31**, 203.0 mg; **32**, 4.9 mg; **33**, 47.0 mg; **34**, 4.2 mg and **35**, 30.0 mg) were isolated as the following:

Preparative TLC was applied to purify fraction BR1 (25.0 mg) using *n*-hexane-acetone (1:9) to give **21** (10.0 mg). Fraction BR2 (350 mg) was further chromatographed on a silica gel column eluting with gradient of *n*-hexane-EtOAc (100:0 → 45:55) to obtain five sub-fractions (BR2A-BR2E). Sub-fraction BR2A (170.0 mg) was subjected to RP-FC using a gradient elution of ACN-H_2O (35-45%, 1 h) to give **20** (17.0 mg); **22** (5.0 mg); **23** (3.0 mg) and **26** (14.0 mg). Sub-fractions BR2B (130.0 mg), BR2D (20.0 mg) and BR2E (10 mg) were each subjected to preparative TLC using *n*-hexane-EtOAc (4:6), EtOAc and MeOH-Et_2O (1:49) to give **16** (110.0 mg), **14** (6.0 mg) and **4** (2.6 mg), respectively. Sub-fraction BR2C (22 mg) was purified using preparative TLC (diethyl ether) to afford compounds **1** (6.0 mg) and **3** (5.8 mg). Fractions BR3 (128.9 mg) and BR4 (37 mg) were purified separately by preparative TLC using *n*-hexane-acetone (1:1 and 6:4) to afford **8** (13.0 mg) and **7** (4.1 mg), respectively. Preparative TLC (diethyl ether) was applied to fraction BR5 (109 mg) to afford **5** (4.5 mg) and **24** (15.4 mg). Fraction BR6 (375 mg) was fractionated by applying it on RP-FC with an isocratic gradient elution (20-20%, ACN-H_2O, 1 h) to give **15** (160.0 mg) and **19** (60.0 mg). Fraction BR7 (600 mg) was resolved by a silica gel CC eluted with gradients of *n*-hexane-EtOAc and EtOAc-MeOH with increasing polarity, respectively, to yield four sub-fractions (BR7A-BR7D). Sub-fraction BR7A (51.5 mg) was chromatographed on RP-FC using a gradient elution of ACN-H_2O (20-23%, 1 h) to afford **6** (6.0 mg) and **27** (14.7 mg). RP-FC was applied on sub-fraction BR7B (33.0 mg) using ACN-H_2O (20-23%, 1 h) as a gradient elution to obtain **28** (3.0 mg). Sub-fraction BR7C (242.0 mg) was subjected to RP-FC using a gradient elution of ACN-H_2O (20-23%, 1 h) to obtain four main fractions (BR7C1-BR7C4), and then the second peak (BR7C2) (38 mg) was further chromatographed on RP-FC using a gradient elution of ACN-H_2O (06-06-10-11%, 2 h) to afford **17** (16.5 mg) and **18** (19.5 mg). Sub-fraction BR7D (97.0 mg) was resolved on RP-FC using a gradient elution of ACN-H_2O (15-20%, 1 h) to give **25** (4.0 mg). Fraction BR8 (119.7 mg) was subjected to RP-FC using a gradient elution of MeOH-H_2O (40-50%, 1 h) to give **10** (11.6 mg) and **29** (4.0 mg). Fraction BR9 (110 mg) was separated with RP-FC using a gradient elution of MeOH-H_2O (40-50%, 1 h) to obtain four sub-fractions (BR9A-BR9D). Sub-fractions BR9A, BR9B and BR9D gave **11** (3.2 mg), **12** (9.1 mg) and **35** (30.0 mg), respectively. The purification of sub-fraction BR9C (15.0 mg) on RP-FC using gradient elution (25-30% ACN-H_2O, 1 h) yielded **13** (3.8 mg). Fraction BR11 (261.7 mg) was resolved on RP-FC using MeOH-H_2O (40-50%, 1 h) as a mobile phase to obtain **2** (11.0 mg), **31** (203.0 mg) and **33** (47.0 mg). Fraction BR13 (200 mg) was further fractionated by applying it to RP-FC with a gradient elution (10-25% ACN-H_2O, 1 h) to obtain four sub-fractions (BR13A-BR13D). Compounds **32** (4.9 mg), **30** (10.2 mg) and **34** (4.2 mg) were obtained

from sub-fractions BR13A, BR13B and BR13C, respectively, while sub-fraction BR13D (30 mg) was re-subjected to RP-FC using a gradient elution (40-50% ACN-H_2O, 1 h) to afford **9** (3.0 mg).

4.4. Physico-chemical parameters of the new compounds

Rhedynosin A (**1**); Yellow powder; $[\alpha]_D^{24}$ -4.31 (*c* 0.33, $CHCl_3$); UV (MeOH) λ_{max} nm (log ε): 211 (4.16), 241 (3.77), 258 (3.85), 306 (2.99); IR (film) ν_{max} 3418, 3014, 2928, 1704, 1605, 1446, 1380, 1048, 755, 666 cm^{-1}; for ^1H and ^{13}C NMR spectroscopic data, see Tables 1 & 4; FT-ICR-MS *m/z* 247.1330 $[M+H]^+$ (calcd for $C_{15}H_{19}O_3$, 247.1334).

Rhedynoside A (**2**): White powder; $[\alpha]_D^{24.2}$ -26.07 (*c* 0.33, MeOH); UV (MeOH) λ_{max} nm (log ε): 216 (4.27), 259 (3.92), 304 (2.99); IR (film) ν_{max} 3369, 2927, 1692, 1602, 1444, 1378, 1075, 918 cm^{-1}; for ^1H and ^{13}C NMR spectroscopic data, see Tables 1 & 4; FT-ICR-MS *m/z* 409.1865 $[M+H]^+$ (calcd for $C_{21}H_{29}O_8$, 409.1862).

Rhedynosin B (**3**): Yellow powder; $[\alpha]_D^{24}$ -12.78 (*c* 0.33, $CHCl_3$); UV (MeOH) λ_{max} nm (log ε): 209 (4.31), 260 (3.96), 313 (3.09); IR (film) ν_{max} 3419, 3018, 2926, 1715, 1603, 1446, 1379, 1290, 1196, 1096, 985, 856, 754, 666 cm^{-1}; for ^1H and ^{13}C NMR spectroscopic data, see Tables 1 & 4; FT-ICR-MS *m/z* 247.0967 $[M+H]^+$ (calcd for $C_{14}H_{15}O_4$, 247.0970).

Rhedynosin C (**4**): White powder; $[\alpha]_D^{24.2}$ +3.76 (*c* 0.33, MeOH); UV (MeOH) λ_{max} nm (log ε): 214 (3.24), 242 (2.97), 258 (2.94), 306 (2.51); IR (film) ν_{max} 3428, 2924, 1703, 1608 1458, 1379, 1260, 1034, 800 cm^{-1}; for ^1H and ^{13}C NMR spectroscopic data, see Tables 1 & 4; FT-ICR-MS *m/z* 245.0821 $[M-H]^-$ (calcd for $C_{14}H_{13}O_4$, 245.0814).

Rhedynosin D (**5**): Yellow solid; $[\alpha]_D^{24}$ -19.12 (*c* 0.33, $CHCl_3$); UV (MeOH) λ_{max} nm (log ε): 215 (4.13), 259 (3.75), 303 (2.76); IR (film) ν_{max} 3418, 2925, 1714, 1602, 1447, 1379, 1093, 855, 756, 666 cm^{-1}; for ^1H and ^{13}C NMR spectroscopic data, see Tables 1 & 4; FT-ICR-MS *m/z* 269.0941 $[M+H]^+$ (calcd for $C_{14}H_{18}{}^{35}ClO_3$, 269.0944).

Rhedynosin E (**6**): Off-white powder; $[\alpha]_D^{24.2}$ -14.94 (*c* 0.33, MeOH); UV (MeOH) λ_{max} nm (log ε): 217 (4.35), 258 (4.02), 295 (3.13); IR (film) ν_{max} 3419, 2932, 1699, 1600, 1465, 1382, 1203, 1099, 995, 884 cm^{-1}; for ^1H and ^{13}C NMR spectroscopic data, see Tables 2 & 4; FT-ICR-MS *m/z* 263.1280 $[M+H]^+$ (calcd for $C_{15}H_{19}O_4$, 263.1283).

Rhedynosin F (**7**): Light yellow crystalline powder; $[\alpha]_D^{24}$ +15.36 (*c* 0.33, $CHCl_3$); UV (MeOH) λ_{max} nm (log ε): 219 (4.27), 259 (3.87), 298 (2.92); IR (film) ν_{max} 3417, 2929, 1698, 1598, 1455, 1379, 1223, 1042, 923, 859, 755 cm^{-1}; for ^1H and ^{13}C NMR spectroscopic data, see Tables 2 & 4; FT-ICR-MS *m/z* 283.1098 $[M+H]^+$ (calcd for $C_{15}H_{20}{}^{35}ClO_3$, 283.1101).

Rhedynosin G (**8**): Yellow gum; $[\alpha]_D^{24.2}$ +4.04 (*c* 0.33, MeOH); UV (MeOH) λ_{max} nm (log ε): 218 (4.34), 260 (3.97), 299 (3.03); IR (film) ν_{max} 3405, 2929, 1705, 1599, 1447, 1378, 1217, 1094, 983, 887, 751 cm^{-1}; for ^1H and ^{13}C NMR spectroscopic data, see Tables 2 & 4; FT-ICR-MS *m/z* 269. 0941 $[M+H]^+$ (calcd for $C_{14}H_{18}{}^{35}ClO_3$, 269.0944).

Rhedynosin H (**9**): Off-white powder; $[\alpha]_D^{24}$ -28.049 (*c* 0.33, $CHCl_3$); UV (MeOH) λ_{max} nm (log ε): 217 (4.71), 258 (4.37), 303 (3.55); IR (film) ν_{max} 2919, 1704, 1601, 1456, 1377, 1325, 1221, 1129, 1020, 970, 885, 756, 702 cm^{-1}; for ^1H and ^{13}C NMR spectroscopic data, see Tables 2 & 4; FT-ICR-MS *m/z* 297. 0802 $[M-H]^-$ (calcd for $C_{14}H_{17}O_5S$, 297.0797).

Rhedynoside B (**10**): White crystalline compound; $[\alpha]_D^{24.2}$ -10.82 (*c* 0.33, MeOH); UV (MeOH) λ_{max} nm (log ε): 219 (4.48), 263 (4.12), 304 (3.11), nm; IR (film) ν_{max} 3391, 2926, 1703, 1601 1451, 1376, 1327, 1227, 1074, 918, 872 cm^{-1}; for ^1H and ^{13}C NMR spectroscopic data, see Tables 3 & 4; FT-ICR-MS *m/z* 415.1527 $[M+H]^+$ (calcd for $C_{20}H_{28}{}^{35}ClO_7$, 415.1523).

Rhedynoside C (**11**): Off-white crystalline powder; $[\alpha]_D^{24.6}$ -0.488 (*c* 0.33, MeOH); UV (MeOH) λ_{max} nm (log ε): 216 (4.43), 257 (3.98), 303 (2.93); IR (film) ν_{max} 3391, 2927, 1699, 1601, 1440, 1379, 1326, 1077, 918, 888 cm^{-1}; for ^1H and ^{13}C NMR spectroscopic data, see Tables 3 & 4; FT-ICR-MS *m/z* 427.1530 $[M-H]^-$ (calcd for $C_{21}H_{28}{}^{35}ClO_7$, 427.1524).

Rhedynoside D (**12**): Yellow powder; $[\alpha]_D^{24.6}$ -0.643 (*c* 0.33, MeOH); UV (MeOH) λ_{max} nm (log ε): 216 (4.43), 256 (4.01), 303 (2.98); IR (film) ν_{max} 3374, 2928, 1700, 1600, 1440, 1376, 1312, 1163, 1075, 921, 890 cm^{-1}; for ^1H and ^{13}C NMR spectroscopic data, see Tables 3 & 4; FT-ICR-MS *m/z* 413.1374 $[M-H]^-$ (calcd for $C_{20}H_{26}{}^{35}ClO_7$, 413.1367).

Rhedynoside E (**13**): Off-white crystalline powder; $[\alpha]_D^{24.6}$ +0.436 (*c* 0.33, MeOH); UV (MeOH) λ_{max} nm (log ε): 218 (4.40), 258 (3.92), 300 (2.63); IR (film) ν_{max} 3390, 3018, 2928, 1703, 1599, 1462, 1380, 1325, 1162, 1076, 898, 757 cm^{-1}; for ^1H and ^{13}C NMR spectroscopic data, see Tables 3 & 4; FT-ICR-MS *m/z* 427.1530 $[M-H]^-$ (calcd for $C_{21}H_{28}{}^{35}ClO_7$, 427.1524).

Acknowledgements

Vera Thoss, Martina Lahmann and Mohammad Nur-e-Alam acknowledge the European Regional Development Fund through the BEACON project. Rizgar Hassan Mohammad acknowledges funding by the Kurdish Ministry of Higher Education and Scientific Research-Kurdistan Regional Government (MHE-SR-KRG) for his scholarship. Muhammad Yousaf, King Saudi University, Saudi Arabia confirmed previously undescribed compounds. Stephania Christou, Manchester University, UK, measured the specific rotations for the previously unreported compounds. Ana Winters, Aberystwyth University, conducted the HPLC-ESI-MS^n analysis. Kathleen Tailliart, Shon Glyn Jones, David Davenport Hughes, Sam Page and Toby Vye provided technical assistance. An anonymous reviewer and Prof. Michael D. Threadgill (University of Bath) provided useful suggestions to improve the manuscript.

Appendix A. Supplementary data

Supplementary data associated with this article can be found, in the online version, at ----------website----------

References

Almeida Santos, M. de F.M., Dórea, J.G., Luna, H., 2006. Bracken-fern extracts can be clastogenic or aneugenic depending on the tissue cell assay. Food Chem. Toxicol. 44, 1845–1848.

Alonso-Amelot, M., Avendano, M., 2002. Human carcinogenesis and bracken fern: A review of the evidence. Curr. Med. Chem. 9, 675–686.

Alonso-Amelot, M.E., Pérez-Mena, M., Calcagno, M.P., Jaimes-Espinoza, R., Castillo, U., 1992. Ontogenic variation of biologically active metabolites of *Pteridium aquilinum* (L. Kuhn) pterosins A and B, and ptaquiloside in a bracken population of the tropical Andes. J. Chem. Ecol. 18, 1405–1420.

Aranha, P.C.R., Hansen, H.C.B., Rasmussen, L.H., Strobel, B.W., Friis, C., 2014. Determination of ptaquiloside and pterosin B derived from bracken (*Pteridium aquilinum*) in cattle plasma, urine and milk. J. Chromatogr. B. Analyt. Technol. Biomed. Life Sci. 951-952, 44–51.

Campos-da-Paz, M., Pereira, L.O., Bicalho, L.S., Dórea, J.G., Poças-Fonseca, M.J., Santos, M. de F.M.A., 2008. Interaction of bracken-fern extract with vitamin C in human submandibular gland and oral epithelium cell lines. Mutat. Res. 652, 158–163.

Castillo, U.F., Wilkins, A.L., Lauren, D.R., Smith, B.L., Alonso-Amelot, M., 2003. Pteroside A2-a new illudane-type sesquiterpene glucoside from *Pteridium caudatum* L. Maxon, and the spectrometric characterization of caudatodienone. J. Agric. Food Chem. 51, 2559–2564.

Chen, C.-Y., Chiu, F.-Y., Lin, Y., Huang, W.-J., Hsieh, P.-S., Hsu, F.-L., 2015. Chemical constituents analysis and antidiabetic activity validation of four fern species from Taiwan. Int. J. Mol. Sci. 16, 2497–2516.

Chen, Y.-H., Chang, F.-R., Lu, M.-C., Hsieh, P.-W., Wu, M.-J., Du, Y.-C., Wu, Y.-C., 2008. New benzoyl glucosides and cytotoxic pterosin sesquiterpenes from *Pteris ensiformis* Burm. Molecules 13, 255–266.

Felipe, D., Brambilla, L., Porto, C., Pilau, E., Cortez, D., 2014. Phytochemical analysis of *Pfaffia glomerata* inflorescences by LC-ESI-MS/MS. Molecules 19, 15720–15734.

Fenwick, G.R., 1988. Bracken (*Pteridium aquilinum*)—toxic effects and toxic constituents. J. Sci. Food Agric. 46, 147–173.

Fukuoka, M., Kuroyanagi, M., Yoshihira, K., Natori, S., 1978. Chemical and toxicological studies on bracken fern, *Pteridium aquilinum* var. *latiusculum*. II. Structures of pterosins, sesquiterpenes having 1-indanone skeleton. Chem. Pharm. Bull. (Tokyo). 26, 2365–2385.

Fukuoka, M., Yoshihira, K., Natori, S., Mihashi, K., Nishi, M., 1983. Carbon-13 nuclear magnetic resonance spectra of pterosin-sesquiterpenes and related indan-1-one derivatives. Chem. Pharm. Bull. (Tokyo). 31, 3113–3128.

Gomes, J., Magalhães, A., Carvalho, A.S., Hernandez, G.E., Papp, S.L., Head, S.R., Michel, V., David, L., Gärtner, F., Touati, E., Reis, C.A., 2012. Glycophenotypic alterations induced by *Pteridium aquilinum* in mice gastric mucosa: synergistic effect with *Helicobacter pylori* infection. PLoS One 7, 1–11.

Hayashi, Y., Nishizawa, M., Harita, S., Sakan, T., 1972. Structures and syntheses of hypolepin A,

B and C, sesquiterpenes from *Hypolepis Punctata* Mett. Chem. Lett. 375–378.

Hikino, H., Miyase, T., Takemoto, T., 1976. Biosynthesis of pteroside B in *Pteridium aquilinum* var. *Latiusculum*, proof of the sesquiterpenoid origin of the pterosides. Phytochemistry (Elsevier) 15, 121–123.

Hikino, H., Takahashi, T., Takemoto, T., 1972. Structure of pteroside A and C, glycosides of *Pteridium aquilinum* var. *latiusculum*. Chem. Pharm. Bull. (Tokyo). 20, 210–212.

Hikino, H., Takahashi, T., Takemoto, T., 1971. Structure of pteroside Z and D, glycosides of *Pteridium aquilinum* var. *latiusculum*. Chem. Pharm. Bull. (Tokyo). 19, 2424–2425.

Hirono, I., 1986. Carcinogenic principles isolated from bracken fern. Crit. Rev. Toxicol. 17, 1–22.

Hopkins, A., 1990. Bracken (*Pteridium aquilinum*): Its distribution and animal health implications. Br. Vet. J. 146, 316–326.

Hsu, F.-L., Liu, S.-H., Uang, B.-J., 2014. Use of pterosin compounds for treating diabetes and obesity. U.S. Patent 8633252 B2.

Kigoshi, H., Sawada, A., Imamura, Y., Niwa, H., Yamada, K., 1989. Ptaquilosin, the aglycone of a bracken carcinogen ptaquiloside: Chemical derivation from ptaquiloside and the reactivity. Tetrahedron 45, 2551–2556.

Kobayashi, A., Egawa, H., Koshimizu, K., Mitsui, T., 1975. Antimicrobial constituents in *Pteris inaequalis* bak. Agric. Biol. Chem. 39, 1851–1856.

Kobayashi, A., Koshimizu, K., 1980. Cytotoxic effects of bracken fern constituents, pterosins, on sea urchin embryos and a ciliate. Agric. Biol. Chem. 44, 393–398.

Kovganko, N. V., Kashkan, Z.N., Krivenok, S.N., 2004. Bioactive compounds of the flora of Belarus. 4. Pterosins A and B from *Pteridium aquilinum*. Chem. Nat. Compd. 40, 227–229.

Kuraishi, T., Murakami, T., Taniguchi, T., Kobuki, Y., Maehashi, H., Tanaka, N., Saiki, Y., Chen, C., 1985. Chemical and chemotaxonomical studies of ferns. LIV. Pterosin derivatives of the genus *Microlepia* (Pteridaceae). Chem. Pharm. Bull. (Tokyo). 33, 2305–2312.

Kuroyanagi, M., Fukuoka, M., Yoshihira, K., Natori, S., 1979. Chemical and toxicological studies on bracken fern, *Pteridium aquilinum* var. *latiusculum.* III. Further characterization of pterosins and pterosides, sesquiterpenes and the glucosides having 1-indanone skeleton, from the rhizomes. Chem. Pharm. Bull. (Tokyo). 27, 592–601.

Lee, Y.-P., Hsu, F.-L., Kang, J.-J., Chen, C.-K., Lee, S.-S., 2012. Metabolism of (2*S*)-pterosin A: identification of the phase I and phase II metabolites in rat urine. Drug Metab. Dispos. 40, 1566–1574.

Levandi, T., Püssa, T., Vaher, M., Ingver, A., Koppel, R., Kaljurand, M., 2014. Principal component analysis of HPLC–MS/MS patterns of wheat (*Triticum aestivum*) varieties. Proc. Est. Acad. Sci. 63, 86–92.

Madeja, J., Harmata, K., Kolaczek, P., Karpinska-Kolaczek, M., Piatek, K., Naks, P., 2009. Bracken (*Pteridium aquilinum* (L.) Kuhn), Mistletoe (*Viscum album* (L.)) and Bladder-nut (*Staphylea pinnata* (L.))-Mysterious Plants with Unusual Applications. Cultural and Ethnobotanical Studies, in: Morel, J.-P., Mercuri, A.M. (Eds.), Plants and Cultural: Seeds of

the Cultural Heritage of Europe. Edipuglia, pp. 207–215.

Marrs, R.H., Watt, a. S., 2006. Biological flora of the British Isles: *Pteridium aquilinum* (L.) Kuhn. J. Ecol. 94, 1272–1321.

McKee, T.C., II, J.H.C., Riccio, R., D'Auria, M.V., Iorizzi, M., Minale, L., Moran, R.A., Gulakowski, R.J., McMahon, J.B., 1994. HIV-inhibitory natural products. 11. Comparative studies of sulfated sterols from marine invertebrates. J. Med. Chem. 37, 793–797.

Murakami, T., Satake, T., Ninomiya, K., Iida, H., Yamauchi, K., Tanaka, N., Saiki, Y., Chen, C.-M., 1980. Pterosin-derivate aus der familie pteridaceae. Phytochemistry (Elsevier) 19, 1743–1746.

Ng, K.-M.E., McMorris, T.C., 1984. An efficient synthesis of pterosin C and other pterosins. Can. J. Chem. 62, 1945–1953.

Padwa, A., Curtis, E.A., Sandanayaka, V.P., 1996. Generation and cycloaddition behavior of spirocyclic carbonyl ylides. Application to the synthesis of the pterosin family of sesquiterpenes †. J. Org. Chem. 61, 73–81.

Pakeman, R., Marrs, R., Howard, D., Barr, C., Fuller, R., 1996. The bracken problem in Great Britain: Its present extent and future changes. Appl. Geogr. 16, 65–86.

Palatinus, L., Chapuis, G., 2007. *SUPERFLIP* – a computer program for the solution of crystal structures by charge flipping in arbitrary dimensions. J. Appl. Crystallogr. 40, 786–790.

Potter, D.M., Baird, M.S., 2000. Carcinogenic effects of ptaquiloside in bracken fern and related compounds. Br. J. Cancer 83, 914–920.

Qu, J., Liang, Q., Liang, Q., Luo, G., Wang, Y., 2004. Screening and identification of glycosides in biological samples using energy-gradient neutral loss scan and liquid chromatography tandem mass spectrometry. Anal. Chem. 76, 2239–2247.

Rasmussen, L.H., Kroghsbo, S., Frisvad, J.C., Hansen, H.C.B., 2003. Occurrence of the carcinogenic bracken constituent ptaquiloside in fronds, topsoils and organic soil layers in Denmark. Chemosphere 51, 117–127.

Scholz, K., Dekant, W., Völkel, W., Pähler, A., 2005. Rapid detection and identification of *N*-acetyl-*L*-cysteine thioethers using constant neutral loss and theoretical multiple reaction monitoring combined with enhanced product-ion scans on a linear ion trap mass spectrometer. J. Am. Soc. Mass Spectrom. 16, 1976–1984.

Sengupta, P., Sen, M., Kumar Niyogi, S., Chandra Pakrashi, S., Ali, E., 1976. Isolation and structure of wallichoside, a novel pteroside from *Pteris wallichiana*. Phytochemistry (Elsevier) 15, 995–998.

Sheldrick, G.M., 2008. A short history of *SHELX*. Acta Crystallogr. A. 64, 112–122.

Sheridan, H., Frankish, N., Farrell, R., 1999. Smooth muscle relaxant activity of pterosin Z and related compounds. Planta Med. 65, 271–272.

Tanaka, N., Satake, T., Takahashi, A., Mochizuki, M., Murakami, T., Saiki, Y., Yang, J., Chen, C., 1982. Chemical and chemotaxonomical studies of ferns. XXXIX. Chemical studies on the constituents of *Pteris bella* Tagawa and *Pteridium aquilinum* subsp. *wightianum* (Wall)

Shich. Chem. Pharm. Bull. (Tokyo). 30, 3640–3646.

Uddin, S.J., Jason, T.L.H., Beattie, K.D., Grice, I.D., Tiralongo, E., 2011. (2*S*,3*S*)-sulfated pterosin C, a cytotoxic sesquiterpene from the Bangladeshi Mangrove fern *Acrostichum aureum*. J. Nat. Prod. 74, 2010–2013.

Vetter, J., 2009. A biological hazard of our age: Bracken fern [*Pteridium aquilinum* (L.) Kuhn] - A review. Acta Vet. Hung. 57, 183–196.

Warncke, I. , Furche, F., 2012 Circular dichroism: electronic. Wiley Interdiscipl. Rev.: Comp. Mol. Sc. 2, 150-166

Yamada, K., Ojika, M., Kigoshi, H., 2007. Ptaquiloside, the major toxin of bracken, and related terpene glycosides: chemistry, biology and ecology. Nat. Prod. Rep. 24, 798–813.

Yoshihira, K., Fukuoka, M., Kuroyanagi, M., Natori, S., 1971. 1-Indanone derivatives from bracken, *Pteridium aquilinum* var. *latiusculum*. Chem. Pharm. Bull. (Tokyo). 19, 1491–1495.

Supplementary Information 2 (SI2)

Isolation and characterisation of thirteen pterosins and pterosides from bracken (*Pteridium aquilinum* (L.) Kuhn) rhizome

Rizgar Hassan Mohammad[a], Mohammad Nur e-Alam[a,b] , Martina Lahmann[a], Ifat Parveen[c], Graham J. Tizzard[d], Simon J. Coles[d], Mark Fowler[e], Alex F. Drake[f], Derren Heyes[g], Vera Thoss[a,*]

[a] School of Chemistry, Bangor University, Bangor LL57 2UW, United Kingdom

[b] Department of Pharmacognosy, College of Pharmacy, King Saud University, P.O. Box 2457, Riyadh 11451, Saudi Arabia.

[c] IBERS, Aberystwyth University, Penglais, Aberystwyth SY23 3DA, UK

[d] UK National Crystallography Service, School of Chemistry, University of Southampton, University Road, Southampton SO17 1BJ, United Kingdom

[e] Strategic Science Group, Unilever R&D, Colworth Science Park, Bedford, MK44 1LQ, UK.

[f] Biomolecular Spectroscopy Centre, Pharmaceutical Optical & Chiroptical Spectroscopy Facility, King's College London, The Wolfson Wing, WWB10 Hodgkin Building, Guy's Campus, London SE1 1UL, UK

[g] Manchester Institute of Biotechnology, University of Manchester, 131 Princess St, Manchester M1 7DN

*Corresponding Author vera.thoss@bangor.ac.uk

Contents:

Crystallographic data

cis-pterosin C

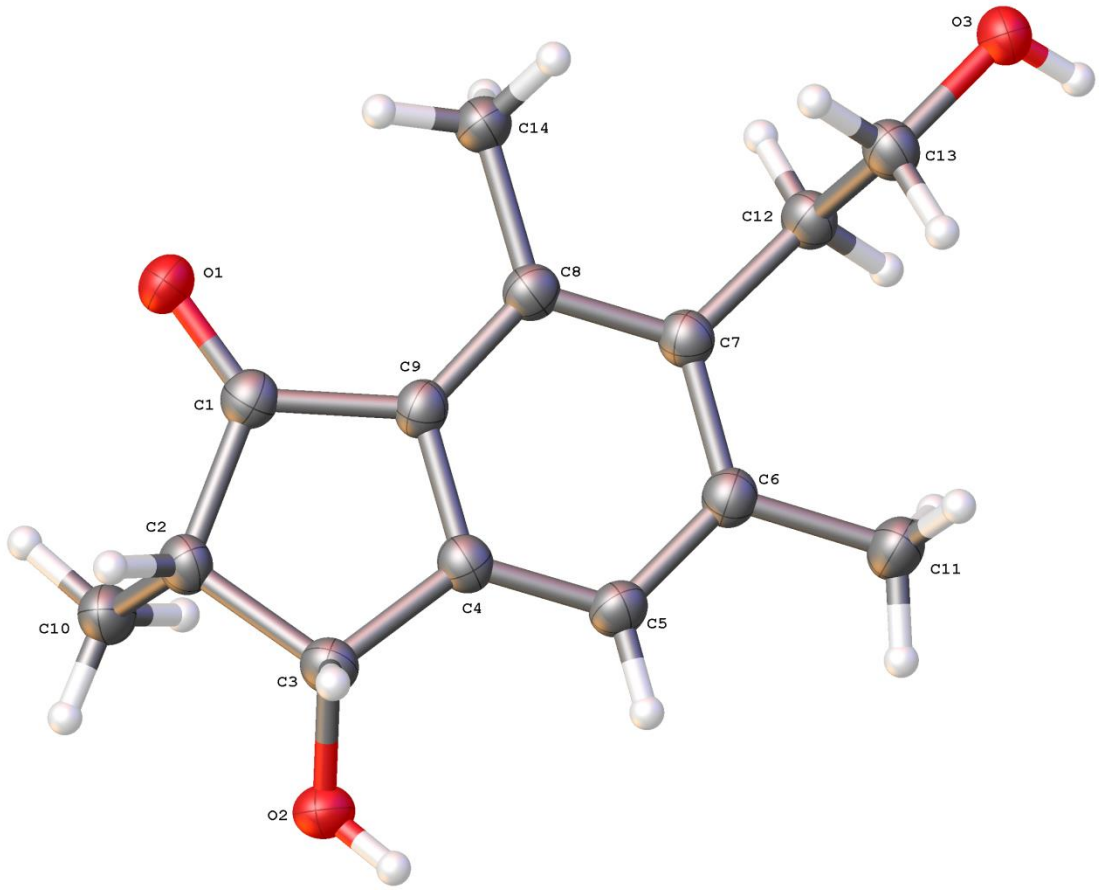

Formula: $C_{14}H_{18}O_3$; M_r = 234.28; crystal dimensions: 0.41 x 0.07 x 0.04 mm; crystal system: Monoclinic; space group: $P2_1$; a = 4.58360(6) Å, b = 15.93341(16) Å, c = 8.13657(8) Å, α = 90°, β = 93.1583(10)°, γ = 90°; V = 593.330(11) Å^3; Z = 2; ρ_{calcd} = 1.331 Mg/m^3; μ = 0.736 mm^{-1}; Cu $K\alpha$ radiation, λ = 1.54184 Å; T = 100 K; $2\Theta_{max}$ = 138.0°; 20930/2179 measured/independent reflections; R_{int}: 0.0516; Flack parameter/Hooft parameter -0.03(9)/-0.12(4); R = 0.0285, wR = 0.0752; $\Delta\rho_{max}$ = 0.133 eÅ^{-3}, $\Delta\rho_{min}$ = −0.121 eÅ^{-3}. Colourless lath crystals. CCDC deposition number 1050917.

trans-pterosin C

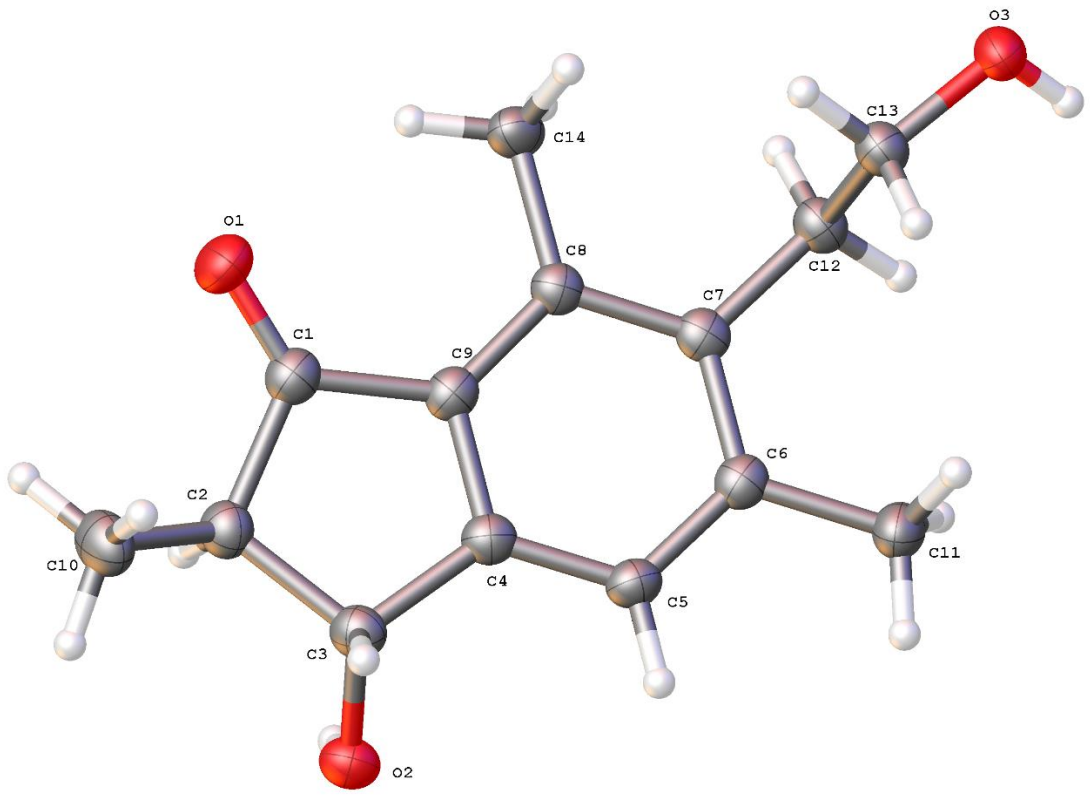

Formula: $C_{14}H_{18}O_3$; M_r = 234.28; crystal dimensions: 0.15 x 0.12 x 0.10 mm; crystal system: Orthorhombic; space group: $P2_12_12_1$; a = 7.07508(11) Å, b = 11.4381(2) Å, c = 14.9966(2) Å, α = 90°, β = 90°, γ = 90°; V = 1213.61(4) Å^3; Z = 4; ρ_{calcd} = 1.282 Mg/m^3; μ = 0.719 mm-1; Cu $K\alpha$ radiation, λ = 1.54184 Å; T = 100 K; $2\Theta_{max}$ = 138.5°; 14992/2138 measured/independent reflections; R_{int}: 0.0563; Flack parameter/Hooft parameter 0.11(13)/0.05(9); R = 0.0301, wR = 0.0779; $\Delta\rho_{max}$ = 0.147 eÅ^{-3}, $\Delta\rho_{min}$ = −0.119 eÅ^{-3}. Colourless plate crystals. CCDC deposition number 1418453.

(2*S*)-pterosin A

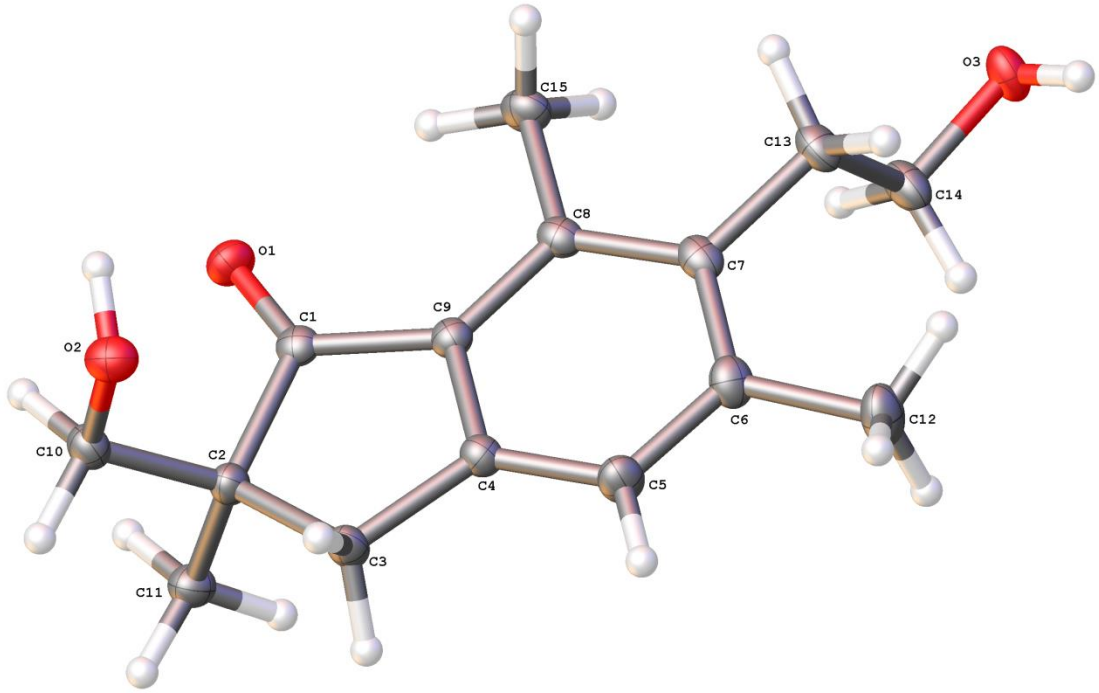

Formula: $C_{15}H_{20}O_3$; M_r = 248.31; crystal dimensions: 0.64 x 0.31 x 0.06 mm; crystal system: Monoclinic; space group: $P2_12_12_1$; a = 7.48123(6) Å, b = 8.18005(9) Å, c = 21.39110(19) Å, α = 90°, β = 90°, γ = 90°; V = 1309.07(2) Å^3; Z = 4; ρ_{calcd} = 1.260 Mg/m^3; μ = 0.695 mm^{-1}; Cu $K\alpha$ radiation, λ = 1.54184 Å; T = 100 K; $2\Theta_{max}$ = 137.5°; 13898/2395 measured/independent reflections; R_{int}: 0.0372; Flack parameter/Hooft parameter 0.09(8)/0.05(3); R = 0.0312, wR = 0.0841; $\Delta\rho_{max}$ = 0.220 eÅ^{-3}, $\Delta\rho_{min}$ = −0.220 eÅ^{-3}. Colourless plate crystals. CCDC deposition number 1050918.

(2*S*)-pteroside K

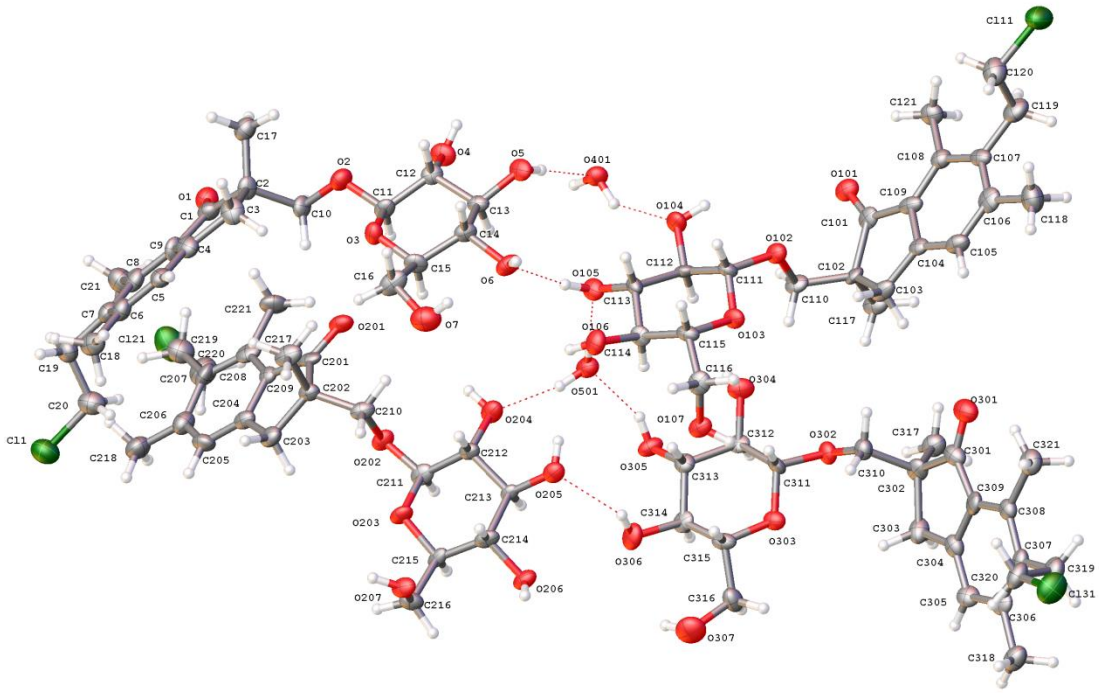

Formula: $C_{21}H_{30}ClO_{7.5}$; M_r = 437.90; crystal dimensions: 0.09 x 0.07 x 0.01 mm; crystal system: Triclinic; space group: *P*1; a = 8.108(4) Å, b = 9.341(4) Å, c = 28.660(12) Å, α = 81.739(14)°, β = 88.818(16)°, γ = 89.745(14)°; V = 2147.6(17) Å^3; Z = 4; ρ_{calcd} = 1.354 Mg/m^3; μ = 0.220 mm^{-1}; Mo $K\alpha$ radiation, λ = 0.71075 Å; T = 100 K; $2\Theta_{max}$ = 55.3°; 57447/19551 measured/independent reflections; R_{int}: 0.1941; Flack parameter/Hooft parameter -0.16(9)/0.09(8); R = 0.0995, wR = 0.2401; $\Delta\rho_{max}$ = 0.843 eÅ^{-3}, $\Delta\rho_{min}$ = −0.360 eÅ^{-3}. Colourless plate crystals. CCDC deposition number 1050920.

Rhedynoside B

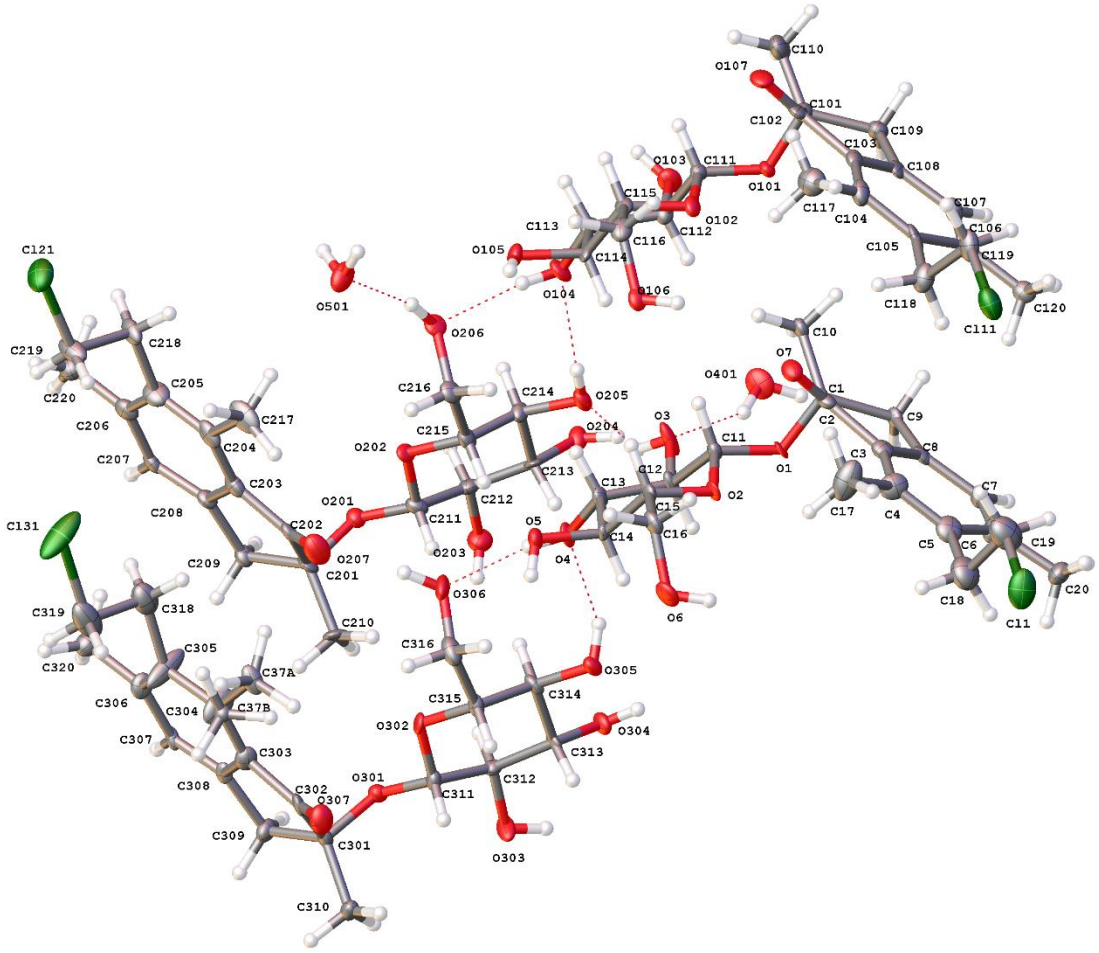

Formula: $C_{20}H_{28}ClO_{7.5}$; M_r = 423.87; crystal dimensions: 0.20 x 0.08 x 0.01 mm; crystal system: Monoclinic; space group: $P2_1$; a = 8.05004(19) Å, b = 43.4268(10) Å, c = 11.4031(3) Å, α = 90°, β = 90.034(2)°, γ = 90°; V = 3986.38(16) Å^3; Z = 8; ρ_{calcd} = 1.413 Mg/m^3; μ = 0.235 mm^{-1}; Mo $K\alpha$ radiation, λ = 0.71075 Å; T = 100 K; $2\Theta_{max}$ = 55.3°; 52007/18325 measured/independent reflections; R_{int}: 0.0382; Flack parameter/Hooft parameter 0.02(2)/0.011(17); R = 0.0691, wR = 0.1779; $\Delta\rho_{max}$ = 1.383 eÅ^{-3}, $\Delta\rho_{min}$ = −0.459 eÅ^{-3}. Colourless plate crystals. CCDC deposition number 1406891.

N.B. this structure was refined as a 2-componant twin with the twin law [-1 0 0 0 -1 0 0 0 1], BASF 0.520(2)

(2*R*)-pteroside B

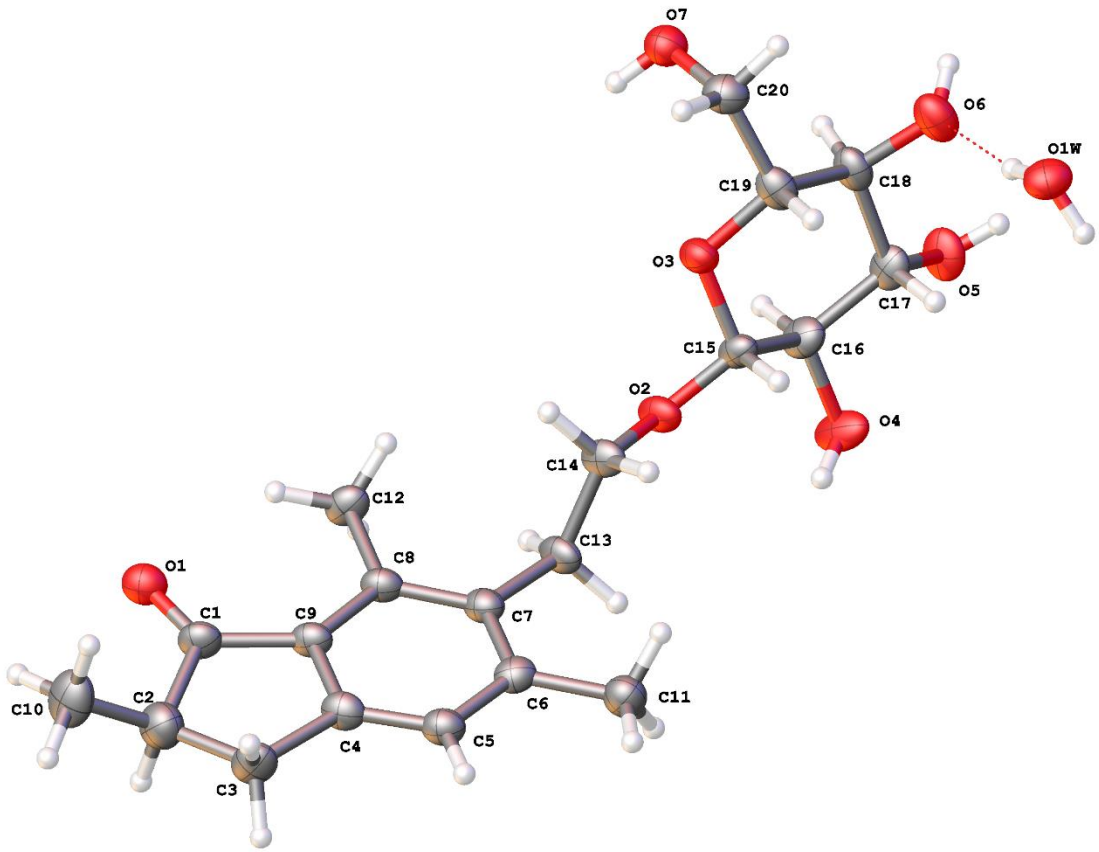

Formula: $C_{20}H_{30}O_8$; M_r = 398.44; crystal dimensions: 0.20 x 0.10 x 0.02 mm; crystal system: Monoclinic; space group: $P2_1$; a = 5.7210(4) Å, b = 10.3060(7) Å, c = 16.4249(13) Å, α = 90°, β = 93.254(7)°, γ = 90°; V = 966.87(12) Å^3; Z = 2; ρ_{calcd} = 1.369 Mg/m^3; μ = 0.879 mm^{-1}; Cu $K\alpha$ radiation, λ = 1.54184 Å; T = 100 K; $2\Theta_{max}$ = 134.8°; 9102/3371 measured/independent reflections; R_{int}: 0.0778; Flack parameter/Hooft parameter 0.1(4)/0.3(3); R = 0.0670, wR = 0.1803 $\Delta\rho_{max}$ = 0.485 eÅ^{-3}, $\Delta\rho_{min}$ = −0.260 eÅ^{-3}. Colourless plate crystals. CCDC deposition number 1418452.

HPLC-ESI-MS^n Method

In order to confirm the presence of chlorinated isolated compounds, bracken rhizomes (10 g, dry weight) were extracted with 100 ml of non-chlorinated organic solvents, methanol and ethyl acetate, and the extracts were analysed by reverse-phase HPLC with on-line photodiode array detection with and without electrospray ionisation-ion trap mass spectrometry. HPLC/ion trap mass spectrometry (HPLC/ESI-MS^n) analysis was performed on a Thermo Finnigan LC-MS system (Thermo Electron Corporation, USA) comprising a Finnigan Surveyor PDA Plus detector, a Finnigan LTQ linear ion trap with ESI source and a Waters C_{18} Nova-Pak column (4 µm, 3.9 mm x 100 mm). The autosampler tray temperature was maintained at 5°C and the column temperature at 30°C. Sample injection volume was typically 10µL, the detection wavelength was set to 210–400 nm and the flow rate was 1 ml min^{-1}, with 100 µL min^{-1} going to the mass spectrometer. The mobile phase consisted of water:formic acid (A; 100:0.1, v/v) and MeOH:formic acid (B; 100:0.1, v/v). The column was equilibrated with 95% solvent A, and the percentage of B increased linearly to 100% over 25 min. Ionisation parameters were optimised by infusion of chlorogenic acid standard at a constant rate into the LC flow. Mass spectra were acquired in negative ionisation mode with the following interface and MS parameters: nitrogen sheath gas 30 arbitrary units, nitrogen auxiliary gas 15 units, spray voltage 4 KV, capillary temperature 320°C, capillary voltage −1 V

and tube lens offset −68 V. MS/MS fragmentation was carried out at normalised collision energy of 35% and isolation width 2.0 (*m/z*).

HPLC-ESI-MS^n Chromatograms

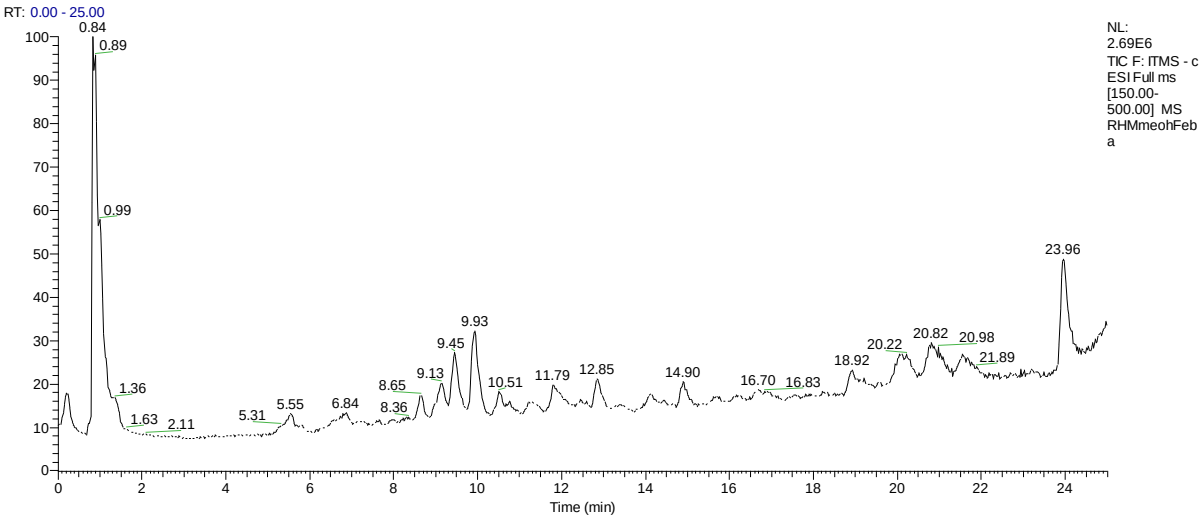

Fig. SD1. Reverse phase HPLC-ESI-MS total ion current (TIC) chromatogram of methanol extract of bracken rhizomes in the negative ion mode.

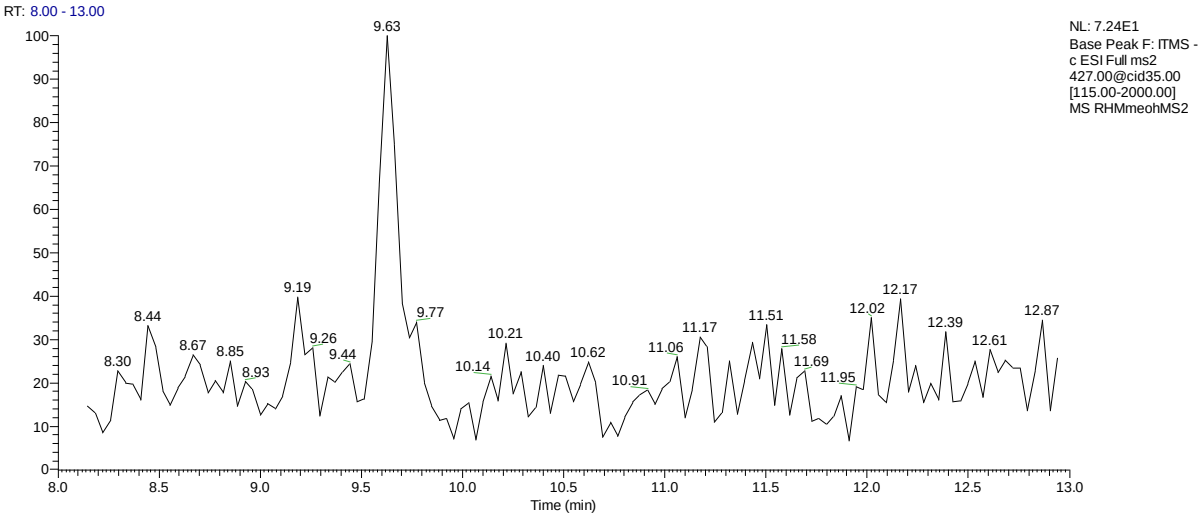

Fig. SD2. HPLC-ESI–MS/MS base peak chromatogram of methanol extract of bracken rhizomes in the negative ion mode.

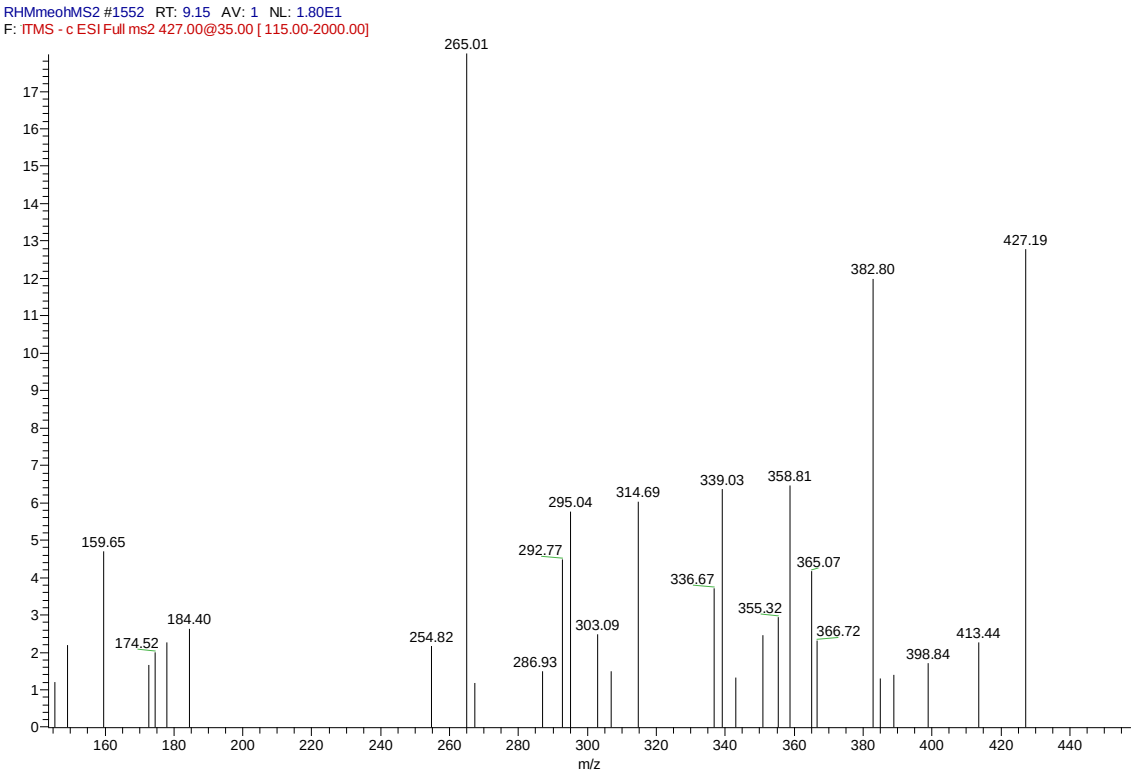

Fig. SD3. HPLC/ESI–MS/MS total ion current (TIC) chromatogram of selected peak (relative retention time (*RR*t) of 9.15 min) of methanol extract of bracken rhizomes in the negative ion mode.

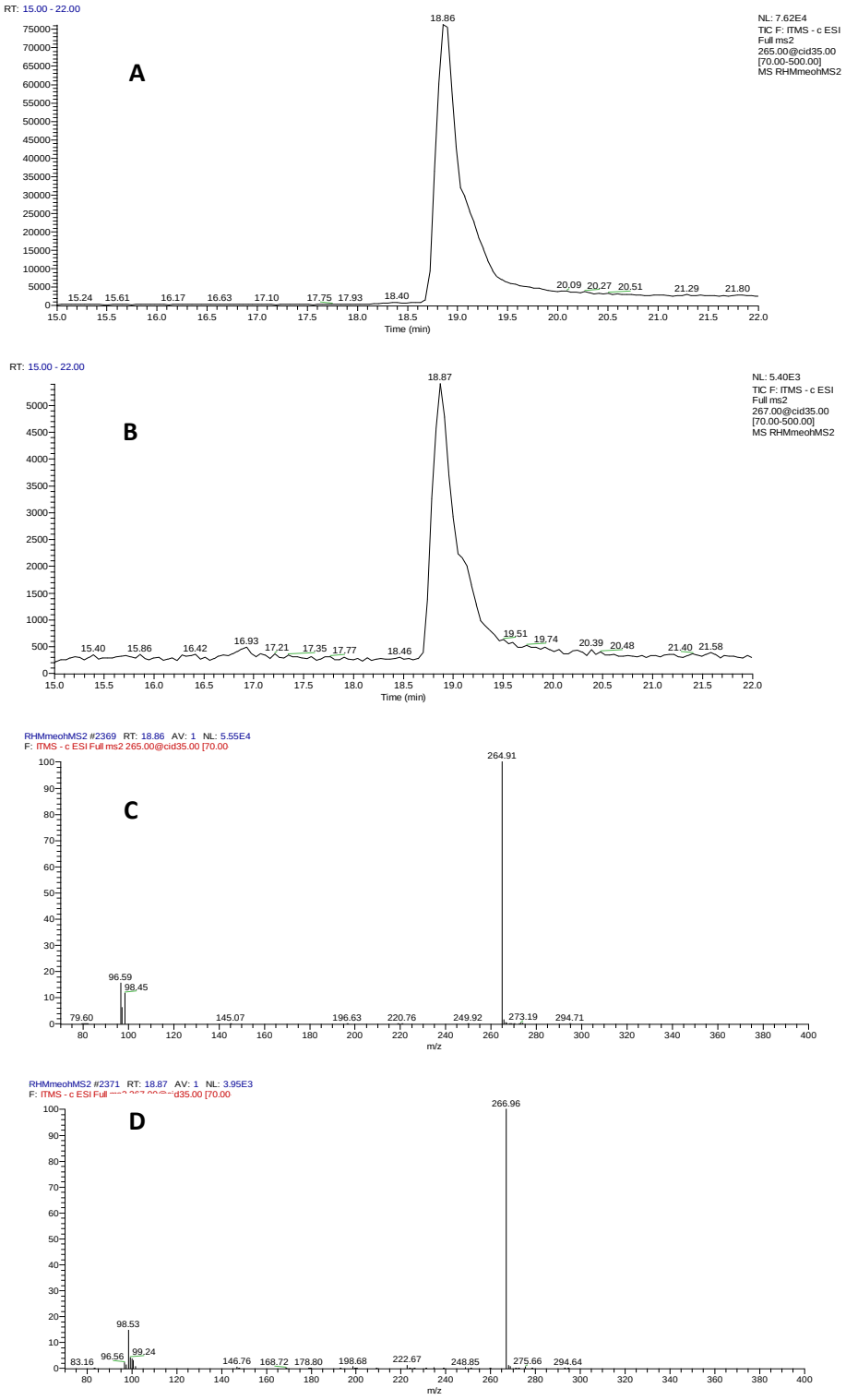

Fig. SD4. Further HPLC/MS/MS identification of the chlorinated compounds (**11**, **13** and **35**) (loss of 162 amu) in methanol extract of bracken rhizomes. Total ion current (TIC) of compounds at *RR*t of 18.8 min: (**A**) with ^{35}Cl isotope; (**B**) with ^{37}Cl isotope. HPLC/MS/MS spectrum showing $[M\text{-}H\text{-}Glc]^{-}$ (265 amu) in the negative mode at *RR*t of 18.8 min for (**C**) ^{35}Cl-compounds and (**D**) ^{37}Cl-compounds.

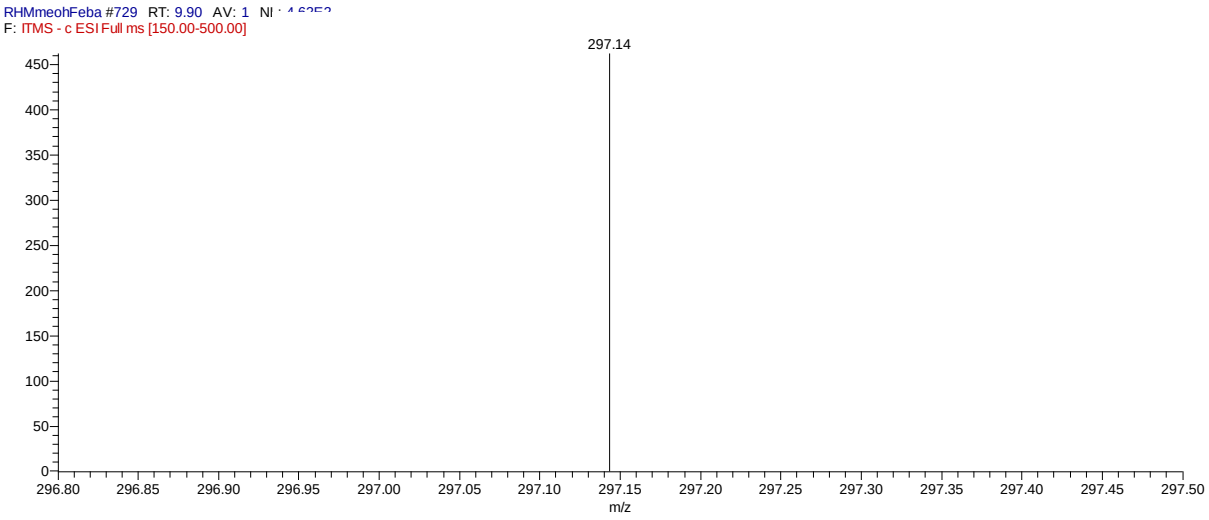

Fig. SD5. HPLC/MS identification of the sulfated-pterosin (**9**) in methanol extract of bracken rhizomes. HPLC/MS spectrum showing $[M\text{-}H]^{-}$ (297.14 amu) in the negative mode at *RR*t of 9.90 min for compound (**9**).

Identification of SGLT1 and GLUT2 transporter inhibitors

Routine cell culture - Human epithelial colorectal adenocarcinoma (Caco-2) cells were obtained from the American Type Culture Collection (ATCC) and cultured in Growth Medium consisting of Dulbecco's modified Eagle's medium (containg Glutamax-1, 4.5g/L D-Glucose & 25mM Hepes (Invitrogen)), 10% Fetal Bovine Serum (Sigma), 1% Non-Essential Amino Acids (Invitrogen) & 1mM Sodium pyruvate (Sigma). The cells were routinely passaged at approximately 80% confluence using TrypLE™ Express Stable Trypsin-Like Enzyme (Invitrogen) to detach the cells, and seeded at approximately 114 cells per mm^2 in fresh tissue culture flasks. Only cells between the passage numbers 45 and 49 were used for experiments.

Preparation of differentiated Caco-2 cell monolayers – Corning® HTS Transwell® 96 well permeable insert supports (Sigma) were collagen coated with 40µl of 50µg/ml Rat Tail Collagen Type I (BD Biosciences) in 0.02M acetic acid for one hour at room temperature under sterile conditions. The inserts were washed twice in Phosphate Buffered Saline (PBS (Invitrogen)) and the Caco-2 cells seeded into the inserts at $9.6x10^5$ cell/ml (75µl per insert) in Growth Medium and 30ml of Growth medium added to the feeder plate below. The cells were left to attach to the collagen matrix and form monolayers over 48hrs at 37°C, 5% CO_2. Both inserts and

feeder plate were washed in PBS and the cells incubated with BD Entero-STIM™ Enterocyte Differentiation Medium containing MITO+™ Serum Extender solution (both BD Biosciences),75µl per insert & 30ml in feeder plate, for a further 48hrs at 37°C, 5% CO_2.

Glucose Transport Inhibitor Cell Screening Assay – Differentiated cell monolayers were washed gently in Dulbecco's Phosphate Buffered Saline containing $CaCl_2$ & $MgCl_2$ (PBS(+) (Invitrogen) and the inserts transferred to a new Corning® HTS Transwell®-96 well receiver plate (Sigma). The cells were incubated with fresh PBS(+) (75µl per insert & 225µl per well) for 60mins at 37°C, 5% CO_2. The PBS(+) was gently aspirated and replaced with 75µl per insert of either 5mM D-Glucose (Sigma) ± test active or 25mM D-Glucose ± test active in triplicate and 225µl per well of PBS(+) quickly added to each well. The 5mM glucose wells and the 45mM glucose wells were incubated at 37°C, 5% CO_2 for 15mins and 30mins, respectively. Details of all the actives tested can be found in Table 1. The cell inserts were transferred to a new receiver plate, the supernatant gently aspirated from the cells and replaced with 100µl of 100µM of Lucifer Yellow (Sigma) solution to confirm the integrity of the monolayers. 225µl of PBS(+) was added to each well and incubated at 37°C, 5% CO_2 for 1hr. The cell inserts were then discarded and the permeability of the membranes to Lucifer Yellow checked by measuring the fluorescence of the

samples at 485nm (excitation) & 530nm (emission) on a Spectramax Gemini EM fluorescence microplate reader.

Glucose Assay – The amount of glucose transported across the cell monolayers was measured using a glucose assay based on Invitrogen's Amplex Red Glucose/Glucose oxidase Assay Kit. Briefly, 50µl of each unknown sample was transferred to a black sided/clear bottom 96-well plate (Greiner Bio-One) to which 100µl of reaction buffer (0.5µl 10mM Ampliflu Red, 1µl 10U/ml HRP, 1µl 100U/ml Glucose Oxidase and 97.5µl PBS (all Sigma)) was added. After 10mins incubation at room temperature, the fluorescence of the samples were measured at 530nm (excitation) & 590nm (emission) on a Spectramax Gemini EM fluorescence microplate reader and the glucose concentration extrapolated from a standard curve.

Table 1 - details of the actives tested for SGLT1 and GLUT2 inhibition activity in Caco-2 cells using 5mM D-glucose for 15 minutes and 25mM D-glucose for 30 minutes, respectively. The assigned class of transporter inhibited by each active is based on SGLT1 inhibitors having ≥20% inhibition of glucose transport at 5mM D-glucose and ≤20% inhibition at 25mM D-glucose, and GLUT2 inhibitors having ≥20% inhibition at both 5mM & 25mM D-glucose levels.

Test Active[a]	Solvent	% inhibition of glucose transport					Class[b]
		5mM Glucose			25mM Glucose		
		Ave.	S.D.		Ave.	S.D.	
Phloridzin	DMSO	34.81	2.64		8.42	1.42	SGLT1
Phloretin	DMSO	83.60	0.95		76.20	3.88	GLUT2
Pterosin A	DMSO	6.18	6.58		-2.93	1.93	None
Pterosin B	DMSO	16.80	3.09		4.38	2.61	None
Pterosin C	DMSO	4.34	6.75		-2.20	2.49	None
Pterosin A glucoside	DMSO	-3.41	7.81		-7.64	4.12	None
Pterosin B glucoside	DMSO	-1.38	5.95		-6.89	2.72	None
Pteroside Z	DMSO	9.18	6.03		-4.49	6.46	None
[a] - All actives tested at 300uM.							
[b] - Based on SGLT1 inhibitors having >20% inhibition at 5mM (glucose) and <20% inhibition at 25mM, and GLUT2 having >20% inhibition at both 5mM & 25mM							

Table 1 shows the percentage of inhibition of each test active against the transport of glucose across a differentiated Caco-2 cell monolayer. At the lower D-glucose concentration of 5mM, the early transport of glucose across the cell monolayer is predominantly through the apically expressed, high affinity, low capacity SGLT1 glucose transporter. At higher D-glucose concentrations, the SGLT1 transporter becomes saturated and consequently the majority of glucose transport across the monolayer is driven by the low affinity, high capacity GLUT2 transporter that is targeted to the apical membrane only following an initial SGLT1-dependent transport of glucose. The screening cell model, detailed in the methods above, is designed to take advantage of these differences in the optimal conditions for each transporter to identify both SGLT1 and GLUT2 specific inhibitors. While both SGLT1 & GLUT2 on the apical membrane transport glucose into the enterocyte, GLUT2 is also expressed in the basolateral membrane where it is essential for the transport of glucose out of the cell. Hence, GLUT2 specific inhibitors will not only block the

apically expressed transporters at high D-glucose concentrations (25mM), they will also enter the cell and block the exit of glucose from the enterocyte at low D-glucose concentrations (5mM). Therefore, to differentiate between inhibition of apical and basolateral transporters, each active was tested at both 5mM D-glucose for 15 minutes and 25mM D-glucose for 30minutes. Actives were classed as SGLT1 inhibitors if they exhibited a greater than 20% inhibition of glucose transport at 5mM D-glucose and a corresponding less than 20% inhibition at 25mM D-glucose. Actives that were able to inhibit glucose transport by greater than 20% in both conditions were classed as GLUT2 specific inhibitors. This approach was qualified through the use of the widely recognised specific inhibitors of both SGLT1 and GLUT2, namely Phloridzin and Phloretin respectively.

Figure 1 - Glucose Concentration Timeline During a Meal

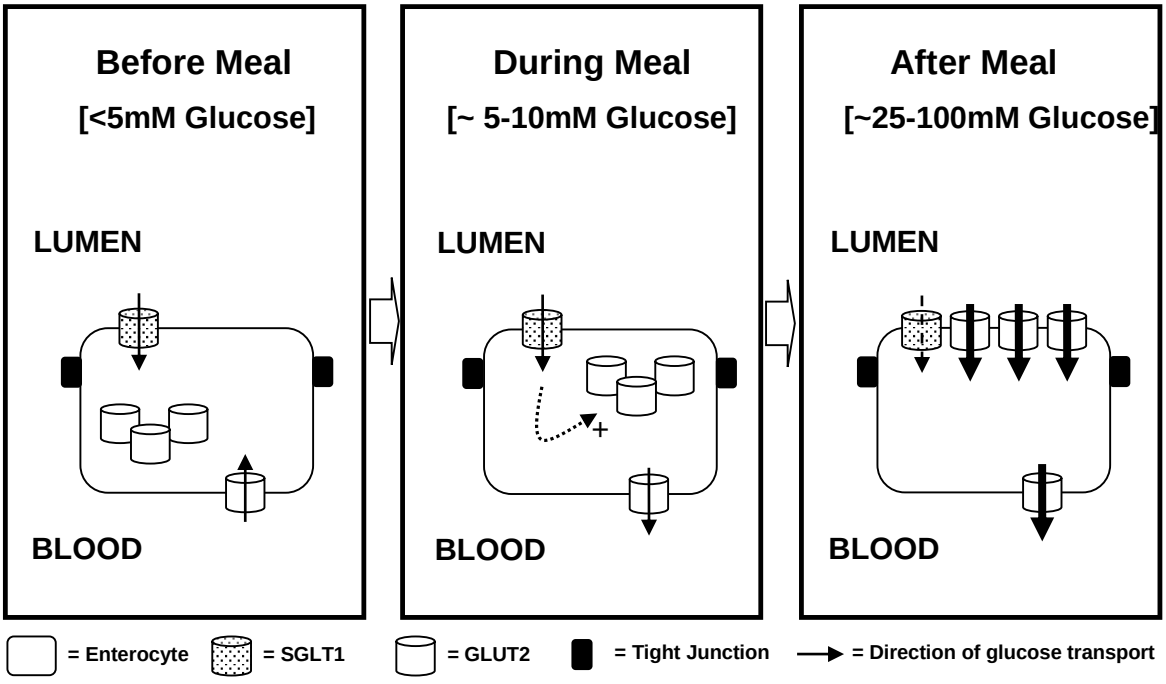

The glucose transport cell model, detailed in the methods above, is a novel *in vitro* cell system designed to mimic the localised changes in glucose concentration in the small intestine during the consumption of a carbohydrate rich meal (Figure 1) (Kellett & Brot-Laroche, 2005). Before the meal, the concentration of free glucose in the lumen of the intestine is low (<5mM) and the apically expressed SGLT1 transporter actively transports any available glucose into the enterocyte. GLUT2 transporters are also active on the basolateral membrane of the enterocyte, transporting glucose from the blood into the cell to maintain cellular metabolism if required. During a meal, the local concentration of glucose begins to increase (5-10mM) and is transported from the intestinal lumen by SGLT1 and subsequently into the systemic circulation via GLUT2. As a consequence of this initial glucose transport across the enterocyte, intracellular stores of GLUT2 are mobilised and targeted to the apical membrane. Shortly after the meal, very high local concentrations of glucose occur (25-100mM) as the carbohydrate content of the meal is broken down into monosaccharides by alpha-glucosidase enzymes located on the apical enterocyte membrane. At these high levels of glucose, the high affinity, low capacity transporter SGLT1 becomes saturated and the majority of glucose transport across the enterocyte is due to the low affinity, high capacity GLUT2 transporters now present in the apical membrane. These localised changes in luminal glucose concentrations are mimicked *in vitro* through an initial short

incubation of differentiated Caco-2 cells with a low level of D-glucose (5mM for 15mins) immediately followed by a sustained incubation with a high level of D-glucose (final concentration of 25mM for 45mins).

References:

Kellett & Brot-Laroche (2005) Apical GLUT2: a major pathway of intestinal sugar absorption. Diabetes **54**(10), 3056-62.

SUPPORTING INFORMATION 1 (SI 1)

Isolation and characterisation of thirteen pterosins and pterosides from bracken (*Pteridium aquilinum* (L.) Kuhn) rhizome

Rizgar Hassan Mohammad[a], Mohammad Nur e-Alam[a,b] , Martina Lahmann[a], Ifat Parveen[c], Graham J. Tizzard[d], Simon J. Coles[d], Mark Fowler[e], Alex F. Drake[f], Derren Heyes[g], Vera Thoss[a,*]

[a] School of Chemistry, Bangor University, Bangor LL57 2UW, United Kingdom

[b] Department of Pharmacognosy, College of Pharmacy, King Saud University, P.O. Box 2457, Riyadh 11451, Saudi Arabia.

[c] IBERS, Aberystwyth University, Penglais, Aberystwyth SY23 3DA, UK

[d] UK National Crystallography Service, School of Chemistry, University of Southampton, University Road, Southampton SO17 1BJ, United Kingdom

[e] Strategic Science Group, Unilever R&D, Colworth Science Park, Bedford, MK44 1LQ, UK.

[f] Biomolecular Spectroscopy Centre, Pharmaceutical Optical & Chiroptical Spectroscopy Facility, King's College London, The Wolfson Wing, WWB10 Hodgkin Building, Guy's Campus, London SE1 1UL, UK

[g] Manchester Institute of Biotechnology, University of Manchester, 131 Princess St, Manchester M1 7DN

*Corresponding Author vera.thoss@bangor.ac.uk

List of Supporting Information:

Figure S93. UV spectrum of compound **11** in CH_3OH.
Figure S94. FT-IR spectrum of compound **11** in CH_3OH.
Figure S95. ^1H NMR ($CDCl_3$, 400 MHz) spectrum of compound **11** after acetylation reaction.
Figure S96. ^1H-^1H COSY NMR spectrum of compound **11** after acetylation reaction.
Figure S97. DEPTQ NMR ($CDCl_3$, 100 MHz) spectrum of compound **11** after acetylation reaction.
Figure S98. ^1H NMR (CD_3OD, 400 MHz) spectrum of compound **12**.
Figure S99. DEPTQ NMR (CD_3OD, 100 MHz) spectrum of compound **12**.
Figure S100. ^1H-^1H COSY NMR spectrum of compound **12**.
Figure S101. HSQC NMR spectrum of compound **12**.
Figure S102. HMBC NMR spectrum of compound **12**.
Figure S103. FT-ICR-MS spectrum of compound **12**.
Figure S104. UV spectrum of compound **12** in CH_3OH.
Figure S105. FT-IR spectrum of compound **12** in CH_3OH.
Figure S106. ^1H NMR ($CDCl_3$, 400 MHz) spectrum of compound **12** after acetylation reaction.
Figure S107. ^1H-^1H COSY NMR spectrum of compound **12** after acetylation reaction.
Figure S108. DEPTQ NMR ($CDCl_3$, 100 MHz) spectrum of compound **12** after acetylation reaction.
Figure S109. ^1H NMR (CD_3OD, 400 MHz) spectrum of compound **13**.
Figure S110. DEPTQ NMR (CD_3OD, 100 MHz) spectrum of compound **13**.
Figure S111. ^1H-^1H COSY NMR spectrum of compound **13**.
Figure S112. HSQC NMR spectrum of compound **13**.
Figure S113. HMBC NMR spectrum of compound **13**.
Figure S114. FT-ICR-MS spectrum of compound **13**.
Figure S115. UV spectrum of compound **13** in CH_3OH.
Figure S116. FT-IR spectrum of compound **13** in CH_3OH.
Figure S117. ^1H NMR ($CDCl_3$, 400 MHz) spectrum of compound **13** after acetylation reaction.
Figure S118. ^1H-^1H COSY NMR spectrum of compound **13** after acetylation reaction.
Figure S119. DEPTQ NMR ($CDCl_3$, 100 MHz) spectrum of compound **13** after acetylation reaction.
Figure S120. ^1H-^1H NOESY NMR (CD_3OD, 400 MHz) spectrum of compound **13**.
Acetylation of compounds **2** and **10**-**13**.

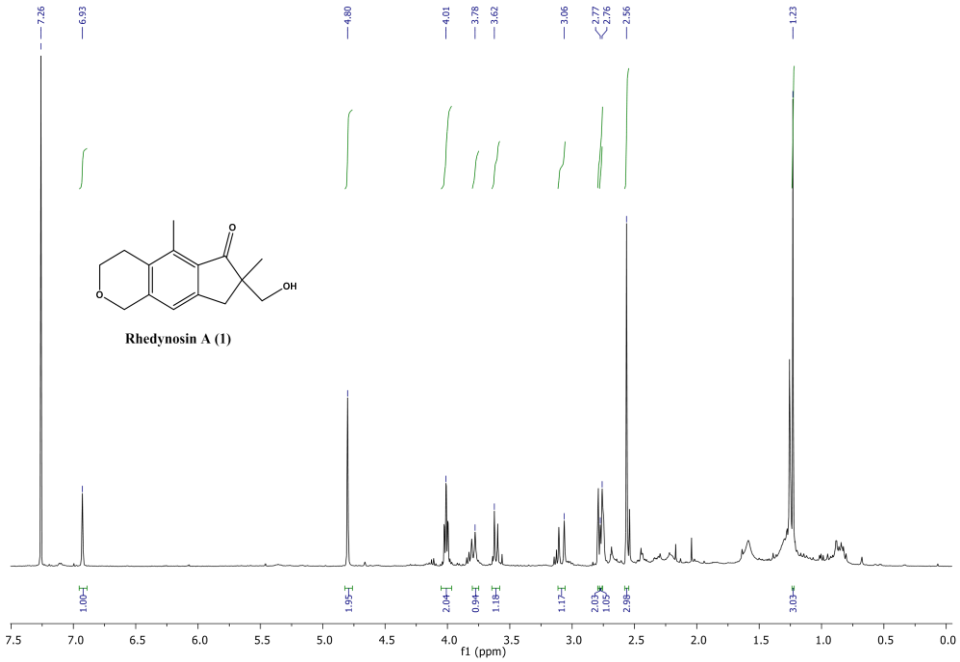

Figure S1. ^{1}H NMR ($CDCl_3$, 400 MHz) spectrum of compound **1**.

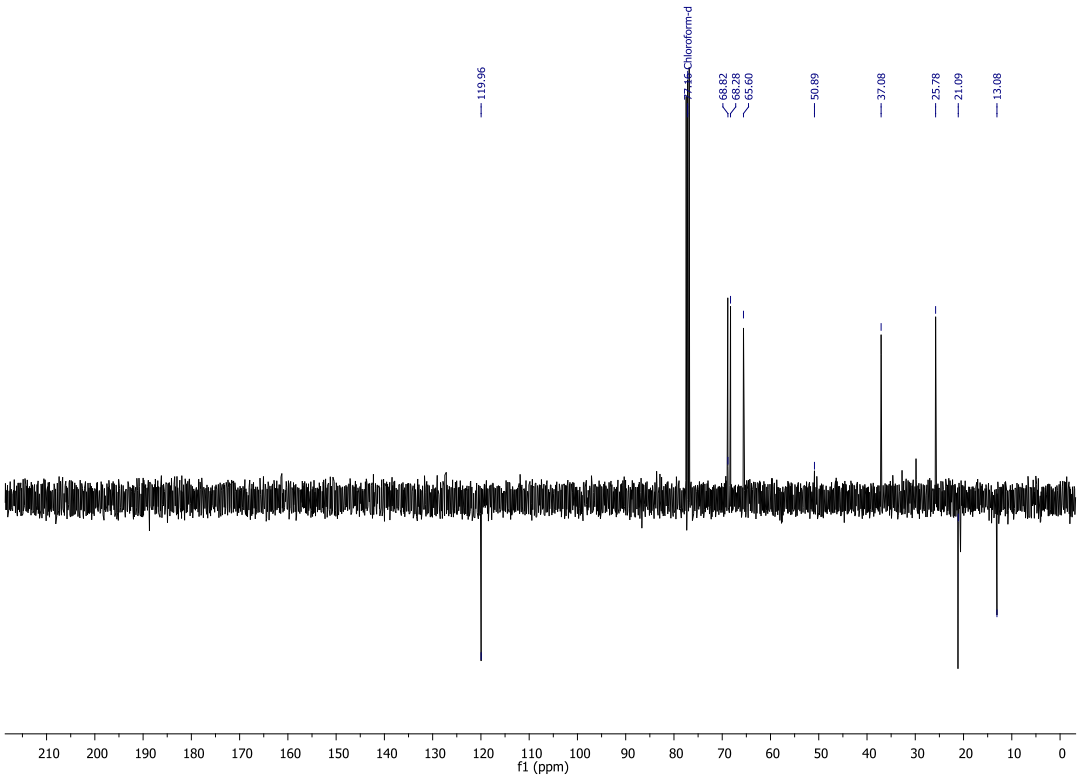

Figure S2. DEPTQ NMR ($CDCl_3$, 100 MHz) spectrum of compound **1**.

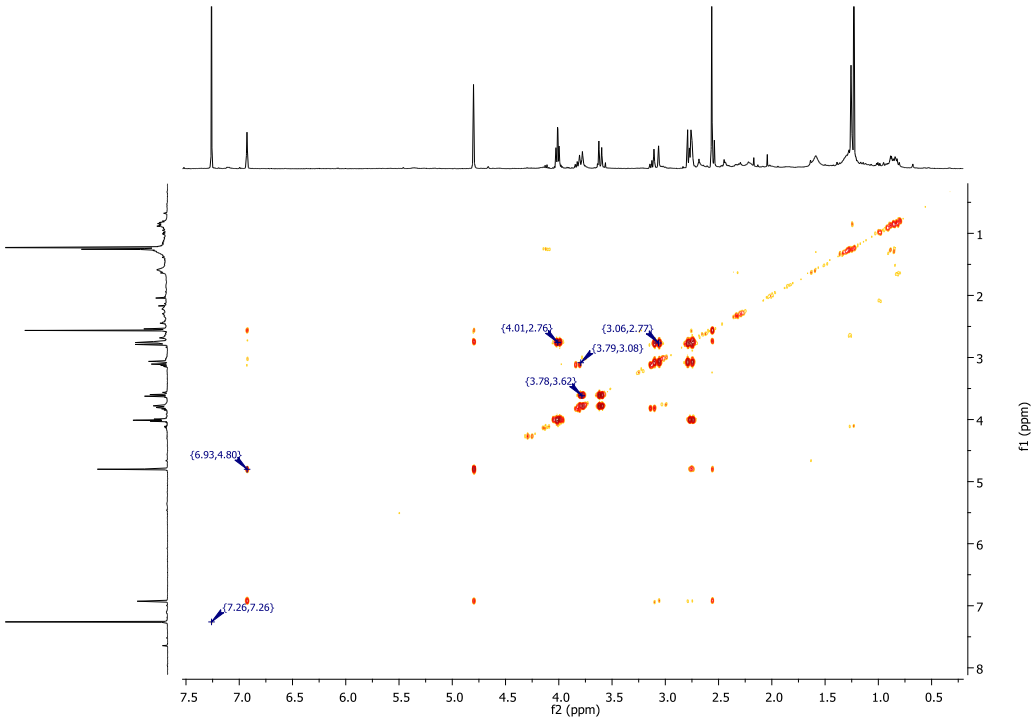

Figure S3. ^{1}H-^{1}H COSY NMR spectrum of compound **1**.

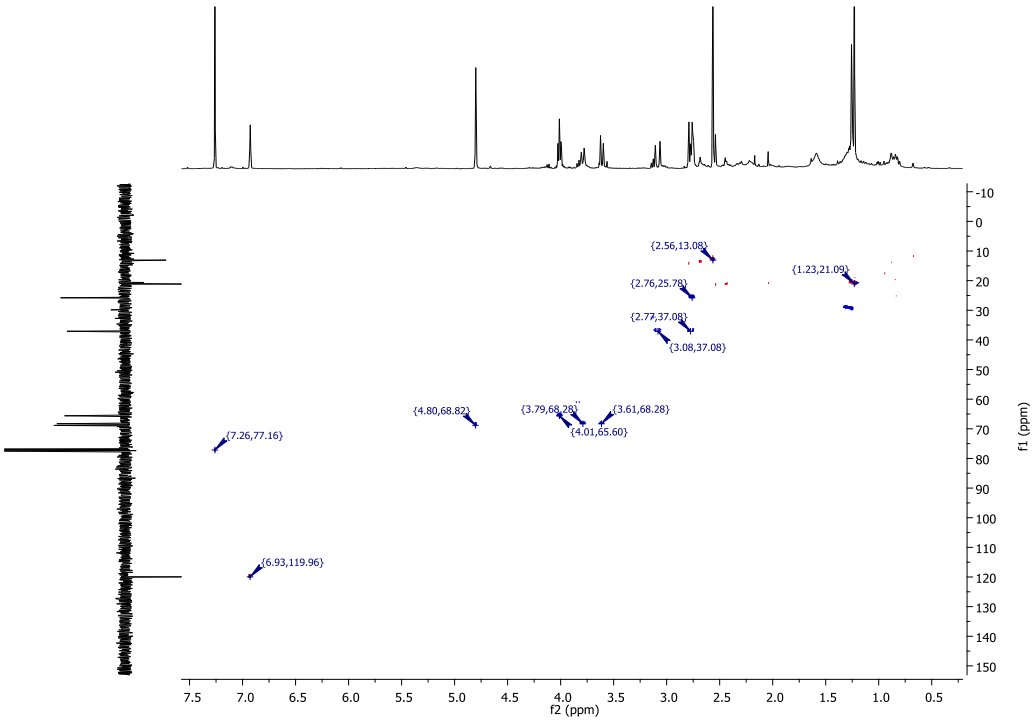

Figure S4. HSQC NMR spectrum of compound **1**.

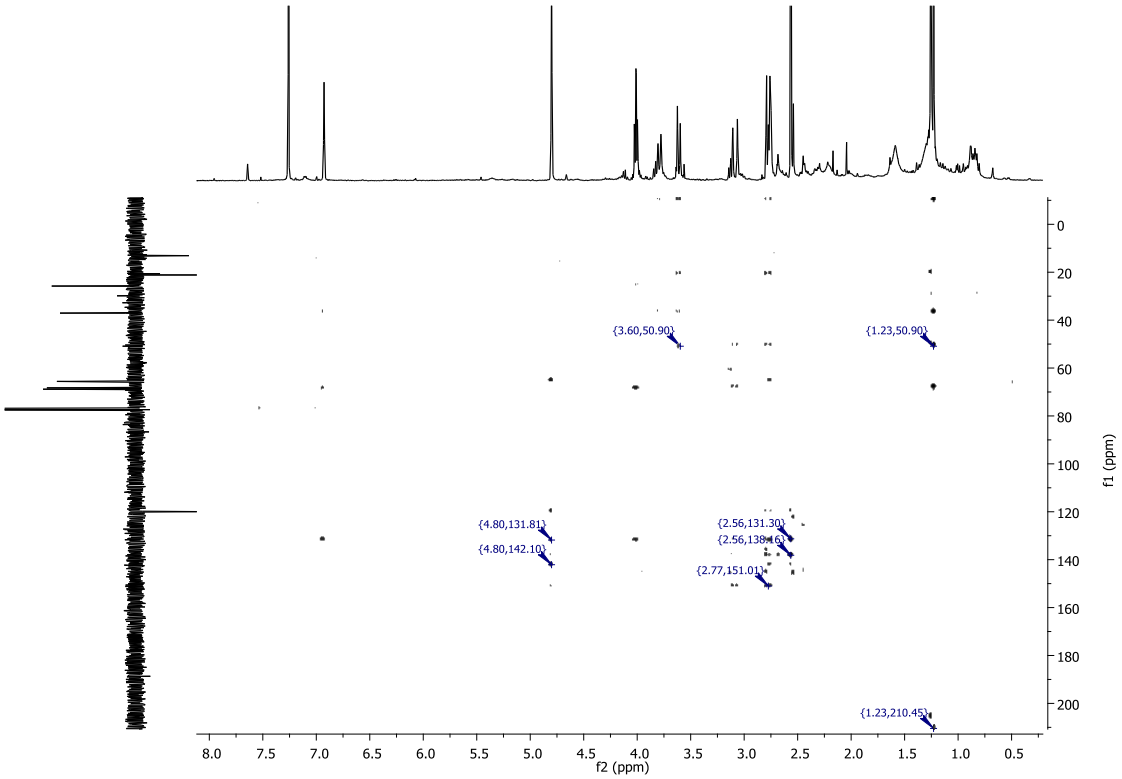

Figure S5. HMBC NMR spectrum of compound **1**.

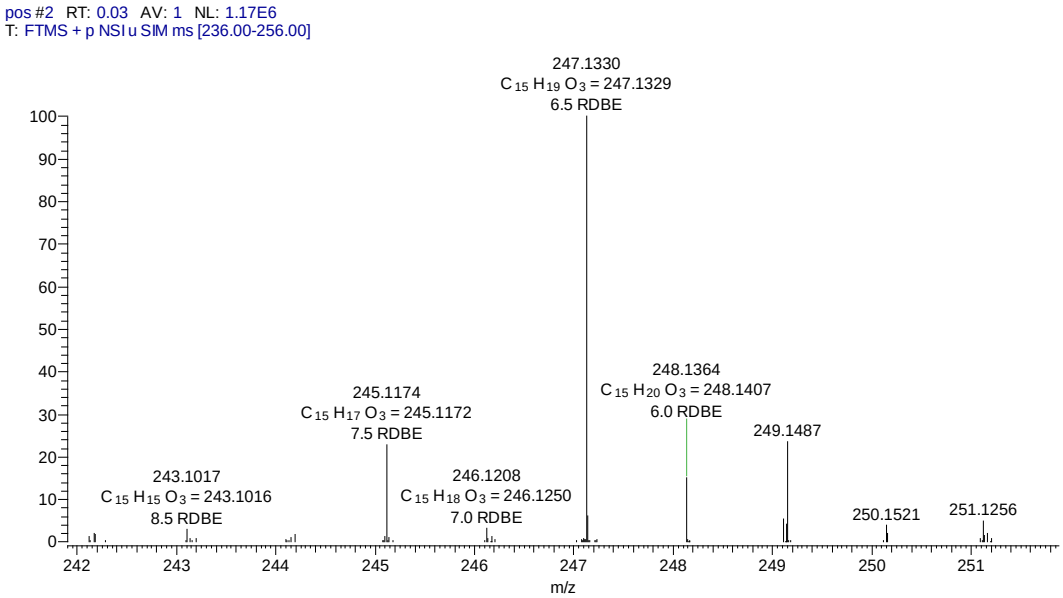

Figure S6. FT-ICR-MS spectrum of compound **1**.

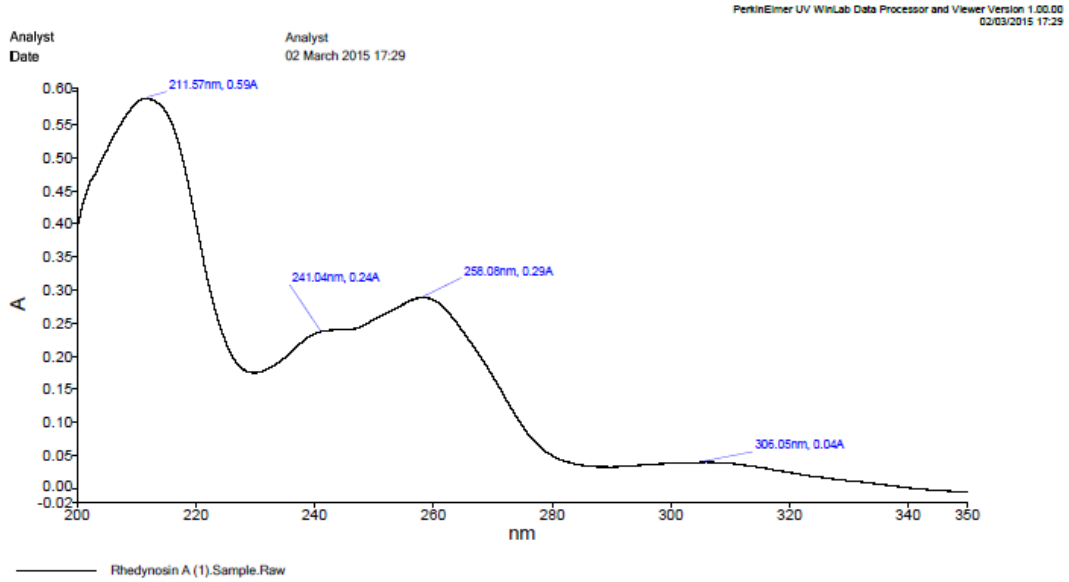

Figure S7. UV spectrum of compound **1** in CH_3OH.

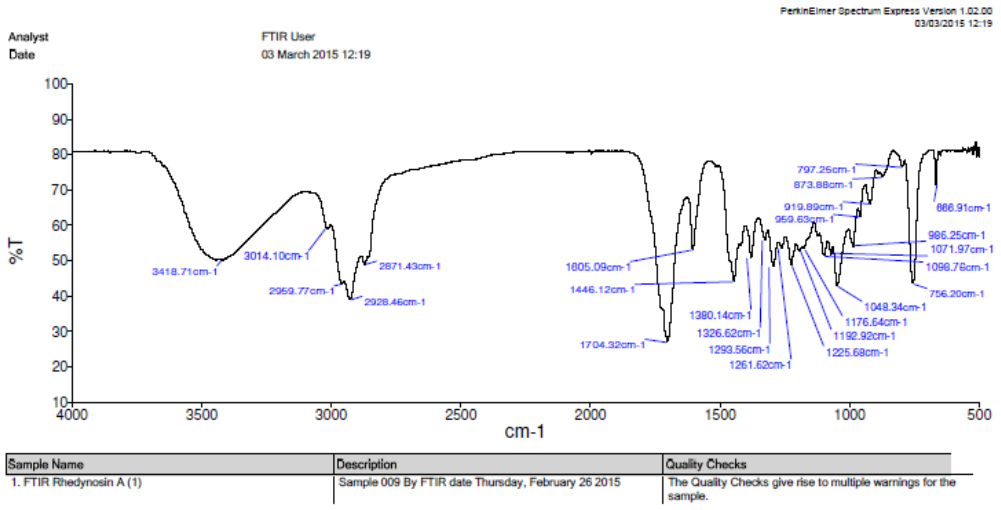

Figure S8. FT-IR spectrum of compound **1** in $CHCl_3$.

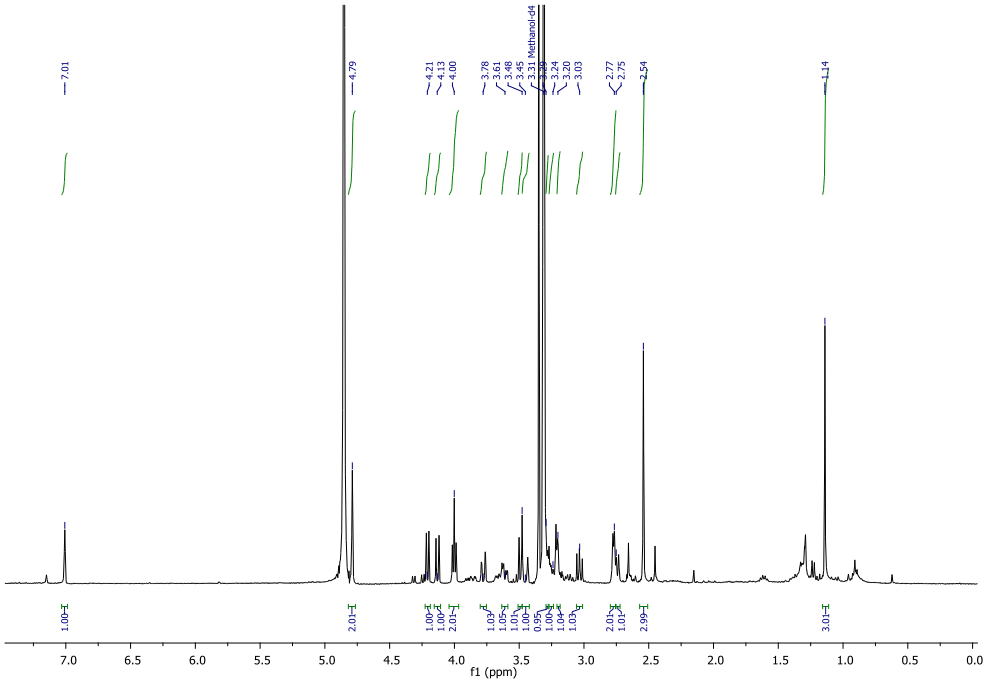

Figure S9. ^{1}H NMR (CD_3OD, 400 MHz) spectrum of compound **2**.

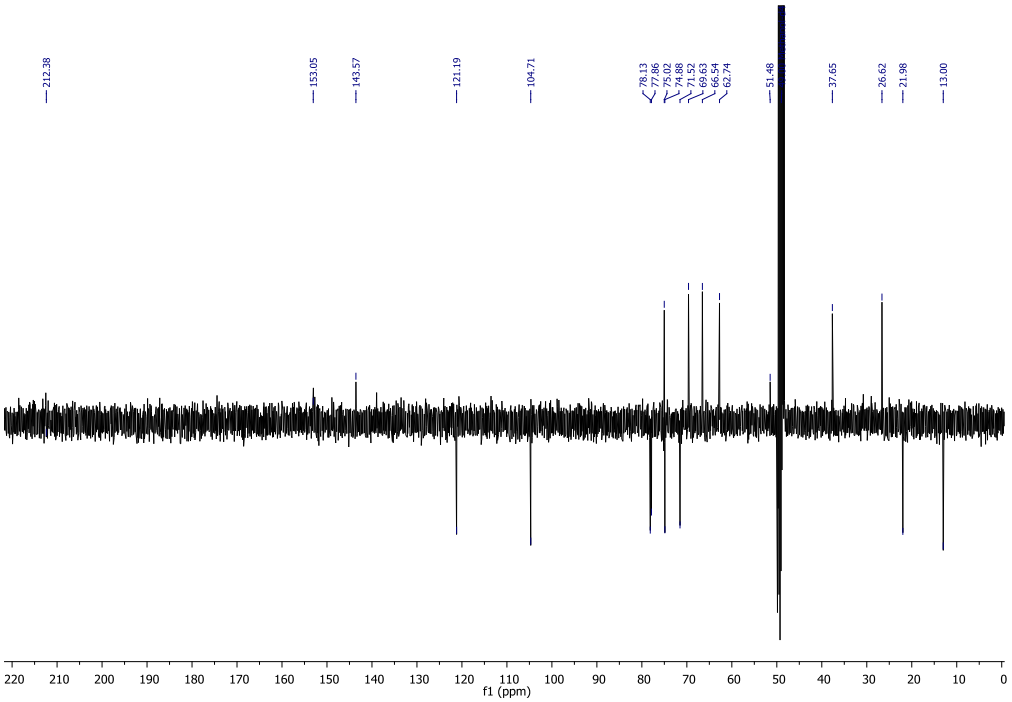

Figure S10. DEPTQ NMR (CD_3OD, 100 MHz) spectrum of compound **2**.

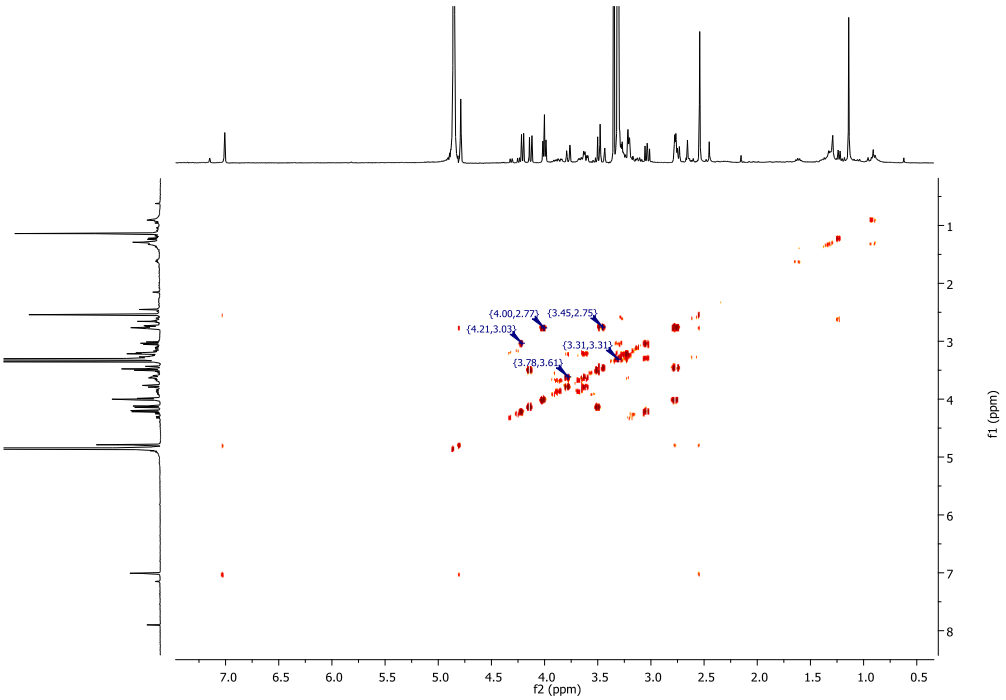

Figure S11. ^{1}H-^{1}H COSY NMR spectrum of compound **2**.

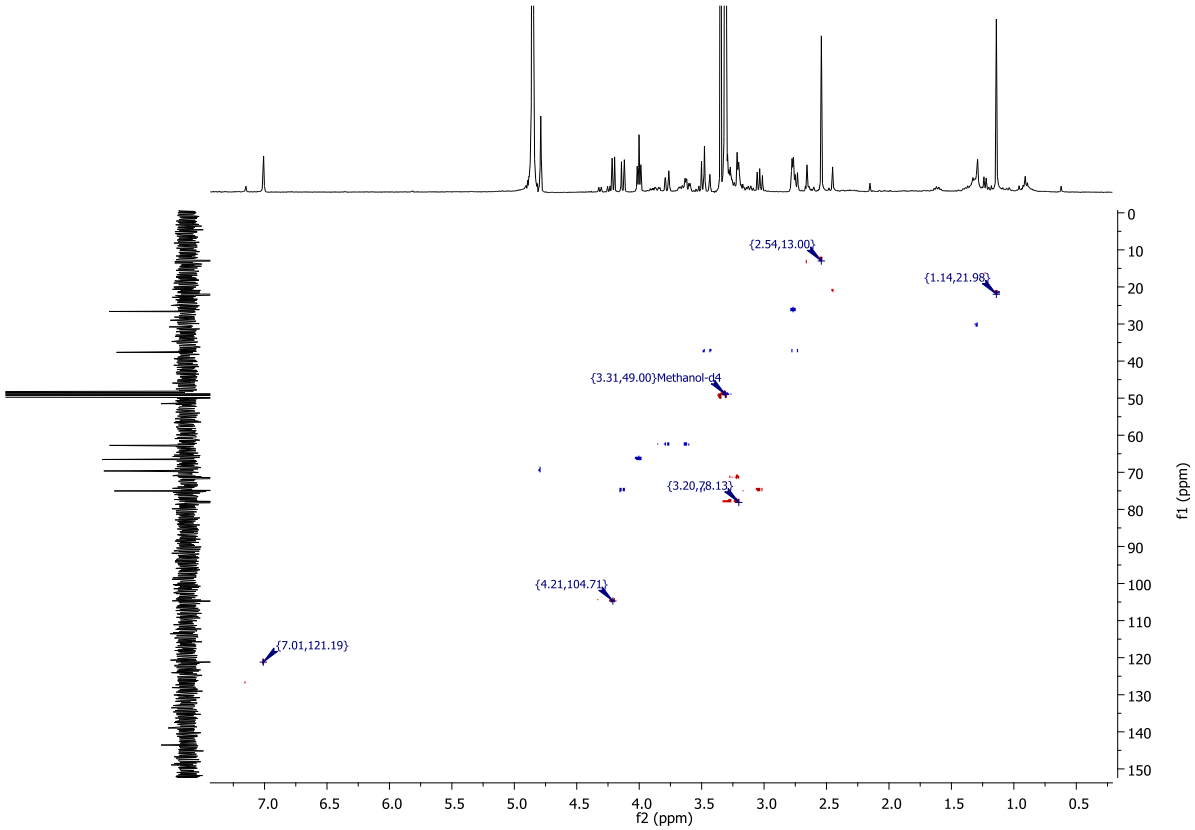

Figure S12. HSQC NMR spectrum of compound **2**.

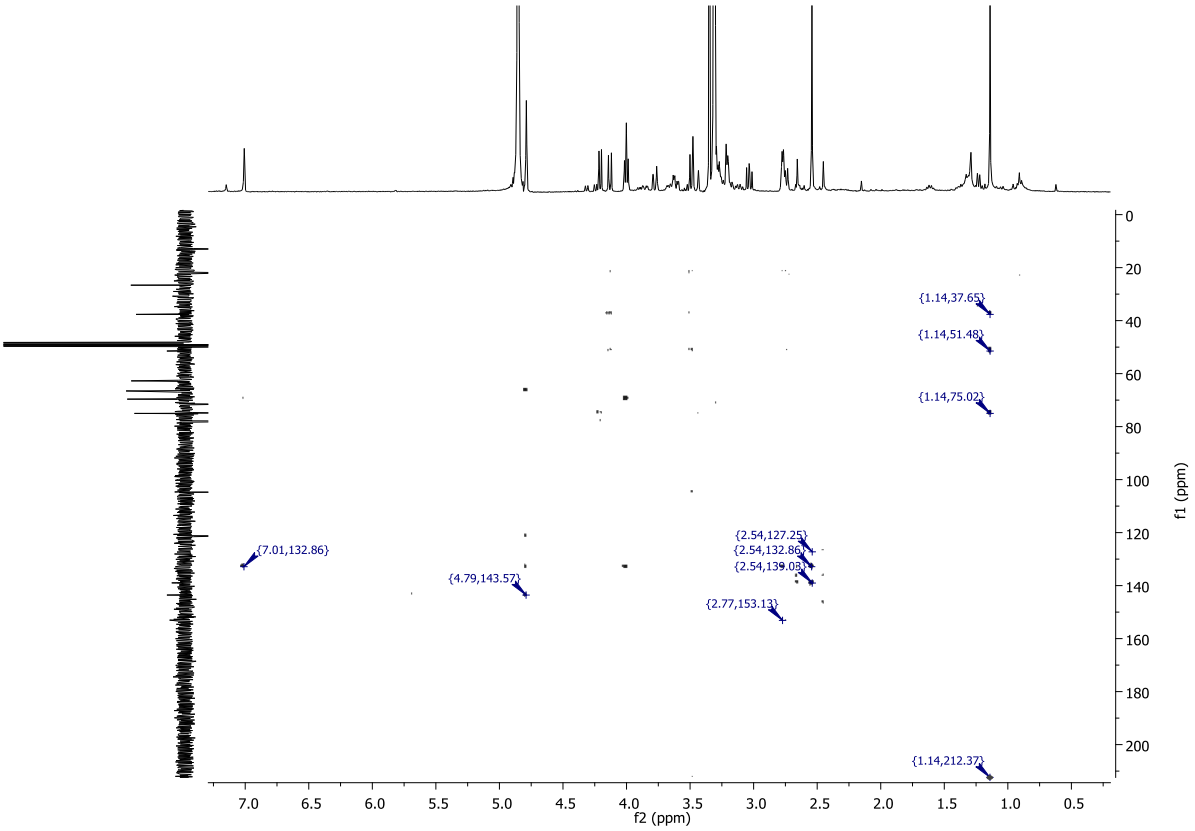

Figure S13. HMBC NMR spectrum of compound **2**.

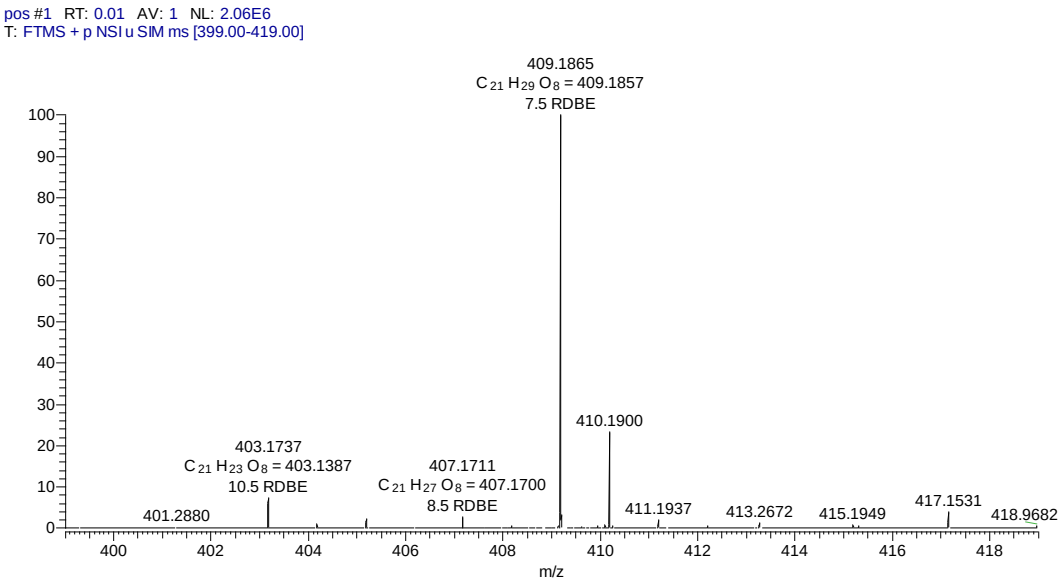

Figure S14. FT-ICR-MS spectrum of compound **2**.

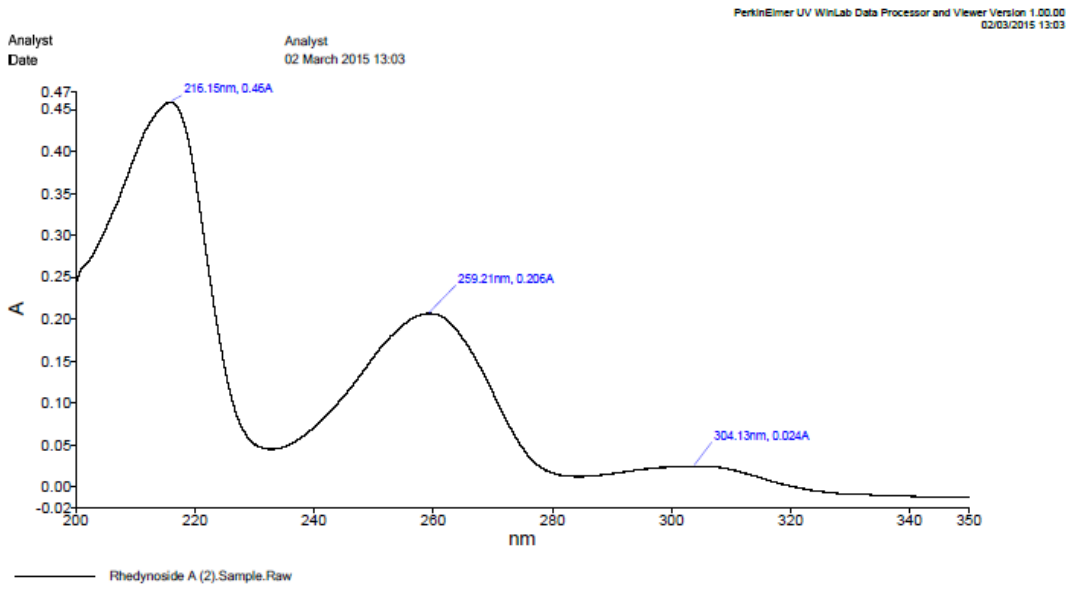

Figure S15. UV spectrum of compound **2** in CH_3OH.

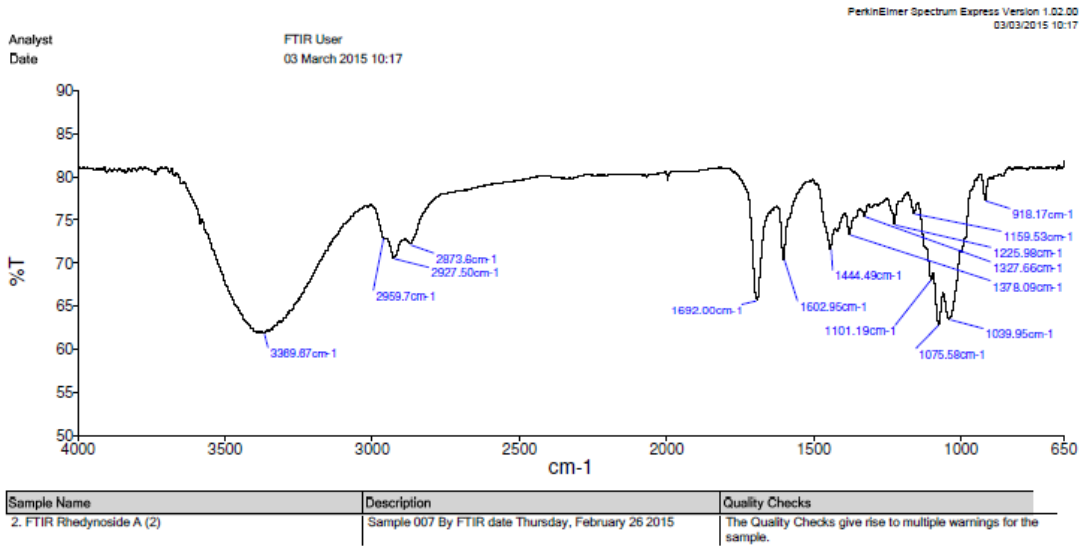

Sample Name	Description	Quality Checks
2. FTIR Rhedynoside A (2)	Sample 007 By FTIR date Thursday, February 26 2015	The Quality Checks give rise to multiple warnings for the sample.

Figure S16. FT-IR spectrum of compound **2** in CH_3OH.

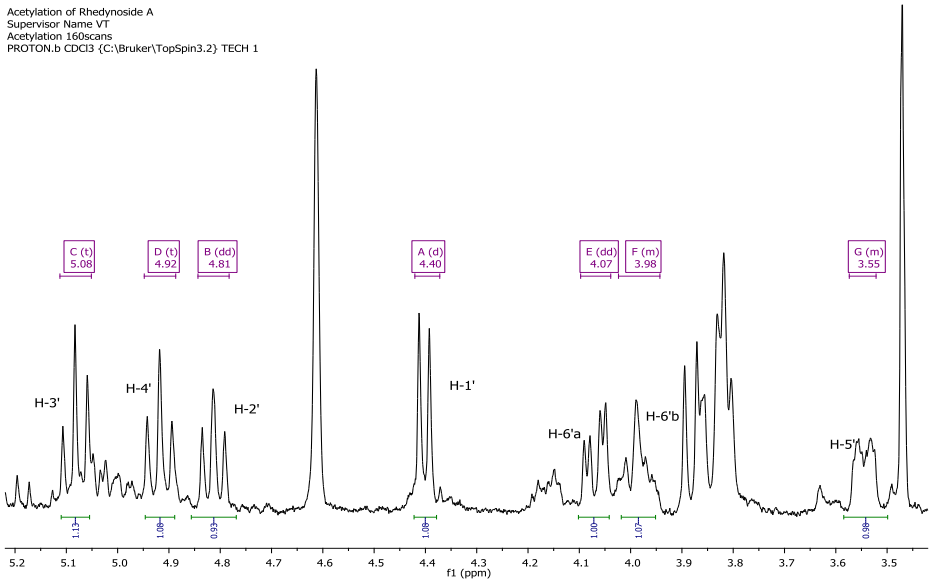

Figure S17. ^{1}H NMR ($CDCl_3$, 400 MHz) spectrum of compound **2** after acetylation reaction

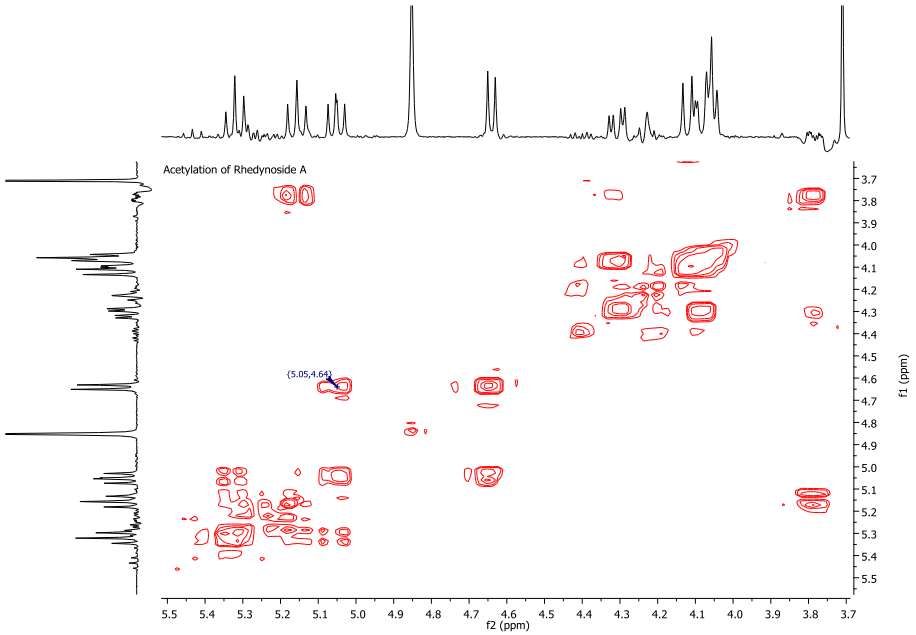

Figure S18. ^{1}H-^{1}H COSY NMR spectrum of compound **2** after acetylation reaction

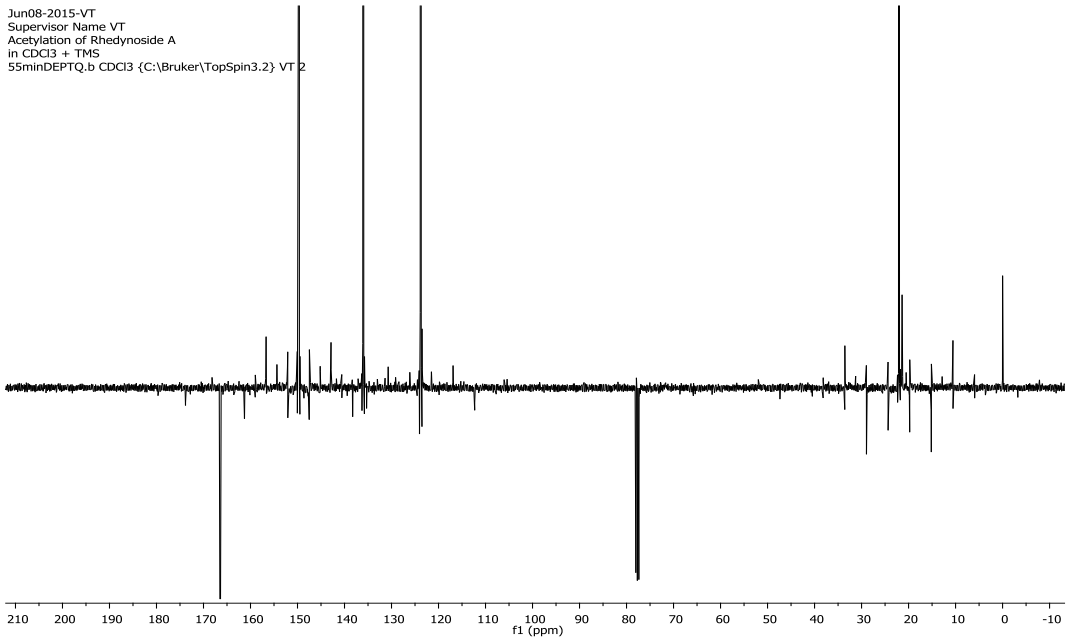

Figure S19. DEPTQ NMR ($CDCl_3$, 100 MHz) spectrum of compound **2** after acetylation reaction

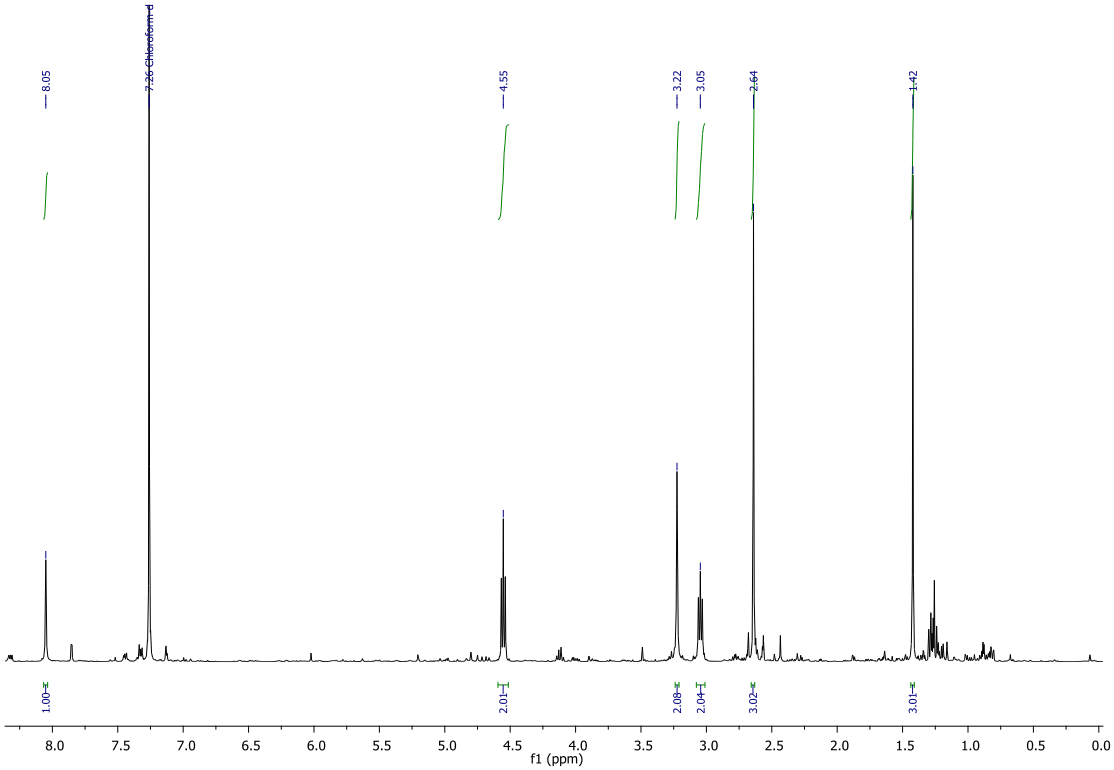

Figure S20. ^1H NMR ($CDCl_3$, 400 MHz) spectrum of compound **3**.

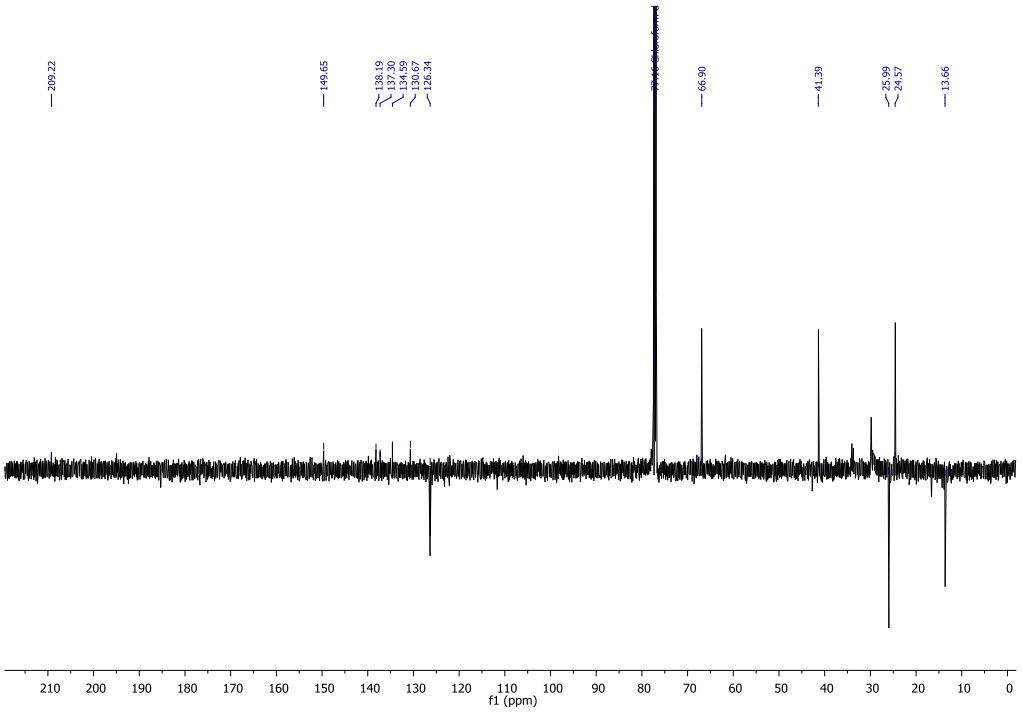

Figure S21. DEPTQ NMR ($CDCl_3$, 100 MHz) spectrum of compound **3**.

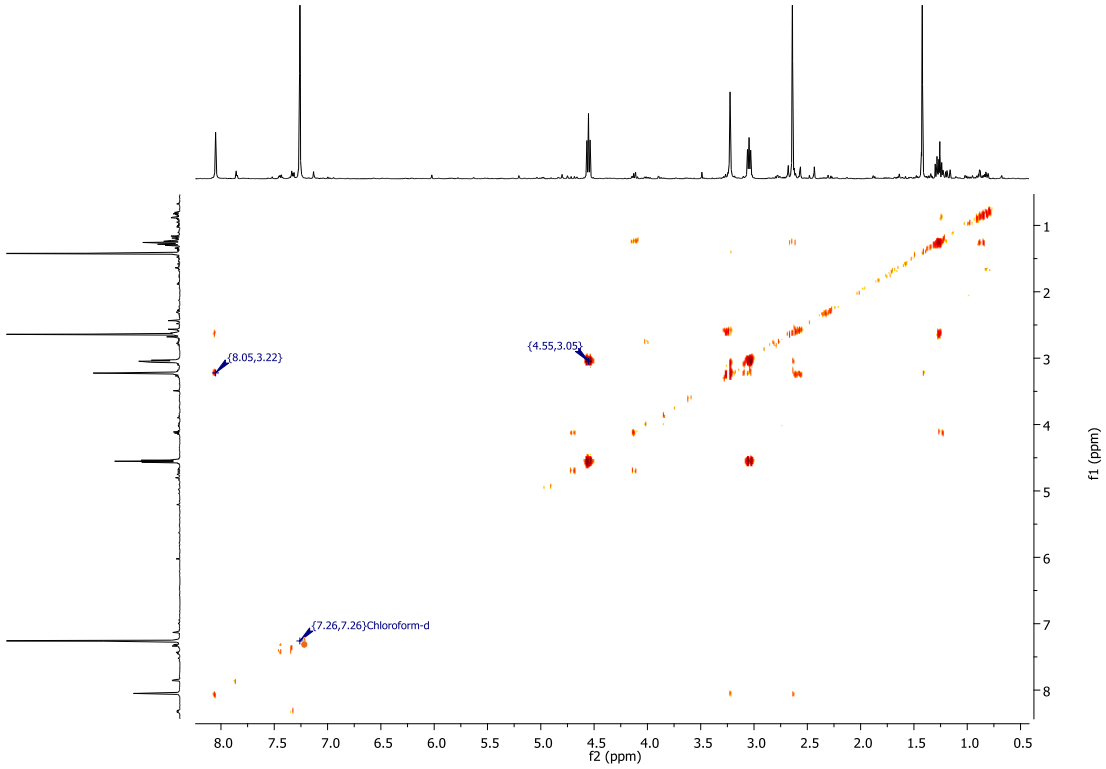

Figure S22. ^{1}H-^{1}H COSY NMR spectrum of compound **3**.

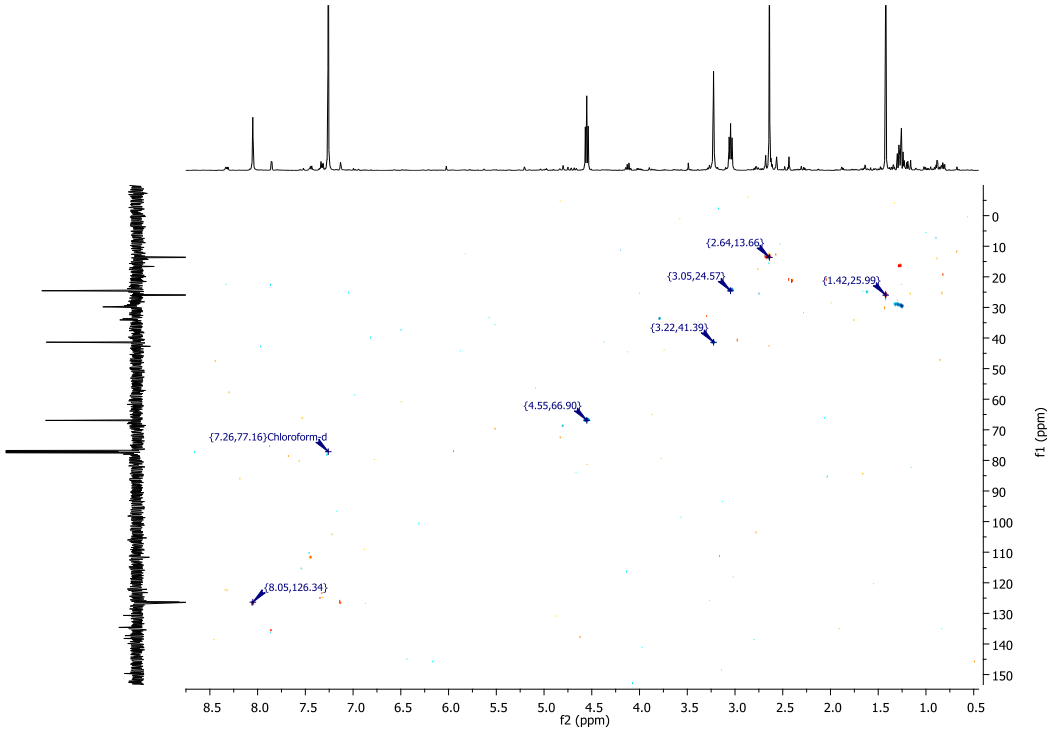

Figure S23. HSQC NMR spectrum of compound **3**.

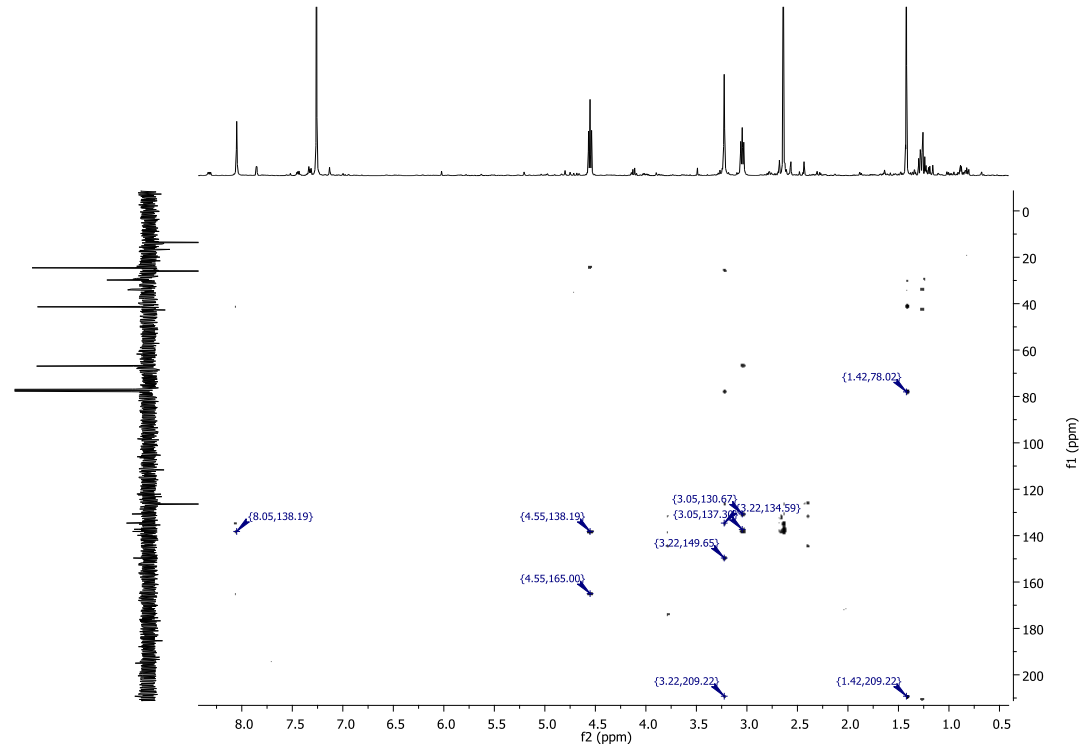

Figure S24. HMBC NMR spectrum of compound **3**.

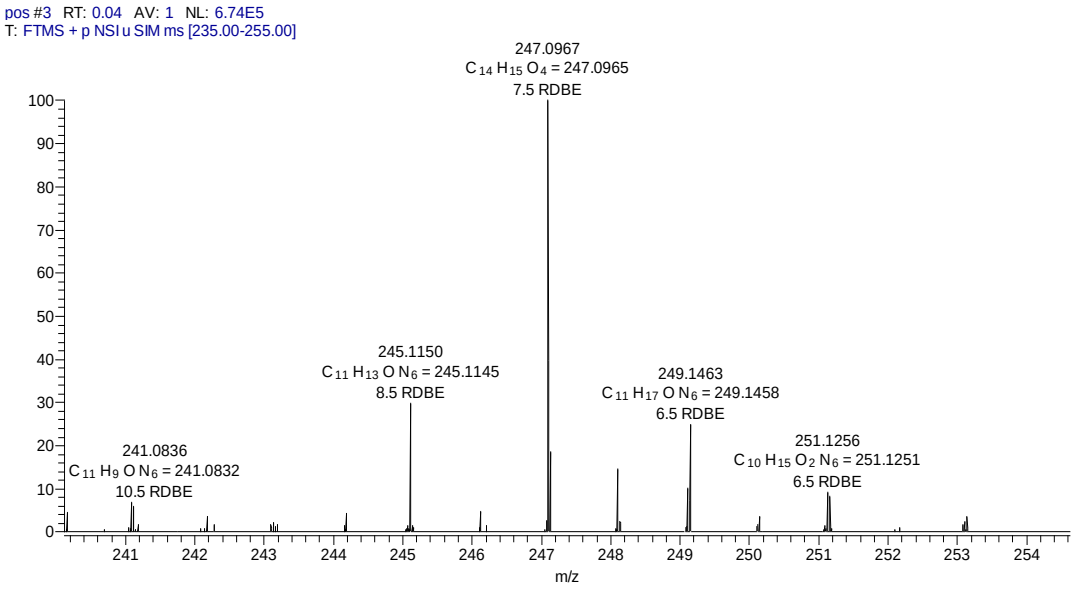

Figure S25. FT-ICR-MS spectrum of compound **3**.

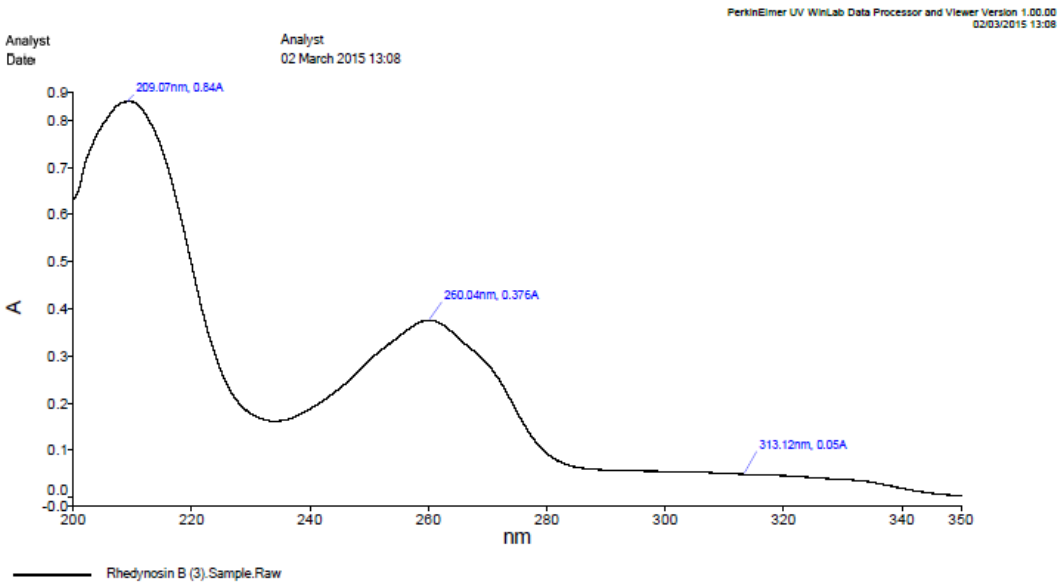

Figure S26. UV spectrum of compound **3** in CH_3OH.

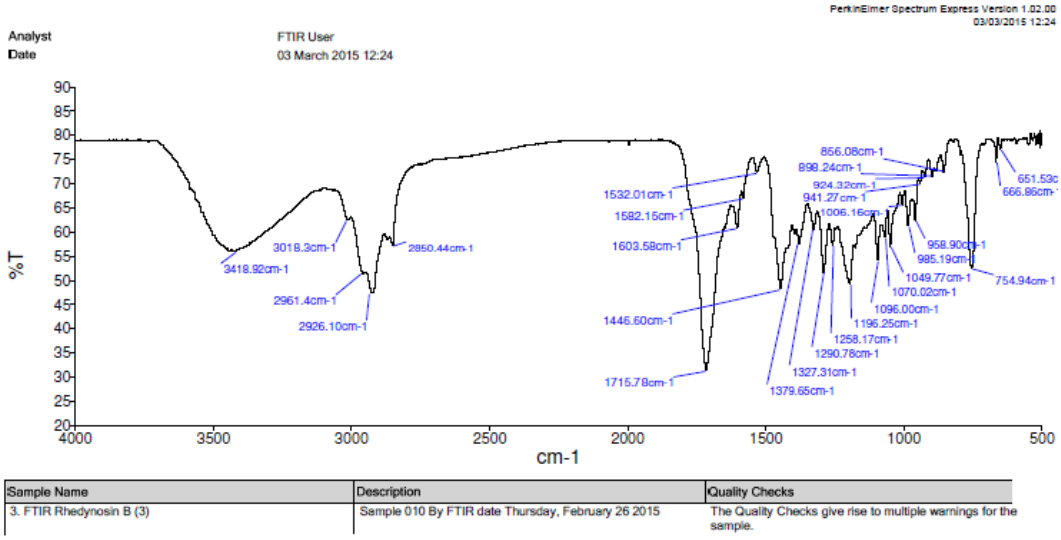

Figure S27. FT-IR spectrum of compound **3** in $CHCl_3$.

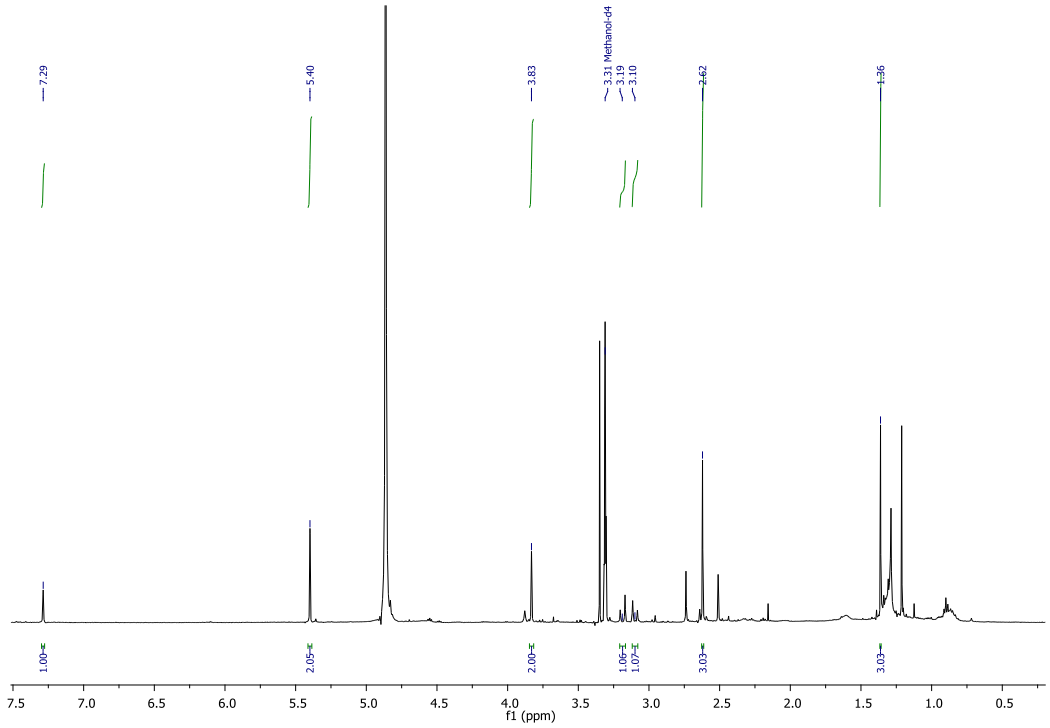

Figure S28. ^1H NMR (CD_3OD, 400 MHz) spectrum of compound **4**.

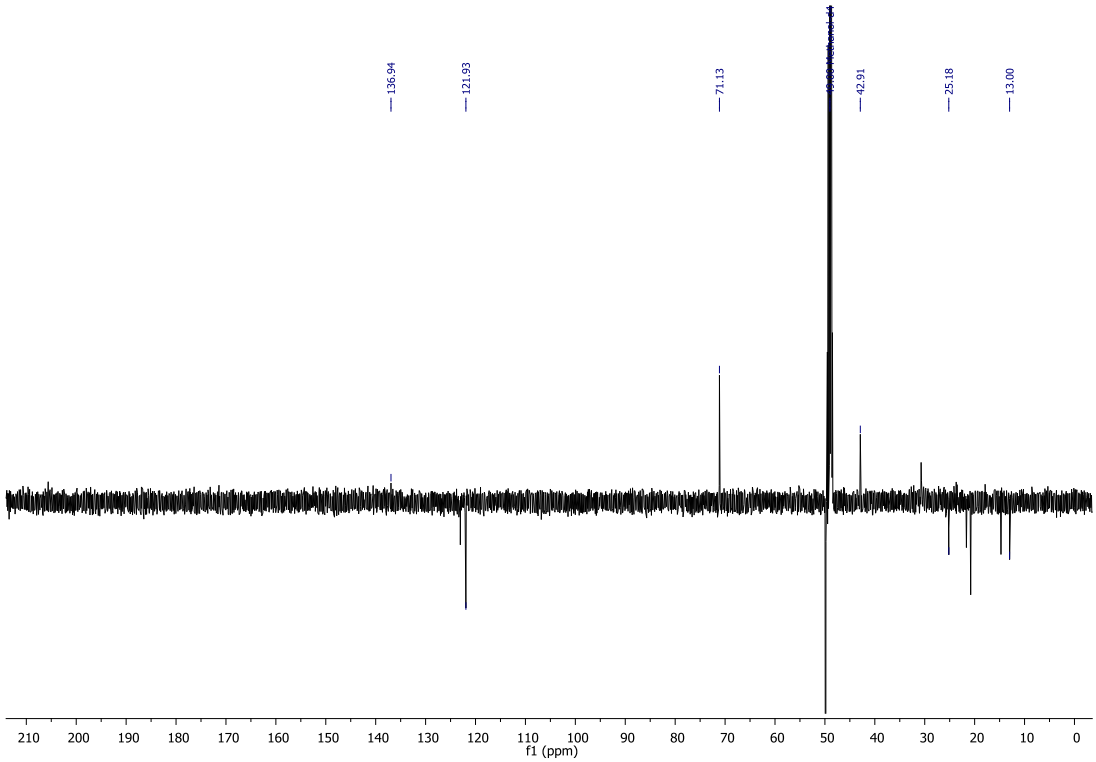

Figure S29. DEPTQ NMR (CD_3OD, 100 MHz) spectrum of compound **4**.

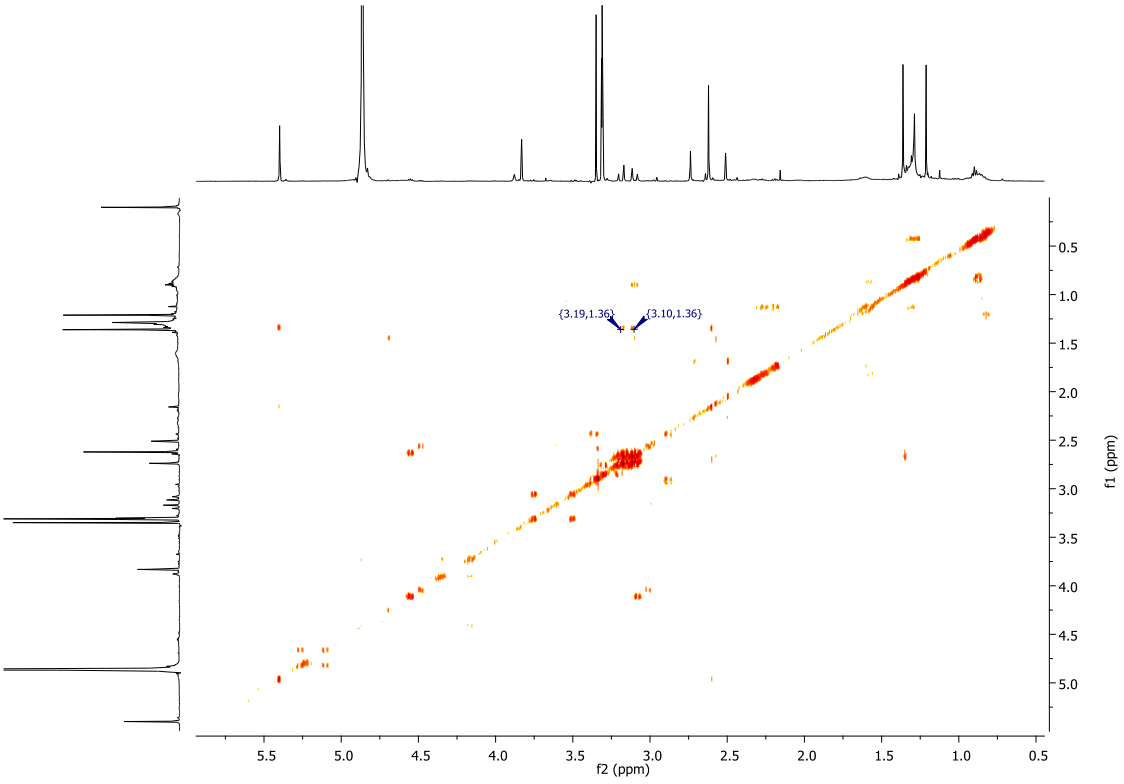

Figure S30. ^{1}H-^{1}H COSY NMR spectrum of compound **4**.

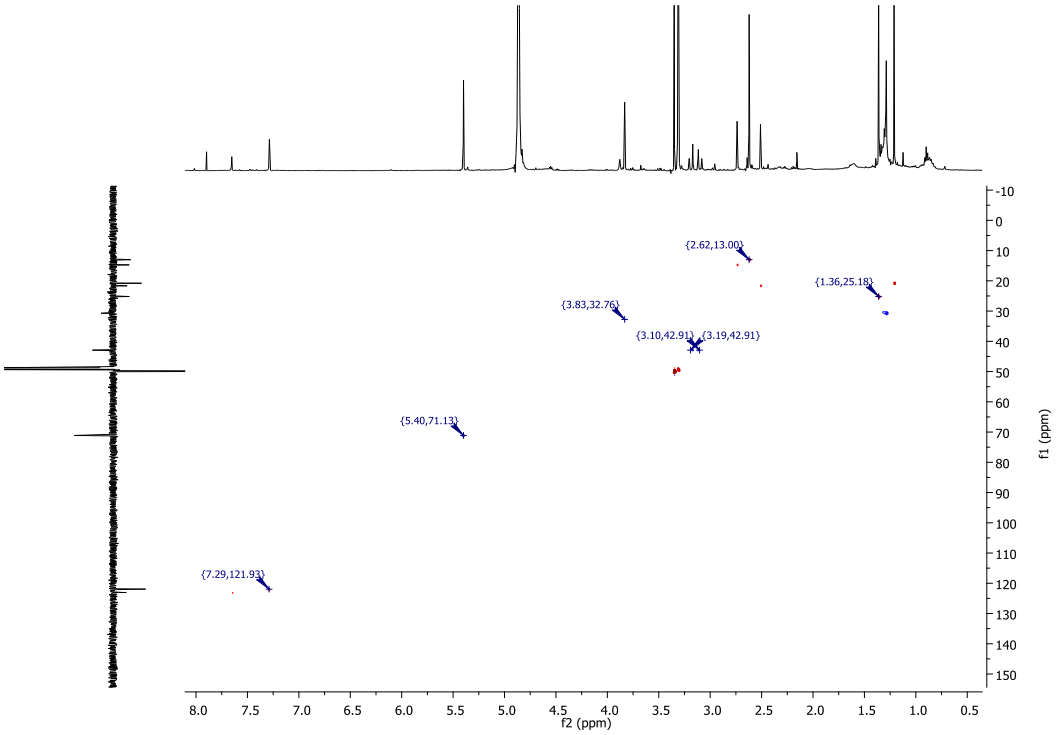

Figure S31. HSQC NMR spectrum of compound **4**.

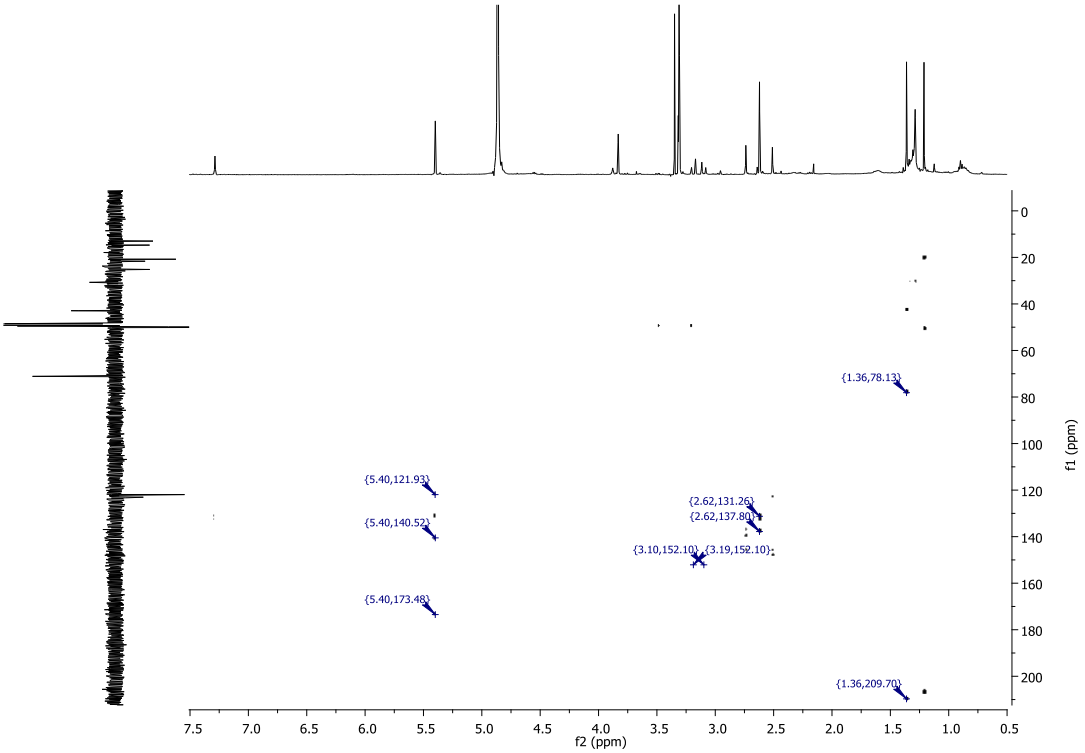

Figure S32. HMBC NMR spectrum of compound **4**.

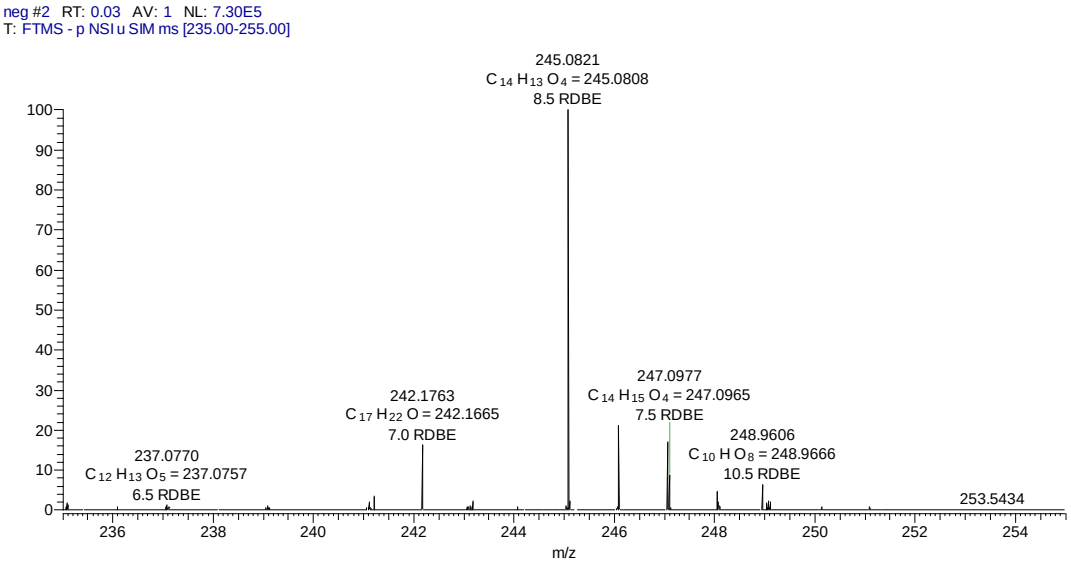

Figure S33. FT-ICR-MS spectrum of compound **4**.

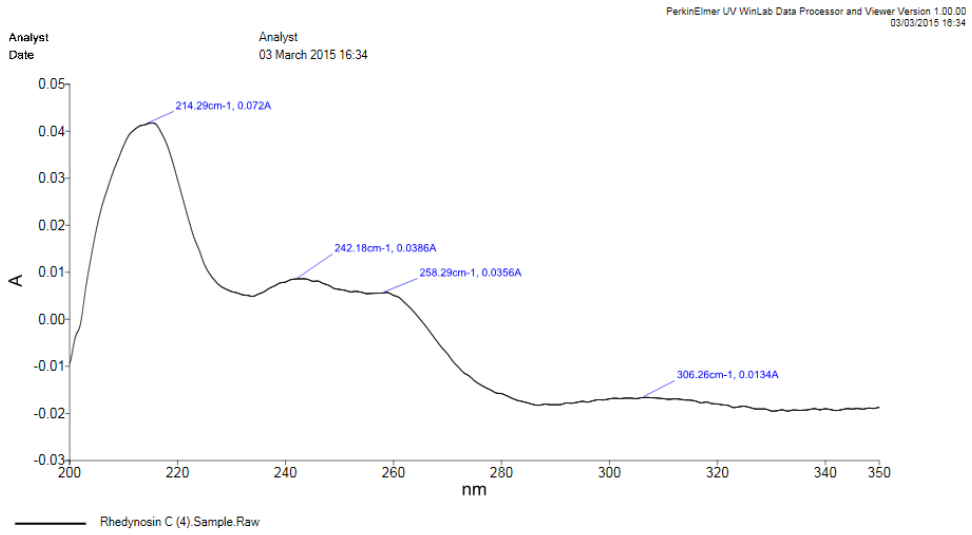

Figure S34. UV spectrum of compound **4** in CH_3OH.

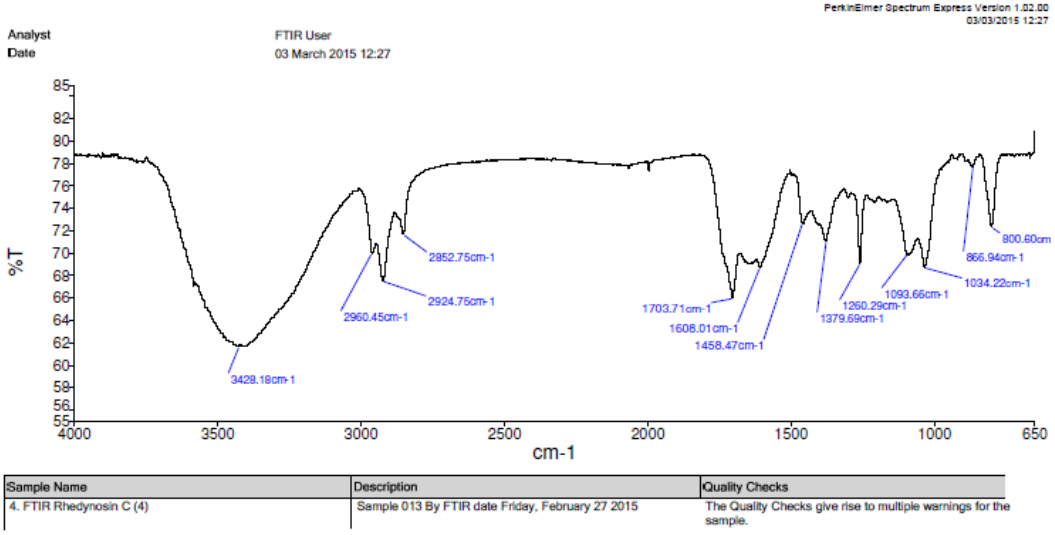

Figure S35. FT-IR spectrum of compound **4** in CH_3OH.

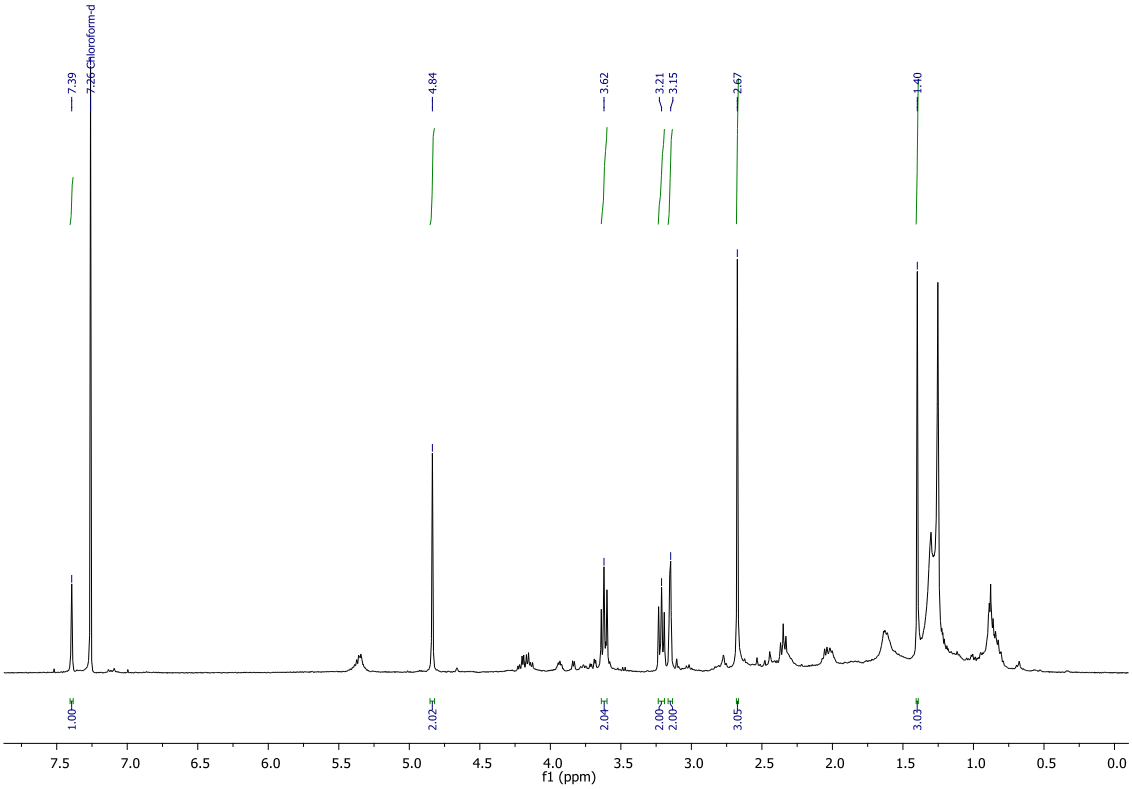

Figure S36. ^1H NMR ($CDCl_3$, 400 MHz) spectrum of compound **5**.

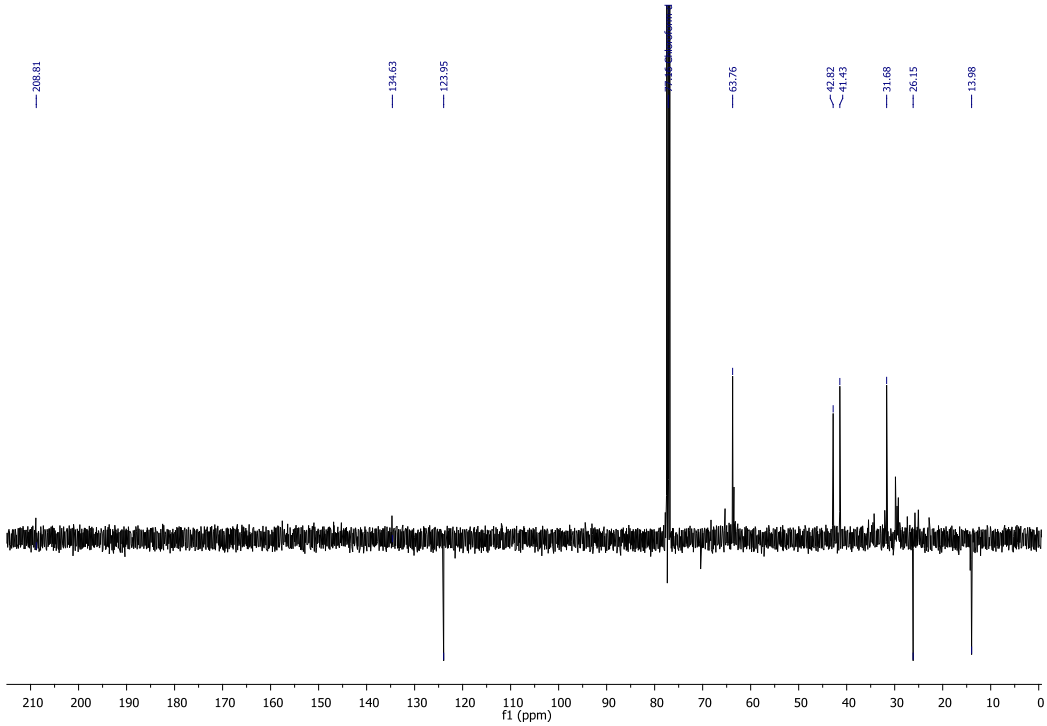

Figure S37. DEPTQ NMR ($CDCl_3$, 100 MHz) spectrum of compound **5**.

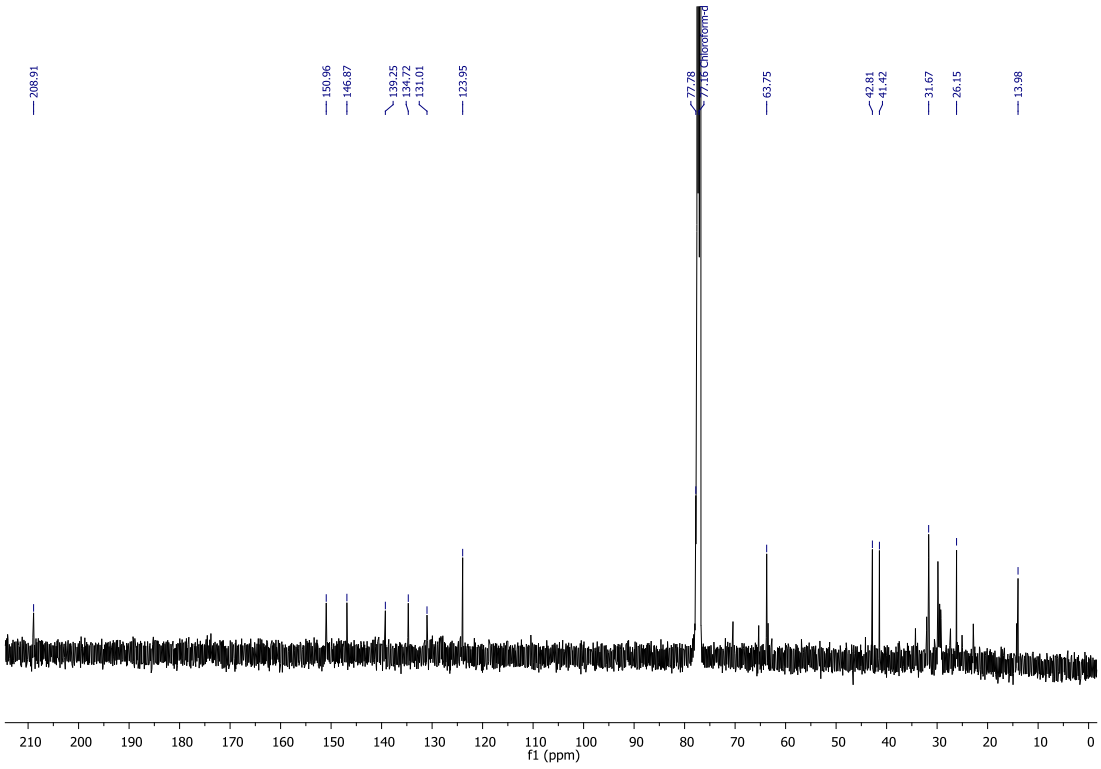

Figure S38. ^{13}C NMR ($CDCl_3$, 100 MHz) spectrum of compound **5**.

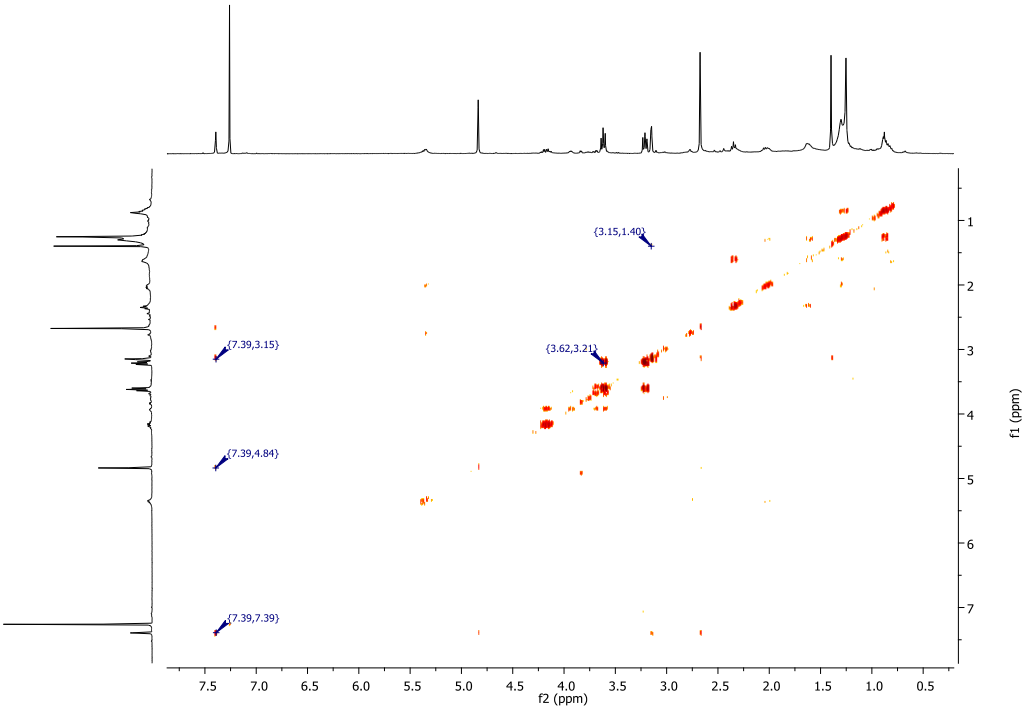

Figure S39. ^{1}H-^{1}H COSY NMR spectrum of compound **5**.

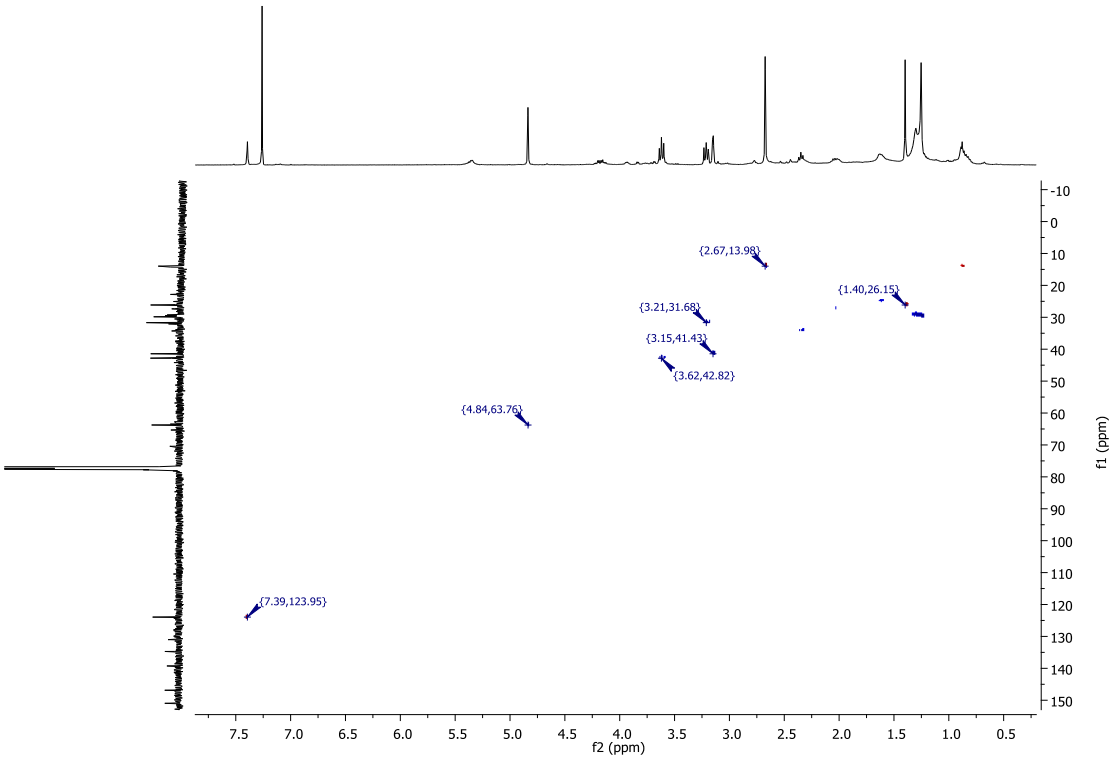

Figure S40. HSQC NMR spectrum of compound **5**.

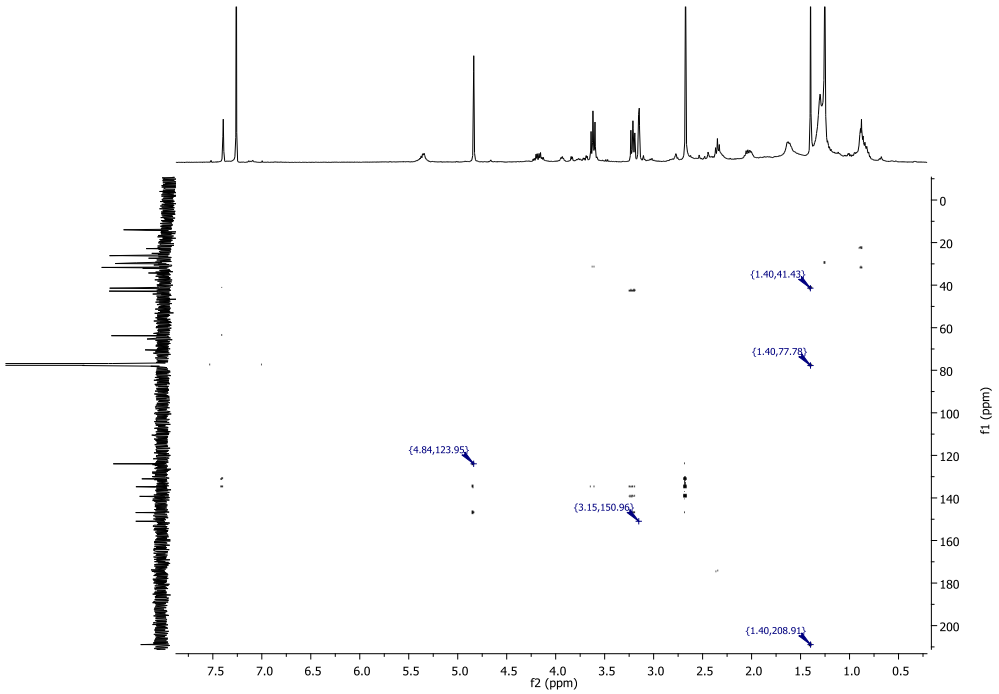

Figure S41. HMBC NMR spectrum of compound **5**.

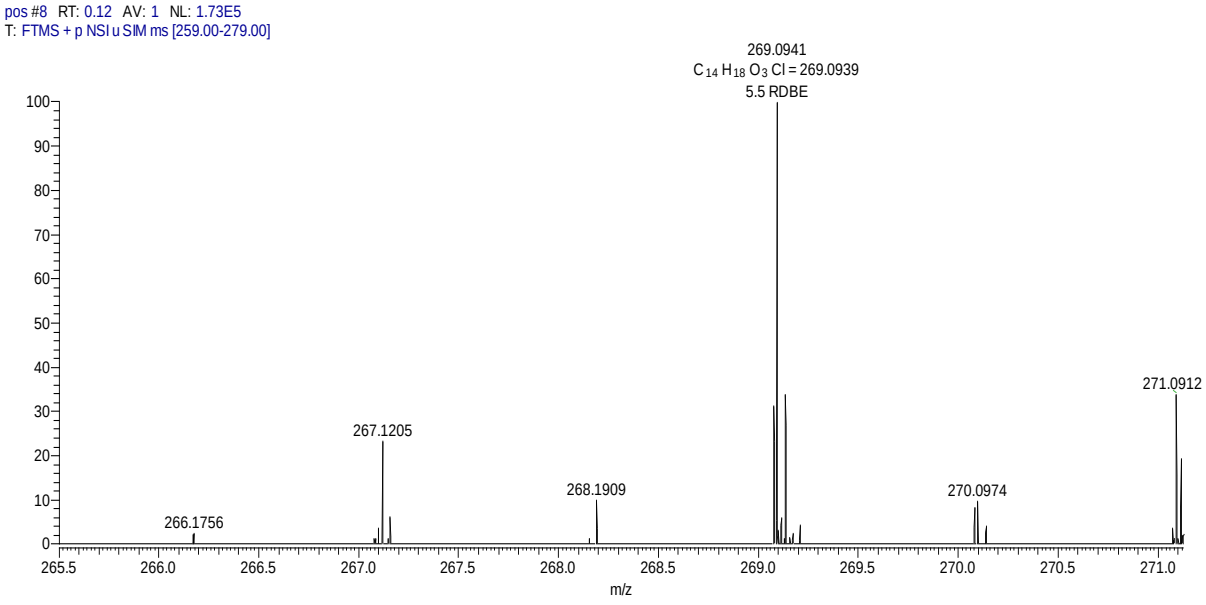

Figure S42. FT-ICR-MS spectrum of compound **5**.

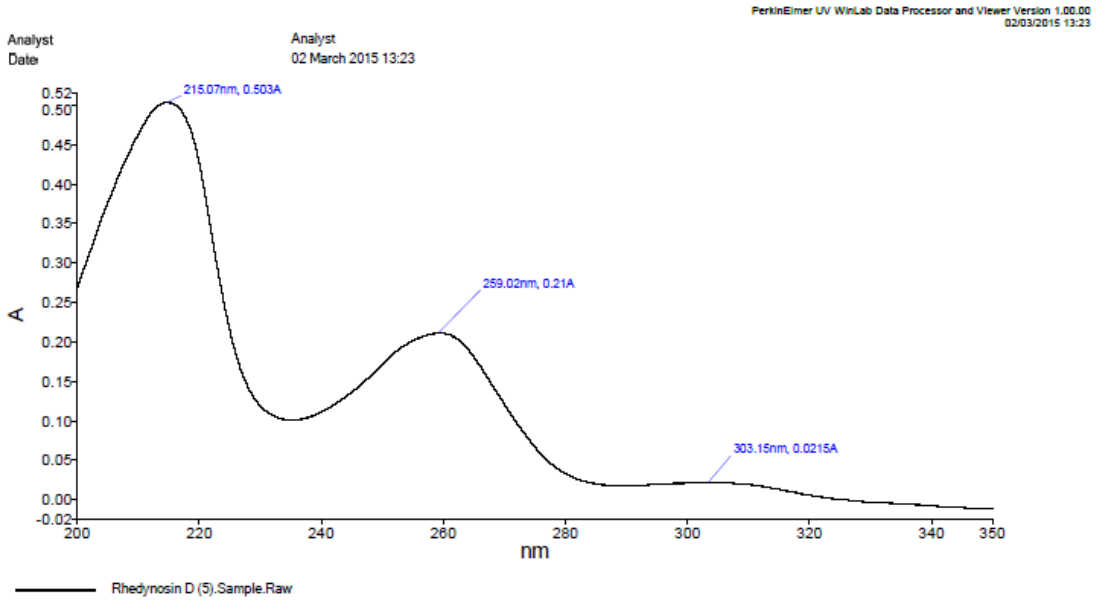

Figure S43. UV spectrum of compound **5** in CH_3OH.

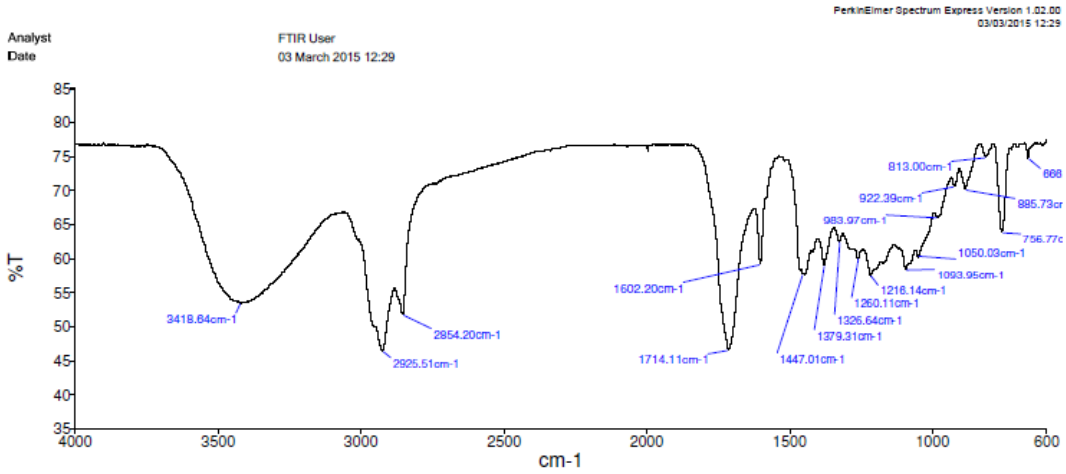

Sample Name	Description	Quality Checks
5. FTIR Rhedynosin D (5)	Sample 015 By FTIR date Friday, February 27 2015	The Quality Checks give rise to multiple warnings for the sample.

Figure S44. FT-IR spectrum of compound **5** in $CHCl_3$.

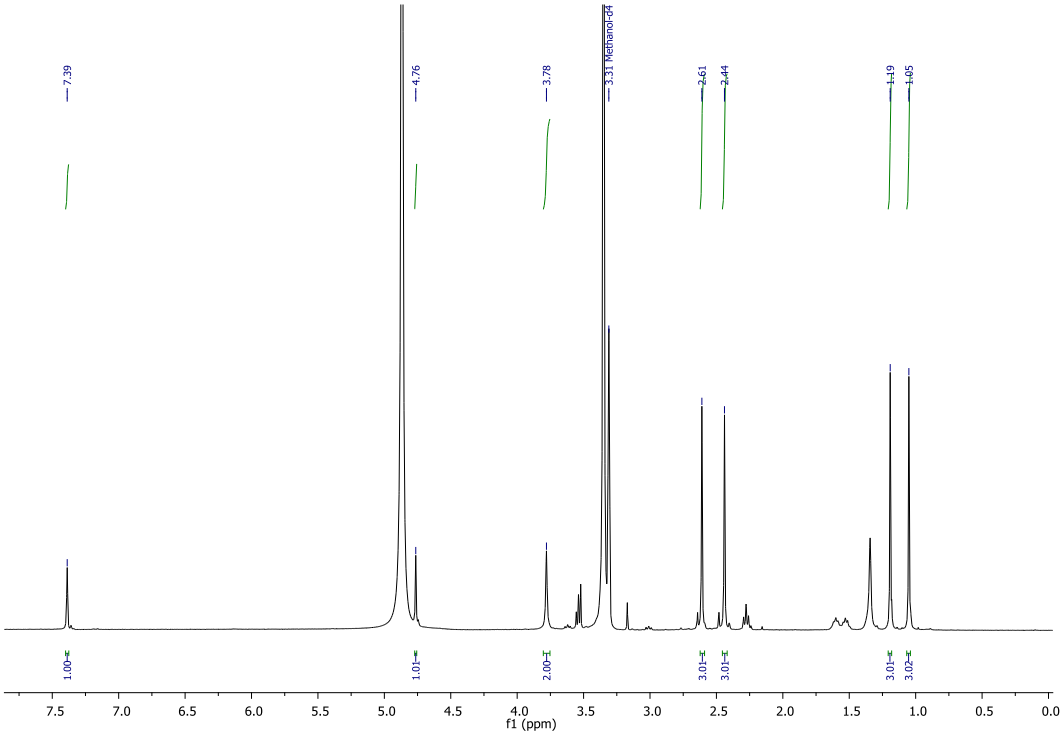

Figure S45. ^{1}H NMR (CD_3OD, 400 MHz) spectrum of compound **6**.

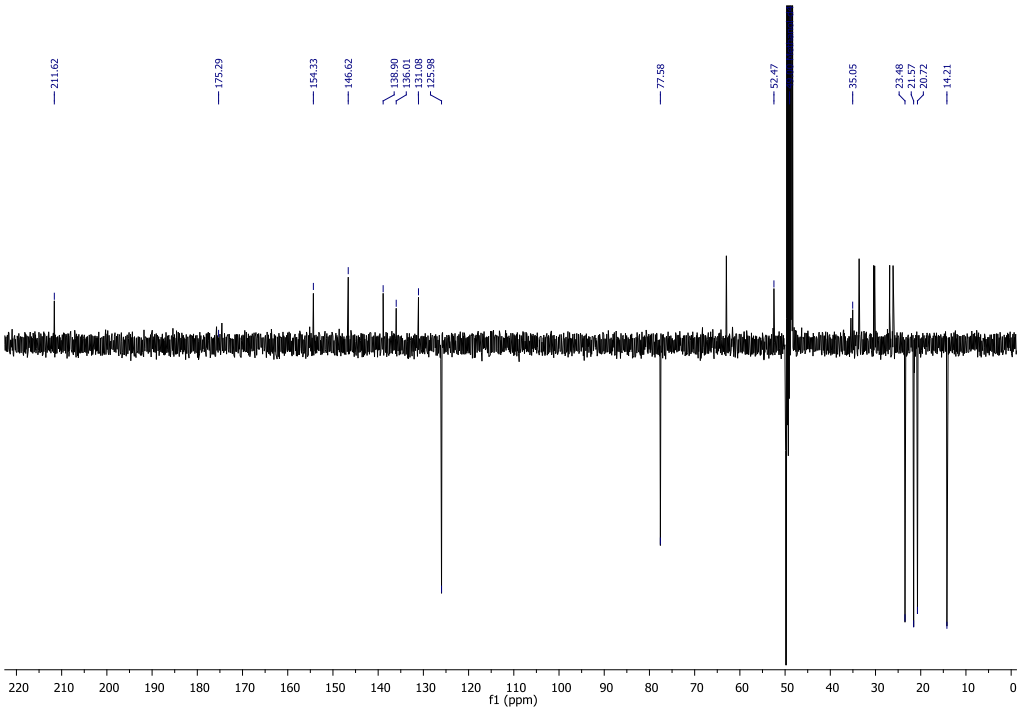

Figure S46. DEPTQ NMR (CD_3OD, 100 MHz) spectrum of compound **6**.

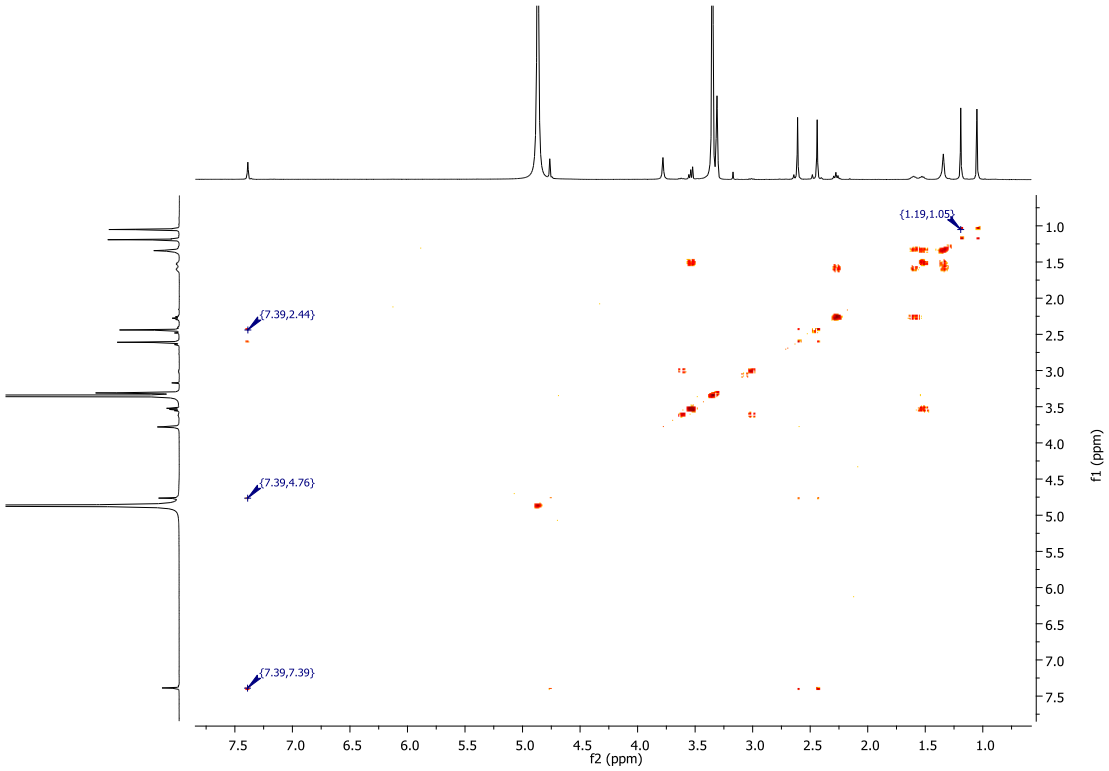

Figure S47. ^{1}H-^{1}H COSY NMR spectrum of compound **6**.

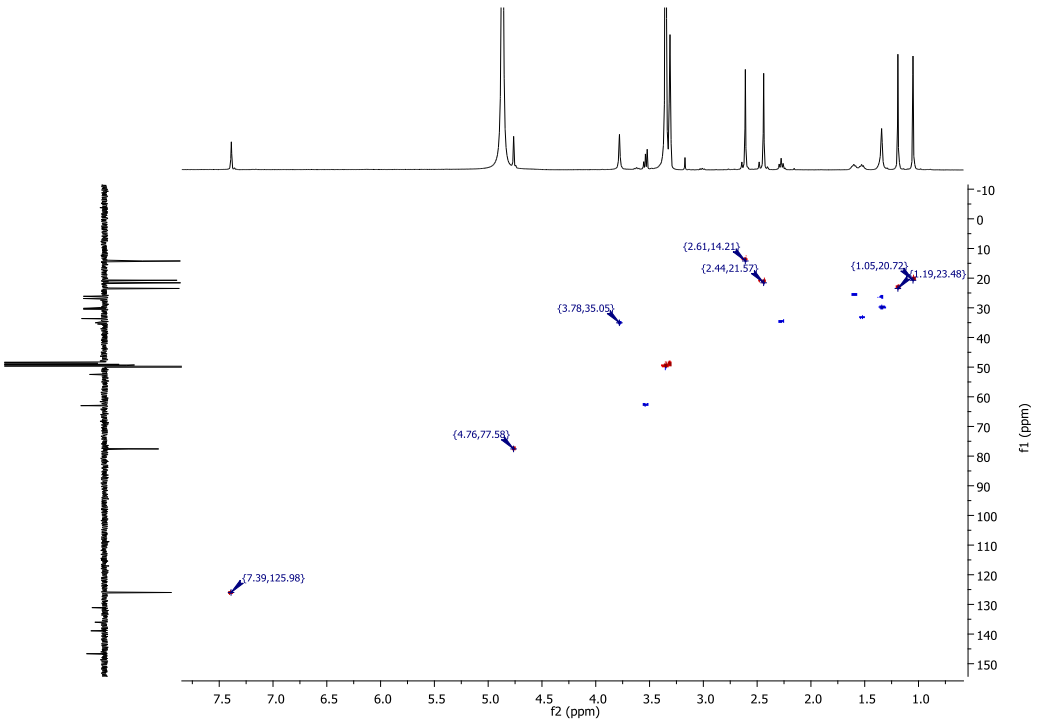

Figure S48. HSQC NMR spectrum of compound **6**.

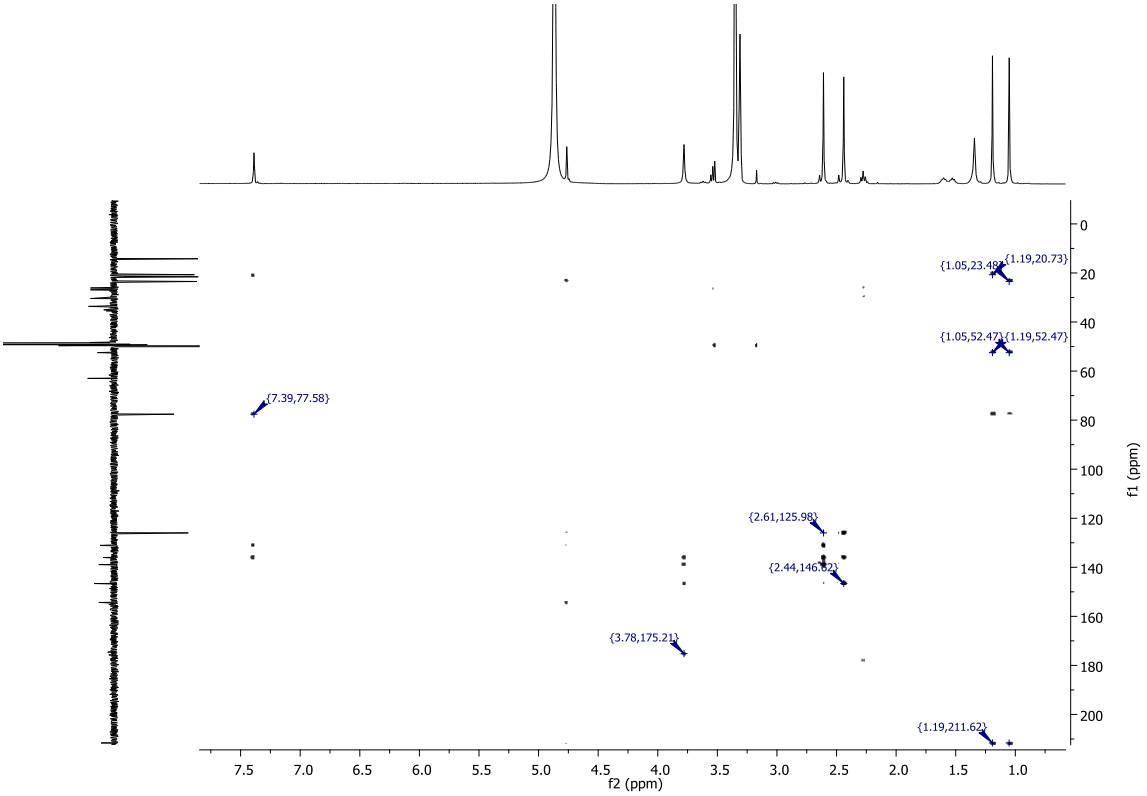

Figure S49. HMBC NMR spectrum of compound **6**.

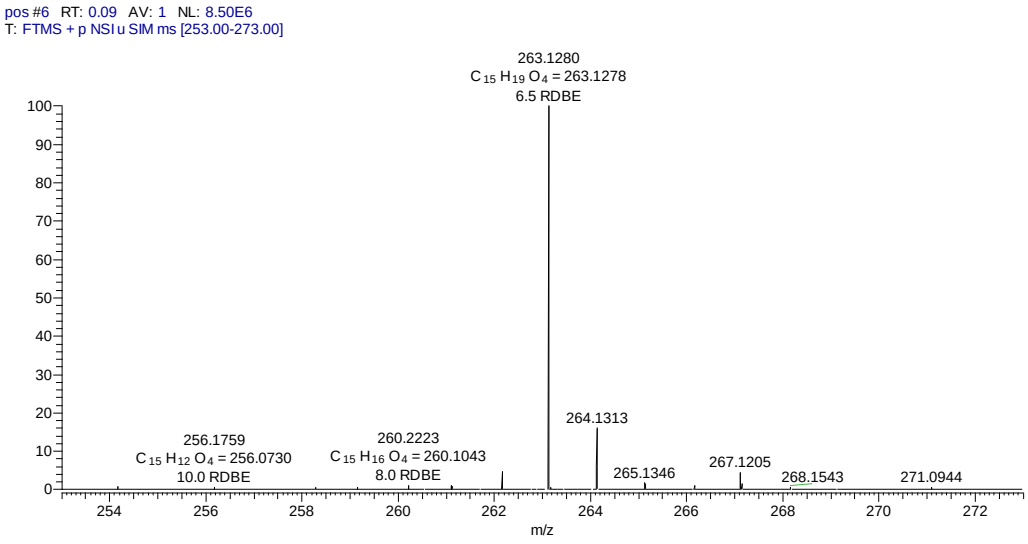

Figure S50. FT-ICR-MS spectrum of compound **6**.

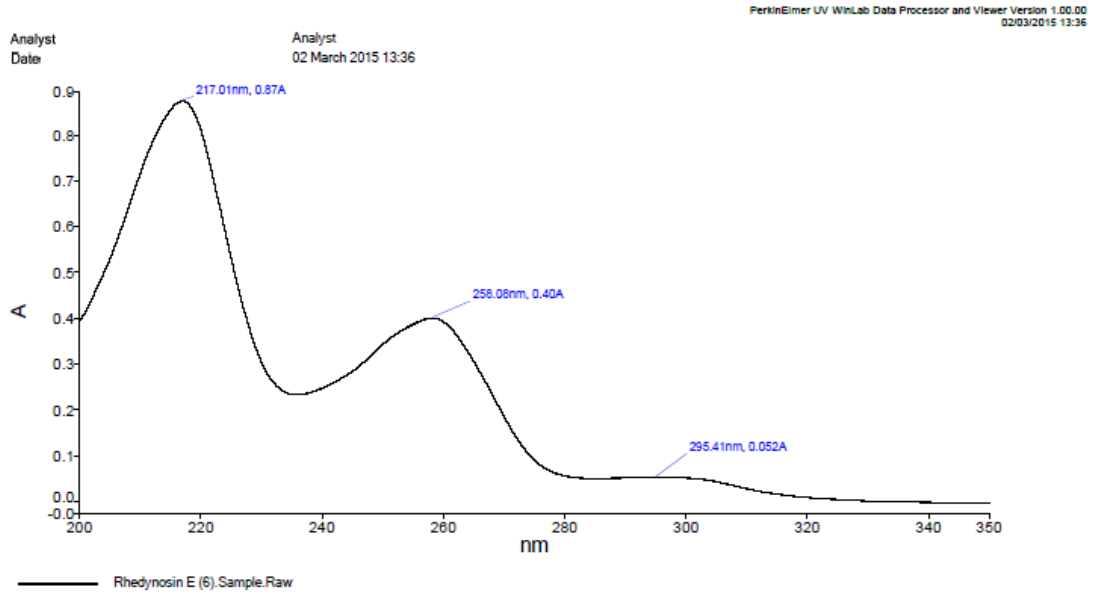

Figure S51. UV spectrum of compound **6** in CH_3OH.

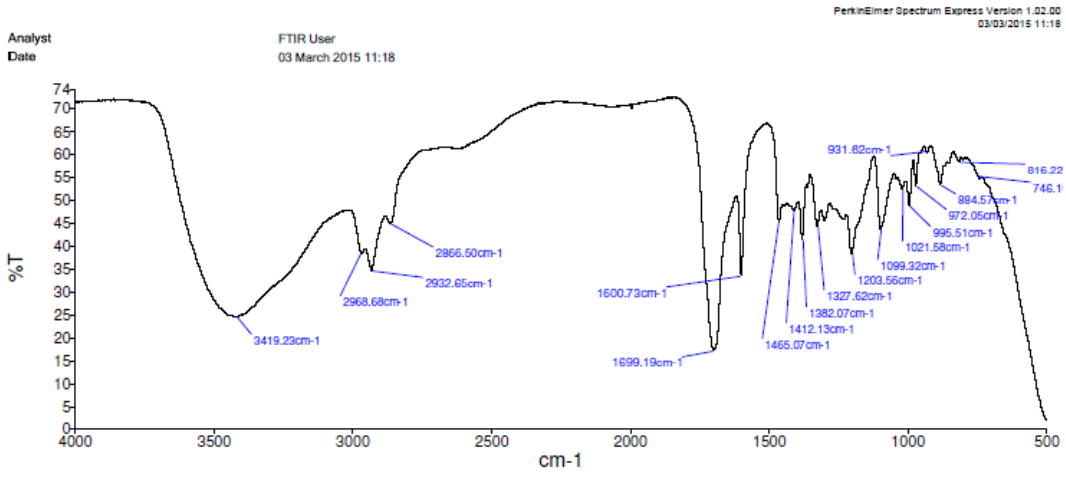

Sample Name	Description	Quality Checks
6. FTIR Rhedynosin E (6)	Sample 016 By FTIR date Friday, February 27 2015	The Quality Checks give rise to multiple warnings for the sample.

Figure S52. FT-IR spectrum of compound **6** in CH_3OH.

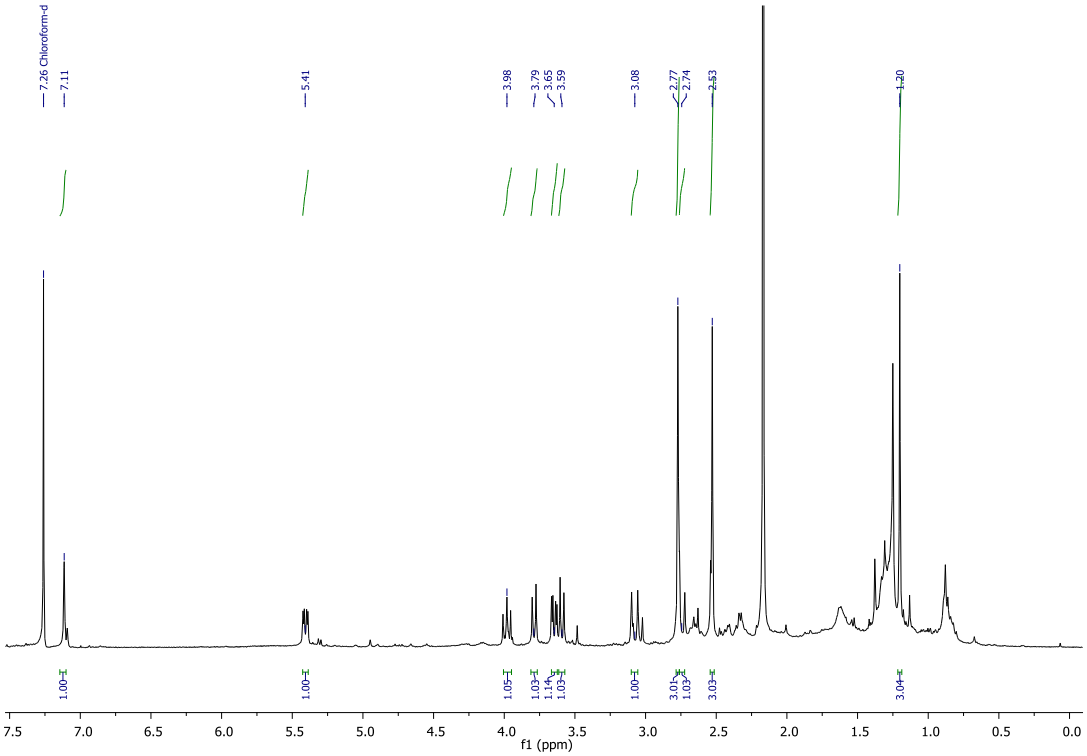

Figure S53. ^{1}H NMR ($CDCl_3$, 400 MHz) spectrum of compound **7**.

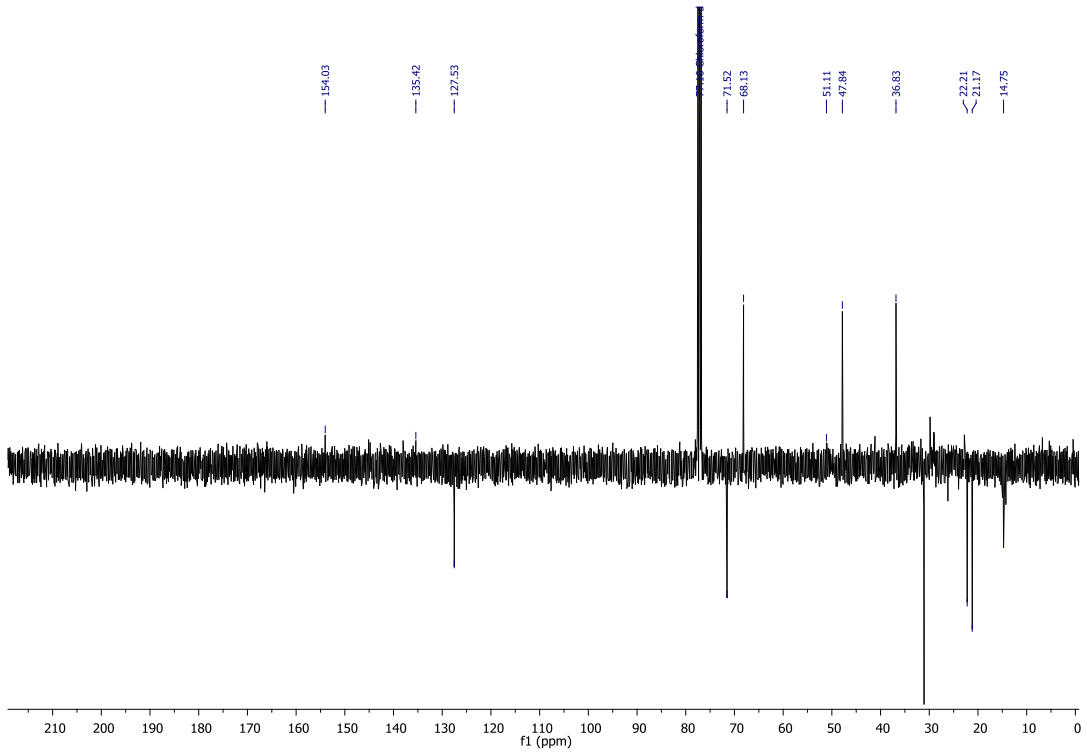

Figure S54. DEPTQ NMR ($CDCl_3$, 100 MHz) spectrum of compound **7**.

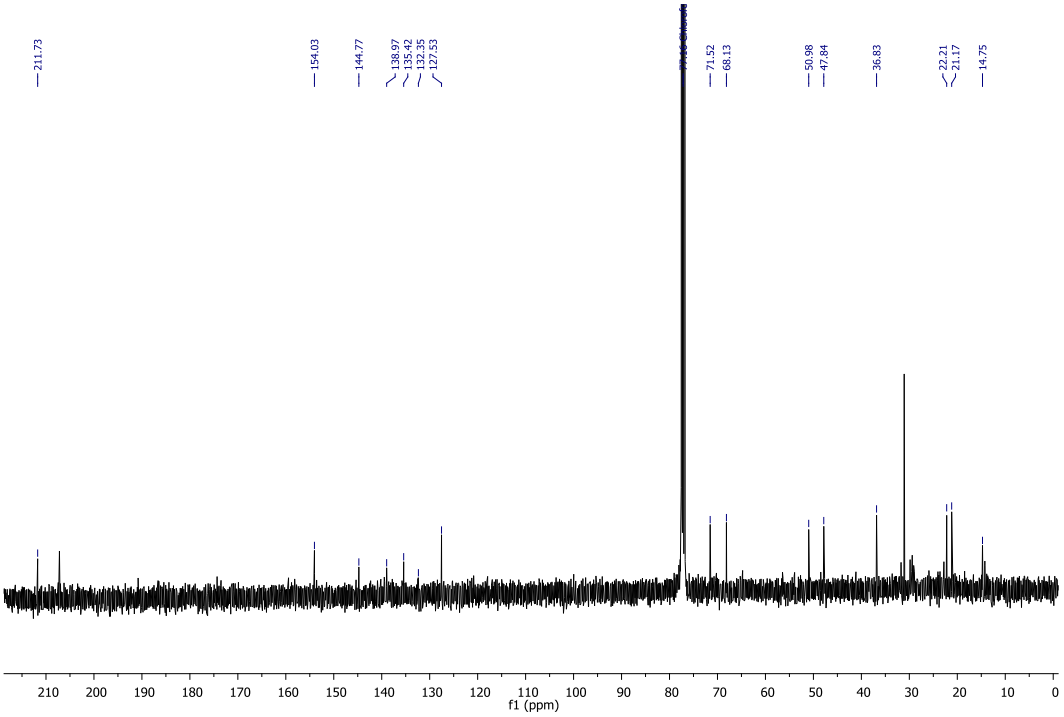

Figure S55. ^{13}C NMR ($CDCl_3$, 100 MHz) spectrum of compound **7**.

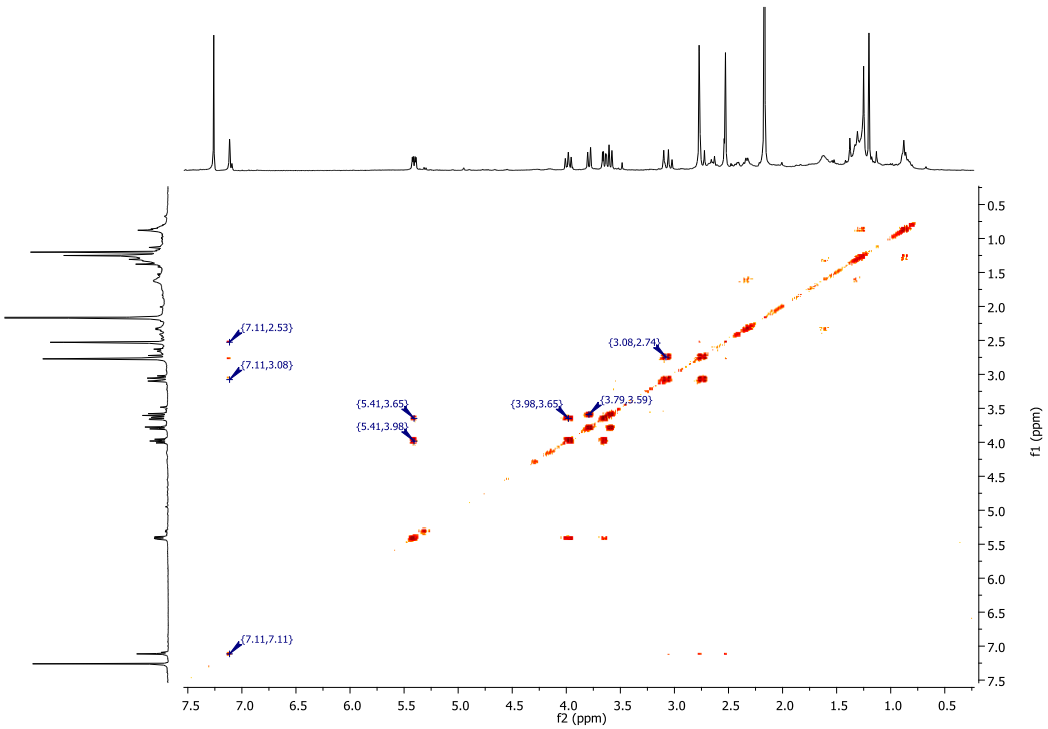

Figure S56. ^{1}H-^{1}H COSY NMR spectrum of compound **7**.

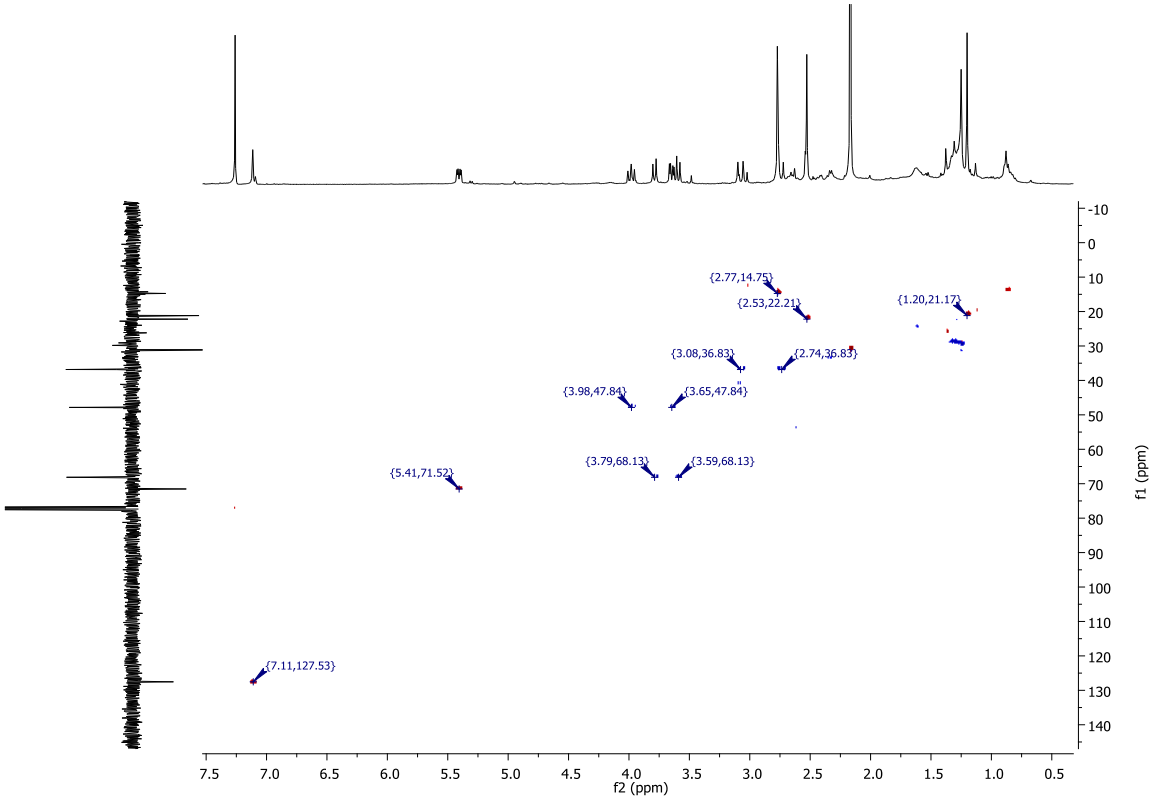

Figure S57. HSQC NMR spectrum of compound **7**.

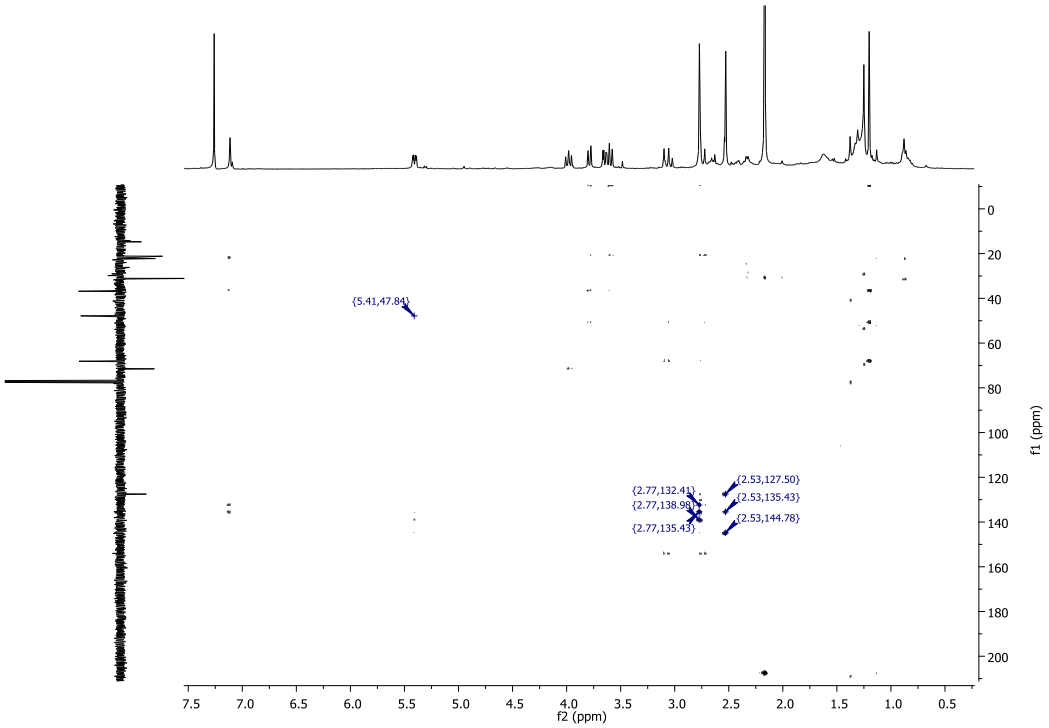

Figure S58. HMBC NMR spectrum of compound **7**.

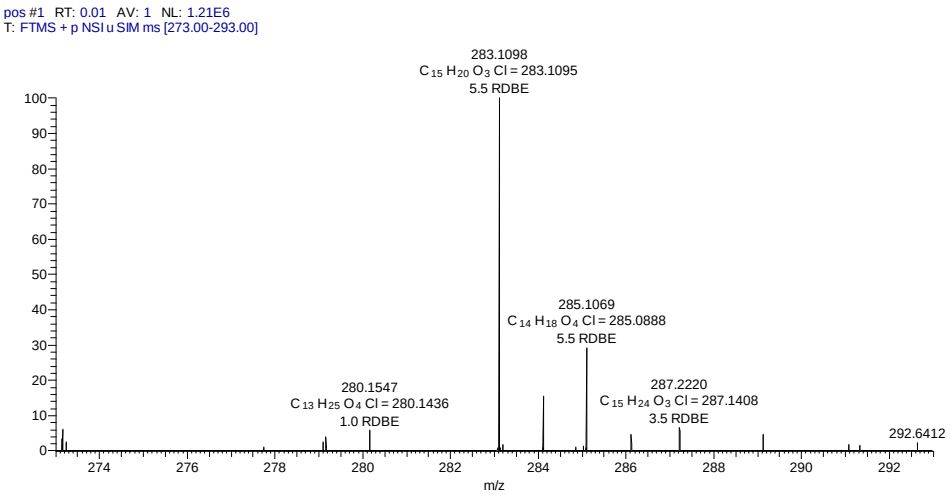

Figure S59. FT-ICR-MS spectrum of compound **7**.

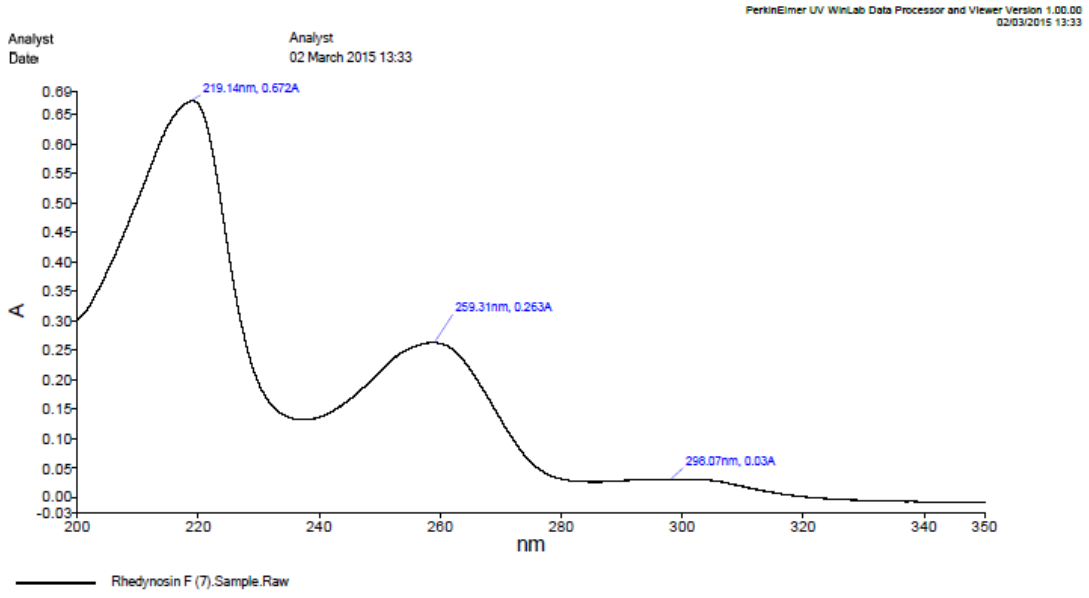

Figure S60. UV spectrum of compound **7** in CH_3OH.

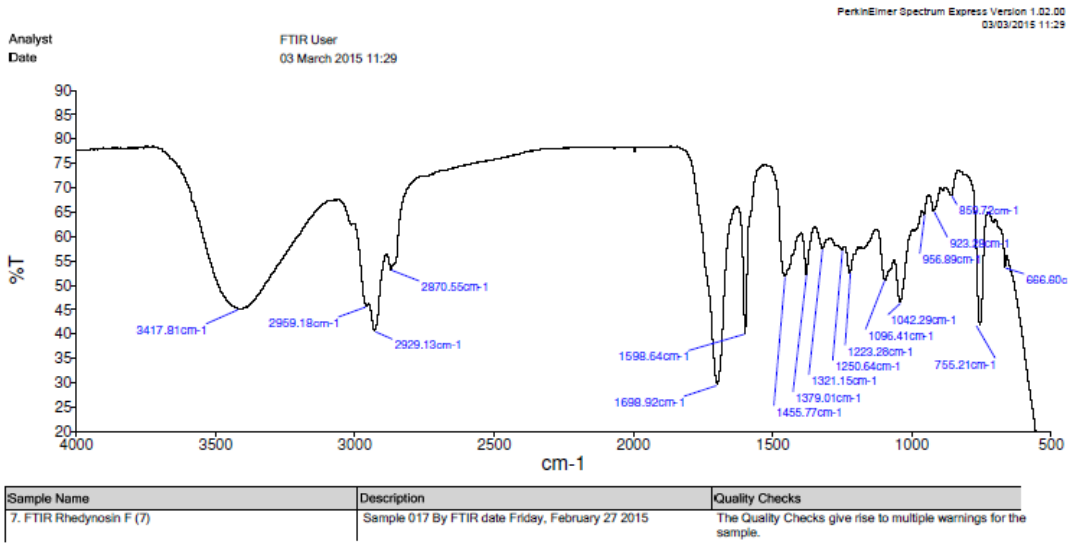

Figure S61. FT-IR spectrum of compound **7** in $CHCl_3$.

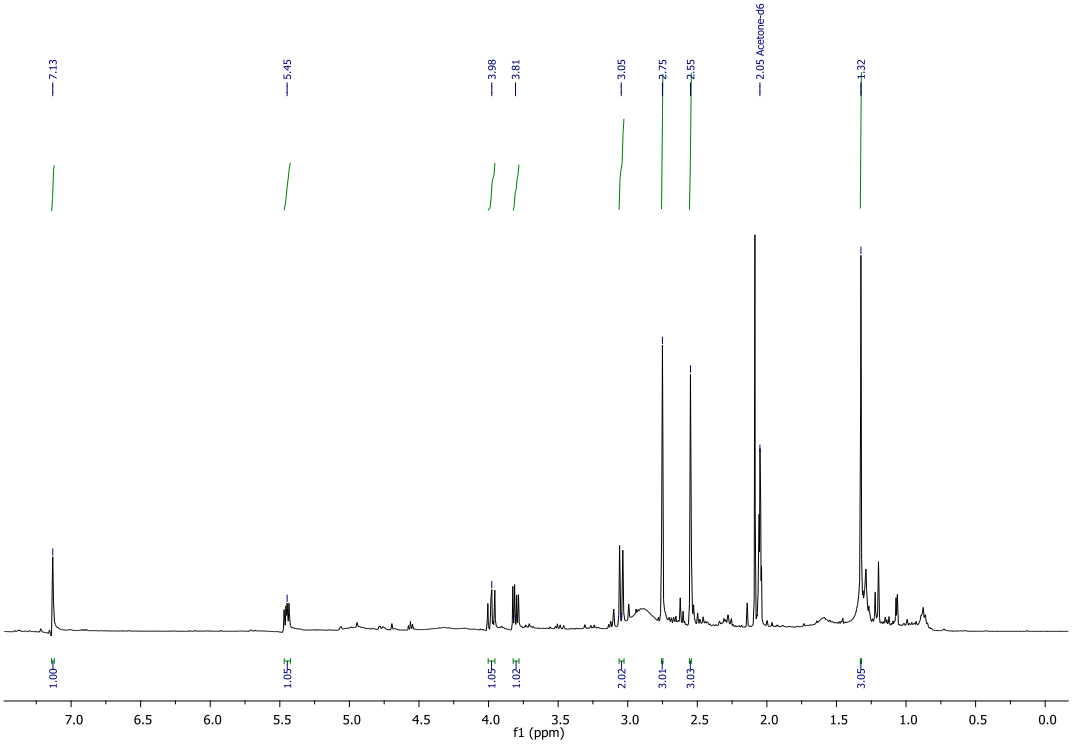

Figure S62. ^1H NMR ($(CD_3)_2CO$, 400 MHz) spectrum of compound **8**.

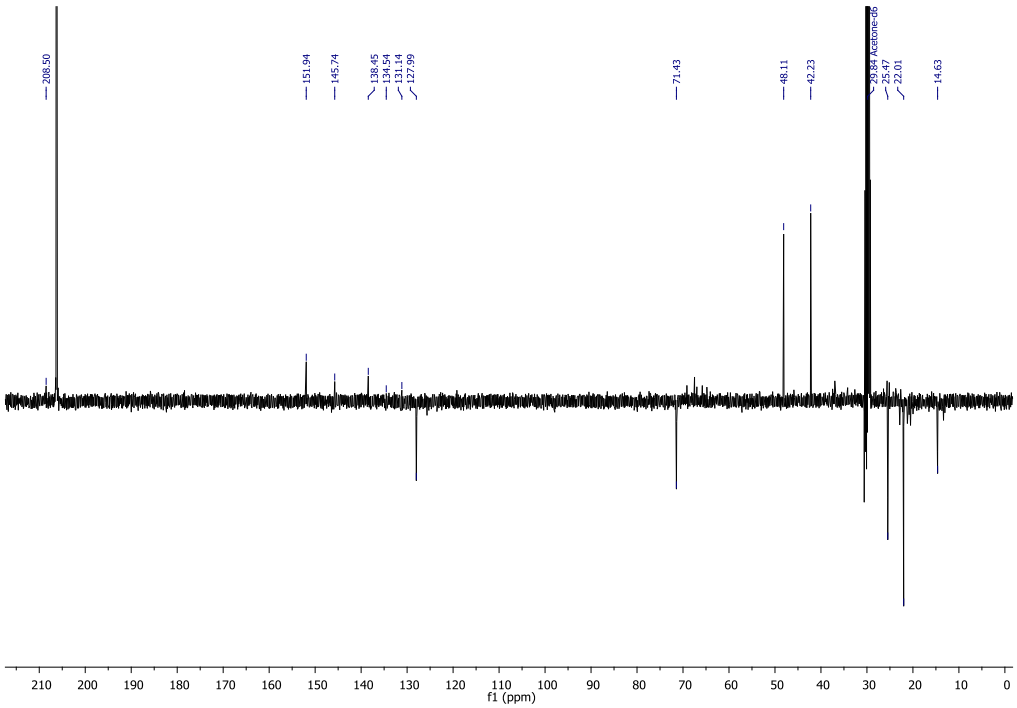

Figure S63. DEPTQ NMR ($(CD_3)_2CO$, 100 MHz) spectrum of compound **8**.

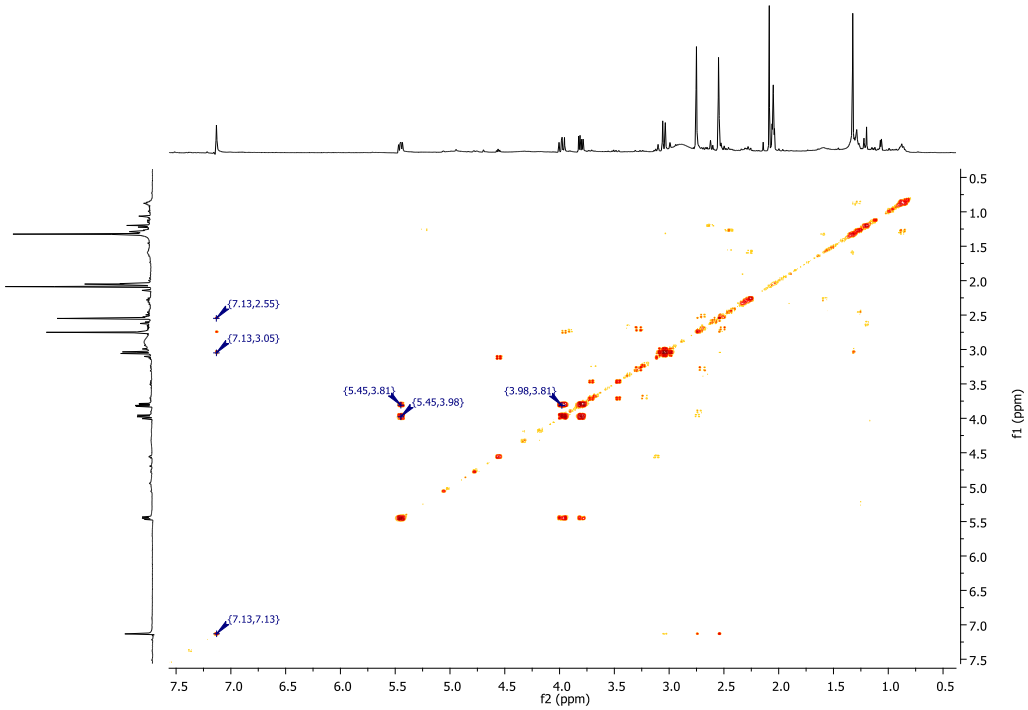

Figure S64. ^{1}H-^{1}H COSY NMR spectrum of compound **8**.

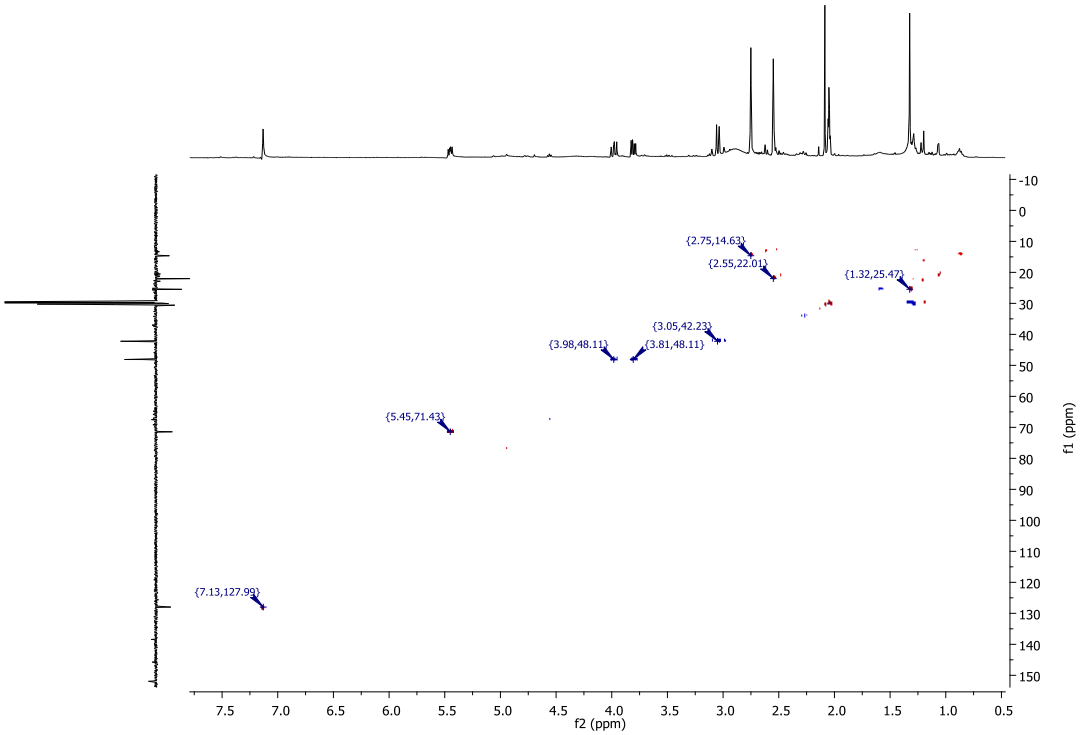

Figure S65. HSQC NMR spectrum of compound **8**.

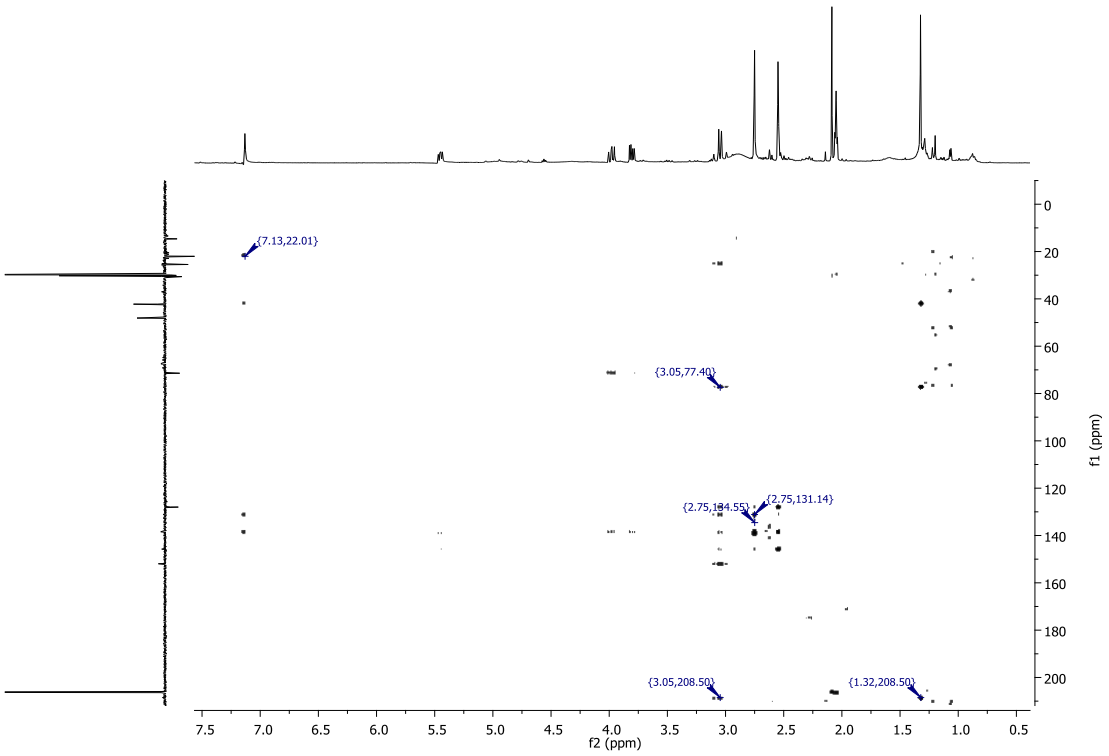

Figure S66. HMBC NMR spectrum of compound **8**.

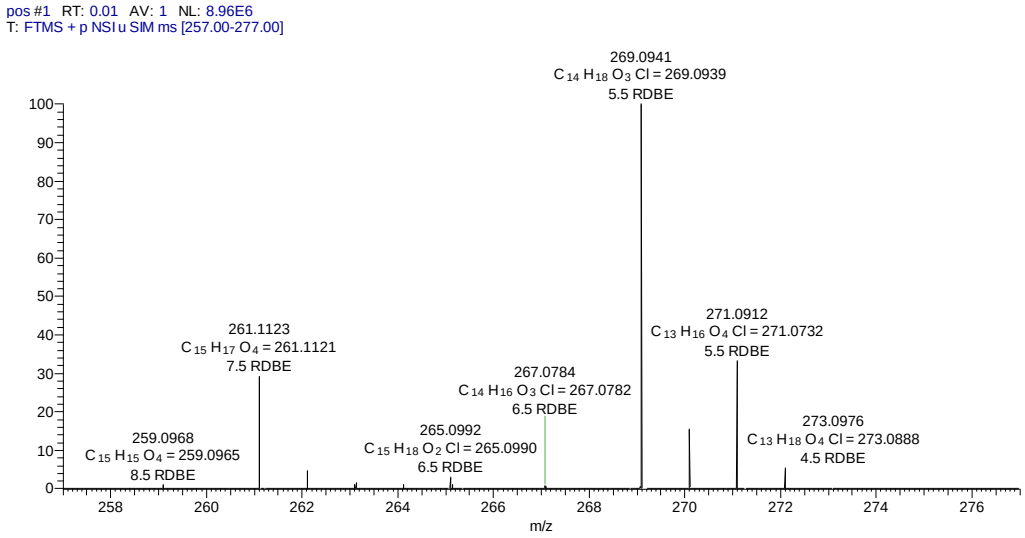

Figure S67. FT-ICR-MS spectrum of compound **8**.

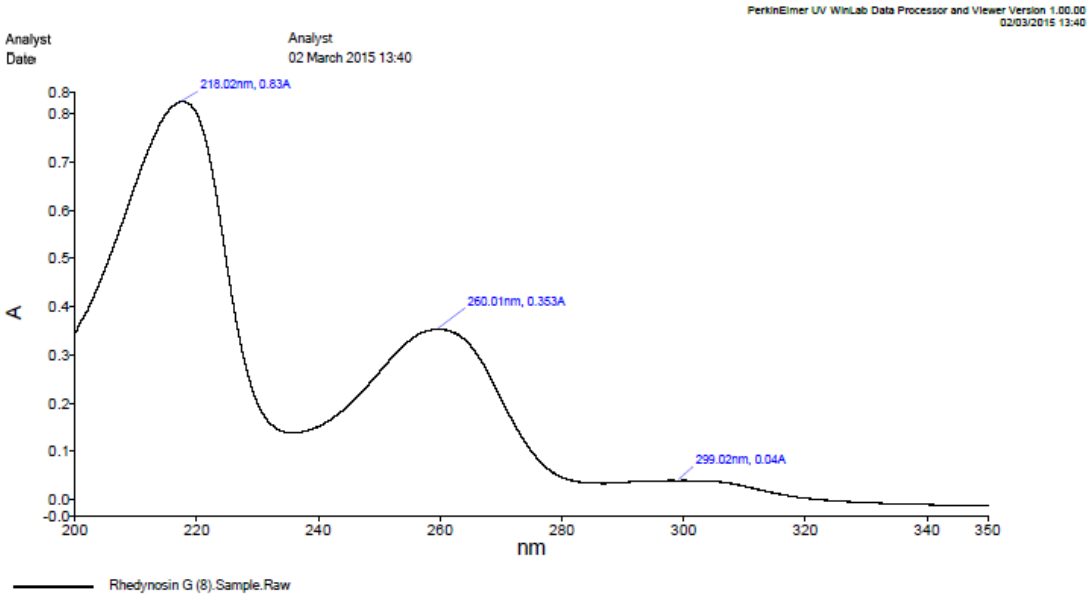

Figure S68. UV spectrum of compound **8** in CH_3OH.

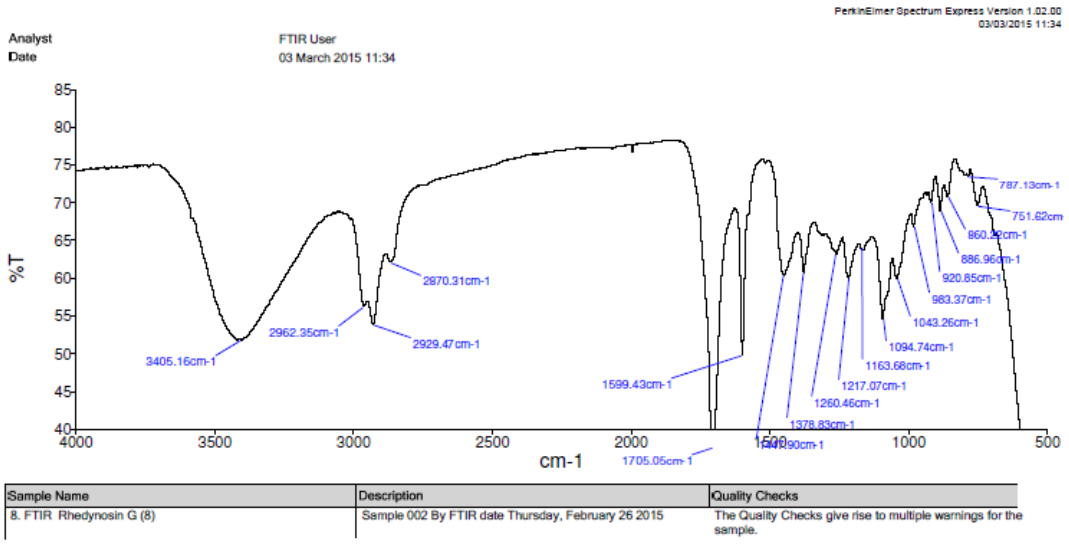

Figure S69. FT-IR spectrum of compound **8** in CH_3OH.

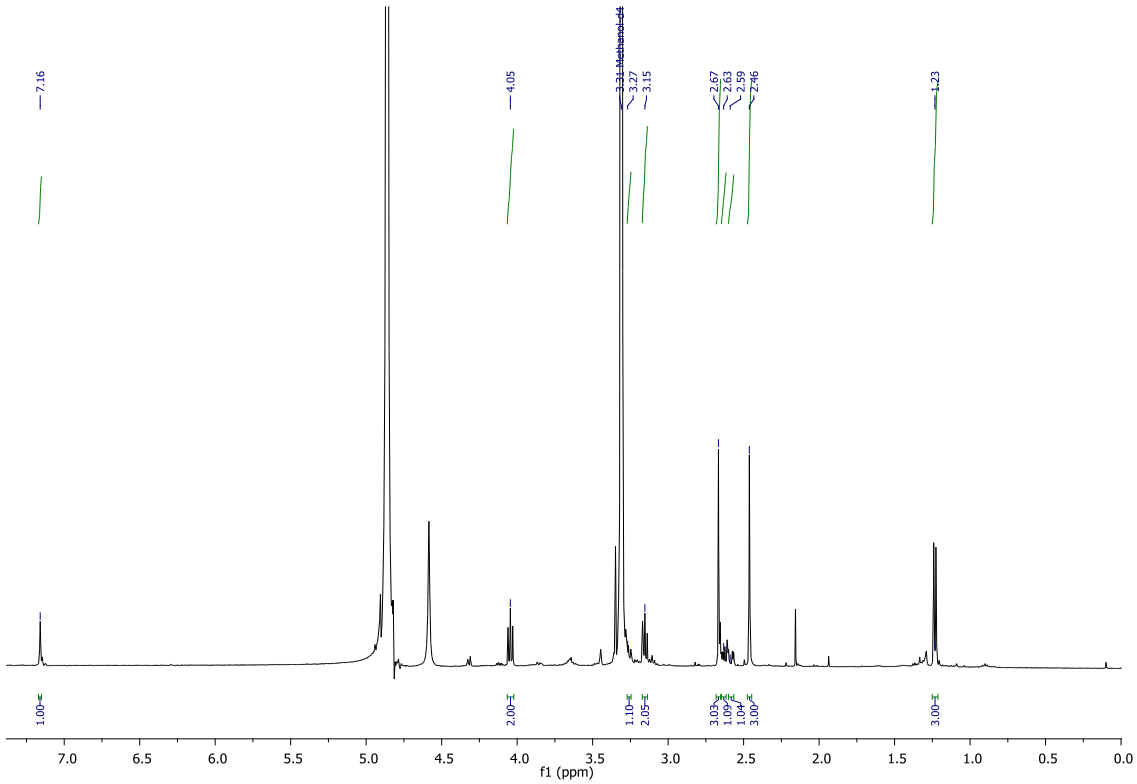

Figure S70. ^1H NMR (CD_3OD, 500 MHz) spectrum of compound **9**.

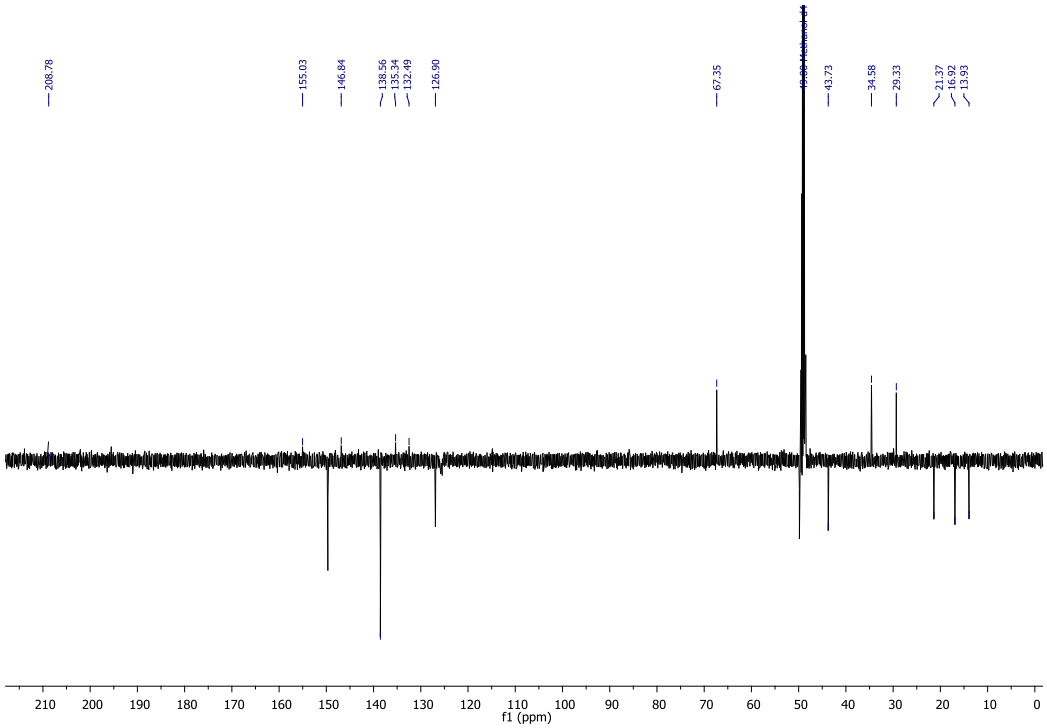

Figure S71. DEPTQ NMR (CD_3OD, 125 MHz) spectrum of compound **9**.

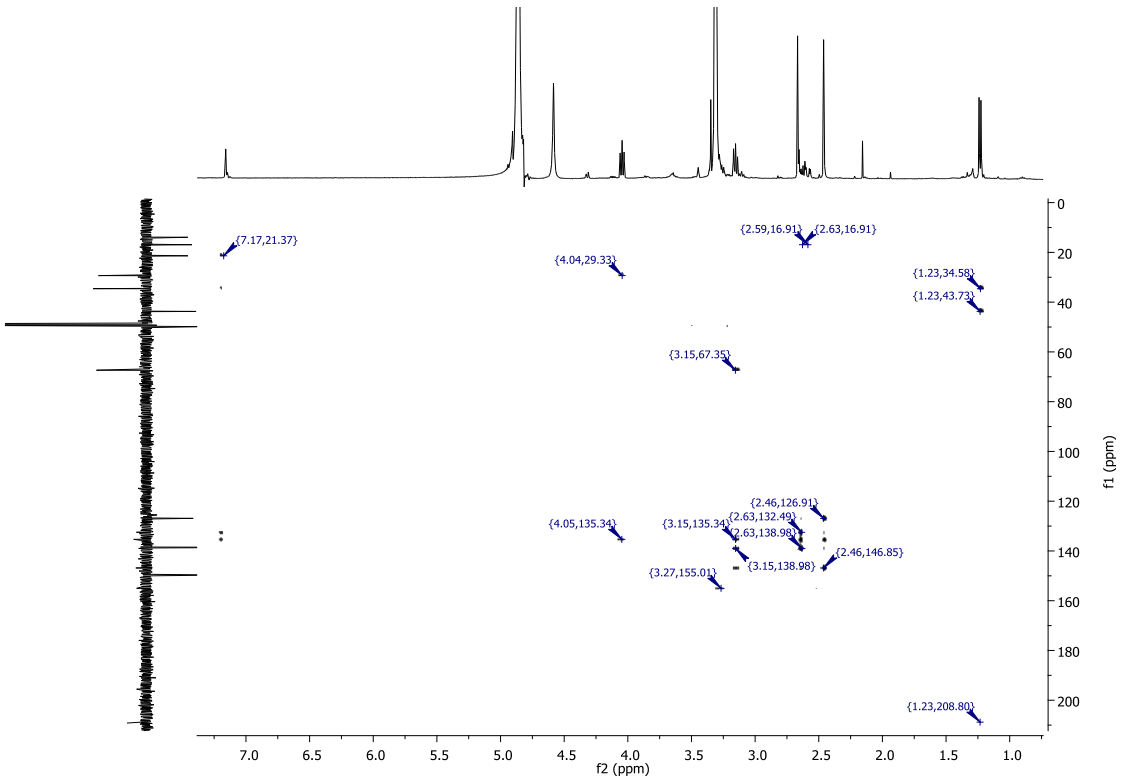

Figure S72. HMBC NMR spectrum of compound **9**.

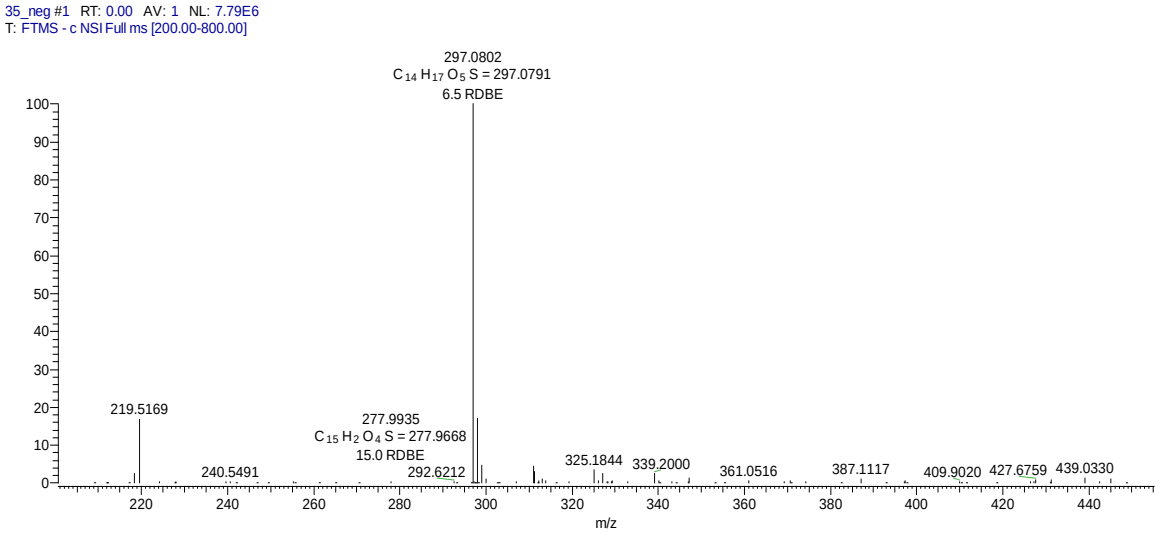

Figure S73. FT-ICR-MS spectrum of compound **9**.

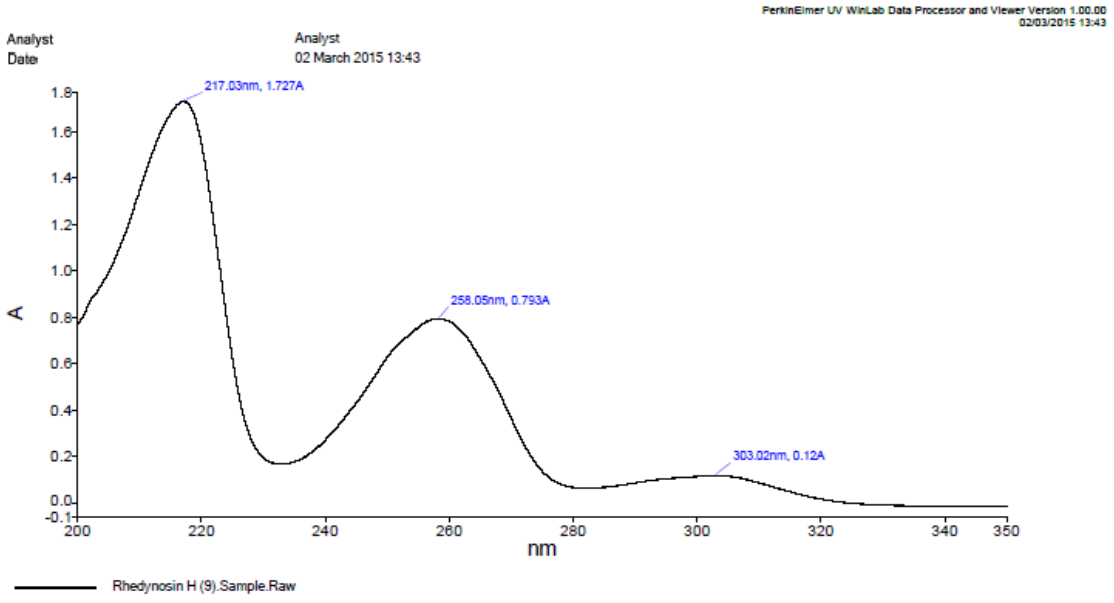

Figure S74. UV spectrum of compound **9** in CH_3OH.

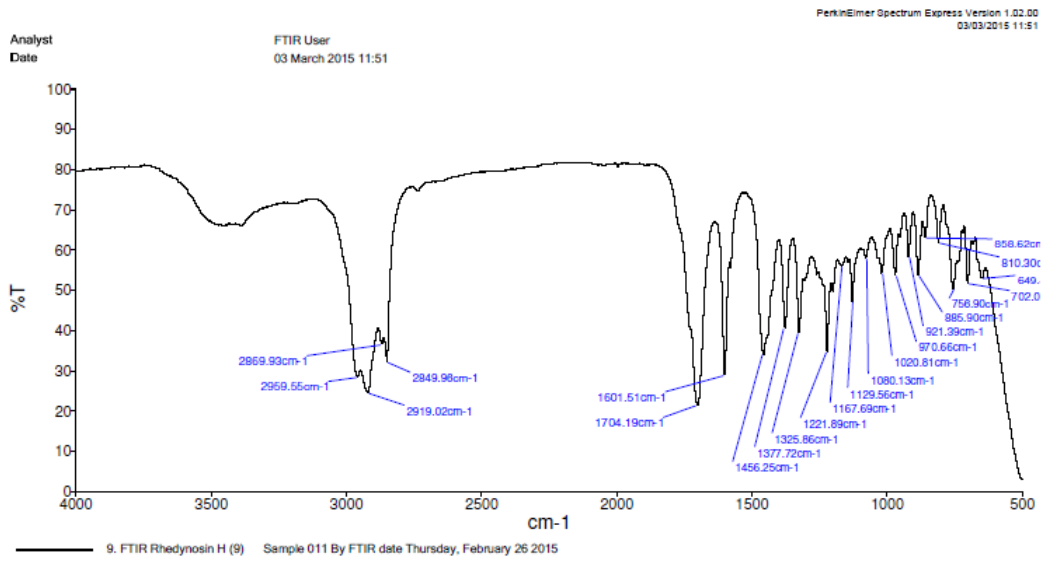

Figure S75. FT-IR spectrum of compound **9** in CH_3OH.

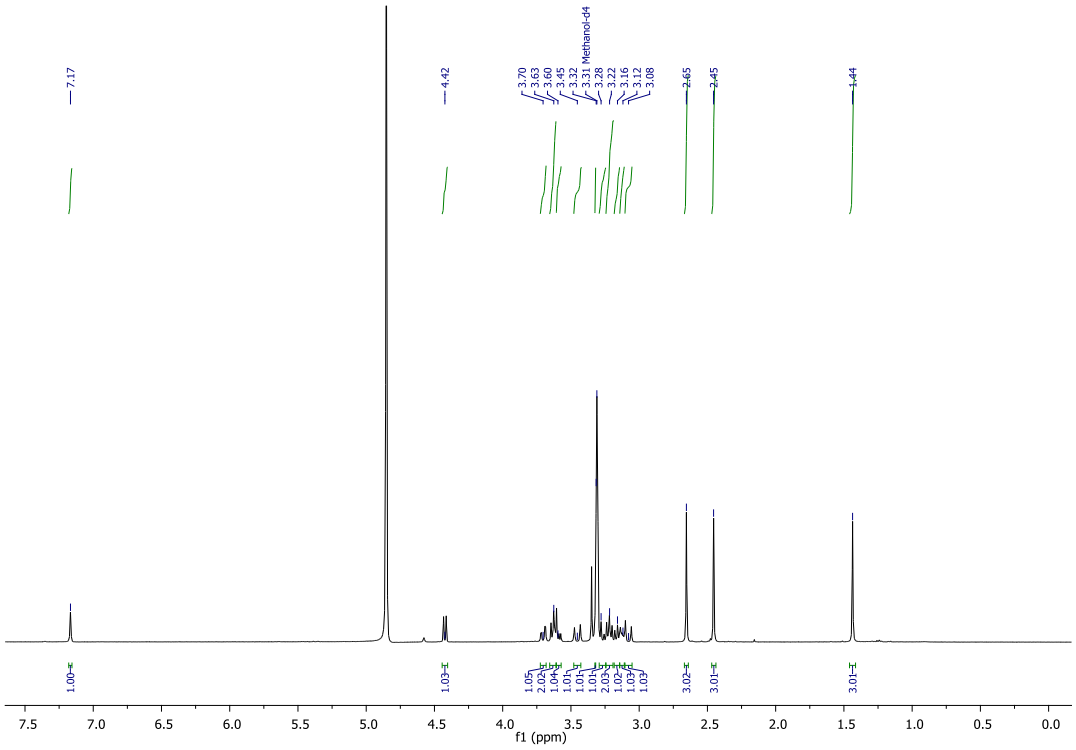

Figure S76. ^{1}H NMR (CD_3OD, 400 MHz) spectrum of compound **10**.

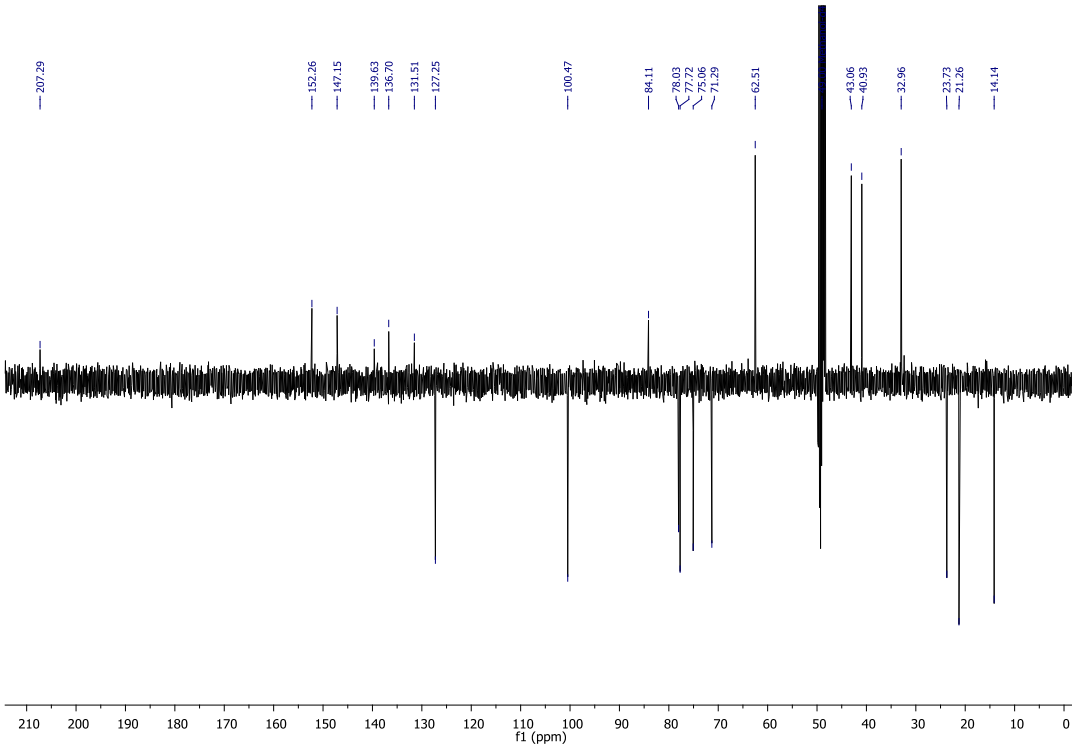

Figure S77. DEPTQ NMR (CD_3OD, 100 MHz) spectrum of compound **10**.

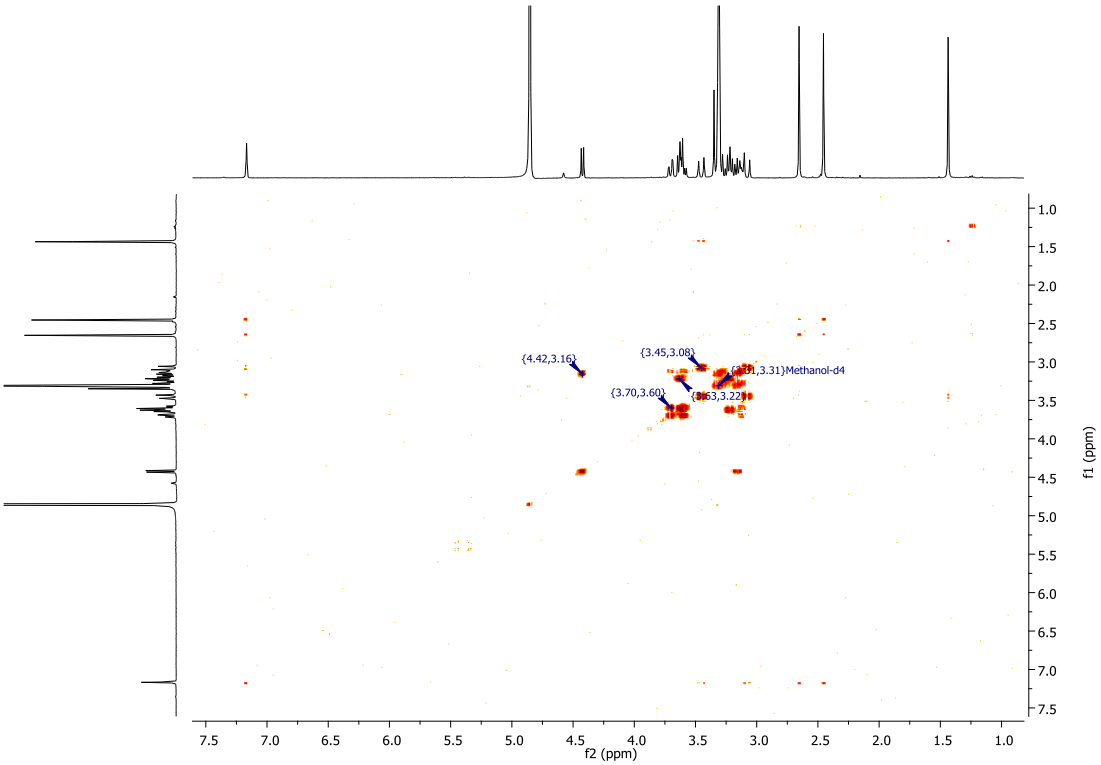

Figure S78. ^1H-^1H COSY NMR spectrum of compound **10**.

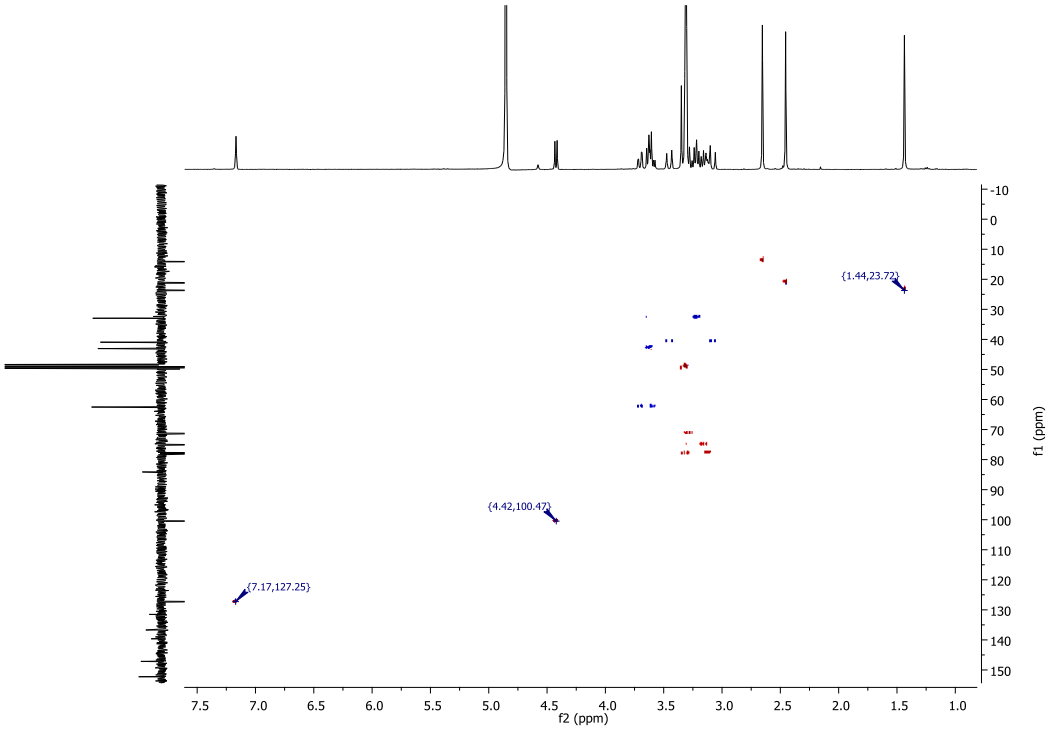

Figure S79. HSQC NMR spectrum of compound **10**.

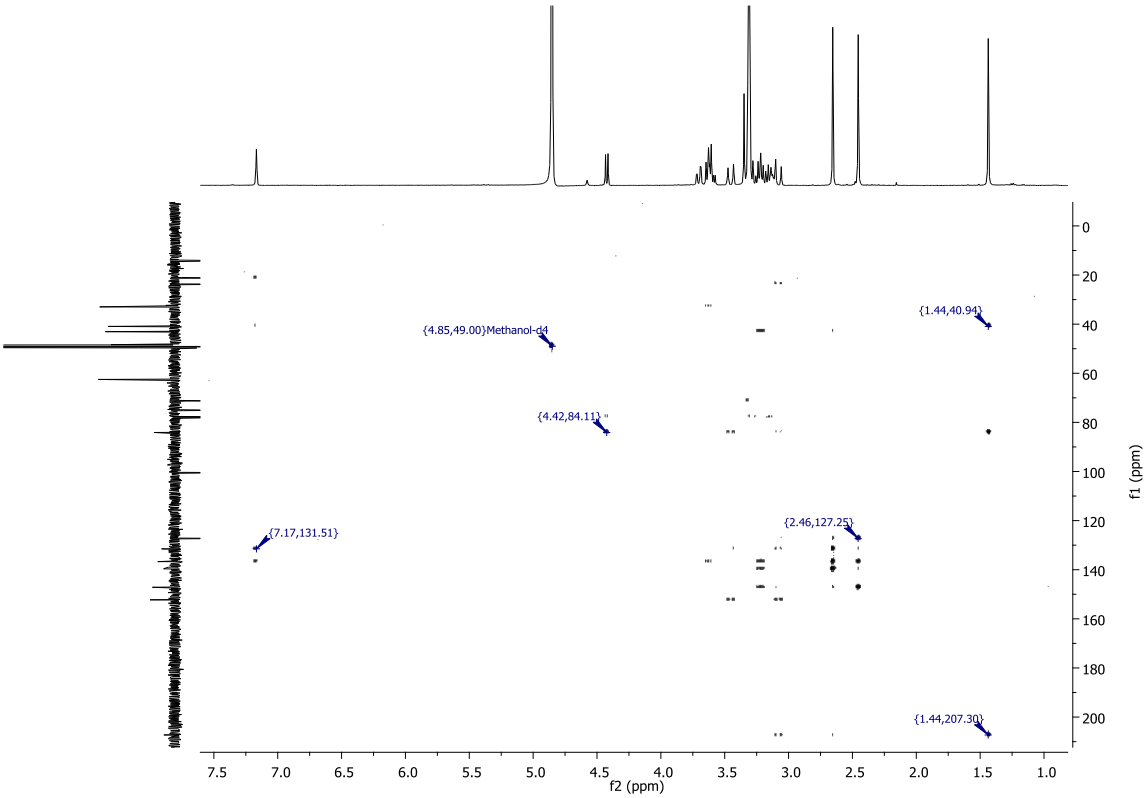

Figure S80. HMBC NMR spectrum of compound **10**.

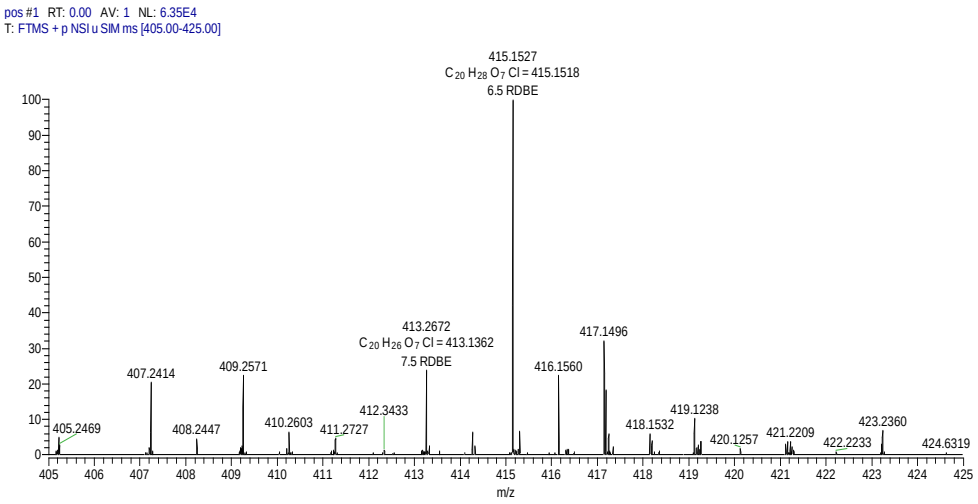

Figure S81. FT-ICR-MS spectrum of compound **10**.

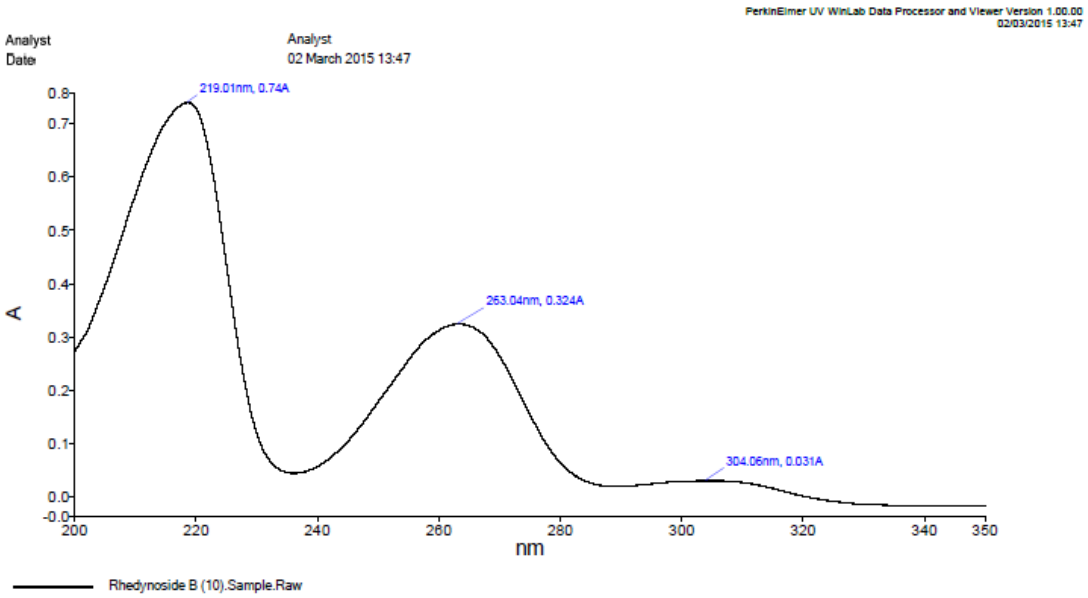

Figure S82. UV spectrum of compound **10** in CH_3OH.

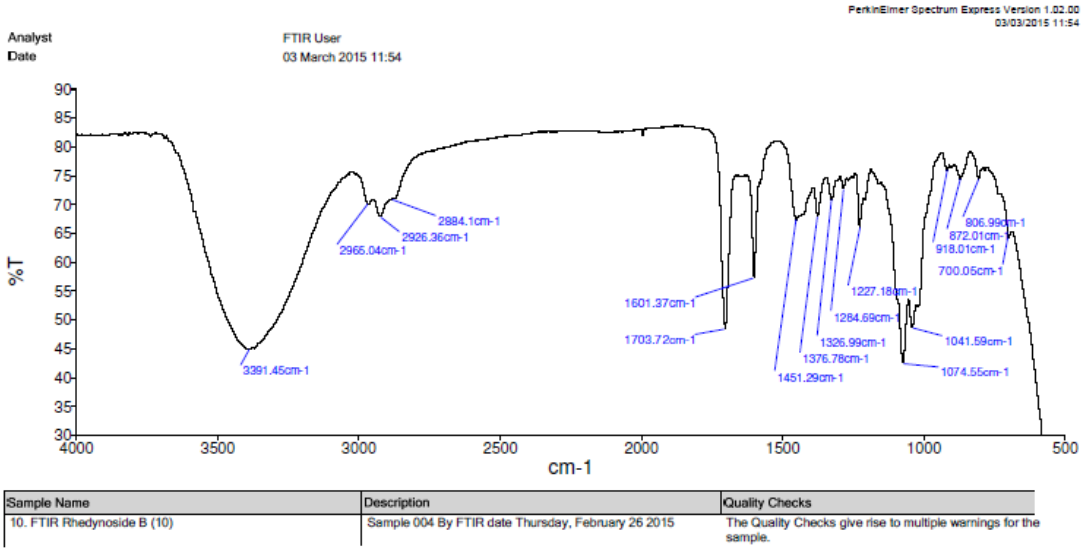

Figure S83. FT-IR spectrum of compound **10** in CH_3OH.

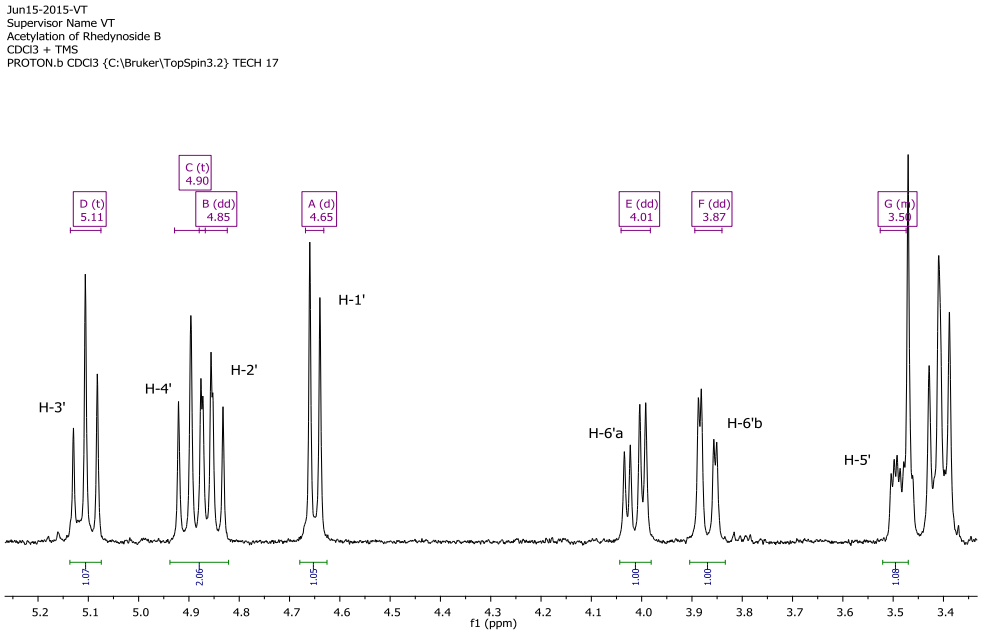

Figure S84. ^1H NMR ($CDCl_3$, 400 MHz) spectrum of compound **10** after acetylation reaction

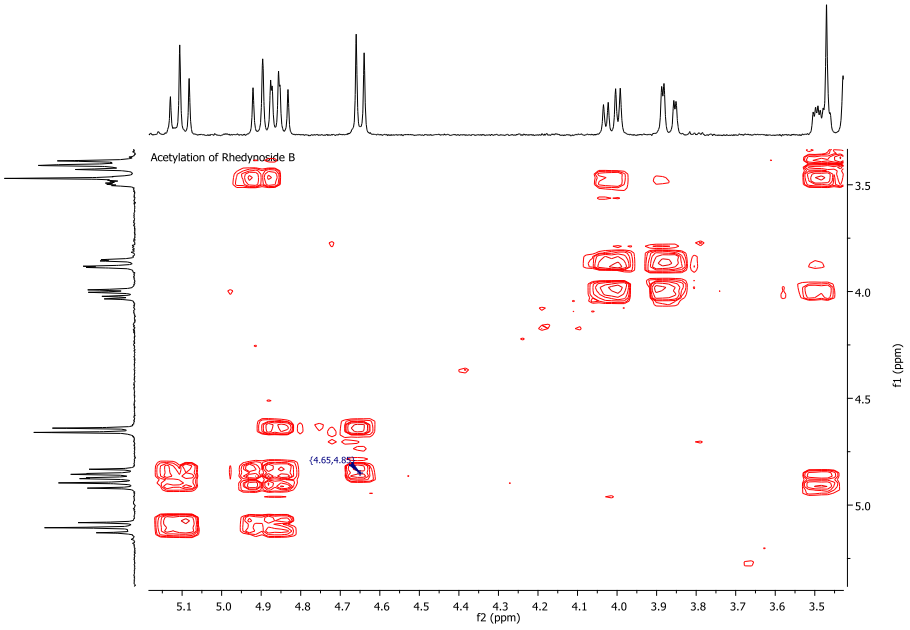

Figure S85. ^{1}H-^{1}H COSY NMR spectrum of compound **10** after acetylation reaction

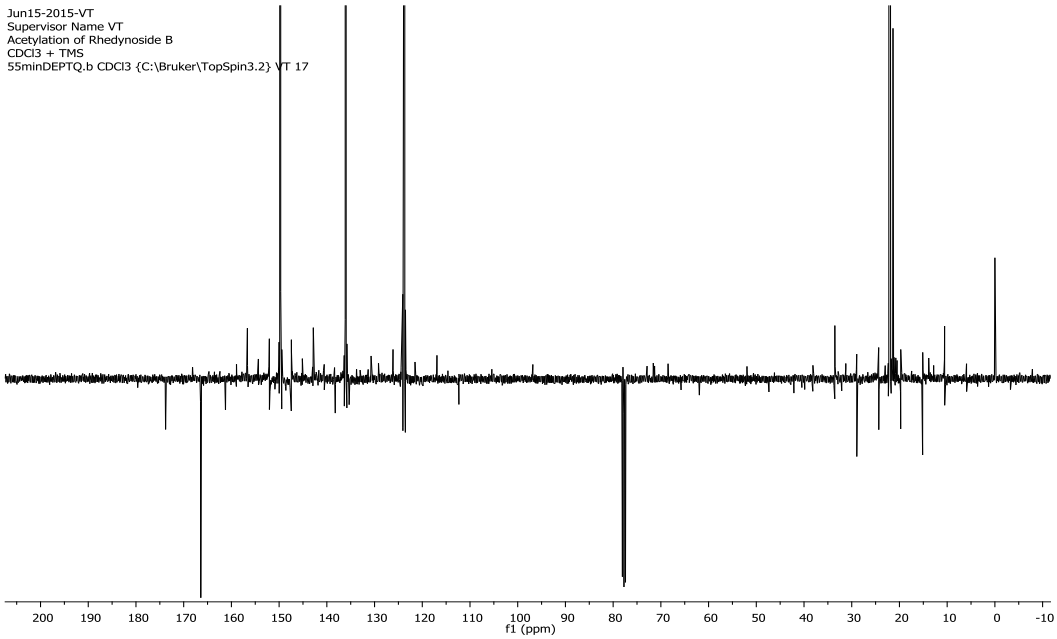

Figure S86. DEPTQ NMR ($CDCl_3$, 100 MHz) spectrum of compound **10** after acetylation reaction

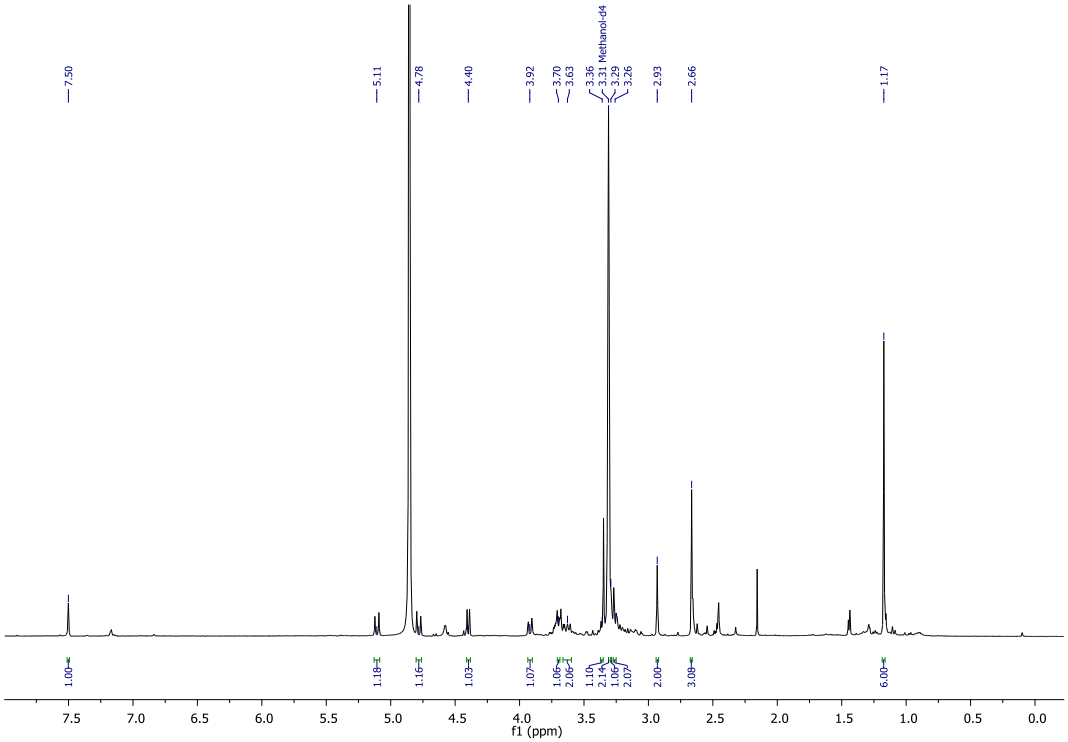

Figure S87. ^{1}H NMR (CD_3OD, 400 MHz) spectrum of compound **11**.

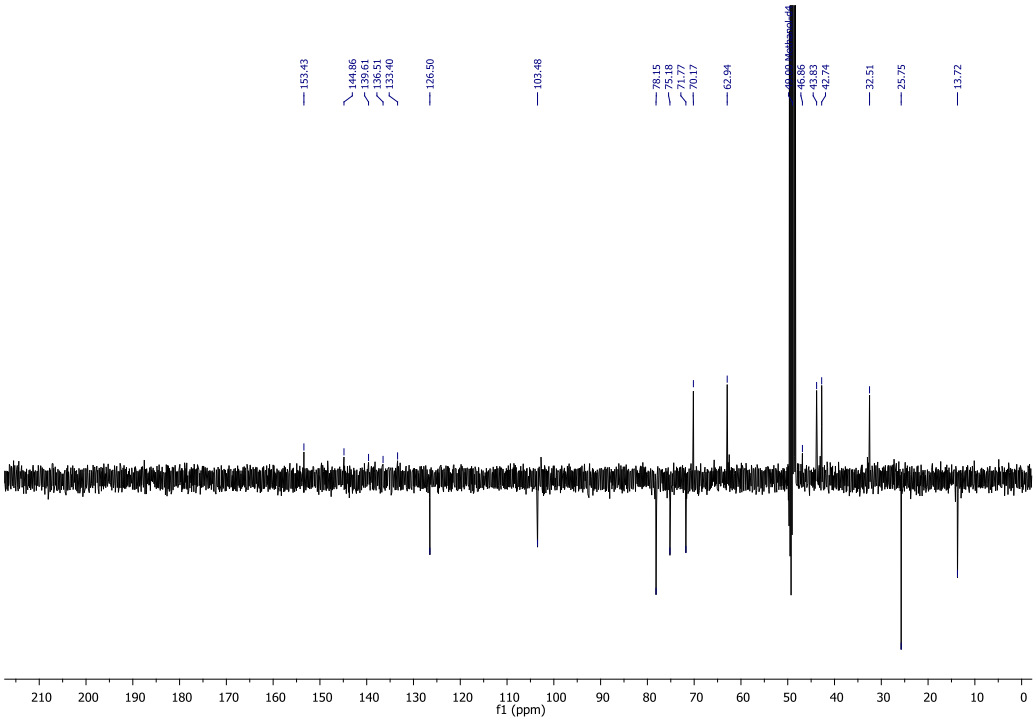

Figure S88. DEPTQ NMR (CD_3OD, 100 MHz) spectrum of compound **11**.

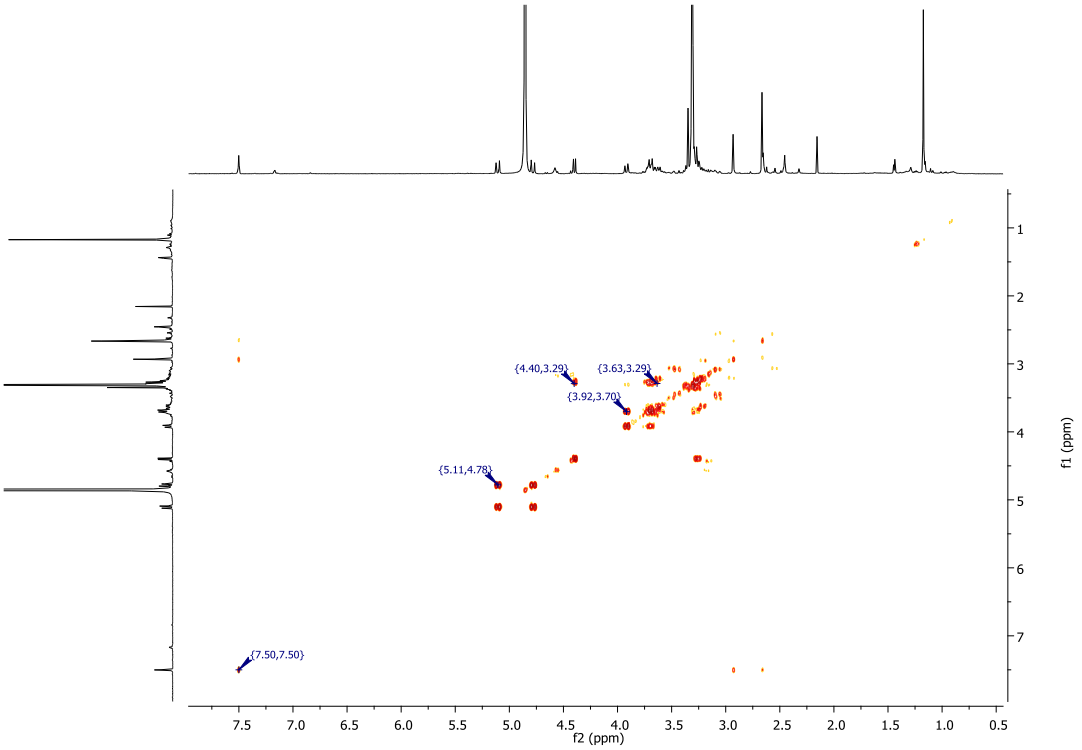

Figure S89. ^{1}H-^{1}H COSY NMR spectrum of compound **11**.

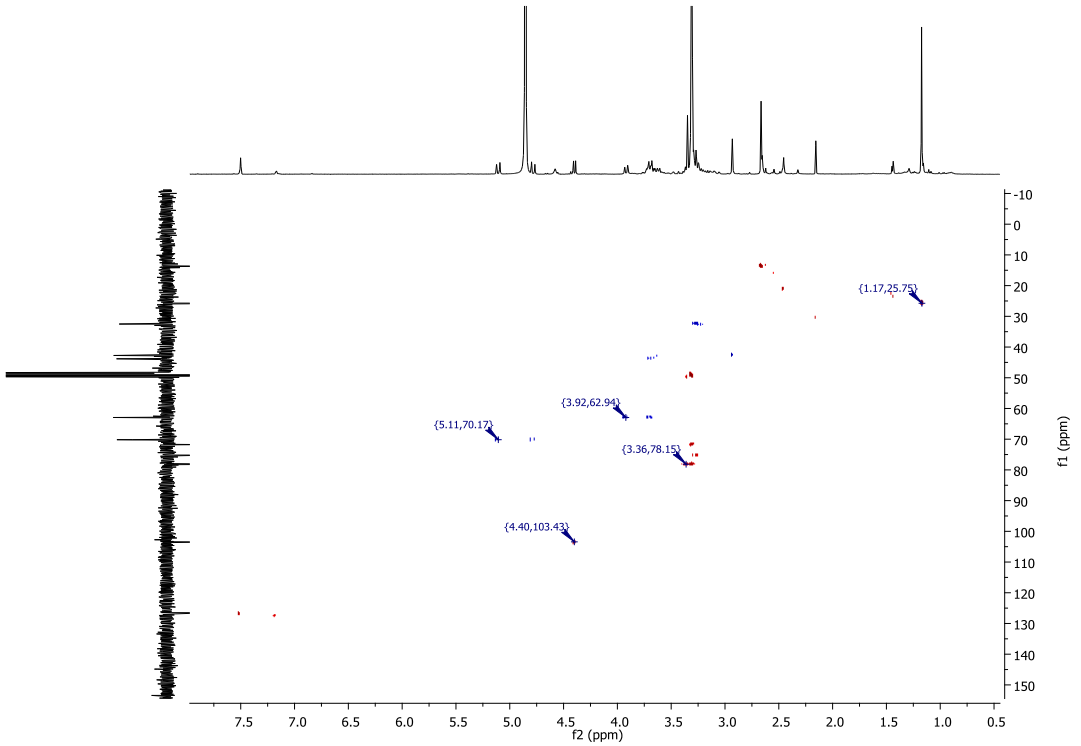

Figure S90. HSQC NMR spectrum of compound **11**.

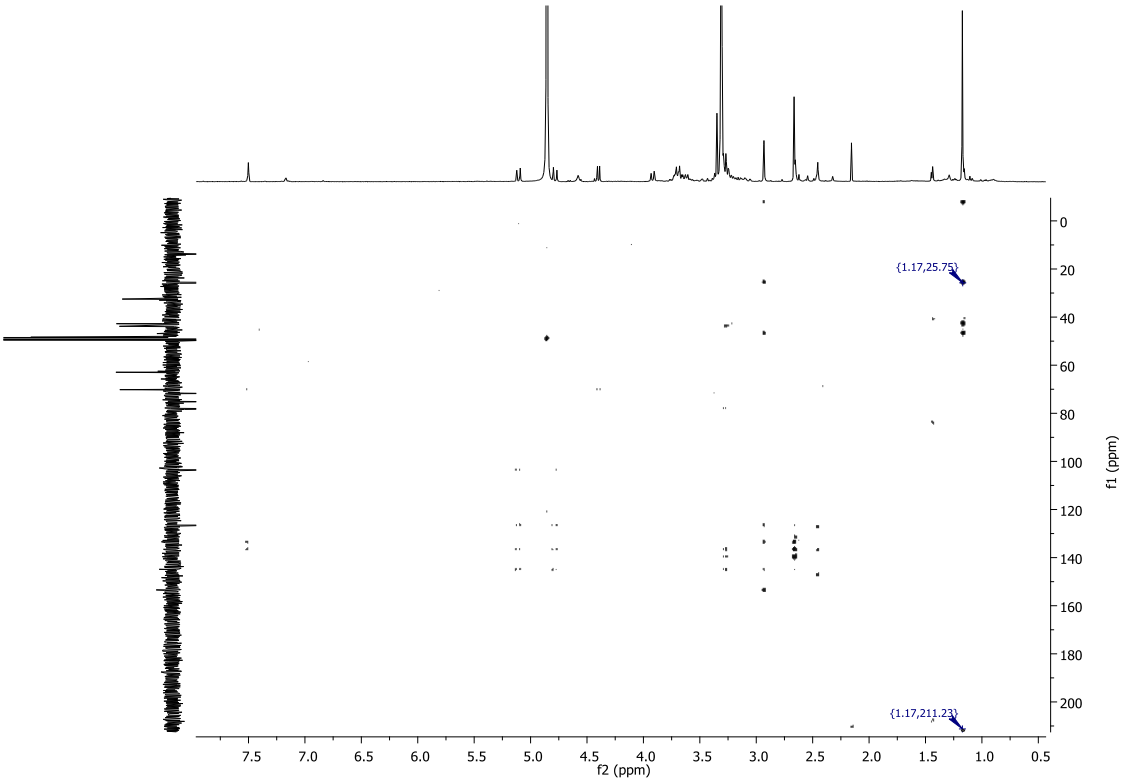

Figure S91. HMBC NMR spectrum of compound **11**.

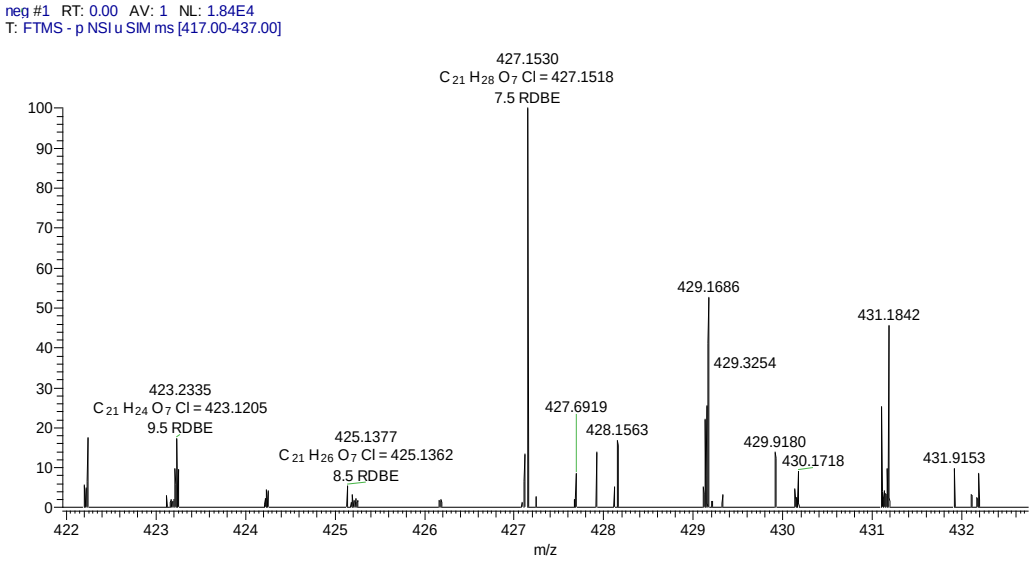

Figure S92. FT-ICR-MS spectrum of compound **11**.

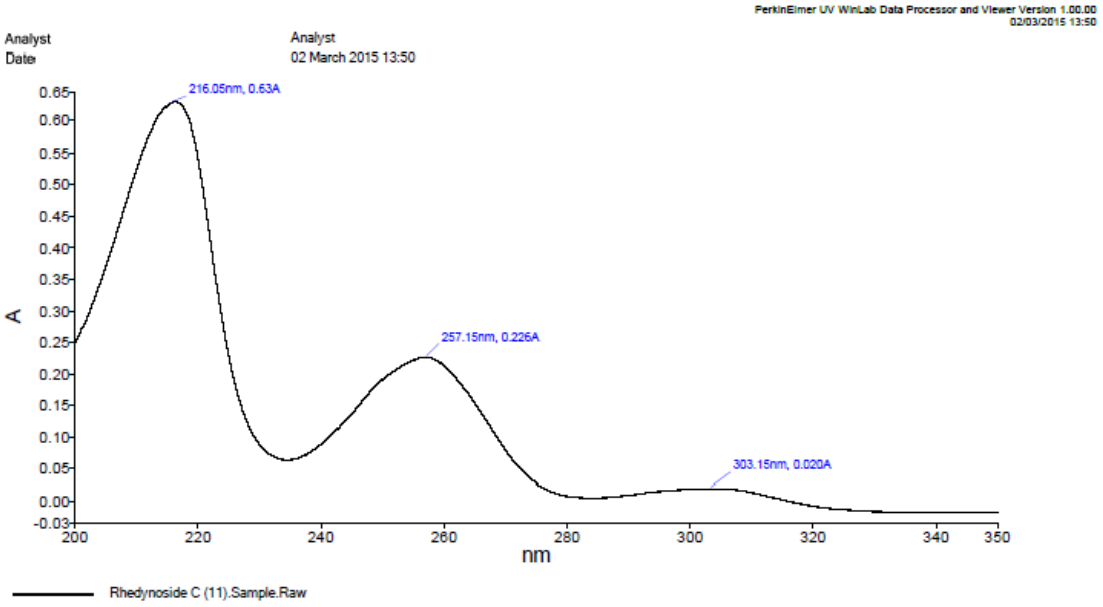

Figure S93. UV spectrum of compound **11** in CH_3OH.

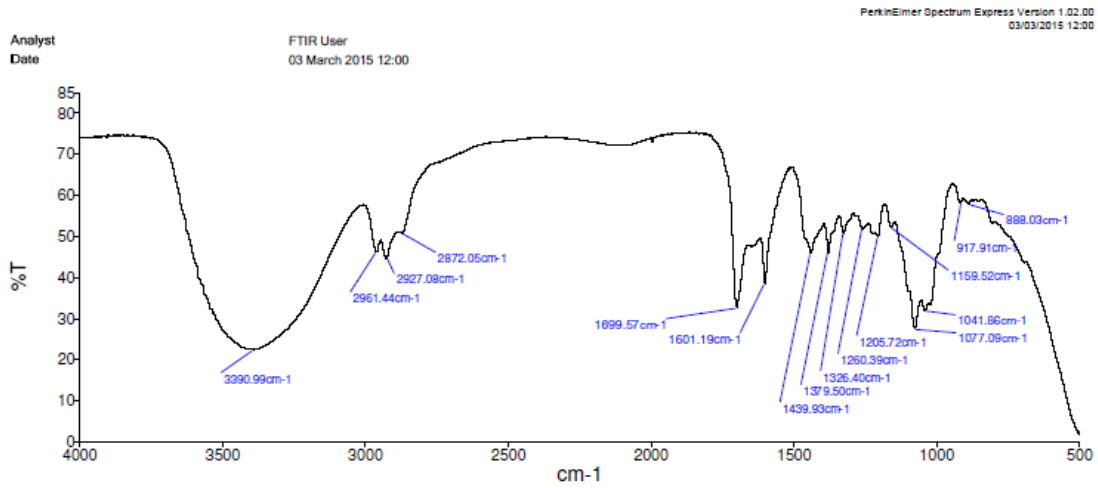

Sample Name	Description	Quality Checks
11. FTIR Rhedynoside C (11)	Sample 018 By FTIR date Friday, February 27 2015	The Quality Checks give rise to multiple warnings for the sample.

Figure S94. FT-IR spectrum of compound **11** in CH_3OH.

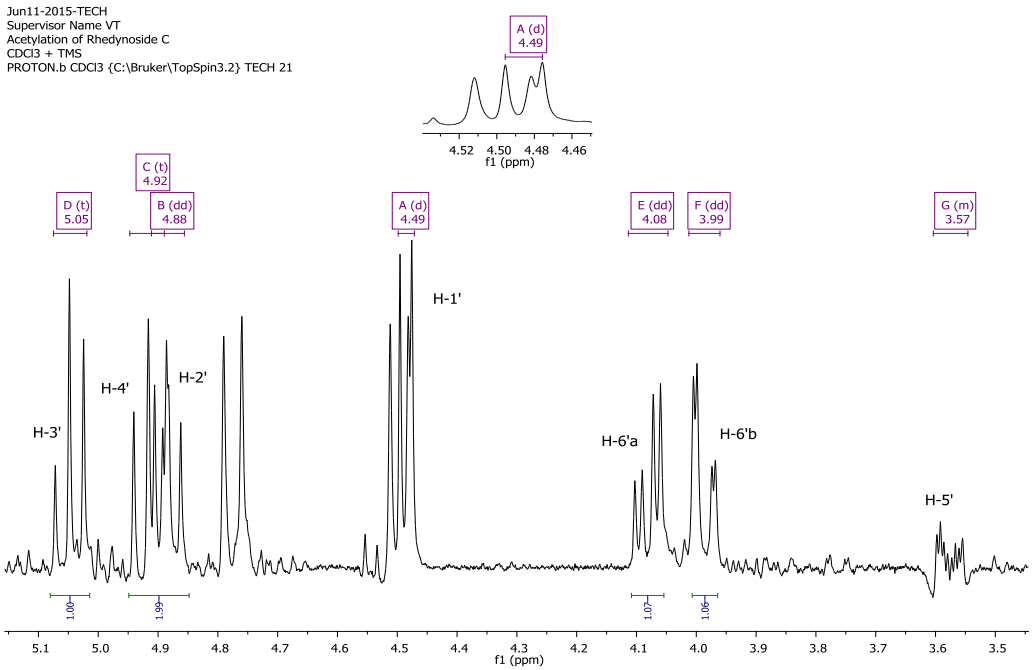

Figure S95. ^{1}H NMR ($CDCl_3$, 400 MHz) spectrum of compound **11** after acetylation reaction

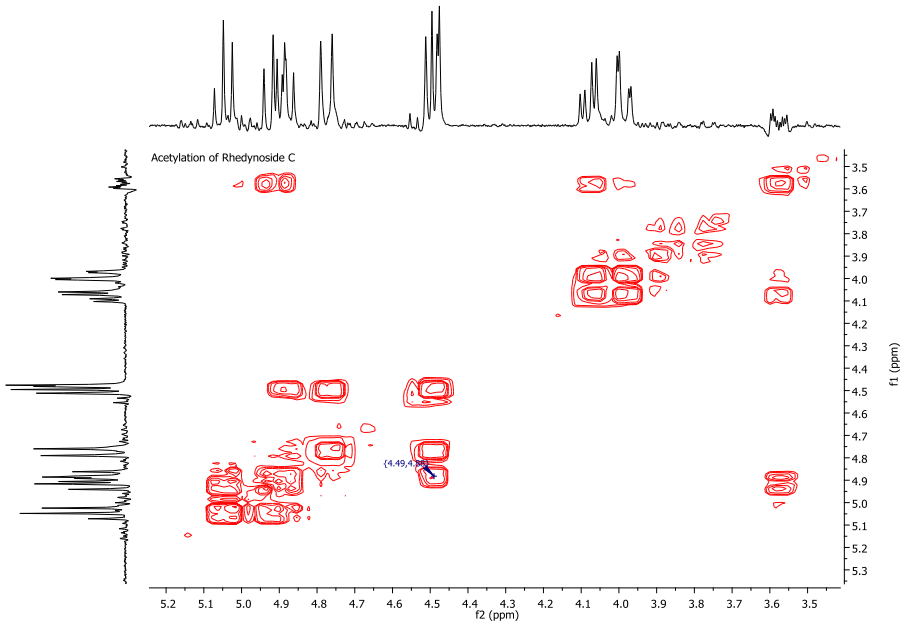

Figure S96. ^{1}H-^{1}H COSY NMR spectrum of compound **11** after acetylation reaction

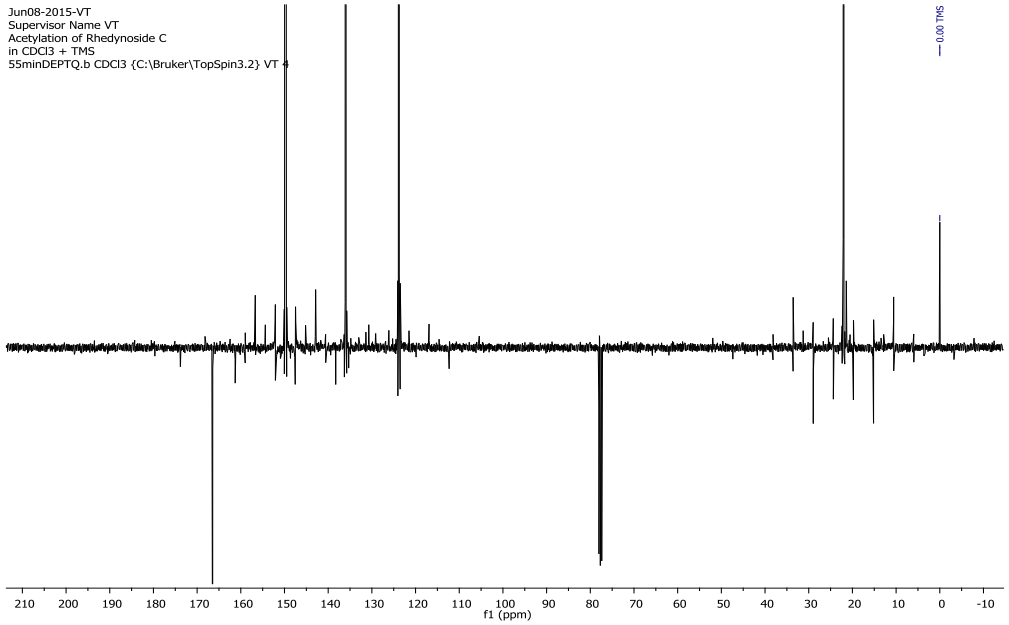

Figure S97. DEPTQ NMR ($CDCl_3$, 100 MHz) spectrum of compound **11** after acetylation reaction

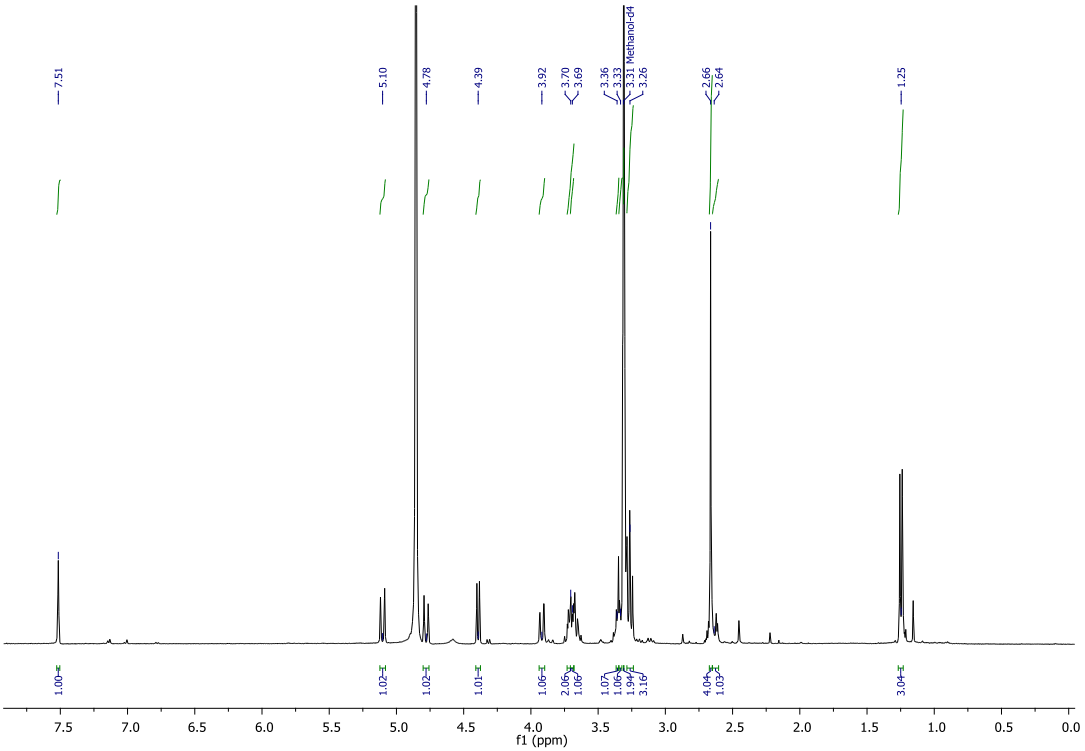

Figure S98. ^1H NMR (CD_3OD, 400 MHz) spectrum of compound **12**.

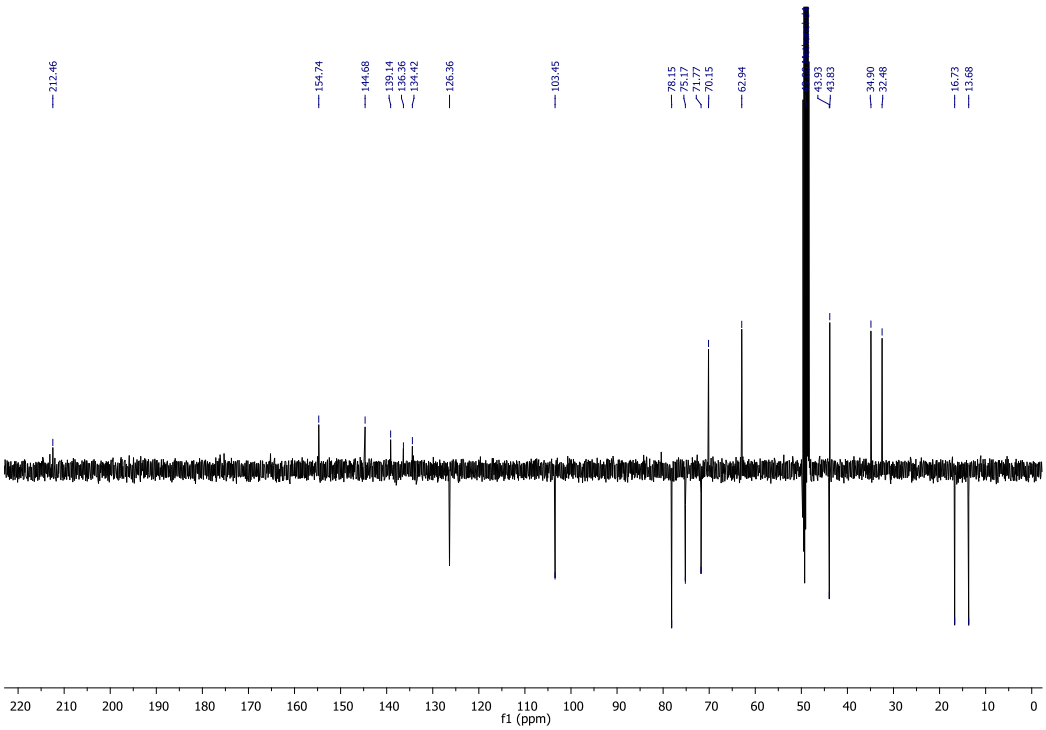

Figure S99. DEPTQ NMR (CD_3OD, 100 MHz) spectrum of compound **12**.

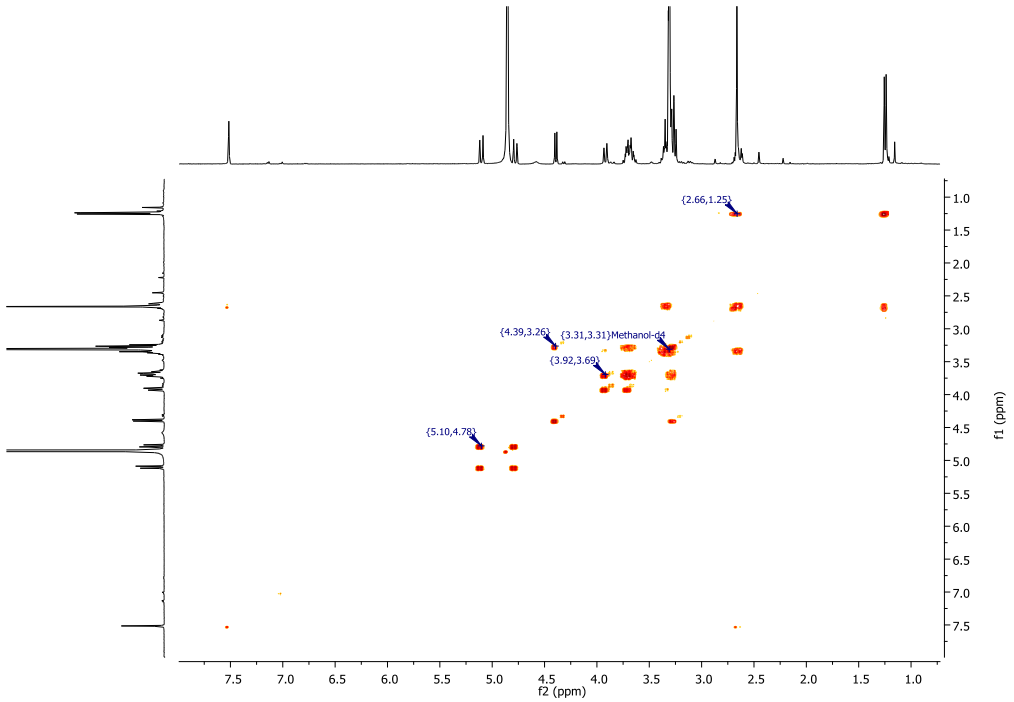

Figure S100. ^1H-^1H COSY NMR spectrum of compound **12**.

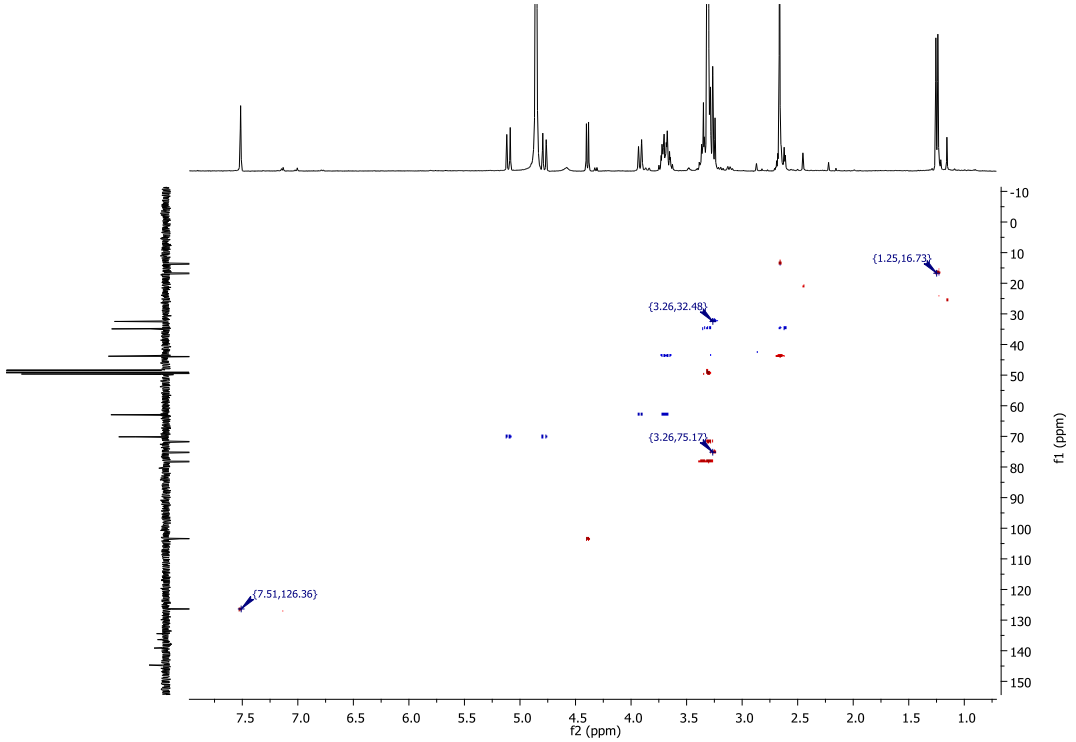

Figure S101. HSQC NMR spectrum of compound **12**.

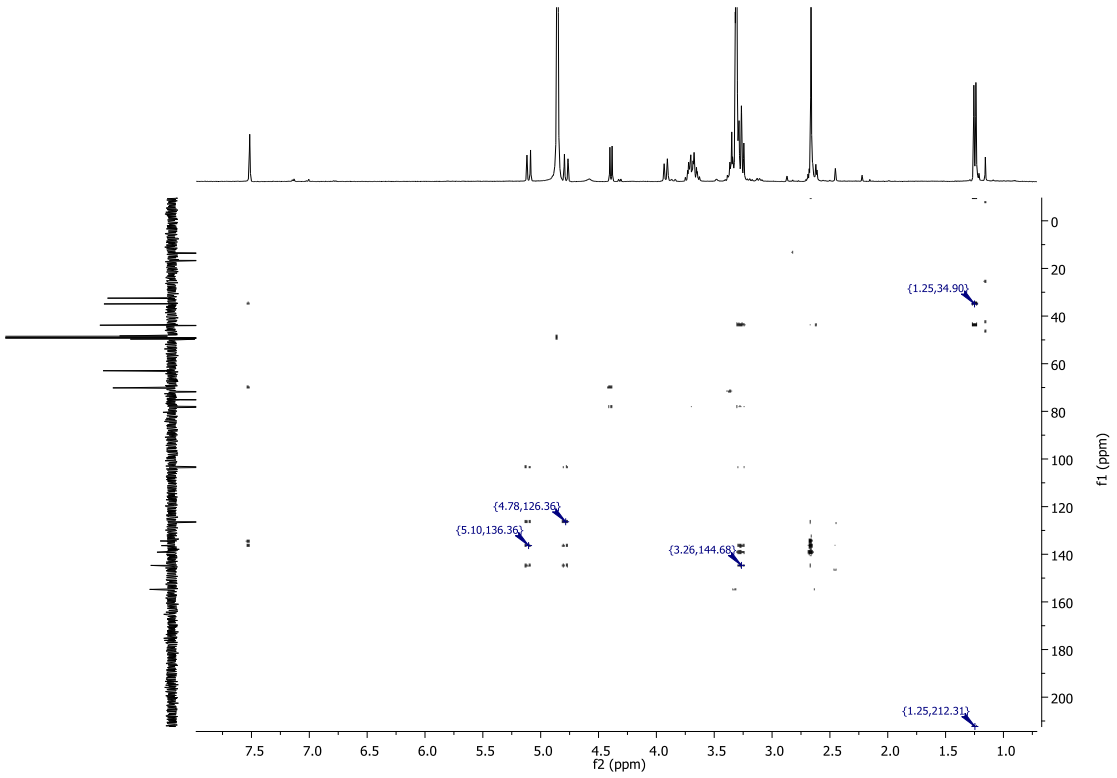

Figure S102. HMBC NMR spectrum of compound **12**.

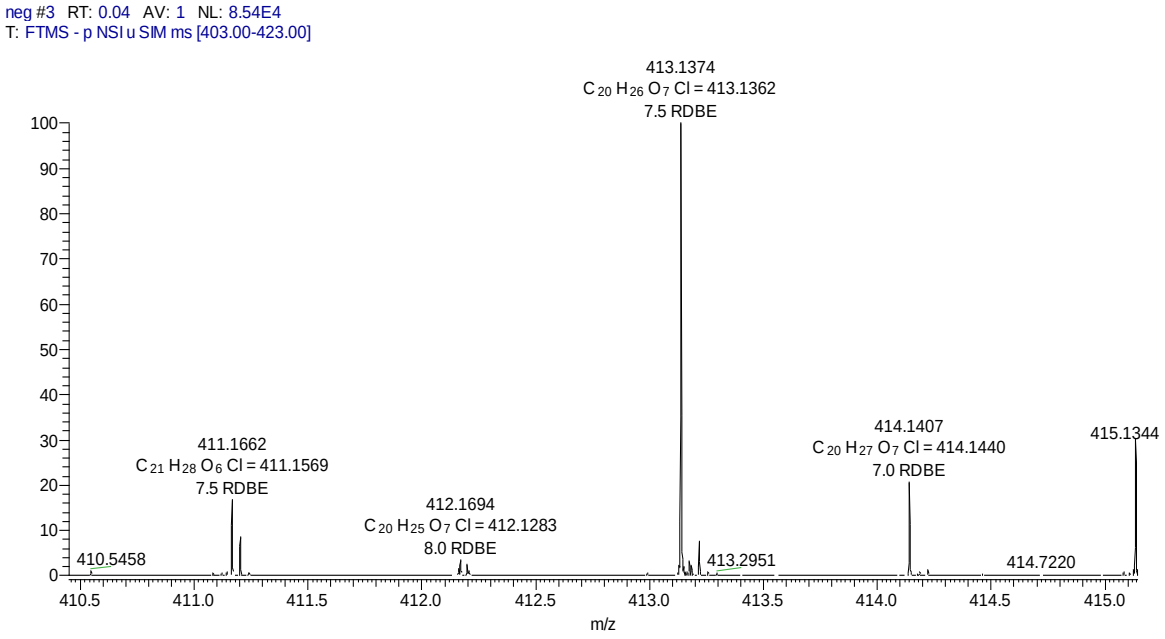

Figure 103. FT-ICR-MS spectrum of compound **12**.

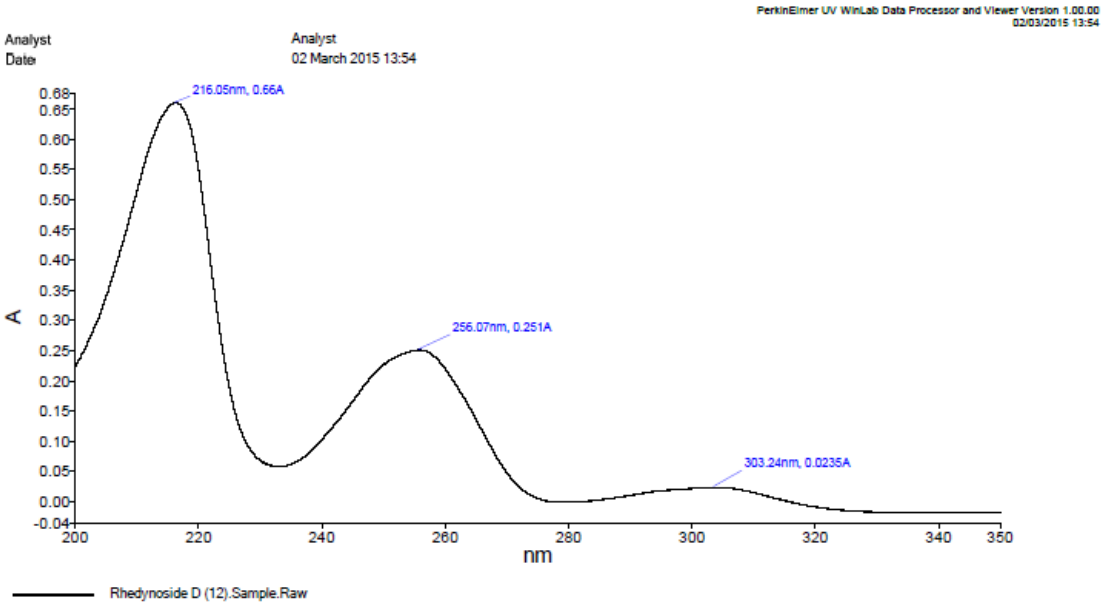

Figure S104. UV spectrum of compound **12** in CH_3OH.

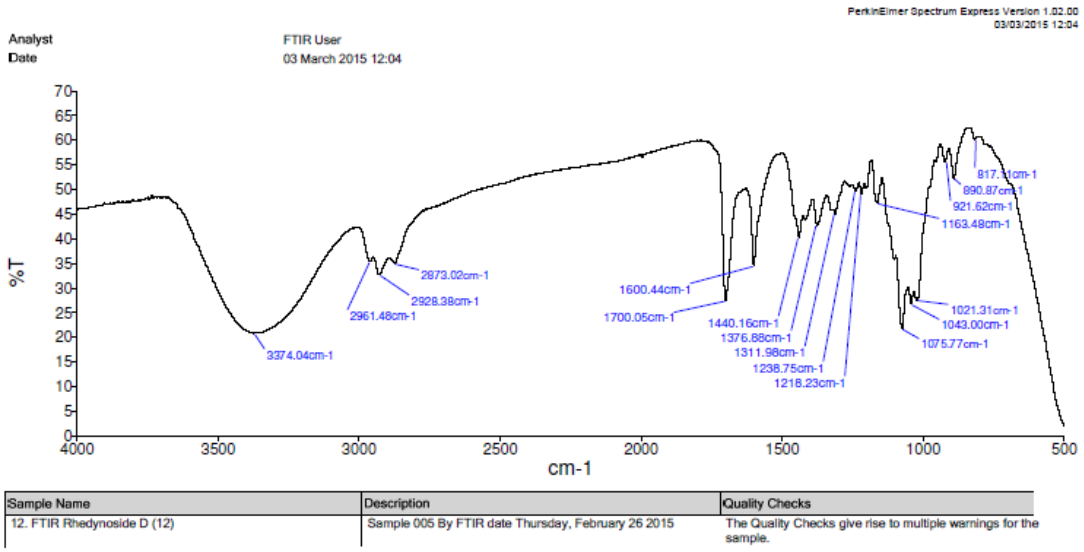

Figure S105. FT-IR spectrum of compound **12** in CH_3OH.

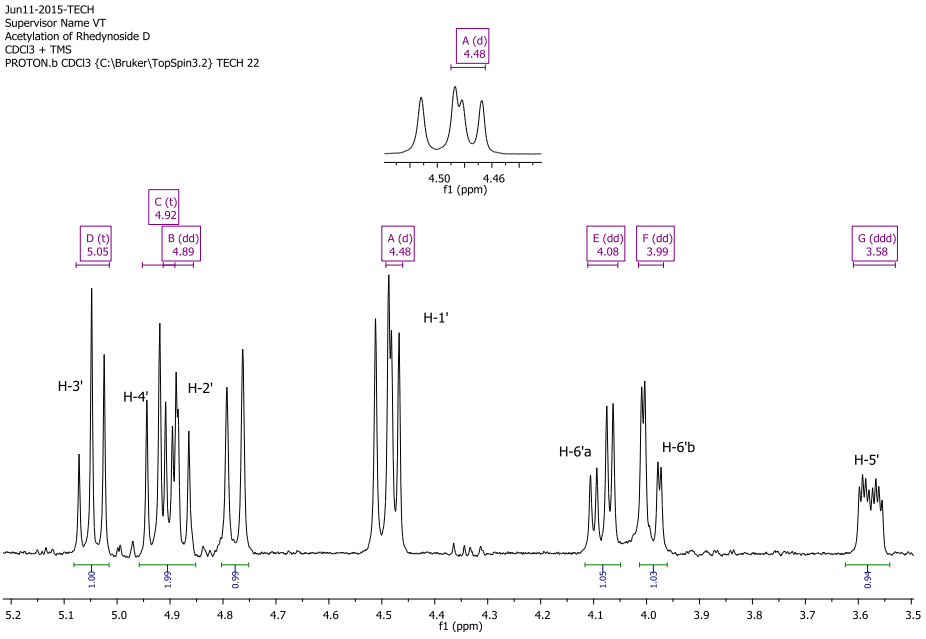

Figure S106. ^{1}H NMR ($CDCl_3$, 400 MHz) spectrum of compound **12** after acetylation reaction

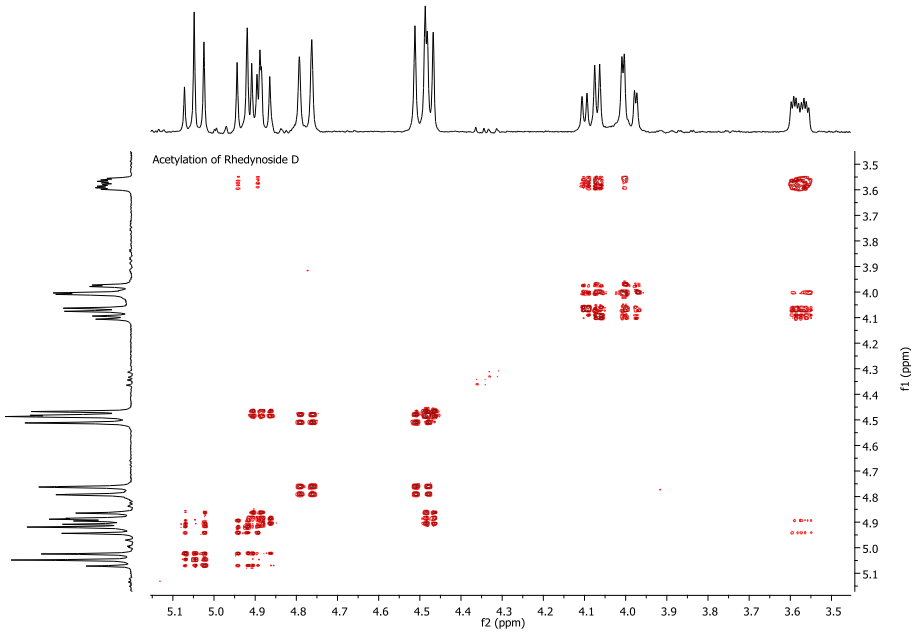

Figure S107. ^{1}H-^{1}H COSY NMR spectrum of compound **12** after acetylation reaction

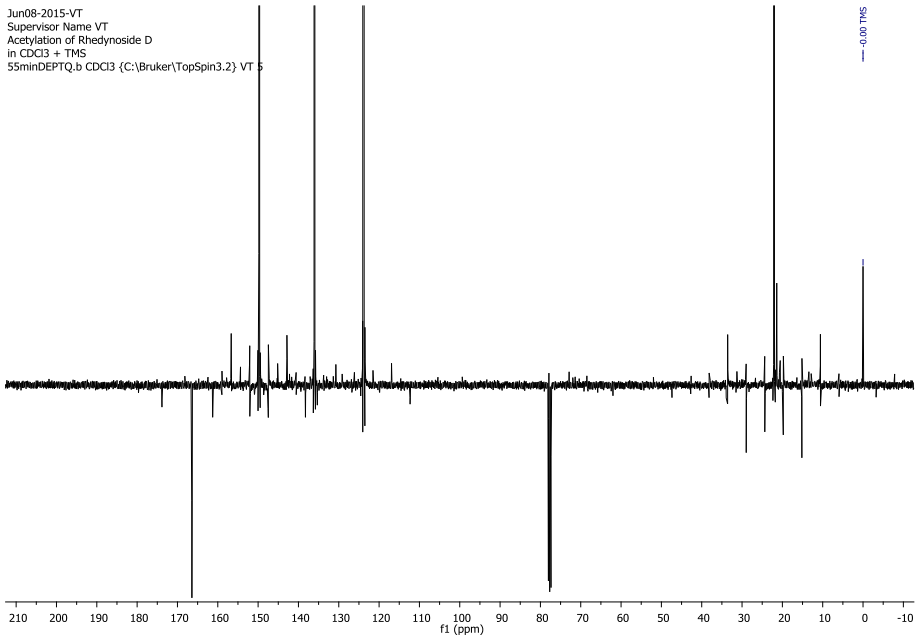

Figure S108. DEPTQ NMR ($CDCl_3$, 100 MHz) spectrum of compound **12** after acetylation reaction

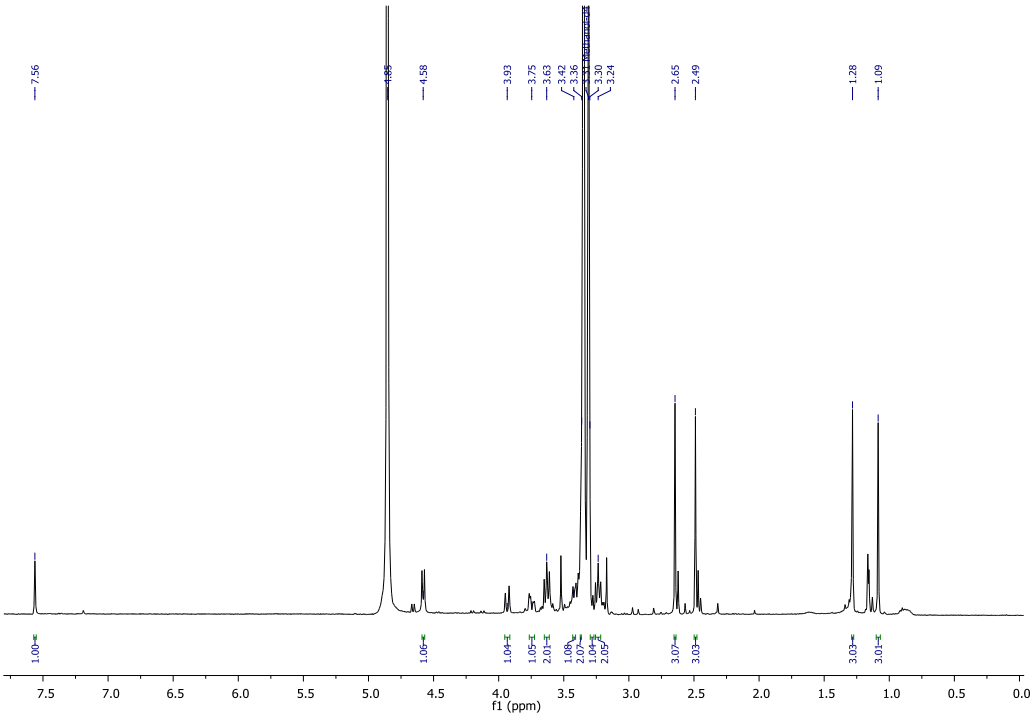

Figure S109. ^{1}H NMR (CD_3OD, 400 MHz) spectrum of compound **13**.

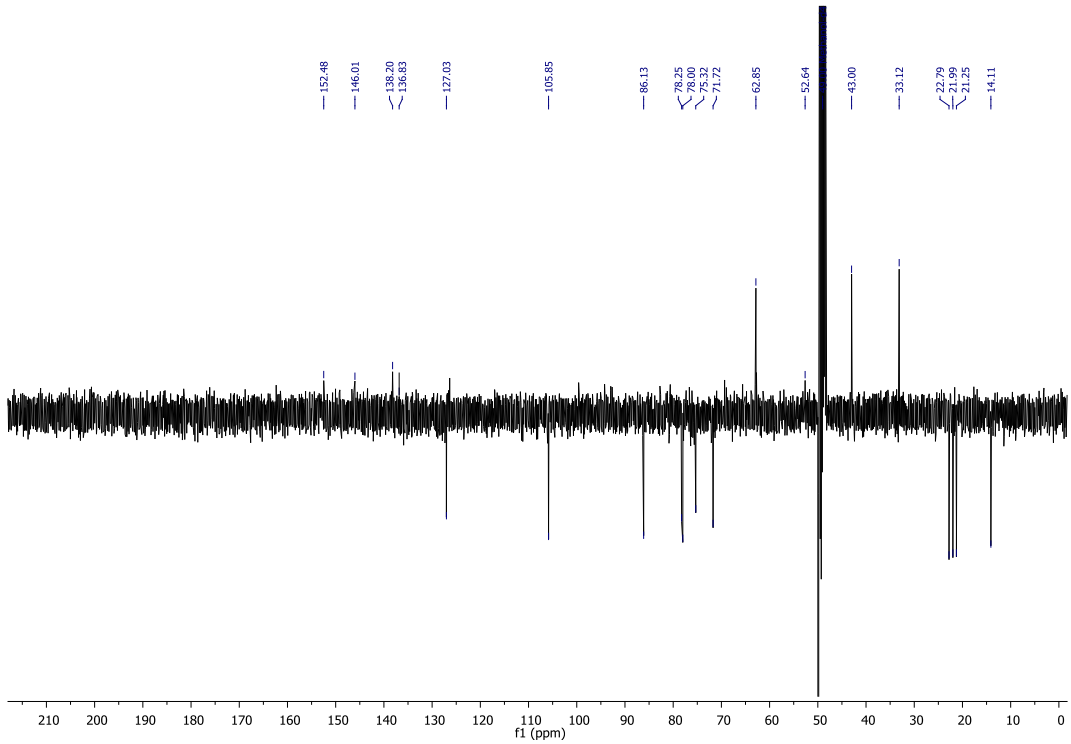

Figure S110. DEPTQ NMR (CD_3OD, 100 MHz) spectrum of compound **13**.

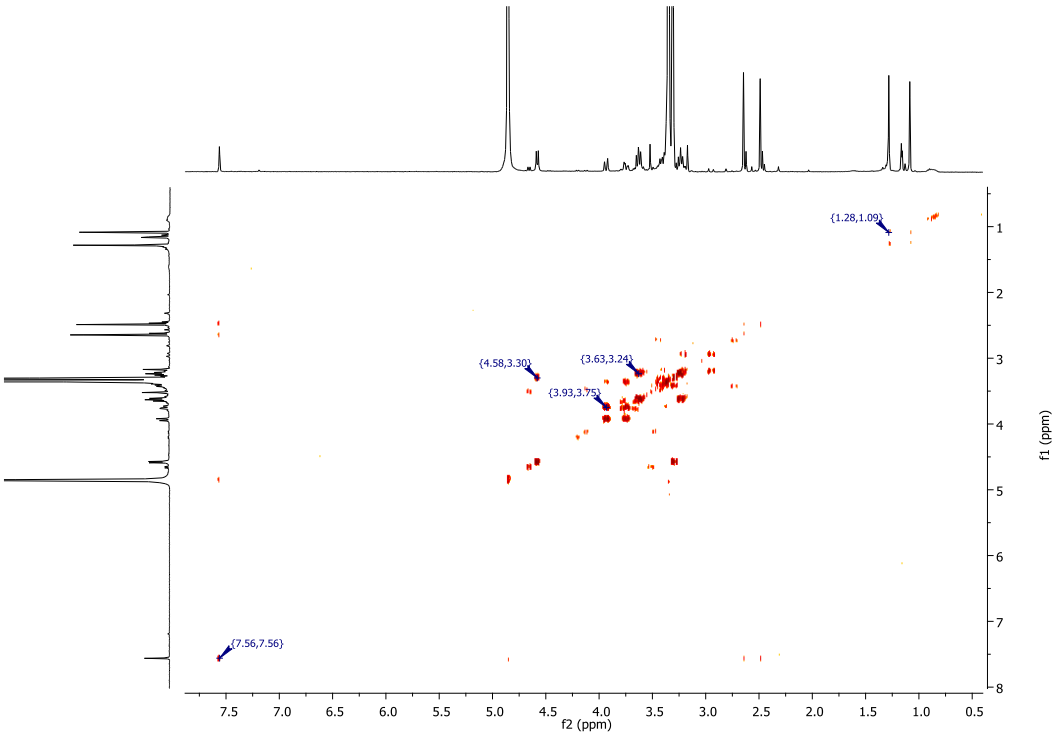

Figure S111. ^{1}H-^{1}H COSY NMR spectrum of compound **13**.

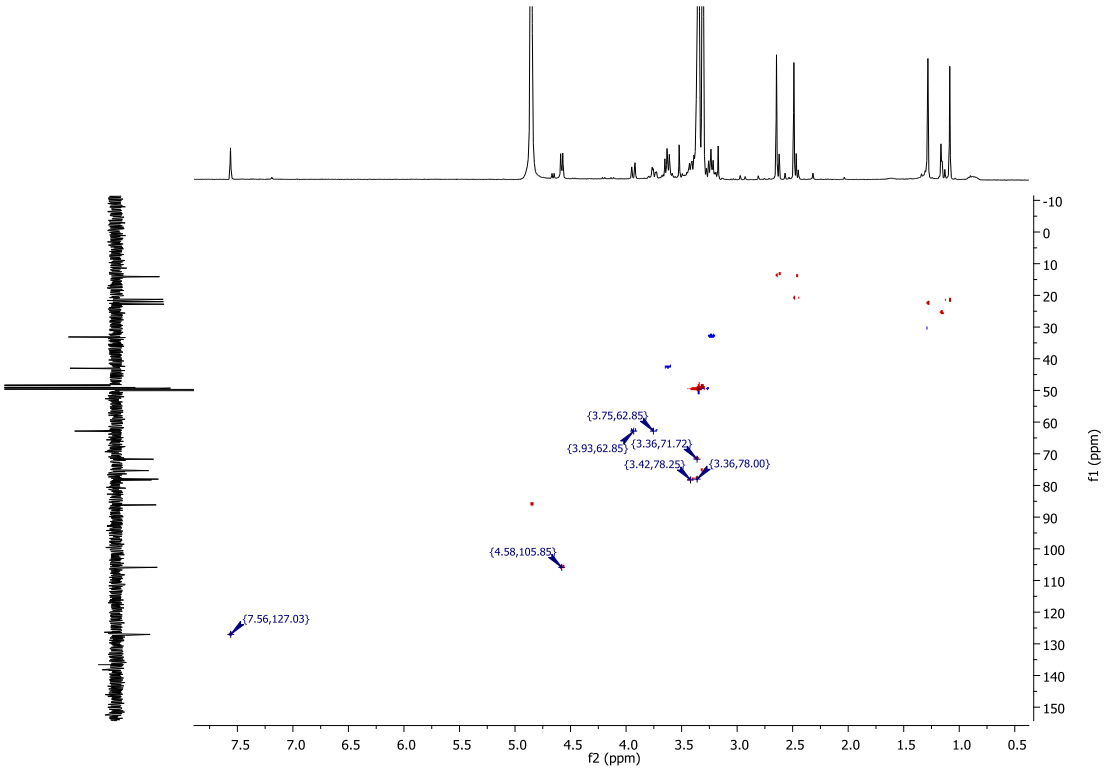

Figure S112. HSQC NMR spectrum of compound **13**.

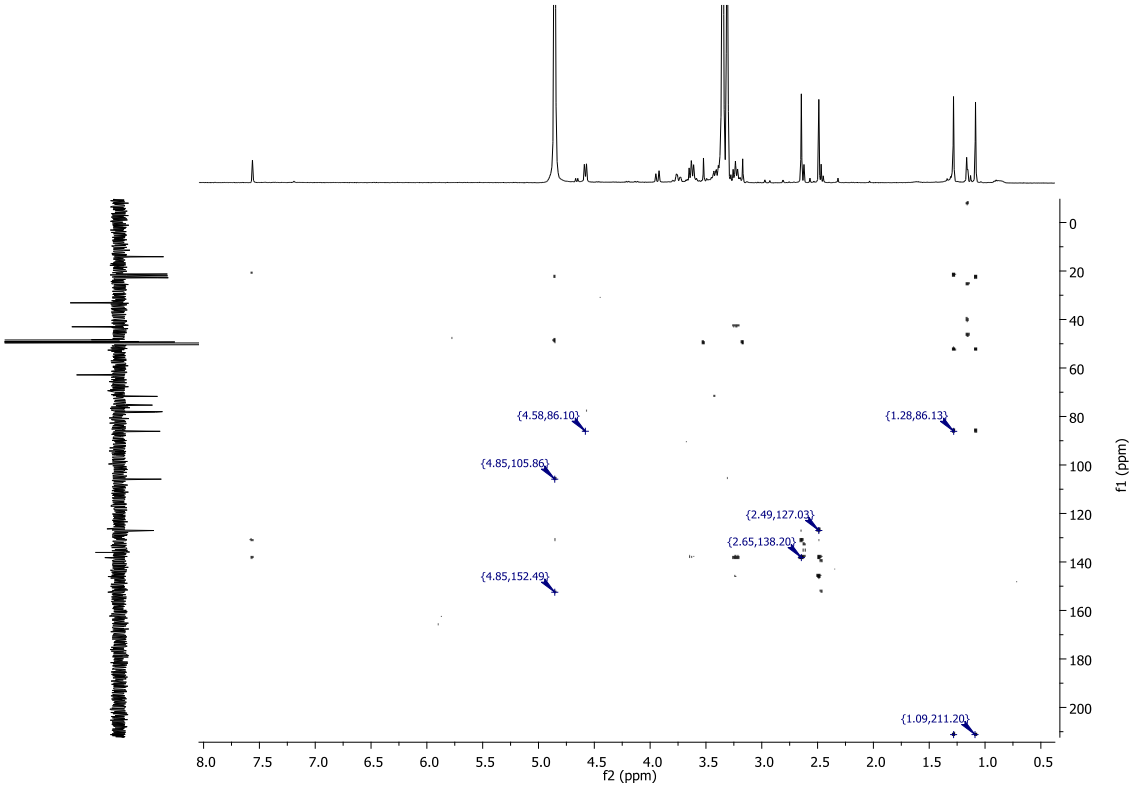

Figure S113. HMBC NMR spectrum of compound **13**.

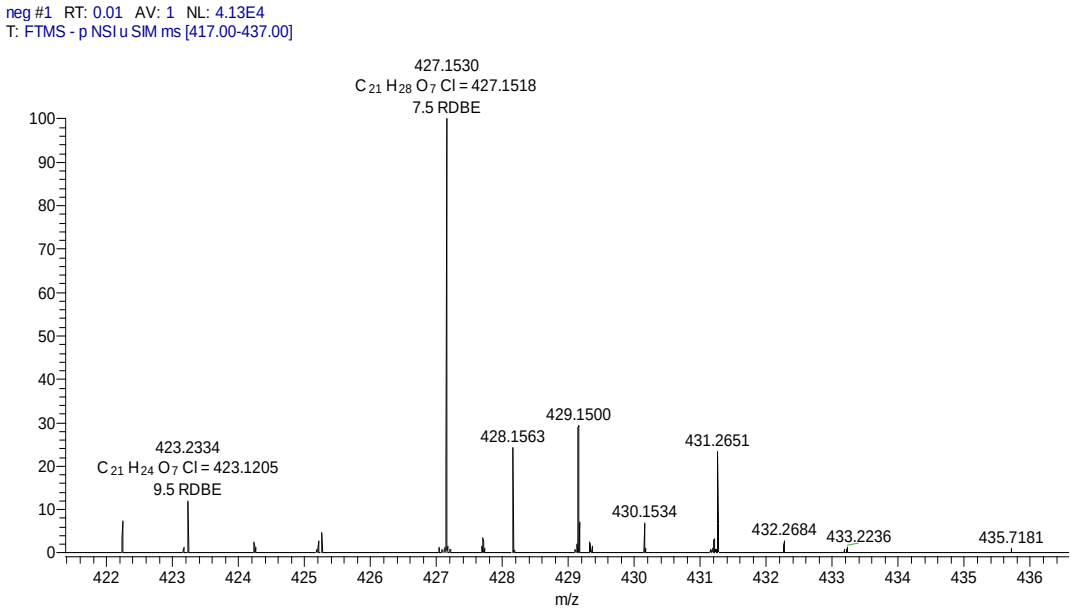

Figure S114. FT-ICR-MS spectrum of compound **13**.

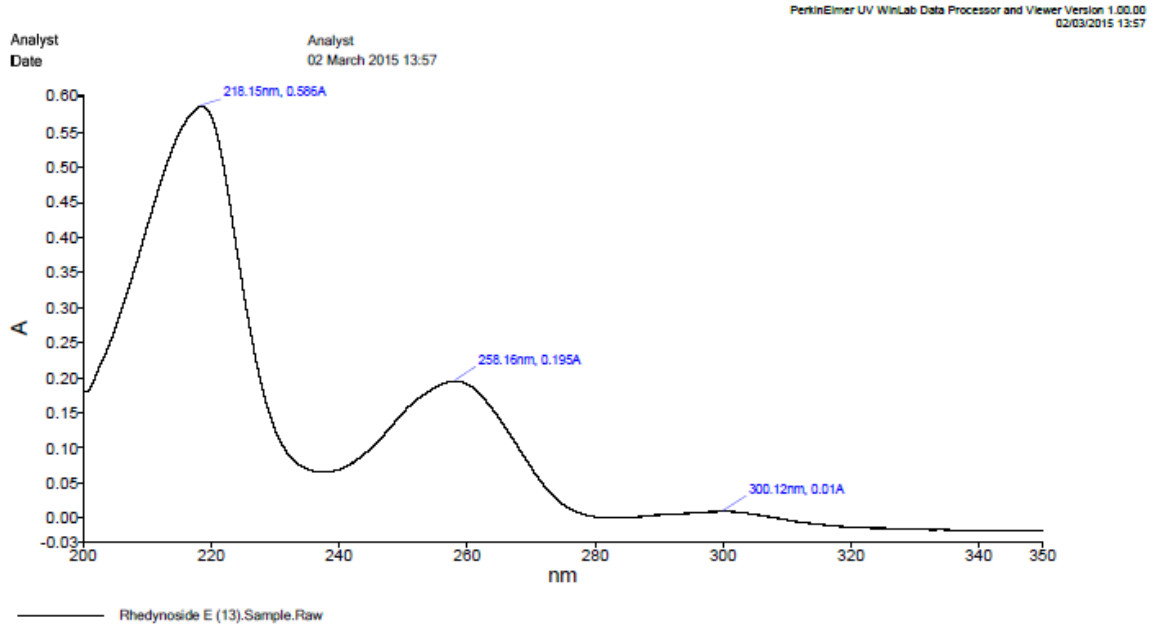

Figure S115. UV spectrum of compound **13** in CH_3OH.

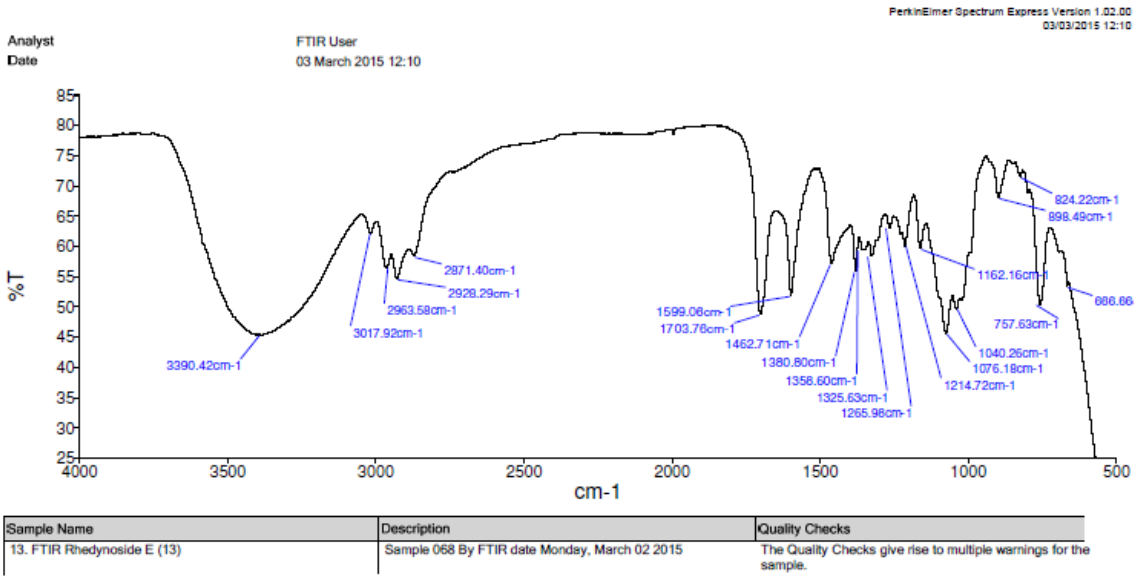

Figure S116. FT-IR spectrum of compound **13** in CH_3OH.

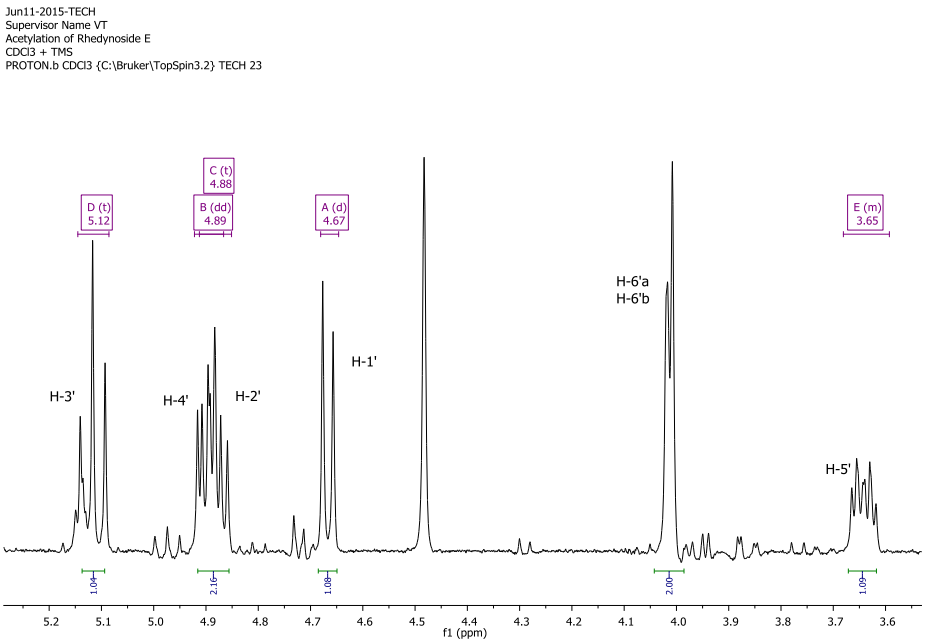

Figure S117. ^{1}H NMR ($CDCl_3$, 400 MHz) spectrum of compound **13** after acetylation reaction

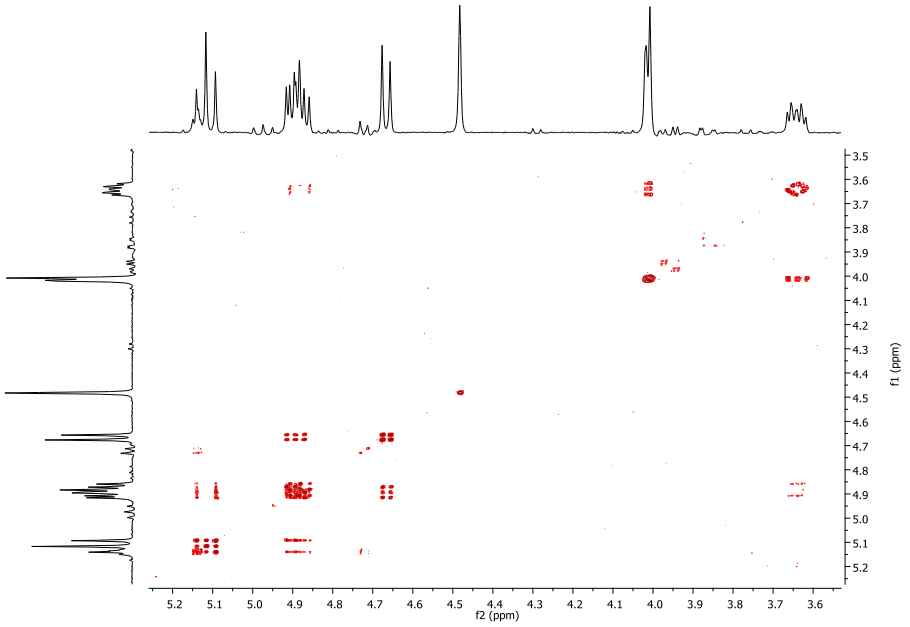

Figure S118. ^{1}H-^{1}H COSY NMR spectrum of compound **13** after acetylation reaction

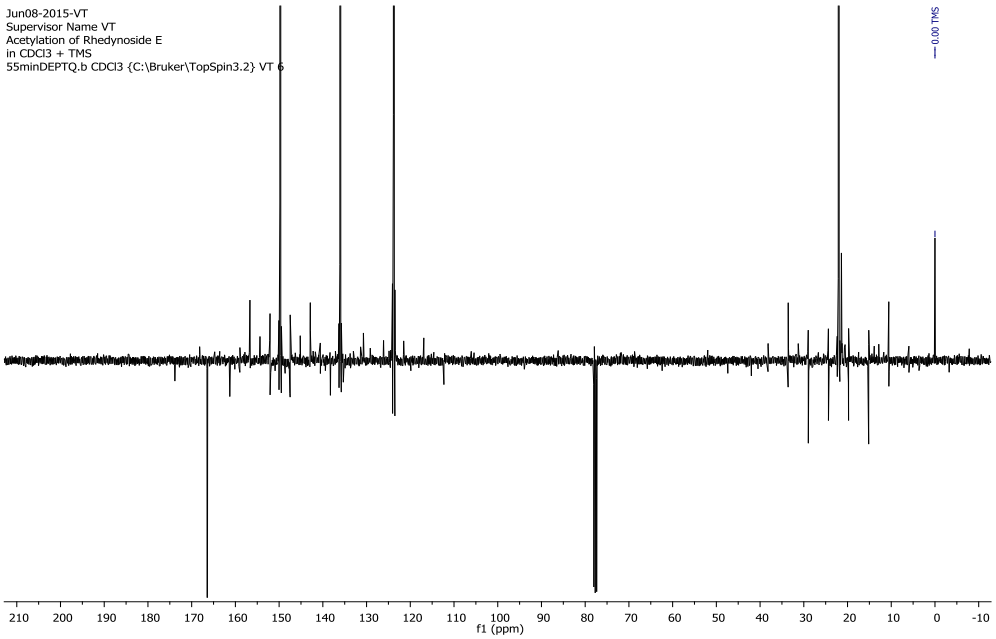

Figure S119. DEPTQ NMR ($CDCl_3$, 100 MHz) spectrum of compound **13** after acetylation reaction

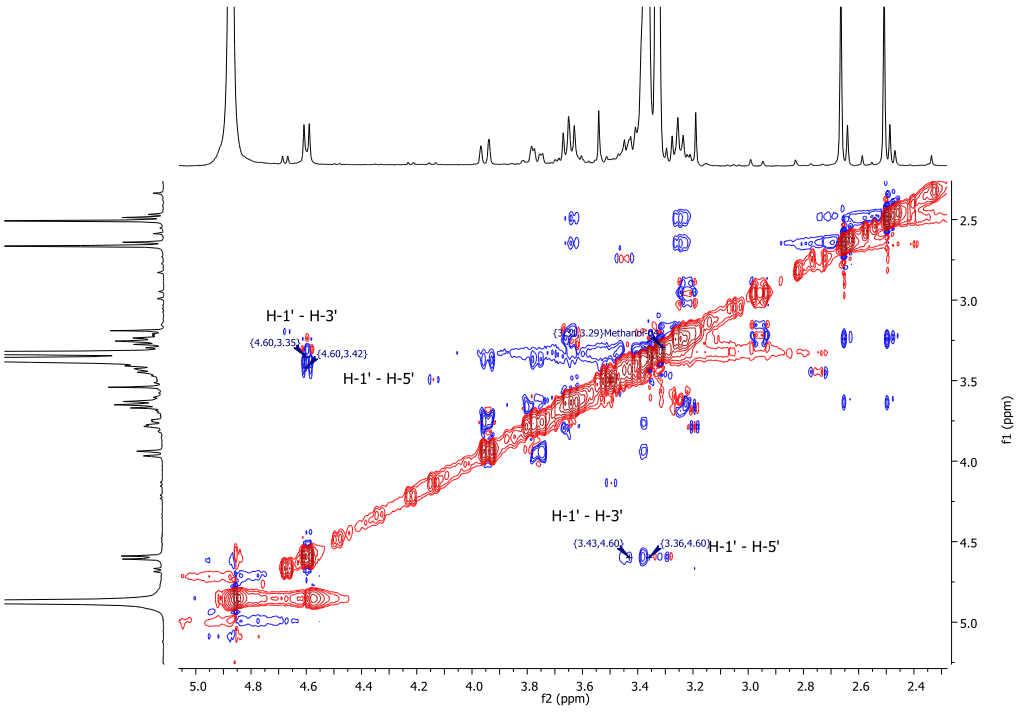

Figure S120. ^{1}H-^{1}H NOESY NMR (CD_3OD, 400 MHz) spectrum of compound **13**.

Acetylation of compounds **2** and **10-13**

Accurately 1 mg of each compound was dissolved with 100 µL of dry pyridine in a HPLC vial and then 50 µL of acetic anhydride was added. The vial was immersed and sonicated for 1 hour and left overnight. The reaction mixture was diluted with 400 µL of $CDCl_3$ containing tetramethylsilane (TMS) as an internal standard. ^1H NMR and COSY were recorded in the range of 3.0-6.0 ppm. DEPTQ was recorded from -50 to 250 ppm.

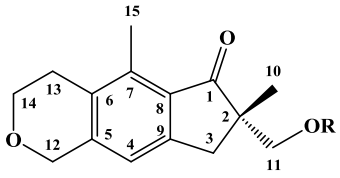

	R
(1)	H
(2)	*β*-D-Glc

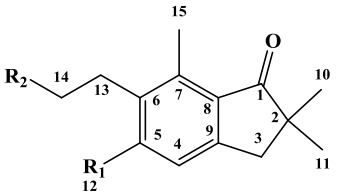

	R_1	R_2
(11)	CH_2-*O*-*β*-D-Glc	Cl
(26)	CH_3	OH
(33)	CH_3	*O*-*β*-D-Glc

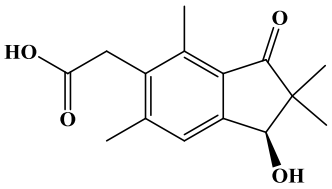

(6)

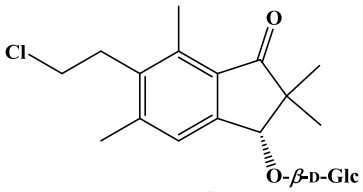

(13)

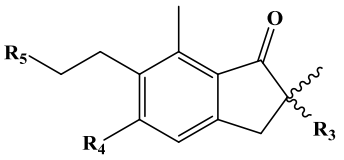

	R_3	R_4	R_5
(5)	OH	CH_2OH	Cl
(9)	H	CH_3	OSO_3H
(12)	H	CH_2-*O*-*β*-D-Glc	Cl

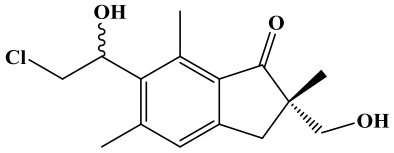

(7)

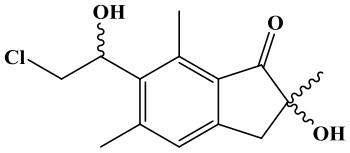

(8)

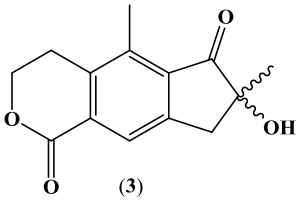

(3)

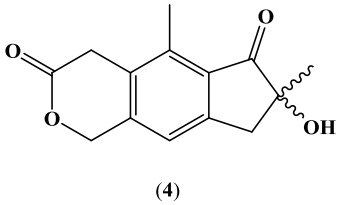

(4)

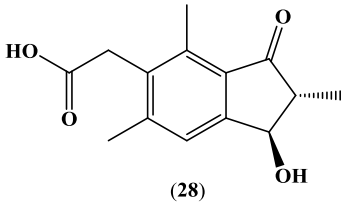

(28)

Fig. 1. Chemical structures of isolated novel and known compounds from bracken rhizomes where compounds **1-9** & **11-13** represent new natural products.

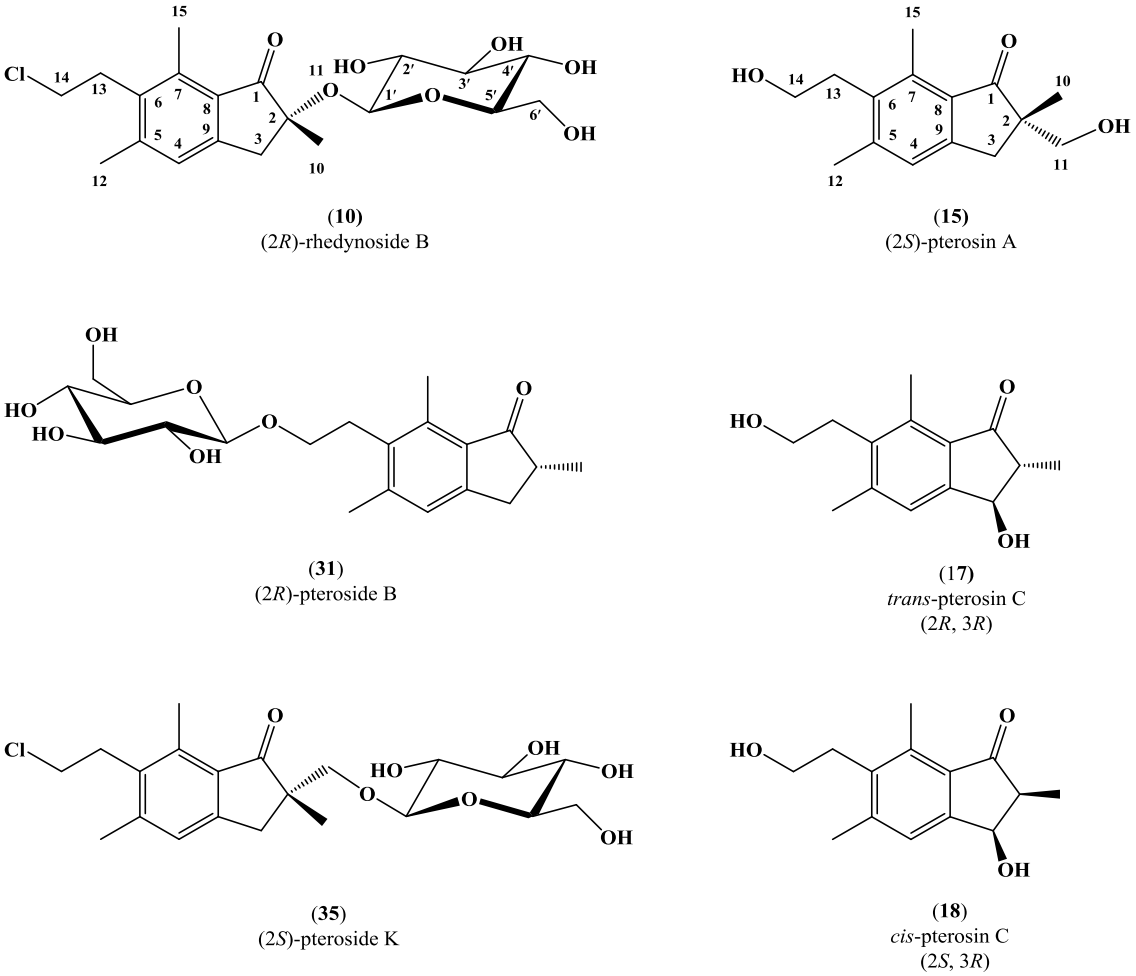

Fig. 2. The absolute stereochemistry of compounds **10**, **15**, **17**, **18**, **31** and **35** obtained from bracken rhizomes, as established by X-ray crystallography (Figs. 5, 6 and SI2). Compound **10** represent a new natural product. The aglycone moiety is numbered 1-15; the sugar moiety is numbered 1′-6′.

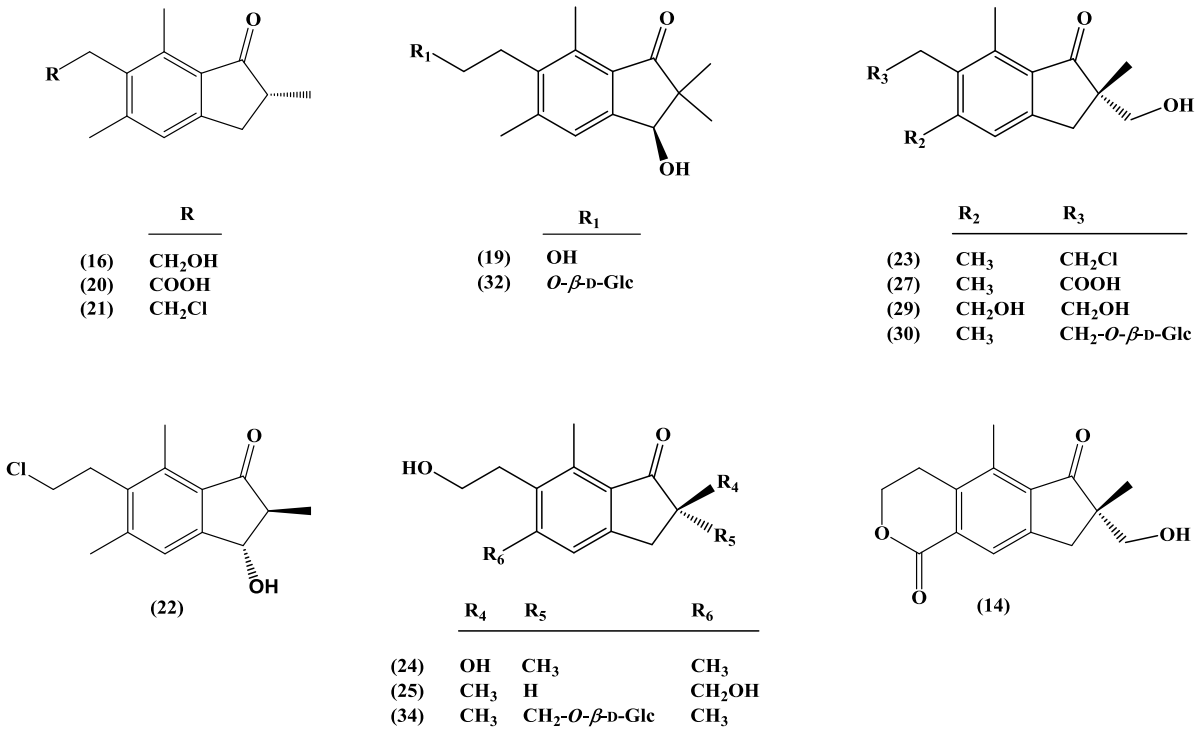

Fig. 3. Chemical structures of pterosins and pterosides **14**, **27**, **29** (Lee et al., 2012), **16**, **30**, **32** (Kuroyanagi et al., 1979), **19-25** (Fukuoka et al., 1978) and **34** (Castillo et al., 2003) obtained from bracken rhizomes with their absolute stereochemistry.

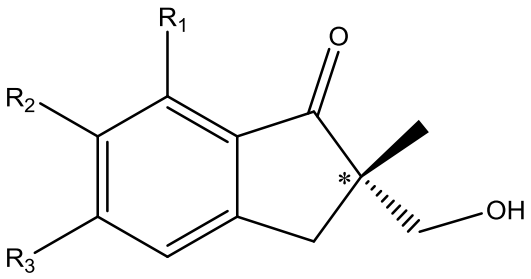

Fig. 4. Chromophore core in compounds **1**, **2**, **7**, **14**, **15**, **23**, **27**, **29** and **30**,.

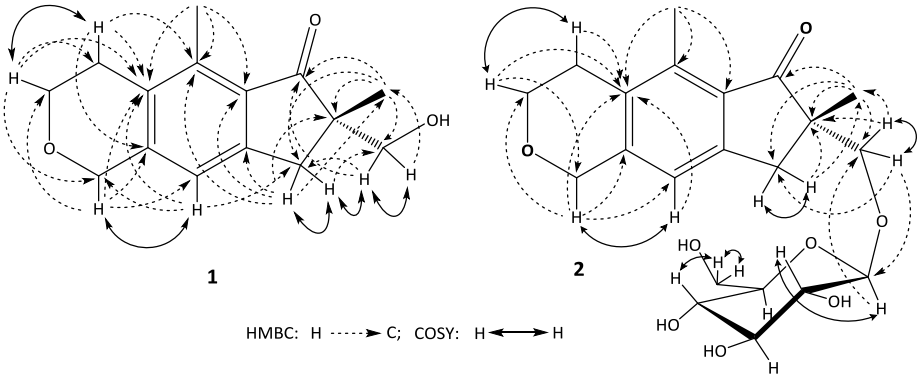

Fig. 5. Key HMBC and COSY correlations of compounds **1** and **2**.

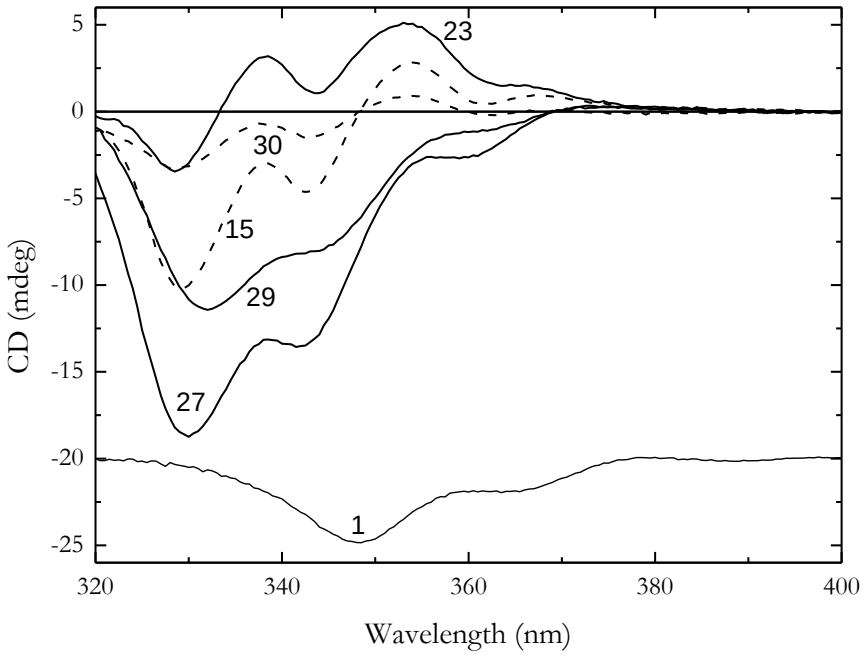

Fig. 6. The CD spectra of **1**, **15**, **23**, **27**, **29**, and **30** in methanol illustrating the superposition of a longer wavelength positively signed vibronic progression and a shorter wavelength negatively signed vibronic progression. The CD of **1** has been offset by -20 mdeg to indicate the overall shift to longer wavelength of the n $\rightarrow\pi^*$ as the compound is tricyclic.

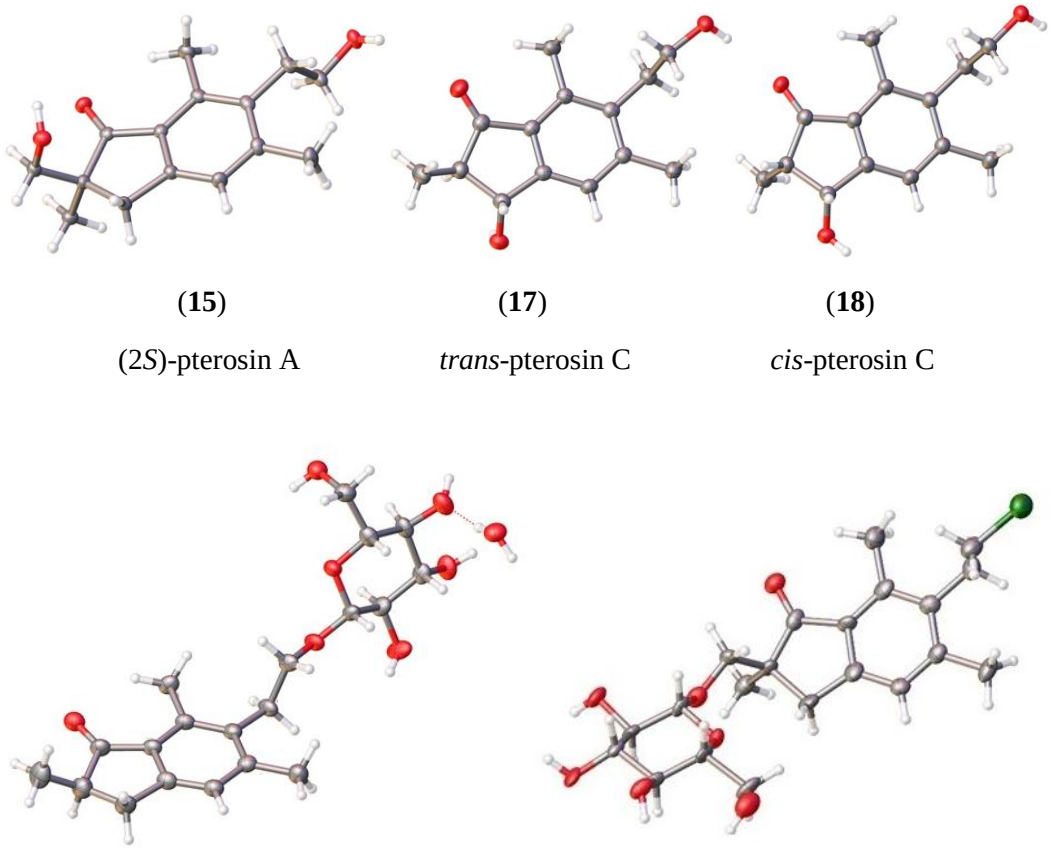

Fig. 7. X-ray crystal structures showing absolute configurations of **15**, **17**, **18**, **31** and **35**.

Note:

In Fig. 7, thermal ellipsoid plots of four crystal structures (*cis*-pterosin C, *trans*-pterosin C, (2*S*)-pterosin A, (2*R*)-pteroside B and (2*S*)-pteroside K) with ellipsoids shown at 50% probability. N.B. pteroside K crystallises as a hemihydrate with four molecules of pteroside K and two molecules of water in the asymmetric unit. Only one molecule of the pteroside K structure is shown here for clarity.

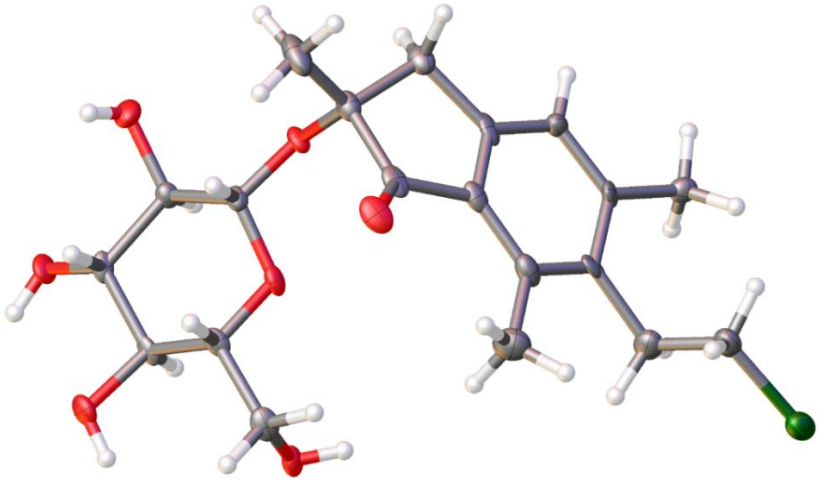

Fig. 8. Thermal ellipsoid plot of rhedynoside B (**10**) with ellipsoids shown at 50% probability. N.B. rhedynoside B crystallises as a hemihydrate with four molecules of rhedynoside B and two molecules of water in the asymmetric unit. Only one molecule of the rhedynoside B structure is shown here for clarity.

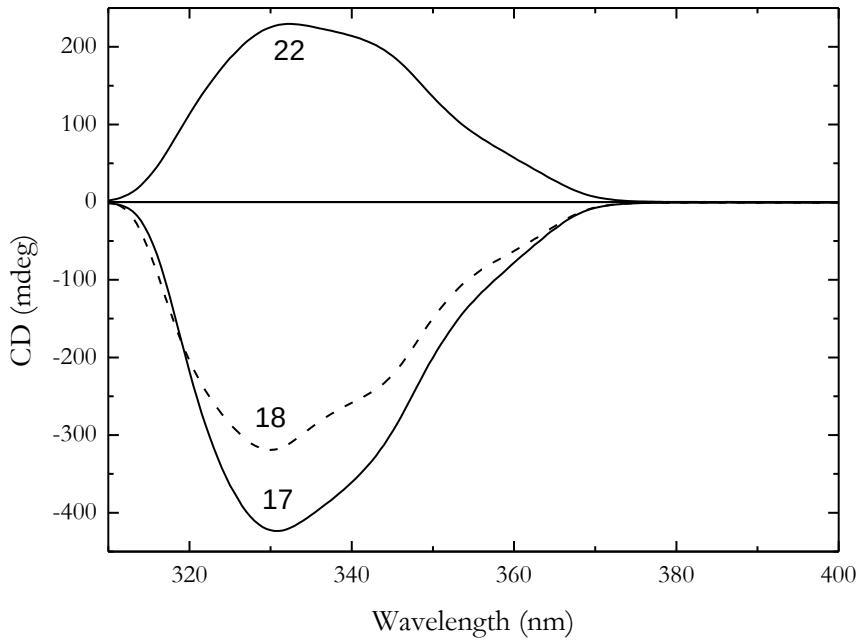

Fig. 9. The CD spectra of **17**, **18**, and **22** recorded in methanol.

Table 1

^{1}H NMR (400 MHz) spectral data$^{\pm}$ of compounds **1**, **3** & **5** in $CDCl_3$ and **2** & **4** in CD_3OD (δ in ppm, *J* in Hz).

No.	**1** δ_H	**2** δ_H	**3** δ_H	**4** δ_H	**5** δ_H
1	-	-	-	-	-
2	-	-	-	-	-
3	3.06, 2.77 (d, *J* = 17.5)	3.45, 2.75 (d, *J* = 17.4)	3.22 (s)	3.19, 3.10 (d, *J* = 17.0)	3.15 (d, *J* = 2.8)
4	6.93 (s)	7.01 (s)	8.05 (s)	7.29 (s)	7.39 (s)
5	-	-	-	-	-
6	-	-	-	-	-
7	-	-	-	-	-
8	-	-	-	-	-
9	-	-	-	-	-
10	1.23 (s)	1.14 (s)	1.42 (s)	1.36 (s)	1.40 (s)
11	3.78, 3.62 (d, *J* =10.8)	4.13, 3.48 (d, *J* = 9.4)	-	-	-
12	4.80 (s)	4.79 (s)	-	5.40 (s)	4.84 (s)
13	2.76 (t, *J* = 5.9)	2.77 (t, *J* = 5.9)	3.05 (t, *J* = 6.0)	3.83 (s)	3.21 (t, *J* = 8.0)
14	4.01 (td, *J* = 1.3, 5.9, 11.8)	4.00 (t, *J* = 5.9)	4.55 (t, *J* = 6.0)	-	3.62 (t, *J* = 8.0)
15	2.56 (s)	2.54 (s)	2.64 (s)	2.62 (s)	2.67 (s)
1′		4.21 (d, $J_{1',2'}$ = 7.8)			
2′		3.03 (dd, $J_{2',3'}$ = 8.9)			
3′		3.29 (m)			
4′		3.24 (m)			
5′		3.20 (m)			
6′a		3.78 (dd, $J_{5',6'a}$ = 1.5, $J_{6'a,6'b}$ = 12.0)			
6′b		3.61 (dd, $J_{5',6'b}$ = 4.6)			

$^{\pm}$ Assignments were confirmed by coupling constants, COSY, DEPTQ, HSQC and HMBC experiments.

Table 2

^{1}H NMR spectral data[±, ‡] of compounds **6** & **9** in CD_3OD, **7** in $CDCl_3$ and **8** in $(CD_3)_2CO$ (δ in ppm, J in Hz).

No.	**6** δ_H	**7** δ_H	**8** δ_H	**9** δ_H
1	-	-	-	-
2	-	-	-	2.63 (m)
3	4.76 (s)	3.08, 2.74 (d, J = 17.3)	3.05 (d, J = 9.5)	3.27, 2.59 (m)
4	7.39 (s)	7.11 (s)	7.13 (s)	7.16 (s)
5	-	-	-	-
6	-	-	-	-
7	-	-	-	-
8	-	-	-	-
9	-	-	-	-
10	1.19 (s)	1.20 (s)	1.32 (s)	1.23 (d, J = 7.5)
11	1.05 (s)	3.79, 3.59 (d, J = 10.7)	-	-
12	2,44 (s)	2.53 (s)	2.55	2.46 (s)
13	3.78 (s)	5.41 (dd, J = 3.5, 10.0)	5.45 (dd, J = 5.2, 8.7)	3.15 (t, J = 8.0)
14	-	3.98 (dd, $J_{13,\ 14a}$ = 10.2, $J_{14a,\ 14b}$ =11.4) 3.65 (dd, $J_{13,\ 14b}$ = 3.7)	3.98 (dd, $J_{13,\ 14a}$ = 8.7, $J_{14a,\ 14b}$ = 11.2) 3.81 (dd, $J_{13,\ 14b}$ = 5.2)	4.05 (t, J = 8.0)
15	2.61 (s)	2.77 (s)	2.75 (s)	2.67 (s)

[±] Assignments were confirmed by coupling constants, COSY, DEPTQ, HSQC and HMBC experiments.

[‡] ^{1}H NMR data measured at 400 MHz for compounds **6**, **7** & **8**, and at 500 MHz for compound **9**.

Table 3

No.	**10** δ_H	**11** δ_H	**12** δ_H	**13** δ_H
1	-	-	-	-
2	-	-	2.66 (m)	-
3	3.45, 3.08 (d, J = 17.4)	2.93 (s)	3.33, 2.64 (m)	4.85 (s)
4	7.17 (s)	7.50 (s)	7.51 (s)	7.56 (s)
5	-	-	-	-
6	-	-	-	-
7	-	-	-	-
8	-	-	-	-
9	-	-	-	-
10	1.44 (s)	1.17 (s)	1.25 (d, J = 7.2)	1.28 (s)
11	-	1.17 (s)	-	1.09 (s)
12	2.45 (s)	4.78, 5.11 (d, J = 12.4)	4.78, 5.10 (d, J = 12.3)	2.49 (s)
13	3.22 (t, J = 8.0)	3.26 (m)	3.26 (t, J = 8.0)	3.24 (t, J = 8.0)
14	3.63 (t, J = 8.0)	3.63 (m)	3.70 (t, J = 8.0)	3.63 (t, J = 8.0)
15	2.65 (s)	2.66 (s)	2.66 (s)	2.65 (s)
1′	4.42 (d, $J_{1',2'}$ = 7.8)	4.40 (d, J = 7.7)	4.39 (d, J = 7.7)	4.58 (d, J = 7.7)
2′	3.16 (dd, $J_{2',3'}$ = 8.0)	3.29 (m)	3.26 (m)	3.30 (m)
3′	3.32[++]	3.31 (m)	3.31 (m)	3.36 (m)
4′	3.28 (dd ~ t, $J_{3',4'}$ = 8.9)	3.31 (m)	3.31 (m)	3.36 (m)
5′	3.12 (m)	3.36 (m)	3.36 (m)	3.42 (m)
6′a	3.70 (dd, $J_{5',6'a}$ = 2.5, $J_{6'a,6'b}$ = 12.0)	3.92 (dd, $J_{5',6'a}$ = 2.0, $J_{6'a,6'b}$ = 12.0)	3.92 (dd, $J_{5',6'a}$ = 1.5, $J_{6'a,6'b}$ = 11.5)	3.93 (dd, $J_{5',6'a}$ = 1.5, $J_{6'a,6'b}$ = 11.8)
6′b	3.60 (dd, $J_{5',6'b}$ = 5.0)	3.70 (dd, $J_{5',6'b}$ = 4.0)	3.69 (dd, $J_{5',6'b}$ = 3.0)	3.75 (dd, $J_{5',6'b}$ = 4.0)

[±] Assignments were confirmed by coupling constants, COSY, DEPTQ, HSQC and HMBC experiments.

[++] Signal under solvent, confirmed by HSQC experiment.

^{1}H NMR (400 MHz) spectral data[±] of compounds **10**-**13** in CD_3OD (δ in ppm, J in Hz).

Table 4

No.	**1**[+] δ_C	**2**[+] δ_C	**3**[+] δ_C	**4**[+] δ_C	**5**[+] δ_C	**6**[+] δ_C	**7**[+] δ_C	**8**[†] δ_C	**9**[+] δ_C	**10**[++] δ_C	**11**[++] δ_C	**12**[++] δ_C	**13**[++] δ_C
1	210.5	212.4	209.2	209.7	208.9	211.6	211.7	208.5	208.8	207.3	211.2	212.5	211.2
2	50.9	51.5	78.0	78.1	77.8	52.5	51.0	77.4	43.7	84.1	46.9	43.9	52.6
3	37.1	37.7	41.4	42.9	41.4	77.6	36.8	42.2	34.6	40.9	42.7	34.9	86.1
4	120.0	121.2	126.3	121.9	124.0	126.0	127.5	128.0	126.9	127.3	126.5	126.4	127.0
5	142.1	143.6	138.2	140.5	146.9	146.6	144.8	145.7	146.8	147.2	144.9	144.7	146.0
6	131.8	132.9	134.6	136.9	134.7	136.0	135.4	134.6	135.3	136.7	136.5	136.4	136.8
7	138.2	139.0	137.3	137.8	139.3	138.9	139.0	138.5	139.0	139.6	139.6	139.1	138.2
8	131.3	127.3	130.7	131.3	131.0	131.1	132.4	131.1	132.5	131.5	133.4	134.4	131.0
9	151.0	153.1	149.7	152.1	151.0	154.3	154.0	151.9	155.0	152.3	153.4	154.7	152.5
10	121.1	122.0	126.0	125.2	126.2	123.5	121.2	125.5	116.9	123.7	125.8	116.7	122.8
11	168.3	175.0	-	-	-	120.7	168.1	-	-	-	125.8	-	122.0
12	168.8	169.6	165.0	171.1	163.8	121.6	122.2	122.0	121.4	121.3	170.2	170.2	121.3
13	125.8	126.6	124.6	132.8	131.7	135.1	171.5	171.4	129.3	133.0	132.5	132.5	133.1
14	165.6	166.5	166.9	117.5	142.8	117.5	147.8	148.1	167.4	143.1	143.8	143.8	143.0
15	113.1	113.0	113.7	113.0	114.0	114.2	114.8	114.6	113.9	114.1	113.7	113.7	114.1
1′		110.4								110.5	110.3	110.3	110.5
2′		174.9								175.1	175.2	175.2	175.3
3′		178.1								178.0	178.2	178.2	178.0
4′		171.5								171.3	171.8	171.8	171.7
5′		177.9								177.7	178.2	178.2	178.3
6′		162.7								162.5	162.9	162.9	162.9

[±] ^{13}C NMR data measured at 100 MHz for all compounds except compound **9** which measured at 125 MHz

[+] ^{13}C NMR data were taken in $CDCl_3$

[++] ^{13}C NMR data were taken in CD_3OD

† ^{13}C NMR data were taken in $(CD_3)_2CO$

^{13}C NMR spectral data[±] of compounds **1-13** in (δ in ppm).